Multiscale Modelling of Foodborne Diseases

by

AZWINDINI DELINAH MAPHIRI

Thesis presented in partial fulfillment of the

academic requirements for the degree of

Doctor of Philosophy (Mathematics)

in the

Department of Mathematical and Computational Sciences

Modelling Health and Environmental Linkages Research Group

Applied Mathematics

Supervisor: Dr. K. MUZHINJI

Co-supervisor: Prof. W. GARIRA

Co-supervisor: Prof. D. MATHEBULA

Submitted July 2024

Declaration of Authorship

I, AZWINDINI DELINAH MAPHIRI, declare that this thesis titled, “Multiscale Modelling of Foodborne Diseases”and the work presented in it are my own. I confirm that:

- This work was done wholly or mainly while in candidature for a research degree at this University.
- Where I have consulted the published work of others, this is always clearly acknowledged.
- Where I have quoted from the work of others, the source is always given. With the exception of such quotations, this thesis is entirely my own work.
- I have acknowledged all main sources of help.

Signed: 

Date: 31/07/2024

Abstract

Infectious disease systems are essentially multiscale complex system wherein pathogens multiply within hosts, spread across people, and infect entire populations of hosts. The description of most biological processes involves multiple, interconnected phenomena occurring on different spatial and temporal scales in the human body. Traditional approaches for modelling infectious disease systems rely on the principles and concepts of the transmission mechanism theory that considers transmission to be the primary cause of infectious disease spread at the macroscale. Modellers of infectious diseases are increasingly using multiscale modelling approach in response to this challenge. Multiscale models of infectious disease systems encompass intricate structures that revolve around the interplay of three distinct sub-systems: the host, the pathogen, and the environmental subsystems. The replication-transmission relativity theory is a novel theory designed for the purpose of multiscale modeling of infectious disease systems, accounting for variations in time and space by incorporating pathogen replication that leads to transmission. Replication-transmission relativity theory consists of seven distinct levels of organization within an infectious disease system, each level including the within-host scale (microscale) and between-host scale (macroscale). Five separate classifications of multiscale models can be formulated that integrate the microscale and macroscale. A research gap has been created in an attempt to establish a multiscale framework in order to understand the mechanisms on how foodborne pathogens cause infections on human beings and animals, as very little has been done in modelling of foodborne disease. The primary goal of this study is to create multiscale models for foodborne diseases to examine whether a mutual influence exists between the microscale and macroscale, guided by the principles of replication-relativity theory. The multiscale models are developed by considering three environmental transmitted diseases at host level caused by pathogens: *norovirus*, *E. coli* O157:H7 and *taenia solium*. We start by developing a single-scale model of foodborne diseases caused by viruses in general, which is then extended to create a multiscale model for *norovirus*. We formulate a non-standard finite difference scheme for the single-scale model, *norovirus*, and *E. coli* O157:H7. For *taenia solium*, we use ODE solvers in Python, specifically, ODE int function in the sci.integrate. The numerical findings from the study confirm the applicability of the replication-transmission relativity theory in cases where the reciprocal impact between the within-host scale and the between-host scale involves both infection/super-infection (for the effect of the between-host scale on the within-host scale) and pathogen excretion/shedding (for the effect of the within-host scale on the between-host scale). We expect that our study will help modellers integrate microscale and macroscale dynamics across various levels of organization within infectious disease systems.

Acknowledgements

I thank God Almighty for providing me with the wisdom, good health, and strength needed to initiate and successfully accomplish this research work. My special thanks to my supervisor, Dr K. Muzhinji. This project would not have been achievable without his invaluable guidance, enduring patience, and unwavering support. I owe many thanks to my co-supervisor, Prof W. Garira, for his outstanding knowledge in mathematical modelling in infectious diseases, which has contributed significantly to this study. Also, Prof D. Mathebula, my co-supervisor, I appreciate your contribution to my PhD studies. You were never too busy to assist me whenever I needed you, and you were a source of encouragement. I also like to express my gratitude to Dr. R. Netshikweta, my research assistant, for his invaluable assistance with this project. I express my sincere gratitude to Dr. Mukhodobwane R.M, Dr. Maregere B, Ndivhuwo Ndou, and Nancy Mukwevho for their exceptional support in a unique manner. I have benefited significantly from their individual recommendations and scholarly engagements throughout different stages of this study. I want to express my gratitude to my family for their steadfast support throughout this study, especially to my uncle, Sam Ramatshekgisa, without whose encouragement I would not have been able to complete it. My lovely daughters Murendeni and Mufunwa and grandson Renda, thank you for all your patience, support, and love over the years. Mufunwa, I was inspired by the love you expressed on a daily basis and by the hugs you offered me, especially during the write-up. My sincere gratitude goes out to my dearest friend, Mr. Ntsieni Phaswana, for his love, support, patience and countless prayers that made this project possible. I would like to thank staff and postgraduate students in the Department of Mathematical and Computational Sciences for their outstanding academic and social contribution which made the department an excellent place to research. I would want to express my gratitude to everyone who has helped me, directly or indirectly. Your kindness has been my source of strength as I strive to complete this task. In addition, I would like to thank South Africa Technology Network (SATN) for its support during the PhD study and writing process. In closing, let me express my sincere gratitude for the financial assistance provided by the University Capacity Development Grant (UCDG).

Contents

List of Figures

List of Tables

Chapter 1

Introduction

Many infectious diseases affect humans and other species, they are a major cause of mortality and morbidity [3, 4]. Infectious illnesses result from pathogenic agents that have the capability to spread from hosts to hosts by various means, including direct contact, airborne droplets, food or water, and mother to baby transmission [5]. The problem of infectious diseases has been made worse by the appearance of emerging infectious diseases, encompassing well-known outbreaks such as the outbreak of dengue fever in 1945, the emergence of HIV/AIDS in 1981, the identification of hepatitis C in 1989, the discovery of hepatitis E in 1990, the occurrence of the SARS epidemic in 2002, and the appearance of the H1N1 influenza strain in 2009., as well as the resurgence of some infectious diseases around the globe like tuberculosis. Even more alarming is the fact that infectious agents are increasingly becoming resistant to antibiotics and antiviral drugs. Apart from infectious agents, factors like the method of transmission, duration of latency and infectiousness, as well as social, demographic, and geographical elements, play a pivotal role in influencing the propagation of a disease. Humans and animals are studied through epidemiology in order to determine disease prevalence and to understand its determinants [5–13].

1.1 Overview of Foodborne Diseases

Foodborne diseases are illnesses that result arising due to the ingestion of food that has been tainted with disease-causing bacteria, viruses, parasites, toxic substances, and chemical contaminants. The societal and economic ramifications linked to foodborne illnesses can have substantial impacts on individuals, food industry entities, and a nation's image [14]. Foodborne illnesses

stand as the primary driver of sickness and death and pose a substantial hindrance to global socioeconomic progress [15]. World Health Organization (WHO) further highlighted that the complete scope and weight of hazardous food, particularly the impact stemming from chemical and parasitic pollutants remain largely unknown [15]. About one in every 10 people around the world is sickened by foodborne disease each year. Out of 600 million people, 420,000 die as a result. The comprehensive report by WHO published in 2012, Dec. 3, included 31 potential foodborne risks, comprising bacteria, viruses, parasites, toxins, and chemical substances. Diarrheal diseases were responsible for most of the global burden, causing 550 million illnesses and 230,000 deaths. Children younger than 5 years old carried 40 percent of the foodborne disease burden, despite representing only 9 percent of the global population [16]. Foodborne illnesses result from unhealthy methods employed during food production, harvesting, and cooking. A total of 31 primary pathogens are responsible for causing such diseases. Prominent examples include *Salmonella nontyphoidal*, *Campylobacter*, *Listeria*, and *Escherichia coli* strains that produce Shiga toxin. National authorities closely monitor these significant pathogens, carefully analyzing outbreaks to identify patterns and devise strategies to prevent future occurrences [14].

While foodborne pathogens differ in their population dynamics and interactions with hosts, they share common characteristics in terms of transmission. Many of these pathogens reside in the gastrointestinal tract of animals, making fecal shedding the primary means of pathogen excretion. They can originate from animal reservoirs as well as from food contamination occurring during the preparation process before they reach the final consumer. There is a substantial body of evidence that strongly suggests the transmission of foodborne pathogens takes place through multiple pathways, such as the direct (oral-fecal) transmission occurring between humans and animals, as well as indirect transmission through the environment. The link between humans and animals as a significant route for the spread of foodborne pathogens, along with other transmission pathways, has been extensively documented [17]. A conceptual diagram for the transmission of foodborne diseases is well depicted in [1] reproduced in the figure below:

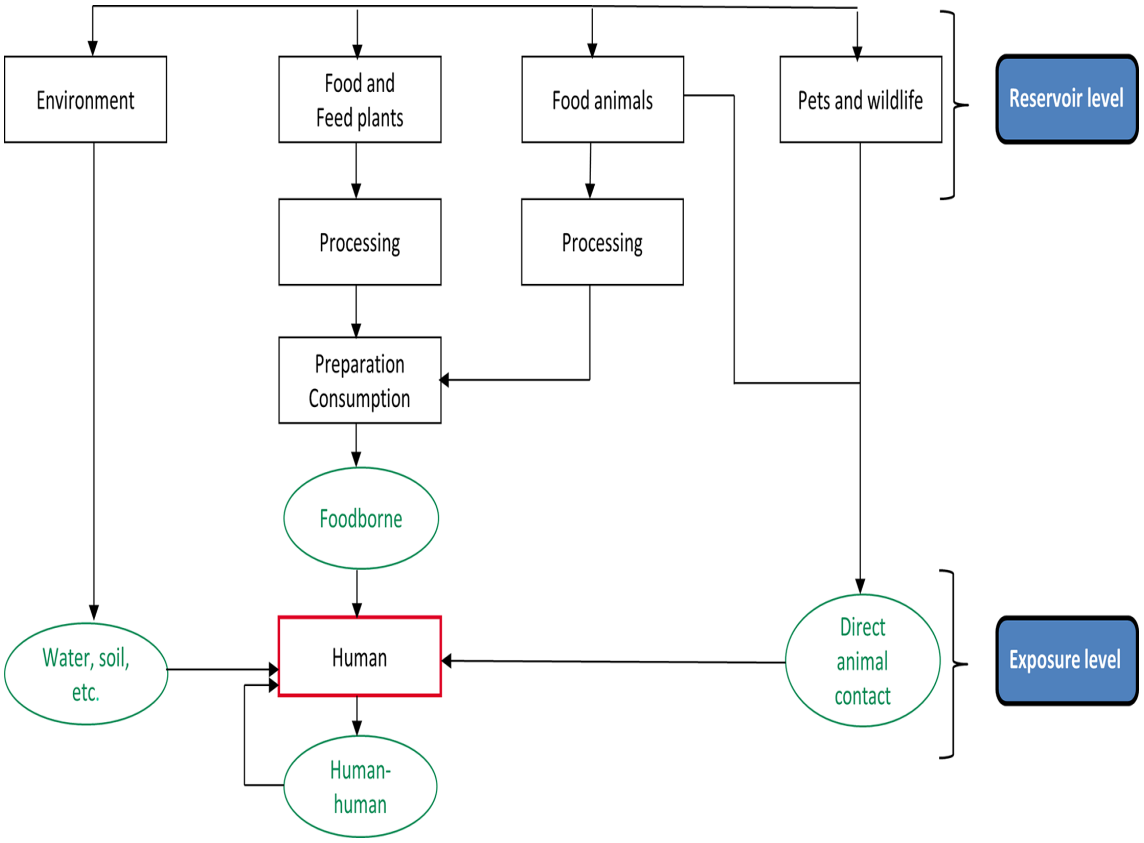

Figure 1.1: Primary pathways for transmitting foodborne illnesses in humans, showcasing two points of origin: the source level and the contact level [1]

Control methods to lessen the spread of foodborne pathogens can be divided into two groups: those that target the gastrointestinal system and modify management. Improvements in hygiene, isolation, and test-and-cull interventions are examples of management control measures. Probiotics, vaccination, therapeutic procedures, and methods such as dietary and nutritional management are examples of control measures that target foodborne pathogens within the digestive system [18]. Vaccinations play a vital role in mitigating the consequences of infectious diseases by offering protection at both the individual and population levels. At the individual level, they can prevent infection, reduce infectiousness, and inhibit colonization. At the population level, general vaccination fosters herd immunity, indirectly protecting both vaccinated and unvaccinated individuals from the disease [19]. Thus, scientific research is required to gather rigorous information on the burden of foodborne diseases which can be vital for supporting policymakers as well as assisting the process for allocating resources appropriately for food safety control and intervention efforts [15].

1.2 Multiscale Modelling

The application of mathematical models to infectious diseases has greatly enriched our understanding of the relationships between pathogens and chronic infections and has shown to be a valuable tool to help public health officials make informed decisions. Our ability to control infectious diseases with fewer resources has been enhanced by using mathematical models to understand infectious disease transmission dynamics [20]. However, the current mathematical frameworks for infectious diseases are founded upon the transmission mechanism theory that elucidates the dynamics of disease propagation, which is based on single scale modelling approach. This theory asserts that transmission is the fundamental dynamic process at every level of the disease system. As per this theory, the dissemination of infectious diseases is based on the transfer of pathogens from one host to another. Consequently, particular transmission models can be constructed to investigate the dynamics of infectious diseases at different organizational levels within the system. To construct transmission models at any organizational level, the conventional method involves dividing the population (which could be cells in a cell model, granulomas in a tissue model, or hosts in a host model) into distinct compartments, where individuals within each compartment exhibit uniform behavior [20]. However, the limitations of using single-scale modelling methodologies to address the challenges in the field of infectious disease modelling are now being recognized. The theory of transmission mechanisms encounters two basic limitation that have lessened its usefulness and applicability. These include the absence of a standardized and comprehensive modelling framework within a single scale for both direct and environmental modes of transmission, as well as the failure to incorporate pathogen replication within models depicting the dynamics of infectious diseases. Based on these facts, it is now understood that relying solely on modelling approaches that focus on a specific scale is inadequate for effectively solving the problems encountered in the study of infectious diseases. Traditional models ignore the reality that the transmission of communicable disease systems results from complex, dynamic connections that take place at many spatial and temporal scales [21]. Whilst single-scale models have been used widely in estimating important parameters from fitting the model to clinical data and for spearheading the science of identifying important drug targets that are key to investigating drug effects on patients under treatment, they lack the rigor to concurrently characterize the complete infectious disease ecosystem [22]. There are three main transmission mechanisms that influence infectious disease dynamics according to this theory.

(a) **Direct transmission mechanism**: This approach involves developing the transmission model by partitioning populations (such as cells, tissues, hosts, etc.) into distinct compartments, including susceptible, exposed, infected, and recovered ($SEIR$), and also different iterations of this concept [20].

(b) **Environmental transmission mechanism**:

In the process of constructing transmission models, this approach involves categorizing the population (including cells, tissues, hosts, etc.) into different compartments, such as susceptible, exposed, infected, recovered, and environmental pathogen load ($SEIRP$), along with possible modifications to this paradigm. Significantly, environmentally transmitted infectious disease systems differ from directly transmitted infectious disease systems by including an extra equation that portrays the behavior of the pathogen within the environment. This distinction is essential as it accounts for the interactions and changes in the pathogen load within the environment, that play a crucial role in comprehending the transmission dynamics of diseases spread through environmental means [20].

(c) **Vector-borne transmission mechanism**:

This mechanism involves developing transmission models based on the disease's intricate life cycle, which mandates engagement with two hosts (a vertebrate host and a vector host) to fulfill its life cycle. Alternatively, the model may be designed for directly transmitted diseases, like malaria, in which the host population is categorized into susceptible, exposed, infected, and recovered groups, denoted as $SEIR$, along with possible variations of these groups. [20].

While the transmission mechanism theory is effective in clarifying the causes of foodborne diseases, it falls short in providing a comprehensive understanding of diseases when examined through multiscale modelling. Consequently, this theory alone is inadequate for describing the complexities of infectious disease phenomena that exhibit changes in time and space, as well as variations at different levels of organization [20]. Yet, due to the interconnected nature of these systems in natural environments, multiscale models are necessary to reflect the cross-scale effects that drive infectious pathogens dynamics. To this date, the field of multiscale modelling has witnessed increased attention due to insights gained from disciplines including fields like molecular biology, immunology, epidemiology, and environmental health. The increased attention arises from a motivation to gain a deeper insight into the intricate transmission dynamics witnessed within systems of infectious diseases. Multiscale modelling of an infectious disease pertains to any characterisation of the disease system that allows for the analysis or study of these diseases at multiple scales simultaneously [22]. By incorporating knowledge from these diverse fields, multiscale modelling offers the potential to unravel the complex interactions and interdependencies that govern the spread of infectious diseases [22]. Consequently, it is currently becoming more and more evident how infectious diseases spread in both large and small sizes. The multiscale modelling approach provides unprecedented opportunities for understanding foodborne diseases by linking growth and progression of pathogens from the agents, humans, the environment etc,

resulting in an all-encompassing population level multiscale model. The potential of such a multiscale modelling technique in providing novel understanding of other complex infectious disease systems has been illustrated before [23, 24]. The Replication-Transmission Relativity Theory is a recent theory designed for multiscale modelling of infectious disease systems. In the context of infectious disease systems, there are three interconnected subsystems that interact to produce the overall system: (i) the host subsystem, (ii) the pathogen subsystem, and (iii) the environment subsystem. These subsystems work together, resulting in infectious disease systems that exhibit hierarchical multilevel, multiscale complexity. This complexity spans multiple levels, ranging from the cellular level, tissue level, and organ level to the microecosystem, host level, community level, and macroecosystem level. Each level plays a distinct role in shaping the dynamics of infectious diseases, contributing to a comprehensive understanding of the entire system [20].

This innovative approach takes into consideration the temporal and spatial variations by incorporating the role of pathogen replication at within-host, which significantly influences disease transmission. By accounting for the interplay between pathogen replication and transmission, this theory offers a more comprehensive understanding of infectious disease phenomena across different scales, providing valuable insights into the dynamics of disease spread [20]. The proposed hypothesis suggests that interactions between the within-host/microscale (where pathogen replication occurs frequently) and between-host/macroscale (where pathogen transmission is frequent) have a significant impact on disease dynamics at all levels of organization within an infectious disease system. For pathogens to effectively spread and persist at a particular level of organization, they must succeed in both the microscale and the macroscale. In essence, there is no single privileged or absolute scale that solely determines disease dynamics at any level of organization in an infectious disease system. Instead, a complex interplay between microscale and macroscale factors influences the overall dynamics of the disease [20]. To comprehensively understand the multiscale dynamics of an infectious disease system at any level of organization, it is crucial to consider the dynamics of these two interconnected scales. [20].

1.2.1 Main hierarchical levels of infectious diseases

There are seven fundamental hierarchical levels within the organization of infectious disease systems. Each of these levels comprises a microscale and a macroscale as its adjacent limiting scales, with both scales reciprocally influencing each other bidirectionally. These multiscale interactions involve the dissemination of the pathogen through infection or superinfection and the process of shedding or excretion, resulting in a cyclical multiscale effect between pathogen replication at the microscale and pathogen transmission at the macroscale [20].

(i) **The cell level**:

The microscale and macroscale within this level of structure are referred to as the within-cell and the between-cell scales, respectively. By integrating these two scales, the multi-scale dynamics of infectious diseases can consider various target cells, such as CD4+ T cells for HIV or red blood cells for malaria [25]. In foodborne illnesses, the cells that are impacted are epithelial cells. Pathogens have the capability to invade the epithelial layer by adhering to and subsequently penetrating through these cells [26].

(ii) **The tissue level**:

The microscale and macroscale of this particular level of organization are referred to as the within-tissue and the between-tissue scales, respectively. Various types of tissues can be taken into account in the multiscale dynamics of infectious disease systems. Examples of such tissues include granulomas [27] in the context of tuberculosis or microabscesses [28] caused by certain bacterial infections [25]. Foodborne pathogens that can live and reproduce inside the tissues and organs of infected people and animals feces include *Cyclospora cayetanensis*, *Toxoplasma gondii*, and *Trichinella spiralis* which are the most prevalent foodborne parasites [26].

(iii) **The organ/anatomical compartment level**:

The within-organ/anatomical compartment and the between-organ/anatomical compartment scales are the microscale and macroscale for this level of organizational structure of an infectious disease system. The lung, brain, gut, kidney, muscle, heart, pancreas, stomach, liver, spleen, bone, adrenal, skin, adipose, and blood are a few of the organs/anatomical compartments taken into account at this level of organization of an infectious disease system [25]. In our case the pathogen such as *Vibrio parahaemolyticus* (*V. parahaemolyticus*) has been considered invasive and can enter circulation through the lamina propria [26].

(iv) **The microecosystem level**:

The many organs/anatomical compartments (lung, gut, kidney, heart, stomach, liver, skin, blood, etc.) are viewed as ecosystems at this level of an infectious disease system's organization. As a result, at this level, infectious disease systems are characterized in terms of several organs, anatomical compartments, and pathogen species. The within-microecosystem and the between-microecosystem scales are the microscale and macroscale for this level of organization of an infectious disease system, respectively. Pathogen such as *E.coli* O157:H7 is one of those which can affect organ such as liver [25].

(v) **The host/organism level**:

Microscale and macroscale of this level of organization are within-host and between-host, respectively. This level is used to demonstrate the viability of the replication-transmission relativity theory when the form of reciprocal influence between the within-host and the between-host scales consists of both super-infection, which is defined as repeated infection before the host recovers from an infectious episode (for the influence of between-host scale on within-host scale), and pathogen excretion/shedding (for the influence of within-host scale on between-host scale) [25]. This study will consider host level to develop multi-scale models for foodborne diseases which are environmentally transmitted for pathogens with replication microscale only, pathogens with replication at both microscale and for pathogens with no replication at both scales.

(vi) **The community level**:

The within-community and the between-community scales are the microscale and macroscale for this level of organizational structure of an infectious disease system. At this level, infectious disease systems are characterized in terms of a single pathogen species or strain, a single host species, and a number of communities. Local communities (village, district, town, province, etc.), territorial communities (i.e., nations), and regional communities [25].

(vii) **The macroecosystem level**:

The various communities (local, national, regional, etc.) are viewed as ecosystems at this level of the organization of an infectious disease system. The within-macroecosystem scale and the between-macroecosystem scale are the microscale and macroscale for this level of organization of an infectious disease system, respectively [25].

Below, we present the conceptual diagram representing the seven hierarchical levels of organization in infectious disease dynamics, derived from the source [20].

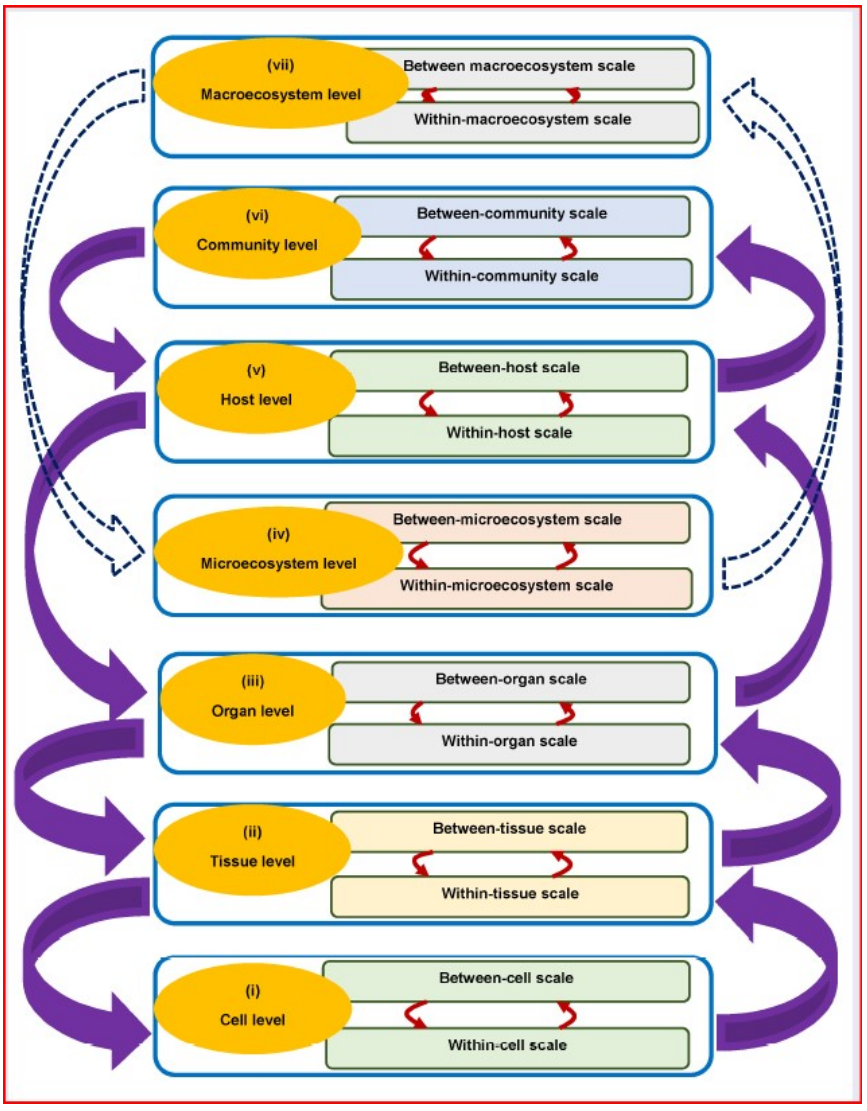

Figure 1.2: The seven hierarchical levels of organisation of infectious disease dynamics are illustrated in this conceptual diagram.

1.2.2 The Reciprocal Influence of Macroscale and Microscale at Hierarchical Levels of an Infectious Disease System

Infectious disease dynamics, as perceived in the context of replication-transmission relativity theory for multiscale modelling of infectious disease systems, can be seen as a continuous cycle of disease processes at each of the seven levels of organizational hierarchy. This cyclical nature is attributed to the reciprocal influence between the microscale and macroscale at every level of hierarchical organization.

The interaction of four important disease processes which are infection/superinfection (a process in which macroscale pathogens move to microscale), pathogen replication, pathogen shedding/excretion (a process in which microscale pathogens move to macroscale), and pathogen transmission is the primary mechanism by which the microscale and the macroscale affect each other reciprocally. At each level, the macroscale influences the microscale through infection or superinfection, while the microscale influences the macroscale through pathogen shedding or excretion. In replication-transmission relativity theory, there are two distinct types of reciprocal influence between microscales, which are:

(a) **Type I reciprocal influence between the macroscale and microscale within a level**:

Through pathogen shedding/excretion, the microscale influences the macroscale this implies the transmission of pathogens from the micro to the macro scale. The influence of the macroscale on the microscale is also evident through the initial infection, as pathogens move from the macroscale to the microscale. Mathematically, this is reflected by the macroscale dictating the initial values of the microscale submodel variables (initial infection) [20].

(b) **Type II reciprocal influence between the macroscale and microscale within a level**:

The microscale also affects the macroscale by releasing or excreting pathogens. As a result of super-infection (repeated infections before the host recovers from an infection), the macroscale influences the microscale, which also involves pathogens moving from the macroscale to the microscale. Mathematically, the macroscale affects the microscale by scaling down the macroscale's variables and parameters [20].

Within the framework of replication-transmission relativity theory, five categories of multiscale models of infectious disease systems have been identified. These models integrate the microscale and macroscale by considering the two types of reciprocal influence that occur between these scales at hierarchical levels of organizational structure in an infectious disease system. The first category of multiscale models of infectious diseases is known as Individual-Based Multiscale Models (IMSMs). In this category, the microscale submodel and the macroscale submodel are integrated through type I reciprocal influence. The macroscale is often regarded as the emergent behavior resulting from the interactions of the microscale entities in this particular category of multiscale models. The second category is **Nested Multiscale Models (NMSMs)**, in this category, type I reciprocal influence integrates the microscale submodel and the macroscale submodel in such a way that the same formalization or mathematical representation is used to describe both

scales. This approach ensures consistency and coherence between the microscale and macroscale components of the model, facilitating a unified understanding of the multiscale dynamics within the infectious disease system. The third category is **Embedded Multiscale Models (EMSMs)**, the microscale and the macroscale submodels are integrated through type II reciprocal influence in this category. The formalism or mathematical representation used to describe the macroscale and microscale submodels must be the same. The fourth category is **Hybrid multiscale models (HMSMs)**, in this context, the integration of the microscale submodel and the macroscale submodel occurs through either type I reciprocal influence or type II reciprocal influence. In this approach, the macroscale submodel and the microscale submodel are described using different mathematical representations, including deterministic/stochastic, discrete time/continuous time, ODE/PDE, and other examples of paired formalisms. This diverse set of mathematical representations allows for a more comprehensive analysis of the multiscale dynamics within the infectious disease system. The fifth category is **Coupled multiscale models (CMSMs)**, in this category, the multiscale models are constructed by merging either a single-scale submodel with some multiscale models from any of the first four categories (applicable to multiscale models that combine an odd number of scales) or by combining multiscale models from any of the previously mentioned categories through either type I or type II reciprocal influence, or a combination of both. This approach allows for the integration of multiple scales and various modelling techniques, leading to a more comprehensive representation of the complex dynamics within infectious disease systems. The multiscale models developed in this category consider a wide range of infections caused by different pathogen strains, species, host groups, host species, communities, and organ/anatomical compartment infections. [20].

Based on the replication relativity theory, infectious diseases pathogens are categorized as environmentally transmitted infectious disease systems, wherein the pathogen undergoes specific free-living life stages in various physical elements of the geographical environment, such as soil, water, contact surfaces, air, and food. In the context of our study, we classify foodborne diseases based on the three different types of environmentally transmitted infectious disease systems described in the in [20]:

(a) **Type I environmentally transmitted foodborne diseases systems**: These pertain to infectious disease systems that are environmentally transmitted, wherein the pathogen does not replicate at the microscale (within the host's scale). An example of such a disease is schistosomiasis [23], Guinea worm [13], and illnesses caused by soil-transmitted helminths like hookworm [29]. In our case we consider *taenia solium* as a soil-transmitted helminths. The pathogen load within an individual host in these infectious disease systems is directly influenced by the number of encountered infective stages from the environment (such as

water, soil, food, air, contact surfaces, etc.) or through super-infection (repeated infection prior to recovery from an infectious episode). The more infective stages an individual absorbs from the environment or experiences through super-infection, the higher the pathogen load within that host. The disease burden of environmentally transmitted infectious diseases is significantly influenced by host behavior, especially with regards to sanitation and hygiene practices. Certain behaviors related to sanitation and hygiene can increase the transmission of diseases within a specific community [20].

(b) **Type II environmentally transmitted foodborne diseases**: These refer to infections that are transmitted through the environment, and in these systems, the pathogen reproduces solely at the microscale. Examples of such diseases include certain bacterial infections, such as paratuberculosis species [30], and viral infections such as influenza [31], Mycobacterium tuberculosis [32], are notable examples of Type II environmentally transmitted infectious disease systems. In our case we consider *norovirus* as a pathogen that replicates at within-host only. In these infectious disease systems, nested multiscale models can be employed, where type I reciprocal influence characterizes the interaction between the microscale and the macroscale at the host level. For modelling such infectious disease systems, embedded multiscale models can also be utilized, utilizing type II reciprocal influence to describe the relationship between the microscale and the macroscale [20].

(c) **Type III environmentally foodborne diseases** In this type of infection, the pathogen undergoes replication at both the microscale and the macroscale. In our case we take into consideration *E.coli* O157:H7. The relationships between the microscale and macroscale in infectious disease systems are described using reciprocal influences of type I and type II at both scales [20].

1.2.3 Multiscale modelling of foodborne diseases

The spread of foodborne pathogenic agents involves the environment which further complicates the life cycle of the pathogens involved. For instance, humans acquire foodborne pathogens when they ingest contaminated food. If humans remain untreated, the pathogens will develop within-humans until they get excreted into the environment or passed back to the agents (animals). The life cycle of foodborne pathogens involves both the gut and the external environment. Pathogen ecology and evolution are influenced by the necessity to survive in both habitats, resulting in a range of pathogen life histories and varying levels of fitness. These differences have significant implications for disease transmission and control strategies [23, 24]. Advancements in molecular biology have provided us with a comprehensive understanding of the fundamental elements of

living organisms and their intricate interactions. This progress has significantly enhanced our capability to identify the molecular identity and dynamics of infectious agents, their hosts, and even vectors. Furthermore, it has greatly expanded our knowledge of the immune responses exhibited by host organisms towards these infectious agents [22]. This research aims to provide a comprehensive understanding of the mechanisms underlying the transmission, growth, and progression of various foodborne bacterial, viral, and parasitic agents. It emphasizes the need to comprehend the progressive infection caused by foodborne pathogens in humans and animals, as well as how immune responses to these infections at the individual level influence disease dynamics at the population level. To achieve this understanding, the application of multiscale techniques becomes essential. The multiscale modelling approach provides unprecedented opportunities for understanding foodborne diseases by linking growth and progression of pathogens from the agents, humans, the environment etc, resulting in an all-encompassing population level multiscale model.

Foodborne infections can manifest at various levels of organization, encompassing cell-level, tissue-level, organ-level, host-level, community-level, and beyond. This wide range of infection levels highlights the complexity of the processes involved in foodborne illnesses. Then there is need to decide which level of multiscale models can best fit the multiscale models. The models in this study are developed at host level where humans and animals such as cattle and pig interact with a pathogen in the physical environmental domains (such as soil, water and food). The multiscale models are developed with the main aim of describing and understanding the complex life cycle of these foodborne pathogens considering the role of humans, plants, animals and the environment and their interconnectedness in sustaining the transmission of foodborne diseases. The reciprocal influence between the microscale and the macroscale plays a crucial role in determining the appropriate categories for developing a multiscale model. This reciprocal influence helps guide the selection of suitable categories that can effectively capture the interactions and dynamics between different scales in the system. At the host level, we construct two nested multiscale models for pathogens that undergo a replication cycle entirely at the microscale and for pathogens that replicate at both microscale and macroscale, additionally we develop a coupled multiscale model for pathogens requiring two hosts to complete their life cycle, the coupled multiscale model proves to be the most suitable category for pathogens with no replication cycle at within-host. Multiscale modelling of infectious disease systems offer several benefits, including the ability to study diseases at the specific scale of infection occurrence, analyze factors influencing disease dynamics (e.g., immune response, health interventions), and explore various aspects of the disease process [20]. At host level we incorporate the immune response and epidemiological scales, in a way to understand how the immune response affect diseases dynamics. It must be noted that at the population level (between-host scale), eliminating foodborne diseases

can be a lengthy process, potentially taking years. However, within an individual host, the time required for disease progression and recovery varies significantly, ranging from days to even years. The duration of healing and recovery at this level is influenced by factors related to the immune response at the site of infection, such as the involvement of different immune cells, the host's medical history, immune memory, and the environmental conditions affecting the immune system [20]. We first develop a single-scale foodborne viral infection to illustrate the weakness of single scale model in foodborne diseases description. In single-scale modelling, the specific details of pathogen replication-transmission interactions are not explicitly represented. Instead, pathogen replication is described in a general manner using a single parameter. Consequently, this approach lacks the ability to study foodborne disease dynamics under constraints imposed by the intricacies of pathogen replication. Models based on the transmission mechanism theory do not account for these highly-detailed dynamics, limiting their capability to comprehensively analyze foodborne diseases. Single-scale models lack the inclusion of specific pathogen replication processes, resulting in a description of the complexity of an infectious disease system without capturing the precise intricacies involved. These models only provide a general understanding of the complexity rather than incorporating the specific details that contribute to the overall complexity of the disease system [33]. The interaction between pathogen replication and pathogen transmission is mutually influential. To gain a broad understanding of foodborne disease dynamics, it is essential to have a thorough understanding of the replication-transmission cycle.

Foodborne diseases are also influenced by four pathogen-specific processes that connect different scales at the host level mentioned earlier. After successful infection/superinfection at the within-host scale, pathogen replication takes place within the host. Subsequently, the process of pathogen replication at the site of infection at within-host scale is followed by pathogen shedding/excretion to the between-host scale. As a result, pathogen shedding/excretion serves as the link between the within-host and between-host scales. The shedding/excretion of the pathogen is then followed by pathogen transmission at the between-host scale. In this way, the entire cycle of infection, replication, shedding, and transmission completes the dynamics of the foodborne disease across different scales. Hence, at each hierarchical level of the foodborne disease system, the processes of infection/superinfection and shedding/excretion of the pathogen establish a cyclic influence between pathogen replication at the within-host scale and pathogen transmission at the between-host scale. These interactions create a continuous loop that impacts disease dynamics across different scales of the system [20].

A nesting principle will be used to link the microscale and macroscale submodels of *norovirus* and *E. coli* O157:H7. The nesting modelling approach consists of three stages. The initial stage focuses on creating a model to examine interactions within the host. The second step involves

constructing an epidemiological model that examines interactions between hosts (between-host model). The third step is the integration of the within-host model into the epidemiological model by incorporating the dynamics of the former using parameters. These parameters in the epidemiological model are expressed as functions derived from the immunological model, thereby linking the two models together [13].

In the context of the third multiscale model focusing on *Taenia Solium*, the relationship between within-host and between-host dynamics is established based on the division of disease processes into three distinct time scales. The first time scale is within-host, which refers to the processes occurring within individual hosts. At this scale, the disease process generally unfolds rapidly, mainly influenced by the pathogen's reproductive cycle and its interaction with the host's immune system. Moving on, the second time scale is the epidemiological time scale, which operates at the between-host level. Disease processes at this scale occur due to interactions between susceptible hosts and the free-living pathogen. In most cases, this process occurs at an intermediate timescale, representing the transmission and spread of the disease among different individuals. The third time-scale in disease processes is known as the environmental time-scale. Infections caused by free-living microorganisms are heavily influenced by environmental factors. In such cases, the pathogen can persist in the environment for an extended period, and its presence can be periodically replenished by infectious hosts that shed the virus into the environment. Disease progression at this environmental time-scale generally occurs at a slow time scale. Incorporating this third time-scale is vital for both between-host and within-host models of infectious diseases to operate effectively. It accounts for the dynamics of pathogen transmission and persistence in the environment, which plays a critical role in shaping the overall epidemiology of the disease and its interactions with individual hosts. By considering this time-scale, the multiscale models can better comprehend the complex relationships between the pathogen, the host, and the environment in the context of infectious diseases [13].

1.2.4 Literature Review for Foodborne Diseases

The early work on mathematical application of infectious diseases is indebted to the current advancement and growth of mathematical models of infectious diseases. In his first publication on mathematical modelling of epidemics published in 1766, Daniel Bernoulli formulated a mathematical model to analyze the mortality caused by smallpox in England, which accounted for approximately one in 14 deaths during that period. Through his model, Bernoulli illustrated that immunization against the virus could potentially increase the life expectancy at birth by approximately three years [34]. After Bernoulli's initial work, Lambert extended the model in 1772 by

integrating age-dependent elements and Laplace also investigated a similar concept [34]. However, this area of research did not undergo systematic development until Ross in 1911 published his benchmark paper that defined modern mathematical epidemiology [35]. In this work, Ross utilized a series of equations to approximate the discrete-time dynamics of malaria transmission through mosquito-borne pathogens, demonstrating the application of the mechanistic a priori modelling technique [36]. After Ross's research, Kermack and McKendrick authored three influential publications that established the foundation for deterministic compartmental epidemic modelling [37].

These publications focused on the mass-action principle in the disease transmission cycle, suggesting that the probability of infection for a susceptible individual is directly proportional to the number of interactions they have with infected individuals. Approximately four decades after Ross's research, MacDonald took Ross's model further to provide a detailed explanation of the malaria transmission cycle and propose effective strategies for eradicating the disease. The resulting Ross-MacDonald models are mathematical tools used to study the dynamics and control of mosquito-transmitted infections, and they owe their advancement to MacDonald's notable contributions to the field, which heavily involved the utilization of computer technology [38]. However, from the beginning of the nineteenth century to the present, the use of dynamical systems techniques in epidemiology has significantly increased. To date, various mathematical models for infectious diseases system including foodborne diseases, were developed.

Ayscue and colleagues [39] created a mathematical model within an ecological metapopulation framework to observe and analyze bacterial population dynamics both within and outside the host. The model aimed to characterize the habitats of *E. coli* O157:H7 at the pen level and incorporate the various population processes of the bacteria in water troughs, feedbunks, cow hosts, and pen flooring. The simulations demonstrated that *E. coli* O157:H7 could persist in the feedlot environment without undergoing a net increase in the cattle's digestive system. The study also revealed that contaminated pen floors and water troughs played a crucial role as sources influencing the dynamics of the *E. coli* O157:H7 population. As a result, these areas were identified as significant environmental targets for interventions aimed at effectively reducing the *E. coli* O157:H7 population [39].

Gautam et al. [40] developed a coupled model to study the spread of infection through the host population, utilizing the SIS (Susceptible-Infectious-Susceptible) model. This was combined with a metapopulation model to examine the *E. coli* O157:H7 free-living stage in the environment, taking into account the impact of ambient temperature on bacterial growth [40]. The primary objective of the model was to investigate how ambient temperature could affect the dynamics of infection transmission for pathogens. The results of the model revealed that changes

in seasonal ambient temperature could exert a notable influence on pathogen populations in the environment, particularly on surfaces within barns and in water troughs. Consequently, these variations in the pathogen population could have implications for the prevalence of infection within the host population [40].

Vanderpas et al. [41] constructed and analyzed a straightforward SEIR (Susceptible, Exposed/Latent phase, Infected/Infectious, and Recovered) compartmental model to study the dynamics of *norovirus* infection within a closed population. The model investigated a *norovirus* outbreak within long-term care facilities. By simulating variations in patient turnover, it explored how the length of hospital stays impacts the endemic level of gastroenteritis and contributes to sustaining the epidemic phase in an open population. The study identified patient turnover in hospital wards as a crucial factor influencing the endemic incidence of norovirus gastroenteritis. As a result, the model's findings highlight the importance of strengthening infection control measures in such settings [41].

Bartsch et al. [42] created an agent-based model to simulate the transmission of *norovirus* among 29 acute care hospitals and five long-term care facilities. The findings from this model highlighted that more effective control of the outbreaks was achieved when hospitals collaborated and acted cooperatively in tracking and managing the spread of the virus [42]. Lee et al. [43] created a computer simulation models to assess the potential financial benefits for hospitals of putting the following *norovirus* outbreak management measures in place: increasing hand hygiene standards, improving disinfection procedures, isolating patients, donning protective gear, enforcing regulations against staff exclusion, and closing wards etc. The findings indicate that implementing improved hand hygiene, utilizing protective apparel, and enhancing disinfection practices, either individually or in combination, are the most cost-effective interventions for controlling and containing a norovirus outbreak [43].

José et al. [44] created a hybrid mathematical model to analyze the dynamics of taeniasis-cysticercosis transmission. This model integrates deterministic equations with stochastic components to represent variations in the mean parasite burden and consider the overall distribution pattern of the parasites. It comprises a coupled system of differential equations, effectively describing the parasite's life cycle progression. The developed model allows for an evaluation of the impact of chemotherapy on all hosts involved in the life cycle of the taeniasis-cysticercosis parasite, including those unintentionally affected by the disease. Nevertheless, the outcomes of the study suggest that achieving the complete elimination of the infection in all hosts through the use of chemotherapeutic therapies alone may not be a feasible goal [44].

Mwasunda et al. [45] developed and analyzed a mathematical model aimed at investigating how taeniasis and cysticercosis spread among humans, pigs, and cattle. The model considered several

factors, such as the mortality rate of taenia eggs and the proportions of infected beef and pork that remain unconsumed. These factors were found to be crucial in devising strategies to control the diseases. The study's results suggest that reducing the number of individuals with taeniasis who defecate in open environments is essential to curbing infections. Additionally, the significance of meat inspection and proper confinement of pigs and cattle should be highlighted in disease control measures [45].

Sánchez-Torres et al. [46] have created a mathematical model that classifies the population into susceptible, infected, and immunized individuals, using the parasite's life cycle as the foundation. They conducted computer numerical experiments to assess the impact of pig vaccination, considering various vaccination schedules and combination intervention methods, which included pig vaccination and anthelmintic treatment for human taeniasis. The findings of the study revealed that achieving the complete elimination of the infection in both pigs and humans requires a protective efficacy and/or coverage rate of 100% for the interventions. However, when these values are less than 100%, different mass interventions, such as vaccinating the pig population twice in combination with chemotherapeutic treatment against human taeniasis, can lead to successful elimination of the infection in both pigs and humans [46].

Researchers developed a mathematical model to study a water-related illness, employing a Nonstandard Finite Difference Scheme (NSFDS) [47]. They investigated the properties of the discrete models and compared them with the corresponding continuous deterministic model. Furthermore, they analyzed and compared the numerical results obtained from NSFDS, Euler method, and MATLAB's ode45. From NSFDS, the results indicated that the discrete model successfully retained important characteristics of the continuous model, such as positivity and stability. These outcomes were further verified through numerical simulations, which demonstrated that the results obtained from NSFDS, Euler method, and ode45 in MATLAB were similar [47].

Berge et al. [48] created a simple mathematical model to study Ebola in Africa. They introduced the NSFD (Nonstandard Finite Difference) approach for numerical analysis and computational purposes. Through analytical proofs and numerical simulations, they demonstrated that the NSFD scheme maintained dynamic consistency with respect to essential properties of the continuous model. These properties included positivity and boundedness of solutions, as well as local and global stability of equilibria. [48].

Treibert et al. [49] constructed a mathematical model with the primary aim of showcasing the impact of varying parameter boundary settings on the estimated incidence rate. The model incorporated data from the COVID-19 survey conducted in Germany, considered an exponentially increasing vaccination rate over time, and used trigonometric functions to represent contact and quarantine rates. To analyze the model numerically, the researchers developed a nonstandard

finite difference (NSFD) scheme. The results of the numerical analysis revealed that the model ensured the positivity of solutions and accurately produced the expected asymptotic behavior [49].

Despite the fact that these studies have been helpful in describing transmission dynamics and identifying potential controls for these infections, transmission still persists because all of these models represent single-scale models constructed using the principles of transmission mechanism theory, which focuses on either immunology or epidemiology, and as a result, they do not take into account the implications of replication-transmission relativity. Additionally, the use of differential equation models of the susceptible-infected-recovered type is less common in the study of foodborne diseases compared to vector-borne and high-impact viral disease systems. This difference in application is primarily attributed to the substantial involvement of contaminated food and water in the transmission of foodborne pathogens [50]. Single-scale models are frequently used to estimate critical parameters from testing the model to clinical information and to advance the science of identifying critical drug targets that are essential to analyzing how drugs affect patients who are being treated, but they lack the rigor to simultaneously describe the entire foodborne disease system. Nevertheless, there are existing nested multiscale modelling frameworks designed for the investigation of other infectious diseases, and the most commonly used mathematical framework at both scales was Ordinary Differential Equations (ODEs). In the multiscale models already in existence, the connection between scales was commonly established by correlating the transmission rate at the between-host scale with the pathogen load at the within-host scale. The functions employed to relate within-host pathogen load to between-host transmission rate were often assumed to follow a linear pattern. Alternatively, logistic and other saturating functions were selected in some instances [51]. Alternatively, the cumulative pathogen load generated by an infected host at the within-host scale was determined by integrating the area under the pathogen load curve, This measure was then utilized as a substitute for the direct transmission rate [52]. Some of the existing coupled multiscale modelling frameworks can be classified as hybrid, as they often utilize Ordinary Differential Equations (ODEs) at the within-host scale and Partial Differential Equations (PDEs) at the between-host scale [53]. In other multiscale models that are coupled, two strains of a pathogen were integrated at the within-host scale and at the between-host scale [54, 55]. Other coupled multiscale modelling frameworks have utilized ODEs models at both the microscale and macroscale [56–58]. Mathebula separately modelled two distinct diseases, namely malaria and schistosomiasis. Several other authors also conducted studies on malaria. The malaria models included both humans and mosquitoes at the between-host scale, categorized into susceptible and infectious individuals [56, 57, 59]. Hite and Cressler examined two parasite strains [58], and Bosia developed a multiscale modelling framework for HIV that incorporated multiple strains [60].

As far as our understanding goes, there are currently no multiscale models available for studying foodborne diseases that have been documented in the literature using the replication-transmission idea outlined in [20]. In this study, we develop two nested multiscale models of foodborne illnesses wherein the microscale and macroscale are the only scales that have an impact at host-level disease dynamics and are defined by ODEs. The first nested multiscale framework is categorized as environmentally transmitted diseases of type II (where there is replication at microscale only) and the second multiscale model framework is categorized as environmentally transmitted diseases of type III (where the replication occurs at both microscale and macroscale). The third multiscale model to be developed is a coupled mutliscale model categorized as environmentally transmitted diseases of type I (where there is no replication at both the microscale and macroscale), and these frameworks are defined by type I and type II reciprocal influence [20]. This study demonstrates the applicability of the replication-transmission relativity theory in cases where the reciprocal influence between the within-host scale and the between-host scale involves both infection/super-infection (for the influence from the between-host scale to within-host scale) and pathogen excretion/shedding (for the influence from the within-host scale to between-host scale).

1.3 Problem Statement

A research gap has been created in an attempt to establish a multiscale framework in order to understand the mechanisms on how foodborne pathogens cause infections on human beings, cattle and pigs since very little has been done in modelling of foodborne disease. The framework will make it easier to fully comprehend the processes involved in the spread, growth, and evolution of diverse foodborne bacterial, viral, parasitic and antibiotic resistant agents. However, such efforts require solid knowledge of disease transmission agents' processes which are known to span a wide spectrum of temporal and spatial scales [22]. Concerning foodborne diseases, these transmission agents can originate from various sources, including the environment, food and feed processing plants, food animals, and domestic as well as wild animals. On the other hand, mathematical models have contributed significantly to the development of the knowledge of the transmission patterns underlying many infectious diseases (including Salmonela, *E. coli* O157:H7, Toxoplasma gondii, HSV, Influenza etc.). However, available literature on mathematical modelling efforts which seek to advance our understanding of key foodborne disease processes have been limited to either humans or food as transmission sources. Such an approach is limited in that it overlooks the pathogen exchange processes between the hosts (at the exposure level) and their respective agents (at the reservoir level) which may help in fully describing and understanding the dynamics that characterize a foodborne disease systems.

With regards to foodborne diseases, several mathematical studies have been carried out and most of them have considered the food supply chain in which food is tracked from its source until it reaches to the point of consumption. Nevertheless, numerous studies have not adequately considered the collective contribution of humans, animals, plants, and the environment in sustaining the life cycle of foodborne diseases. For instance, humans may excrete pathogenic agents into the environment which will in turn get acquired by animals and plants. Therefore, the researcher proposes to fill this gap by developing a multiscale modelling framework that will link between-host submodels and within-host submodels at host level that describe the disease transmission dynamics at different stages of pathogenic life cycle (human to food to human). The multiscale models of foodborne diseases developed in this study will assist in directing policy initiatives aimed at data collection and establishing efficacy levels of various interventions directed towards reducing the burden of food borne diseases.

1.4 Rationale of the Study

There has been very little modelling of foodborne diseases done in the previous studies, and there are currently no multiscale models of these illnesses. This study introduces a multiscale framework for understanding the mechanisms through which foodborne pathogens infect humans, aiming to gain insights into the complexities of these illnesses. The multiscale models give a complete understanding of the complex life cycles of foodborne pathogens.

1.5 Aim and Objectives

1.5.1 Aim of the Study

The primary objective of this study is to create multiscale models of foodborne diseases that demonstrate the relationship between the microscale and macroscale, using the principles of replication-relativity theory.

1.5.2 Objectives of the Study

The objectives of the study are to:

a. construct a nested multiscale model focused on pathogens with a replication cycle at the microscale only, specifically to investigate the impact of within-human scale pathogen replication on the between-host scale using *norovirus* as a paradigm.

b. develop a nested multiscale model for pathogens with replication cycles occurring at both within-cattle scale and between-host scale, specifically to investigate the potential relationship between the environmental pathogen growth rate and the microscale pathogen replication rate at the site of infection, using *E. coli* O157:H7 as a paradigm.

c. to create a coupled multiscale model for pathogens, where there is no replication cycle at both the within-human scale and the within-animal scale. The primary objective of this model is to investigate the influence of the within-human scale and within-animal scale on the between-host scale, as well as the influence of the between-host scale on the within-human scale and within-animal scale using *Taenia solium* as an example.

1.6 Methodology

In this research, we construct nested multiscale models and coupled multiscale model for foodborne diseases using ordinary differential equations to describe the dynamics of type I, type II, and type III of environmentally transmitted disease systems. The multiscale models are formulated at the host level, comprising two distinct scales: the within-host scale and the between-host scale, using *Norovirus*, *E. coli* O157:H7, and *T. solium* as examples. At the within-host scale, the models demonstrate the pathogen replication-transmission relativity theory, while at the between-host scale, it demonstrates the transmission mechanism theory, these scales are linked together to form a multliscale circle. Initially, we construct a single-scale model that characterizes the transmission dynamics of viral foodborne diseases at the between-host scale. Subsequently, we proceed to develop microscale submodels and macroscale submodels, linking them for both to form multiscale models.

In our mathematical analysis, we use numerous techniques to analyze all the models in this study, which are as follows: Next generation operator to evaluate the disease threshold, Routh-Hurwitz criteria to determine the stability of the disease-free equilibrium (DFE), fixed point theory to allow us to guarantee the existence of a solution to the original problem, Center Manifold theory to determine the stability of disease at an endemic equilibrium state, and Lyapunov function to prove global stability. We conduct sensitivity analysis to test the parameters which are sensitive to the models the Latin Hypercube Sampling (LHS) and Partial Rank Correlation Coefficients (PRCCs). The first three models are simulated by constructing non-standard finite difference

schemes (NSFDS). The adoption of these schemes is justified by the possibility that standard schemes could produce erroneous and unstable numerical results that are highly dependent on time step-size [47]. Although a non-standard finite difference method is employed to avoid numerical instability, it might be excessively time-consuming and expensive to compute [61]. Based on this fact and considering that the coupled multiscale is highly nonlinear and too complex, the numerical simulations for the third multiscale model are obtained through using ODE solvers in Python, that is ODE int function in the sci.integrate which solves systems of differential equations. These solvers are ode45 (Runge-Kutta Dormand-Prince method of order (4,5)) with default tolerance) [62].

1.7 Outline of the thesis

The structure of this thesis is outlined as follows:

In **Chapter 2**, we formulate a single-scale model for foodborne diseases caused by viruses in general at the host level. Subsequently, in the following chapter, this model is adapted to develop a nested multiscale model. This single-scale model is developed in an effort to evaluate or assess the efficacy of single-scale models in predicting the dynamics of foodborne infections.

In **Chapter 3**, we construct and analyze a nested multiscale model for pathogens that do not have a replication cycle at the microscale. The main objective is to assess the impact of within-human scale pathogen replication on the between-host scale, with *norovirus* serving as a paradigm in the analysis.

In **Chapter 4**, we develop and analyze a nested multiscale model for pathogens, where the replication cycle occurs at both the within-cattle scale and the between-host scale. The primary aim is to assess the influence of environmental pathogen growth rate on within-cattle scale pathogen replication rate and the influence of within-cattle scale pathogen replication rate on environmental pathogen growth rate using *E. coli* O157:H7 a paradigm.

In **Chapter 5**, we construct and analyze a coupled multiscale model for pathogens, where there is no pathogen replication cycle at both the within-human scale and within-animal scale. The main objective is to examine the influence of the within-human scale and within-animal scale on the between-host scale, as well as the impact of the between-host scale on the within-human scale and within-animal scale. To illustrate these dynamics, we use *Taenia solium* as an example in our investigation.

In **Chapter 6**, provides conclusions and some recommendations for future research directions.

Chapter 2

Single-scale Model for Viral Foodborne Diseases Dynamics at Host-level

2.1 Introduction

A mathematical model that describes or characterizes an infection illness problem exclusively at one scale is referred to as a single-scale model from the perspective of infectious disease systems at any level of organization. Single-scale models have been and will remain instrumental in guiding the management and eradication efforts of various infectious diseases, both on a local and global scale. The application of single-scale models, which are considered to fall within the category transmission mechanism theory of disease dynamics, has improved our understanding of infectious disease transmission dynamics [20]. The assumption used in transmission mechanism theory for foodborne viral infections is that each host would contract the virus at the same rate and experience the same sickness time course. These models of transmission play an important role in guiding public health interventions involving infectious diseases, particularly in the context of new pathogens [63]. The single scale model used in models of the dynamics of infectious diseases, however, does not take into consideration pathogen replication, which is a weakness of this theory. This limitation prevents models based on the transmission mechanism theory from being used to study the dynamics of infectious diseases under the constraints imposed by pathogen replication. The basis for single-scale models in infectious diseases is the

susceptible, exposed, infected, recovered, pathogen load (SEIRP) paradigm and its various variations (SIP, SISP, SIRP, etc.). By adopting this approach, pathogen load is explicitly incorporated into models at each of the seven scales of organization within an infectious disease system [20]. Single-scale models of infectious disease dynamics, which do not account for the intricacies of pathogen replication mechanisms, merely hint at the complexity of the infectious disease system under study without providing specific details about that complexity. Few virus types, such as *norovirus*, *hepatitis A* and E, and *rotavirus*, are responsible for the majority of viral foodborne illnesses [64, 65]. The intestines of humans and animals are where all foodborne viruses originate, because viruses are frequently shed in bodily secretions, such as feces. As viruses cannot replicate in food, foodborne viral transmission occurs due to various factors, such as contaminated food handled by infected individuals with poor hygiene practices. Additionally, transmission can result from consuming animal products that are contaminated with viruses or coming into contact with sewage or sewage-polluted water, for instance, through the consumption of contaminated meat, fish, etc. [64, 66]. To date, only a limited number of mathematical models for foodborne viral diseases have been proposed or analyzed. Most of the transmission mathematical models of foodborne diseases caused by viruses are SIR type. In this chapter we develop a single scale modelling framework for foodborne diseases caused by viruses at host level. The model is used to develop a nested multiscale model for *norovirus* based on the replication-transmissiom relativity theory in the next chapter. The construction of this single scale model is being done to examine or test the efficacy of single-scale models in forecasting the dynamics of foodborne diseases using viral infection in general.

2.2 Mathematical Model for Viral Transmission Dynamics at Host-level

In this subsection, we adapt a single-scale modelling framework for environmentally-transmitted disease systems at the host level in [67] in a way to develop the single-scale model for viral infection. The specific details of pathogen-immune system interactions, which determine the replication and persistence of the pathogen at the within-human scale, are not explicitly modeled in this study. Instead, just one parameter can phenomenologically describe how a pathogen replicates. Our objective is to demonstrate that the limitations arising from pathogen replication render it impractical to study the dynamics of infectious diseases using a single model. The model is constructed by monitoring the dynamics of two susceptible human populations S_F,

infected humans I_F so that the total human population is given by

$$N_F = S_F + I_F,$$

and environmental pathogen population V_F. In developing a single-scale model at the host level for foodborne pathogens, we make the following assumptions:

1. Infection occurs through the ingestion of food containing viral load V_F from contaminated food. However, if there is any indirect transmission, it can be calculated using the environmental viral load V_F.
2. The average extracellular foodborne virus present in each infected individual is phenomenologically modeled as N_f, serving as a proxy for individual infectiousness.
3. The environmental virus V_F does not undergo replication in the environment, i.e., outside the human host.

Taking these assumptions into account, the dynamics of foodborne virus transmission at the human organism scale are as follows:

$$\begin{cases} 1. \ \dfrac{dS_F(t)}{dt} &= \Lambda_F - \dfrac{\beta_F V_F(t) S_F(t)}{P_0 + V_F(t)} - \mu_F S_F(t), \\ 2. \ \dfrac{dI_F(t)}{dt} &= \dfrac{\beta_F V_F(t) S_F(t)}{P_0 + V_F(t)} - [\mu_F + \delta_F] I_F(t), \\ 3. \ \dfrac{dV_F(t)}{dt} &= N_f \alpha_f I_F(t) - \mu_V V_F(t). \end{cases} \tag{2.2.0.1}$$

Equation (1) in the model system (2.2.0.1) describes the dynamics of susceptible humans. New recruits of human population enter this class at a rate, Λ_F at any time, t through birth, this population is reduced through viral infection at a rate $\dfrac{\beta_F V_F(t) S_F(t)}{P_0 + V_F(t)}$ with β_F being the exposure rate to the infective environmental viral load V_F and P_0 is the saturation parameter of the virus that grant 50% probability that an individual will become infected after ingesting the virus. Infection takes place when humans consume contaminated food from the environment. The susceptible population decreases due to natural death at a rate, μ_F. Equation (2) in the model system (2.2.0.1) represents the population of infected humans. This population increases as susceptible individuals get infected and decreases due to natural death at a rate, μ_F. Additionally, this population decreases due to disease-induced death at a rate, δ_F, resulting in an average lifespan of

viral-infected humans in the population of $\frac{1}{(\mu_F + \delta_F)}$. We make the assumption that infected humans spread the disease through shedding into the environment at a rate of $N_f \alpha_f I_F(t)$, where N_f represents the phenomenological modelling of the average number of within-host scale viral load available for excretion into the environment by each infected human, occurring at a rate of α_f. Thus, the population dynamics of viral load in the environment, as described by Equation (3) in the model system (2.2.0.1), increases after viral excretion by the infected human host into the environment through fecal material at a rate, $N_f \alpha_f I_F(t)$. The population of viral load in the environment is assumed to decrease due to natural death at a rate, μ_V. Below is the conceptual diagram of the single-scale model system (2.2.0.1).

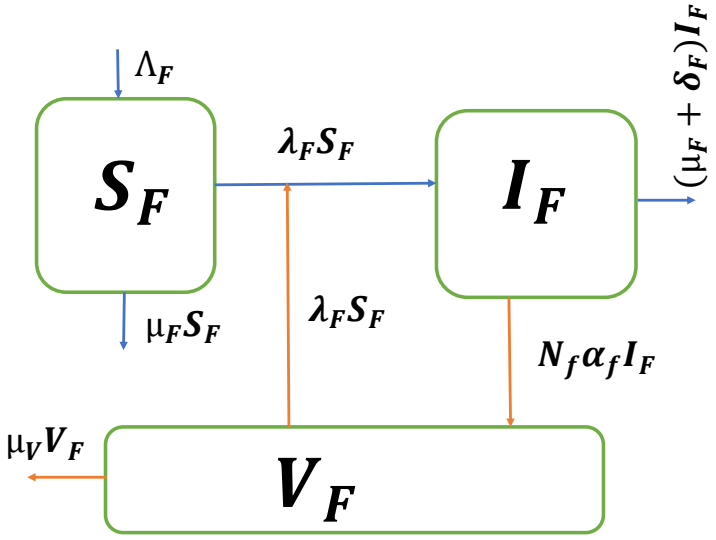

Figure 2.1: Transmission cycle of the foodborne disease in human beings.

2.3 Mathematical analysis

In this sub-section, we analyze the mathematical properties of the model system (2.2.0.1). Firstly, we demonstrate that all solutions of the model system (2.2.0.1) remain positive for all $t > 0$. Next, we establish that the model system (2.2.0.1) is both mathematically and epidemiologically well-posed.

2.3.1 Positivity of Solutions

As the model system presented in (2.2.0.1) describes human and foodborne viral populations, all parameters in the model are non-negative. Furthermore, it can be shown that the solutions of the model (2.2.0.1) are also non-negative, given the initial values $\Big(S_F(0), I_F(0), V_F(0)\Big)$, the solution $\Big(S_F(t), I_F(t), V_F(t)\Big)$ of the model system (2.2.0.1) remain positive for all $t > 0$, so should be in consistence with the basic aspect of the biological reality. We state the following theorem to summarize this:

Theorem 2.1. *Since the initial conditions of the system of equations (2.2.0.1) are non-negative, this implies that* $\Big(S_F(0) > 0, I_F(0) > 0, V_F(0) > 0\Big)$*, resulting solutions* $\Big(S_F(t), I_F(t), V_F(t)\Big)$ *are all positive for all* $t > 0$.

Proof. Based on the model system (2.2.0.1), a differential inequality that illustrates the dynamics of the susceptible human population over time is expressed as:

$$\frac{dS_F(t)}{dt} \geq -(\lambda_F(t) + \mu_F)S_F(t) \tag{2.3.1.1}$$

where

$$\lambda_F(t) = \frac{\beta_F V_F(t)}{P_0 + V_F(t)}.$$

The differential inequality (2.3.1.1) can be solved through the method of separation of variables as shown below:

$$\frac{dS_F(t)}{S_F(t)} \geq -(\lambda_F(t) + \mu_F)dt \tag{2.3.1.2}$$

letting

$$\hat{t} = \sup\{t > 0 : S_F > 0, I_F > 0, V_F > 0\} \in [0, t],$$

and integrating (2.3.1.2), we obtain

$$ln(S_F(t)) \geq -\left(\mu_F t + \int_0^t \lambda_F(\hat{t})d\hat{t}\right) + ln(S_F(0))$$

which yields

$$S_F(t) \geq S_F(0).\exp\left\{-\left(\mu_F t + \int_0^t \lambda_F(\hat{t})d\hat{t}\right)\right\} > 0. \tag{2.3.1.3}$$

This implies that

$$\lim_{t\to\infty} \inf(S_F(t)) \geq 0. \tag{2.3.1.4}$$

Similar method can be used to demonstrate that

$$\lim_{t\to\infty} \inf(I_F(t)) \geq 0. \tag{2.3.1.5}$$

Based on Equation (3) in the model system (2.2.0.1), we can deduce the following:

$$\frac{dV_F(t)}{dt} \geq -\mu_V V_F(t). \tag{2.3.1.6}$$

separation of variables gives

$$V_F(t) \geq V_F(0).\exp\{-\mu_V t\} > 0. \tag{2.3.1.7}$$

This implies that

$$\lim_{t\to\infty} \inf(V_F(t)) \geq 0. \tag{2.3.1.8}$$

Consequently, the state variables (S_F, I_F, V_F) of the model system (2.2.0.1) remain non-negative for all $t \geq 0$. □

2.3.2 Invariant Region

Let N_F represent the total human population, so that $N_F(t) = S_F(t) + I_F(t)$. Substituting the derivatives in system (2.2.0.1) we have

$$\frac{dN_F(t)}{dt} = \Lambda_F - \mu_F N_F - \delta_F I_F \tag{2.3.2.1}$$

so that

$$\frac{dN_F(t)}{dt} \leq \Lambda_F - \mu_F N_F(t). \tag{2.3.2.2}$$

This implies that

$$\lim_{t\to\infty} sup(N_F(t)) \leq \frac{\Lambda_F}{\mu_F}. \tag{2.3.2.3}$$

From (2.3.2.3), we learn that each of the individual state variable is less or equal to $\frac{\Lambda_F}{\mu_F}$ since $N_F(t)$ represent the sum of these state variables. From Equation (3) of the model system (2.2.0.1) we obtain the following:

$$\frac{dV_F(t)}{dt} \leq N_f\alpha_f\frac{\Lambda_F}{\mu_F} - \mu_V V_F, \tag{2.3.2.4}$$

since $I_F(t) \leq \frac{\Lambda_F}{\mu_F}$. Therefore the equation for (2.3.2.4) is obtainable by using an integrating factor $e^{\mu_V t}$, to get

$$V_F(t) \leq \frac{N_f\alpha_f\Lambda_F}{\mu_V\mu_F} + C_2e^{-\mu_V t}. \tag{2.3.2.5}$$

This implies that

$$\lim_{t\to\infty} sup(V_F(t)) \leq \frac{N_f\alpha_f\Lambda_F}{\mu_V\mu_F}. \tag{2.3.2.6}$$

As a result, all feasible solutions of the model system (2.2.0.1) are positive and eventually enter the invariant attracting region $\Omega = (S_F, I_F, V_F)$

$$\begin{cases} \Omega = (S_F(t), I_F(t), V_F(t))|\ 0 \leq S_F(t) + I_F(t) \leq \dfrac{\Lambda_F}{\mu_F}, \\ \qquad 0 \leq V_F(t) \leq \dfrac{N_f \alpha_f \Lambda_F}{\mu_V \mu_F}. \end{cases} \tag{2.3.2.7}$$

Thus, Ω is a positively invariant and attracting region, as all solutions that originate in Ω will stay within Ω for all $t \geq 0$. This establishes that the model system (2.2.0.1) is mathematically and epidemiologically well-posed [68]. Therefore, it is adequate to study the dynamics of the flow generated by the model system (2.2.0.1).

2.3.3 Disease-free equilibrium(DFE) and Reproductive Number

The disease-free equilibrium E_0 represents the point at which there is no virus present to cause infection. This equilibrium is obtained by setting the left-hand side of the model (2.2.0.1) to zero. and further assume that $I_F = V_F = 0$ to get $E^0 = \left(\dfrac{\Lambda_F}{\mu_F}, 0, 0\right)$. It is important for disease-free quilibrium to be analysed because the persistence or the anticipated elimination of viral infection depends fully on whether or not the disease-free is stable or not. The basic reproductive number, R_0 is calculated below.

2.3.3.1 Determination of the Basic Reproductive Number

The basic reproduction number (R_0) is the number of newly infected individuals that arise from one infected individual when almost all individuals are uninfected, when $R_0 < 1$ the infection will die out and the infection will persist in the community when $R_0 > 1$. The R_0 of the single-scale model system (2.2.0.1) will be calculated using the next generation operator as described in [69]. In this case, a subsystem comprising Equation (2) and Equation (3) from the model system (2.2.0.1) shows the progression and exchange of infectious humans and the environmental pathogen load. These equations play a crucial role in the computation of the basic reproductive number. The Jacobian matrix related to the linearized subsystem, evaluated at the disease-free equilibrium point E^0 of the model system (2.2.0.1), is expressed as follows:

$$J_{E^0} = \begin{pmatrix} -(\mu_F + \delta_F) & \dfrac{\beta_F \Lambda_F}{P_0 \mu_F} \\ N_f \alpha_f & -\mu_V \end{pmatrix}. \tag{2.3.3.1}$$

Subsequently, the Jacobian matrix J_{E^0} is divided into two distinct matrices, denoted as F_I and V_I, with the property that $J_{E^0} = F_I V_I$. In this partition, F represents the transmission matrix, which is non-negative and characterizes the generation of secondary infections. On the other hand, V_I stands for the transition matrix, which is non-singular and describes the changes in individual states, including removal due to death and clearance of environmental pathogens. Now, if we incorporate the pathogen shedding ($N_f \alpha_f I_F$) into the environment, it is included in the V_I matrix rather than the F_I matrix. Consequently, the matrices F_I and V_I are modified as follows:

$$F_I = \begin{pmatrix} 0 & \dfrac{\beta_F \Lambda_F}{P_0 \mu_F} \\ 0 & 0 \end{pmatrix}, \quad V_I = \begin{bmatrix} \mu_F + \delta_F & 0 \\ -N_f \alpha_f & \mu_V \end{bmatrix}. \tag{2.3.3.2}$$

and

$$V_I^{-1} = \begin{bmatrix} \dfrac{1}{(\mu_F + \delta_F)} & 0 \\ \dfrac{N_f \alpha_f}{\mu_V (\mu_F + \delta_F)} & \dfrac{1}{\mu_V} \end{bmatrix}, \tag{2.3.3.3}$$

The next generation matrix, $M_I = F_I V_I^{-1}$ is given by

$$F_I V_I^{-1} = \begin{bmatrix} \dfrac{N_f \alpha_f \beta_F \Lambda_F}{P_0 \mu_F \mu_V (\mu_F + \delta_F)} & \dfrac{\beta_F \Lambda_F}{P_0 \mu_F \mu_V} \\ 0 & 0 \end{bmatrix}. \tag{2.3.3.4}$$

The basic reproductive number is determined by calculating the spectral radius, which refers to the dominant eigenvalue of the matrix $F_I V_I^{-1}$. that is $R_0 = \rho(F_I V_I^{-1})$. Therefore, the basic reproductive number is given by:

$$R_0 = \rho(F_I V_I^{-1}) = \frac{N_f \alpha_f \beta_F \Lambda_F}{P_0 \mu_F \mu_V (\mu_F + \delta_F).} \tag{2.3.3.5}$$

We can rewrite the fundamental reproductive number as

$$R_0 = R_{EH}R_{HE}. \tag{2.3.3.6}$$

In this context, the variable R_{EH} represents the effective viral infectious dose of viral cells introduced into a disease-free population of humans at an equilibrium state. The estimated number of individuals likely to be infected by these viral cells can be approximated as follows:

$$R_{EH} = \frac{\beta_F \Lambda_F}{P_0 \mu_F}. \tag{2.3.3.7}$$

The estimated quantity of viral cells generated by an infected individual and subsequently contaminating the environment is approximately given by:

$$R_{HE} = \frac{N_f \alpha_f}{\mu_V(\mu_F + \delta_F)}. \tag{2.3.3.8}$$

The above quantity represents the scenario where a single newly infected individual enters a contamination-free environment at an equilibrium point. Drawing from the expressions of R_{EH} and R_{HE}, it is evident that both the between-host (macroscale) transmission parameters and the within-host (microscale) parameters play significant roles in the transmission of viral infections. These parameters collectively influence the spread of the infection both at the individual level within a host and at the population level among hosts.

2.3.3.2 Local stability of the disease-free equilibrium

In this subsubsection, we examine the local stability of the disease-free equilibrium in the model system (2.2.0.1), following the approach outlined in [70]. The stability of the disease-free equilibrium is determined by analyzing the matrix $F - V$, and its stability properties are assessed based on the following expression:

$$F = \begin{bmatrix} 0 & \frac{\beta_F \Lambda_F}{P_0 \mu_F} \\ 0 & 0 \end{bmatrix} \tag{2.3.3.9}$$

and

$$V = \begin{bmatrix} \mu_F + \delta_F & 0 \\ \\ -N_f\alpha_f & \mu_V \end{bmatrix}. \tag{2.3.3.10}$$

Then,

$$F - V = \begin{bmatrix} -(\mu_F + \delta_F) & \dfrac{\beta_F\Lambda_F}{P_0\mu_F} \\ \\ \hat{N}_f\alpha_f & -\mu_V \end{bmatrix}. \tag{2.3.3.11}$$

The eigenvalues of $F - V$ are determined by solving the equation

$$|(F - V) - \lambda| = \begin{bmatrix} -(\mu_F + \delta_F) - \lambda & \dfrac{\beta_F\Lambda_F}{P_0\mu_F} \\ \\ \hat{N}_f\alpha_f & -\mu_V - \lambda \end{bmatrix}, \tag{2.3.3.12}$$

which gives the characteristic equation in the form:

$$P(\lambda) = \lambda^2 + a_1\lambda + a_0 = 0, \tag{2.3.3.13}$$

where

$$\begin{cases} a_1 &= (\mu_F + \delta_F) + \mu_V, \\ \\ a_0 &= \mu_V(\mu_F + \delta_F)[1 - R_0], \end{cases} \tag{2.3.3.14}$$

Now, to determine the eigenvalues of the polynomial (2.3.3.13) we use the Routh-Hurwitz Criteria in [71]. In this case, we define the following matrices whose elements are the coefficients a_0 and a_1 of the characteristic polynomial $P(\lambda)$ in Equation (2.3.3.13):

$$H_1 = \begin{pmatrix} a_1 \end{pmatrix}, \quad H_2 = \begin{pmatrix} a_1 & 1 \\ 0 & a_0 \end{pmatrix}. \tag{2.3.3.15}$$

Evaluating the determinant of H_1, we obtain

$$\begin{cases} det(H_1) &= \left| a_1 \right|, \\ &= a_1, \\ &= (\mu_F + \delta_F) + \mu_V > 0. \end{cases} \tag{2.3.3.16}$$

The determinant of H_2 is given by:

$$\begin{cases} det(H_2) &= \begin{vmatrix} a_1 & 1 \\ 0 & a_0 \end{vmatrix}, \\ &= a_1 a_0, \\ &= (\mu_F + \delta_F) + \mu_V[\mu_V(\mu_F + \delta_F)(1 - R_0)] > 0, \quad \text{whenever} \quad R_0 < 1. \end{cases} \tag{2.3.3.17}$$

It can be noted that all the coefficients a_0 and a_1 of the polynomial in Equation (2.3.3.13) are greater than zero whenever $R_0 < 1$. And also all the determinants of matrices H_1 and H_2 are positive if and only if $R_0 < 1$. Consequently, all the roots of the polynomial have either negative real parts or are negative. In accordance with the findings presented in [23], we can summarize the results through the following theorem:

Theorem 2.2. *[23] The disease-free equilibrium point of the model system (2.2.0.1) demonstrates local asymptotic stability if the value of the basic reproductive number, denoted by R_0, is less than 1.*

2.3.3.3 Global stability of the disease-free equilibrium

To establish the global stability of the Disease-Free Equilibrium (DFE) in the single-scale model system (2.2.0.1), we employ a next-generation operator, as detailed in [69]. By doing so, the system (2.2.0.1) can be reformulated in the following way:

$$\begin{cases} \dfrac{dX}{dt} &= F(X, Z), \\ \dfrac{dZ}{dt} &= G(X, Z), \end{cases} \tag{2.3.3.18}$$

where

- $X = S_F$ corresponds to a compartment representing uninfected humans and
- $Z = (I_F, V_F)$ refers to compartments representing infected humans and infective viruses present in the physical environment.

We let

$$E_0 = (X^*, 0) = \left(\frac{\Lambda_F}{\mu_F}, 0, 0\right), \tag{2.3.3.19}$$

denote the disease-free equilibrium (DFE) of the model system (2.2.0.1) as X^*. For global asymptotic stability of X^* to be established, it is imperative that we satisfy the prescribed conditions denoted as (H1) and (H2).

H1. $\frac{dX}{dt} = F(X, 0)$ is globally asymptotically stable (g.a.s),

H2. $G(X, Z) = AZ - \hat{G}(X, Z)$, $\hat{G}((X, Z) \geq 0$ for $(X, Z) \in \mathbb{R}^3_+$ where $A = D_Z G(X^*, 0)$ is an M-matrix and $\mathbb{R}^3_+$ which refers to the region in which the model is biologically meaningful.

In this case

$$F(X, 0) = \left[\ \Lambda_F - \mu_F S_F\ \right], \tag{2.3.3.20}$$

and the matrix A is given by

$$A = \begin{bmatrix} -(\mu_F + \delta_F) & \dfrac{\beta_F \Lambda_F}{\mu_F P_0} \\ \\ \widehat{N}_f \alpha_f & -\mu_F \end{bmatrix}, \tag{2.3.3.21}$$

and

$$\hat{G}(X, Z) = \begin{bmatrix} \left(\dfrac{\Lambda_F}{\mu_F P_0} - \dfrac{S_F}{P_0 + V_F}\right) \beta_F V_F \\ \\ 0 \end{bmatrix}. \tag{2.3.3.22}$$

Since $S_F^0 = \Lambda_F/(\mu_F P_0) \geq S_F/(P_0 + V_F)$, it is clear that $\hat{G}(X, Z) \geq 0$ for all $(X, Z) \in \mathbb{R}^3_+$. Furthermore, it is evident that A qualifies as an M-matrix, given that its off-diagonal elements are non-negative. Based on the outcomes derived from applying the theorem used in [72], we can now present a theorem that summarizes the above results.

Theorem 2.3. *[72] The fixed point*

$$E_0 = (X^*, 0) = \left(\frac{\Lambda_F}{\mu_F}, 0, 0\right)$$

of the single-scale model system (2.2.0.1) exhibits global asymptotic stability (GAS) when the value of the basic reproductive number, R_0, is less than or equal to 1, and both assumptions $(H1)$ and $(H2)$ are met.

2.4 The Endemic Equilibrium and its Stability

In this subsection, we will obtain the expressions for the endemic equilibrium, the endemic equilibrium is a state where the infection persists. The endemic equilibrium is determined by setting the system's equations to zero and then solving the resulting equations simultaneously for the state variables.

$$\begin{cases} \Lambda_F - \dfrac{\beta_F V_F(t) S_F(t)}{P_0 + V_F(t)} - \mu_F S_F(t) &= 0, \\ \dfrac{\beta_F V_F(t) S_F(t)}{P_0 + V_F(t)} - [\mu_F + \delta_F] I_F(t) &= 0, \\ N_f \alpha_f I_F(t) - \mu_V V_F(t) &= 0. \end{cases} \tag{2.4.0.1}$$

we obtain the following expressions upon solving for Equation (2.4.0.1)

$$\begin{cases} S_F^* &= \dfrac{\Lambda_F[\beta_F + \mu_F R_0]}{(\beta_F + \mu_F)\mu_F R_0}, \\ I_F^* &= \dfrac{\beta_F \Lambda_F (R_0 - 1)}{(\beta_F + \mu_F)(\mu_F + \delta_F) R_0}, \\ V_F^* &= \dfrac{\mu_F P_0}{\beta_F + \mu_F}(R_0 - 1). \end{cases} \tag{2.4.0.2}$$

We recall that the value of R_0 is defined by Equation (2.3.3.5). Consequently, based on the system (2.4.0.2), we can deduce that the endemic equilibrium exists only when $R_0 > 1$.

2.4.1 Local Stability of the Endemic Equilibrium

In this subsection, we apply the Center Manifold Theory, as described in [73], to analyze the local stability of the endemic equilibrium state in the model system (2.2.0.1). The Center Manifold Theory is employed to assess the stability of a non-hyperbolic equilibrium point. The theorem is stated as follows:

Theorem 2.4. *[73] Let us consider the following general system of ordinary differential equations with a parameter denoted as ϕ:*

$$\frac{dx}{dt} f(x,\phi), \quad f : \mathbb{R}^n \longrightarrow \mathbb{R}, \quad f : \mathbb{C}^2(\mathbb{R}^2 \times \mathbb{R}), \tag{2.4.1.1}$$

where 0 is an equilibrium point of the system (2.2.0.1), (i.e., $f(0,\phi) = 0$, for all ϕ, and assume that

(1) $A = D_x f(0,0) = \left(\frac{\partial f_i(0,0)}{\partial x_i}\right)$ is a linearization of the system around the equilibrium 0 with ϕ evaluated at 0;

(2) Zero is a simple eigenvalue of A and other eigenvalues of A have negative real part;

*(3) Matrix A has a left eigenvector denoted by **u** and a right eigenvector denoted by **v**, corresponding to the zero eigenvalue.*

Let f_k be the k^{th} component of f and

$$a = \sum_{k,i,j=1}^{n} v_k u_i u_j \frac{\partial^2 f_k}{\partial x_i \partial x_j}(0,0), \tag{2.4.1.2}$$

$$b = \sum_{k,i,j=1}^{n} v_k u_i \frac{\partial^2 f_k}{\partial x_i \partial \phi}(0,0). \tag{2.4.1.3}$$

The local dynamics of the system around the equilibrium point 0 is totally governed by the signs of a and b.

(i) $a > 0$, $b > 0$, when $\phi < 0$ with $\mid \phi \mid \ll 1$, 0 is locally asymptotically stable, and there exists a positive unstable equilibrium; when $0 < \phi \ll 1$, 0 is unstable and there exists a negative and locally asymptotically stable equilibrium.

(ii) $a < 0$, $b < 0$, when $\phi < 0$ with $\mid \phi \mid \ll 1$, 0 is unstable; when $0 < \phi \ll 1$, 0 is locally asymptotically stable, and there exists a positive unstable equilibrium point.

(iii) *$a > 0$, $b < 0$, when $\phi < 0$ with $\mid \phi \mid \ll 1$, 0 is unstable and there exists a locally asymptotically stable negative equilibrium; when $0 < \phi \ll 1$, 0 is stable and a positive unstable equilibrium appear.*

(iv) *$a < 0$, $b > 0$, when ϕ changes from negative to positive, 0 changes its stability from stable to unstable. Correspondingly a negative unstable equilibrium becomes positive and locally asymptotically stable.*

To apply the above theorem for our model system, we introduce the following simplification and change of variables. We rewrite the model (2.2.0.1) using the state variables of the food-borne disease model and the center manifold approach on the system. We let $x_1 = S_F(t), x_2 = I_F(t), x_3 = V_F$ and $\beta^* = \beta_F$.

Using vector notation, we denote $\mathbf{x} = (x_1, x_2, x_3)^T$ the model (2.2.0.1) can be written in the form $\mathbf{F} = (f_1, f_2, f_3)^T$. By writing the model (2.2.0.1) in vector form as:

$$\begin{cases} \dot{x_1} = f_1 = \Lambda_F - \dfrac{\beta^* x_1 x_3}{P_0 + x_3} - \mu_F x_1, \\ \dot{x_2} = f_2 = \dfrac{\beta^* x_1 x_3}{P_0 + x_3} - (\mu_F + \delta_F) x_2, \\ \dot{x_3} = f_3 = N_f \alpha_f x_2 - \mu_V x_3. \end{cases} \tag{2.4.1.4}$$

We let $R_0 = 1$ and solving β^* as a birfurcation parameter, we obtain

$$\beta^* = \frac{P_0 \mu_F \mu_V (\mu_F + \delta_F)}{\hat{N}_f \alpha_f \Lambda_F}. \tag{2.4.1.5}$$

The Jacobian matrix at DFE is given by

$$J(E_0, \beta^*) = \begin{bmatrix} -\mu_F & 0 & -\dfrac{\beta^* \Lambda_F}{P_0 \mu_F} \\ 0 & -(\mu_F + \delta_F) & \dfrac{\beta^* \Lambda_F}{P_0 \mu_F} \\ 0 & \hat{N}_f \alpha_f & -\mu_V \end{bmatrix}. \tag{2.4.1.6}$$

The characteristic equation associated with the Jacobian matrix is given by

$$a_2\lambda^2 + a_1\lambda + a_0 = 0 \tag{2.4.1.7}$$

where

$$\begin{cases} a_2 = 1, \\ a_1 = \mu_V + (\mu_F + \delta_F), \\ a_0 = \mu_V(\mu_F + \delta_F)[1 - R_0]. \end{cases} \tag{2.4.1.8}$$

We notice that $a_2 > 0, a_1 > 0$ and $a_0 > 0$ when $R_0 < 1$, $a_0 < 0$ when $R_0 > 1$ and $a_0 = 0$ when $R_0 = 1$. When $R_0 = 1$ we can clearly observe that Jacobian of the linearized system has a single zero eigenvalue and all other eigenvalues are negative or have negative real parts. Therefore, the center manifold theory is one appropriate tool to use in analysing the dynamics of the model (2.2.0.1). When $R_0 = 1$, it is clear that the Jacobian matrix has a right eigenvector that is associated to the zero eigenvalue given by

$$\omega = (\omega_1, \omega_2, \omega_3)$$

we obtain

$$\begin{cases} \omega_1 = -\dfrac{\beta^*\Lambda_F}{P_0\mu_F}, \\ \omega_2 = \dfrac{\beta^*\Lambda_F}{P_0\mu_F(\mu_F + \delta_F)}, \\ \omega_3 = 1. \end{cases} \tag{2.4.1.9}$$

Similarly, we denote the left eigenvector associated to the zero eigenvalue as follows:

$$\mathbf{v} = (v_1, v_2, v_3)^T$$

we obtain

$$\begin{cases} v_1 = 0, \\ v_2 = \dfrac{\hat{N}_f \alpha_f}{\mu_F + \delta_F}, \\ v_3 = 1. \end{cases} \tag{2.4.1.10}$$

We shall demonstrate the conditions on parameter values of a bifurcation to occur in the system, based on the use of center manifold theory. We compute the bifurcation coefficients a and b, for the transformed system model (2.4.1.4), and are defined as follows:

$$\begin{aligned} a &= \sum_{k,i,j=1}^{3} v_k \omega_i \omega_j \frac{\partial^2 f_k(E_0, \beta^*)}{\partial x_i \partial x_j}, \\ b &= \sum_{k,i=1}^{3} v_k \omega_i \frac{\partial^2 f_k(E_0, \beta^*)}{\partial x_i \partial \beta^*}. \end{aligned} \tag{2.4.1.11}$$

Substituting,

$$\begin{cases} a &= \displaystyle\sum_{k,i,j=1}^{3} v_1 \omega_1 \omega_3 \frac{\partial^2 f_k(E_0, \beta^*)}{\partial x_1 \partial x_3} + \sum_{k,i,j=1}^{3} v_2 \omega_1 \omega_3 \frac{\partial^2 f_2(E_0, \beta^*)}{\partial x_1 \partial x_3}, \\ &= -\dfrac{\hat{N}_f \alpha_f \beta^{*2} \Lambda_F}{(\mu_F + \delta_F) P_0^{*2} \mu_F^{*2}} < 0, \end{cases} \tag{2.4.1.12}$$

and similarly,

$$\begin{cases} b &= \displaystyle\sum_{k,i=1}^{3} v_1 \omega_3 \frac{\partial^2 f_1(E_0, \beta^*)}{\partial x_i \partial \beta^*} + \sum_{k,i=1}^{3} v_2 \omega_i \frac{\partial^2 f_2(E_0, \beta^*)}{\partial x_3 \partial \beta^*}, \\ &= \dfrac{\hat{N}_f \alpha_f \Lambda_F}{(\mu_F + \delta_F) \mu_F P_0} > 0. \end{cases} \tag{2.4.1.13}$$

We observe that the bifurcation coefficients $a < 0$ and $b > 0$, then it follows that the model will undergo trans-critical bifurcation at $R_0 = 1$. We can conclude that the model is local asymptotically stable when $R_0 > 1$ but close to 1.

2.4.2 Global Stability of the Endemic Equilibrium

To prove the global asymptotic stability of the endemic equilibrium point E^* of the model system (2.2.0.1) we construct a global Lyapunov function following the work done in [74] to prove global asymptotic stabilty.

Theorem 2.5. *[72] The endemic equilibrium E^* of the model system (2.2.0.1) is globally asymptotically stable when $R_0 > 1$.*

In our case, we perform the global stability analysis of endemic equilibrium state by using the definition of Volterra-type Lyapunov function given by:

$$\begin{aligned} L_1 &= L(S_F, I_F, V_F) \\ &= S_H^* g\left(\frac{S_F}{S_F^*}\right) + I_H^* g\left(\frac{I_F}{I_F^*}\right) + aV_F^* g\left(\frac{V_F}{V_F^*}\right) \end{aligned} \tag{2.4.2.1}$$

where a is positive constant to be determined, and we take advantage of the properties of the function

$g(x) = x - 1 - lnx$, which is positive in $(0, \infty)$ except at $x = 1$, where it vanishes. We note that L_1 is non-negative in the interior of Ω and attain zero at E^*. Differentiating L_1 along the trajectories of the system of equations (2.2.0.1), we obtain

$$\begin{aligned} \frac{dL_1}{dt} &= \frac{dS_F}{dt}\left[1 - \frac{S_F^*}{S_F}\right] + \frac{dI_F}{dt}\left[1 - \frac{I_F^*}{I_F}\right] + \\ &\quad a\frac{dV_F}{dt}\left[1 - \frac{V_F^*}{V_F}\right], \\ &= \left[1 - \frac{S_F^*}{S_F}\right]\left[\Lambda_F - \lambda_F S_F + \frac{\beta_F V_F S_F}{P_0 + V_F} - \mu_F S_F\right] + \left[1 - \frac{I_F^*}{I_F}\right]\left[\frac{\beta_F V_F S_F}{P_0 + V_F} - (\mu_F + \delta_F) I_F\right] \\ &\quad + \left[1 - \frac{V_F^*}{V_F}\right]\left[N_f \alpha_f I_F - \mu_V V_F\right]. \end{aligned} \tag{2.4.2.2}$$

Since E^* is the endemic equilibrium point the following relations hold

$$\begin{cases} \Lambda_F = \dfrac{\beta_F V_F^* S_F^*}{P_0 + V_F^*} + \mu_F S_F^*, \\ (\mu_F + \delta_F) = \dfrac{\beta_F V_F^* S_F^*}{P_0 + V_F^*}, \\ \mu_V = \dfrac{N_f \alpha_f I_F^*}{V_F^*} \end{cases} \tag{2.4.2.3}$$

using the relation in (2.4.2.2), $\dfrac{dL_1}{dt}$ becomes

$$\begin{aligned} \frac{dL_1}{dt} &= \left[1 - \frac{S_F^*}{S_F}\right][\frac{\beta_F V_F^* S_F^*}{P_0 + V_F^*} + \mu_F S_F^* - \frac{\beta_F V_F S_F}{P_0 + V_F} - \mu_F S_F] \\ &+ \left[1 - \frac{I_F^*}{I_F}\right]\left[\frac{\beta_F V_F S_F}{P_0 + V_F} - \frac{\beta_F V_F^* S_F^*}{P_0 + V_F^*}.\frac{I_F}{I_F^*}\right] \\ &+ a\left[1 - \frac{V_F^*}{V_F}\right]\left[N_f \alpha_f I_F - \frac{N_f \alpha_f I_F^* V_F}{V_F^*}\right], \end{aligned} \tag{2.4.2.4}$$

$$\begin{aligned} &= -\frac{\mu_F}{S_F}\left(S_F - S_F^*\right)^2 - \lambda^* \frac{S_F^*}{S_F} + 2\lambda^* S_F^* + I_F\left[aN_f\alpha_f - \frac{\lambda^* S_F^*}{I_F^*}\right] + \lambda_F S_F\left(\frac{S_F^*}{S_F} - \frac{I_F^*}{I_F}\right) + \\ &aN_f\alpha_f I_F^* - aN_F\alpha_f I_F.\frac{V_F^*}{V_F} - aN_f\alpha_f I_F^*\frac{V_F}{V_F^*}. \end{aligned}$$

Let $aN_f\alpha_f - \dfrac{\lambda^* S_F^*}{I_F^*} = 0.$

We get $a = \dfrac{\lambda^* S_F^*}{N_f \alpha_f I_F^*}.$

Substituting the value of a into Equation (2.4.2.1), such that

$$\begin{aligned} \frac{dL_1}{dt} &= \left[1 - \frac{S_F^*}{S_F}\right]\left[\lambda^* S_F^* + \mu_F S_F^* - \lambda_F S_F - \mu_F S_F\right] + \left[1 - \frac{I_F^*}{I_F}\right]\left[\lambda_F S_F - \lambda_F^* S_F^*.\frac{I_F}{I_F^*}\right] + \\ &\frac{\lambda_F^* S_F^*}{N_f \alpha_f I_F^*}\left[N_f \alpha_f I_F - N_f \alpha_f I_F^*.\frac{V_F}{V_F^*}\right]. \end{aligned} \tag{2.4.2.5}$$

By direct calculations from Equation (2.4.2.5), the first term at the right hand side of (2.4.2.5) is as follows

$$\begin{aligned}\left[1-\frac{S_F^*}{S_F}\right]\left[\lambda^* S_F^* + \mu_F S_F^* - \lambda_F S_F - \mu_F S_F\right] &= \left(1-\frac{S_F^*}{S_F}\right)\left[\lambda^* S_F^* - \lambda_F S_F\right] + \\ &\quad (1-\frac{S_F^*}{S_F})\Big[\mu_F S_F^* - \mu_F S_F] \\ &= -\mu_F S_F\left(1-\frac{S_F^*}{S_F}\right)^2 + \\ &\quad \lambda^* S_F^*\left(1-\frac{S_F^*}{S_F}\right)\left(1-\frac{\lambda_F S_F}{\lambda^* S_F^* S_F^*}\right), \\ &< \lambda_F^* S_F^*\left(1-\frac{S_F^*}{S_F}\right)\left(1-\frac{\lambda_F S_F}{\lambda^* S_F^*}\right);\end{aligned} \tag{2.4.2.6}$$

and the second term at the right hand side of Equation (2.4.2.5) is simplified as follows:

$$\left[1-\frac{I_F^*}{I_F}\right]\left[\lambda_F S_F - \lambda_F^* S_F^* - \frac{I_F}{I_F^*}\right] = \lambda_F^* S_F^*\left(1-\frac{I_F^*}{I_F}\right)\left[\frac{\lambda_F S_F}{\lambda_F^* S_F^*} - \frac{I_F}{I_F^*}\right]; \tag{2.4.2.7}$$

lastly, the third term at the right hand side of Equation (2.4.2.5) is given by

$$\frac{\lambda^* S_F^*}{N_f \alpha_f I_F^*}\left[1-\frac{V_F^*}{V_F}\right]\left[N_f \alpha_f I_F - N_f \alpha_f I_F^* \frac{V_F}{V_F^*}\right] = \lambda^* S_F^*\left(1-\frac{V_F^*}{V_F}\right)\left[\frac{I_F}{I_F^*} - \frac{V_F}{V_F^*}\right]. \tag{2.4.2.8}$$

Therefore,

$$\begin{aligned}\frac{dL_1}{dt} &\leq \lambda_F^* S_F^*\left(1-\frac{S_F^*}{S_F}\right)\left(1-\frac{\lambda_F S_F}{\lambda^* S_F^*}\right) + \lambda^* S_F^*\left(1-\frac{V_F^*}{V_F}\right)\left[\frac{I_F}{I_F^*} - V_F^* V_F^*\right] + \\ &\quad \lambda^* S_F^*\left(1-\frac{V_F^*}{V_F}\right)\left[\frac{I_F}{I_F^*} - V_F^* V_F^*\right], \\ &\leq \lambda_F^* S_F^*\left[2 - \frac{\lambda_F S_F I_F^*}{\lambda_F^* S_F^* I_F} + \frac{\lambda_F}{\lambda_F^*} - \frac{S_F^*}{S_F} - \frac{I_F}{I_F^*}\right] + \lambda_F^* S_F^*\left[1 - \frac{I_F}{I_F^*}.\frac{V_F^*}{V_F} + \frac{I_F}{I_F^*} - \frac{V_F}{V_F^*}\right].\end{aligned} \tag{2.4.2.9}$$

By using the function $g(x) = x - 1 - lnx$, we get

$$
\begin{aligned}
\frac{dL_1}{dt} &\leq \lambda_F^* S_F^* \left[-g\frac{S_F^*}{S_F} - g\left(\frac{\lambda_F S_F}{\lambda_F^* S_F^*}.\frac{I_F^*}{I_F}\right) - ln\left(\frac{V_F}{V_F^*}\right) - \frac{I_F}{I_F^*} + ln\left(\frac{I_F}{I_F^*}\right) + ln\left(\frac{P_0+V_F}{P_0+V_F^*}\right)\right] + \\
&\quad \lambda_F^* S_F^* \left[-g\left(\frac{I_F V_F^*}{I_F^* V_F}\right) - ln\left(\frac{I_F}{I_F^*}\right) + \frac{I_F}{I_F^*} + ln\left(\frac{V_F}{V_F^*}\right) - \frac{V_F}{V_F^*}\right], \\
&\leq \lambda_F^* S_F^* \left[-g\left(\frac{S_F^*}{S_F}\right) - g\left(\frac{\lambda_F S_F}{\lambda_F^* S_F^*}.\frac{I_F^*}{I_F}\right) + \frac{V_F}{V_F^*} - ln\left(\frac{V_F}{V_F^*}\right) - \frac{I_F}{I_F^*} + ln\left(\frac{I_F}{I_F^*}\right)\right] \\
&\quad + \lambda_F^* S_F^* \left[\frac{V_F}{V_F^*}.\frac{P_0+V_F}{P_0+V_F^*} - \frac{P_0+V_F}{P_0+V_F^*} - g\left(\frac{P_0+V_F}{P_0+V_F^*}\right) - \frac{V_F}{V_F^*} - 1\right] \qquad (2.4.2.10) \\
&\quad + \lambda_F^* S_F^* \left[-g\left(\frac{I_F V_F^*}{I_F^* V_F}\right) - ln\left(\frac{I_F}{I_F^*} + \left(\frac{I_F}{I_F^*}\right)\right) + ln\left(\frac{V_F}{V_F^*} - \frac{V_F}{V_F^*}\right)\right], \\
&\leq \lambda_F^* S_F^* \left[\frac{V_F}{V_F^*} - ln\frac{V_F}{V_F^*} - \frac{I_F}{I_F^*} + ln\frac{I_F}{I_F^*}\right] + \lambda_F^* S_F^* \left[\frac{I_F}{I_F^*} - ln\left(\frac{I_F}{I_F^*}\right) + ln\left(\frac{V_F}{V_F^*}\right) - \frac{V_F}{V_F^*}\right], \\
&\leq 0.
\end{aligned}
$$

From Equation (2.4.2.10), we have the largest invariant subset, where $\frac{dL_1}{dt} = 0$. Therefore, we conclude from LaSalle's Invariance Principle that E^* is globally asymptotically stable when $R_0 > 1$.

2.5 Sensitivity Analysis

In this section, we conduct a sensitivity analysis of the two viral transmission metrics obtained from the viral dynamics single-scale model system (2.2.0.1) with respect to the parameters of the model. This analysis aims to understand how variations in the model parameters affect the viral transmission metrics. The two viral transmission metrics obtained from the single-scale model system (2.2.0.1) are as follows: the reproduction number, denoted by R_0, which provides insight into the disease dynamics during the initial stages of infection and the endemic value of the environmental viral load, represented by V_F^*, which offers an understanding of the disease dynamics at the epidemic level. For any epidemic model that describes the dynamics of diseases within a population, conducting a sensitivity analysis is essential. Such an analysis helps to identify the model's parameters that can be targeted for disease control, elimination, or even eradication.

Additionally, it enables the monitoring and control of these parameters during an outbreak of the disease. Overall, a sensitivity analysis study plays a crucial role in understanding and managing the spread of diseases. The analysis is conducted using a combination of Latin Hypercube Sampling and partial rank correlation coefficients (PRCCs). For each run, we conduct 1000 simulations to investigate how individual model parameters impact both the basic reproduction numbers (R_0) and the endemic value of the environmental viral load (V_F^*). The sensitivity analysis outcomes for R_0 and V_F^* concerning variations in the model parameters are presented in the Tornado plots. Figure 2.2 illustrates the sensitivity of R_0, while Figure 2.3 shows the sensitivity of V_F^*. These plots provide insights into how changes in individual model parameters impact the respective viral transmission metrics.

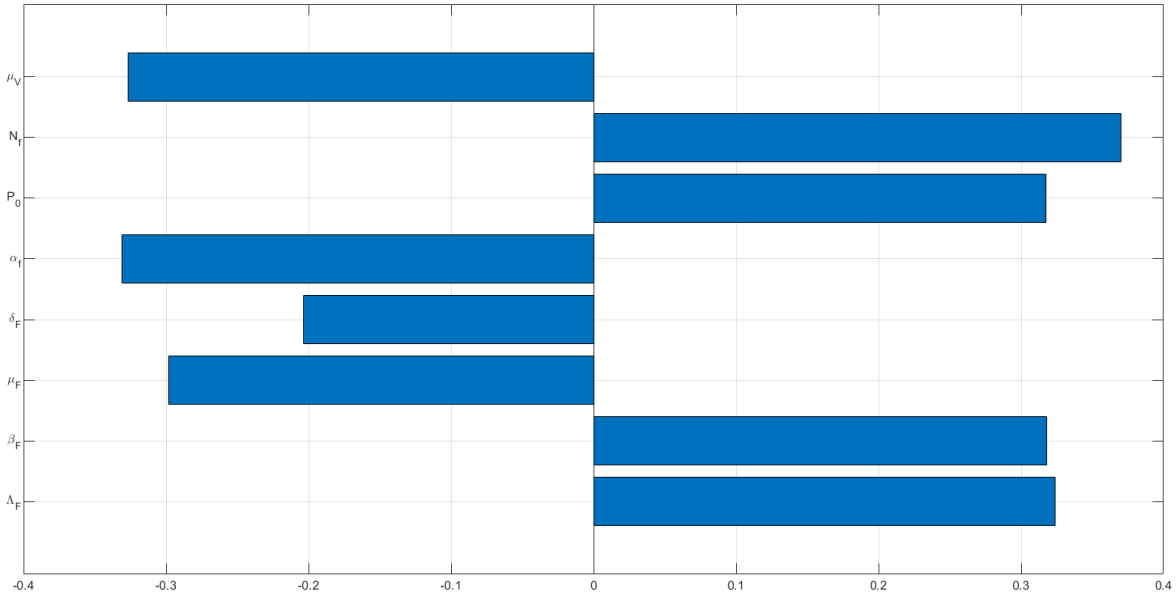

Figure 2.2: Tornado plot of partial rank correlation coefficients (PRCCs) of all the model parameters that influence the viral transmission metric R_0

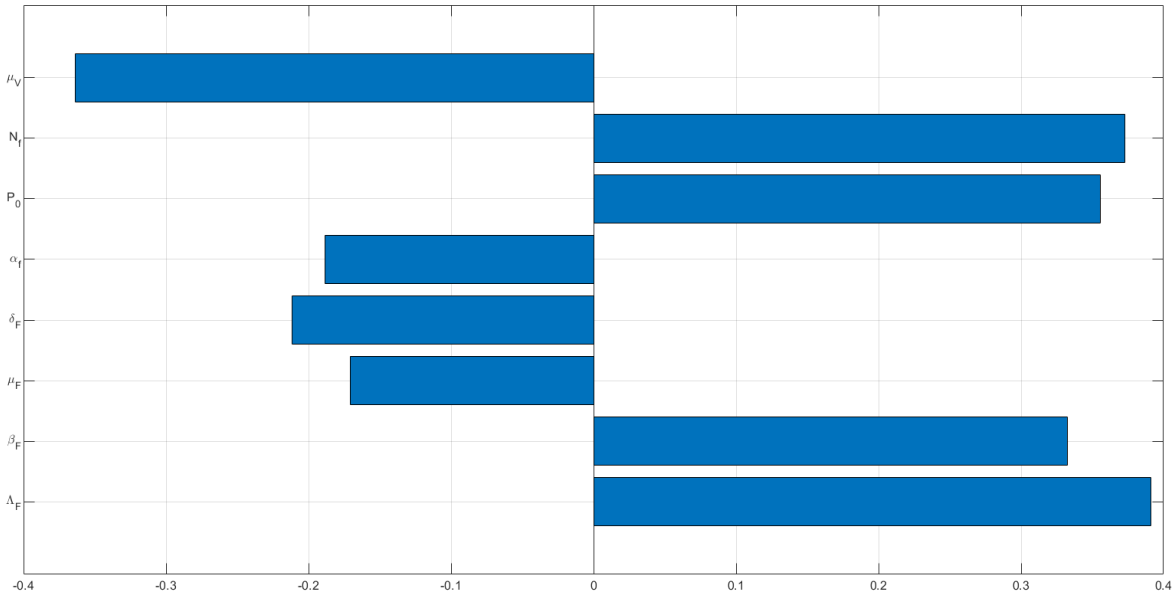

Figure 2.3: Tornado plot of partial rank correlation coefficients (PRCCs) of all the model parameters that influence the viral endemic point metric V_F^*

Drawing from the sensitivity analysis results of both R_0 and V_F^* concerning all the parameters in the single-scale model (2.2.0.1), as presented in Table 2.3, we can deduce the following conclusions:

(i.) The sensitivity analysis reveals that certain parameters in the viral single-scale model (2.2.0.1) exhibit positive partial rank correlation coefficients (PRCCs), while others have negative PRCCs. A positive PRCC suggests that increasing these parameters will lead to higher values for both R_0 and V_F^*. Conversely, parameters with negative PRCCs indicate that increasing them will result in lower values for both R_0 and V_F^*. As an example, when the viral transmission rate β_F at the between-host level is increased, both the values of R_0 and V_F^* will also increase. On the other hand, if the natural decay rate of the virus in the environment μ_V is increased, it will lead to a reduction in the values of both R_0 and V_F^*.

(ii.) The foodborne transmission metrics R_0 and V_F^* are sensitive to almost all of the disease parameters ($\mu_V, N_f, P_0, \alpha_f, \beta_F$), but they are both highly sensitive to (μ_V, N_f). Therefore, special attention should be given to the accuracy of these two parameters during data collection to enhance the validity and utility of the model system (2.2.0.1). Accurate and reliable values for the viral transmission rate β_F and the natural decay rate of the virus in

the environment μ_V are crucial for improving the accuracy and predictive capability of the model.

Since both R_0 and V_F^* are significantly sensitive to N_f, and μ_V, we note that N_f phenomenologically model the within-host dynamics of the infection which can be modified by within-host health intervention mechanisms such as drugs that kill foodborne viral cells at the individual level.

(iii.) On the other hand, R_0 is more sensitive to α_f whereas V_F^* is also more sensitive to β_F. This can imply that any intervention that can limit the shedding rate by the infected individual will have effect on the foodborne disease transmission through reducing human infection. V_F^* characterizes transmission of the disease when the disease has reach an endemic level, this can imply that foodborne diseases interventions such avoiding contaminated food and vaccination will have more effect in controlling the transmission of foodborne infection at endemic level.

2.6 Nonstandard Finite Difference Scheme

In this section, we outline the development of a non-standard finite difference scheme (NSFDs) that ensures compatibility with the positivity of the state variables present in the system. The primary aim of this scheme is to maintain the non-negativity of the state variables throughout the numerical simulation, which is essential for accurate and physically meaningful results.

The NSFD scheme, a unique class of numerical techniques, is introduced to solve single-scale viral model in order to obtain schemes that are dynamically consistent and their solutions preserve the physical properties of the approximated differential system for arbitrary time step-sizes. Such properties include conservation law, positivity, monotonicity, the stability of fixed points. In 1994, Mickens introduced NSFD scheme as an alternative to standard numerical methods for solving differential equations with qualitative properties retained [75]. This technique was used for continuous models in numerous applicable fields, including ecology and epidemiology [47, 76], among others. Generally it has been found that the NSFD scheme overcomes the weaknesses of the traditional standards numerical methods. The NSFDS differs from the standard numerical scheme because it depends on the two main rules. The first modification involves replacing the denominator function with $0 < \phi(h) < 1$, where $\phi(h) = h + O(h^2)$, as proposed in [77]. This change ensures that the step size remains within a specific range to maintain stability and positivity during the numerical computation. The second modification pertains to approximating the nonlinear terms in a nonlocal manner, as described in [78]. This approach helps preserve the positivity of the state variables by treating the nonlinear interactions in a way

that avoids negative values and instability issues during the numerical solution. For example, the term x^2 can be approximated using $x_n x_{n+1}$. This scheme is relatively more consistent than the other traditional methods [78]. By incorporating Micken's scheme, we substitute the constant step size h with functions $\phi_i(h)$, where $i = 1, 2, 3$, to ensure the state variables remain positive and stable. Additionally, we adopt nonlocal representations for the function terms. As a result, the following discrete model for the system (2.2.0.1) is derived:

$$\begin{cases} \dfrac{S_F^{k+1} - S_F^k}{\phi_1(h)} = \Lambda_F - \dfrac{\beta_F S_F^{k+1} V_F^k}{P_0 + V_F^k} - \mu_F S_F^{k+1}, \\ \dfrac{I_F^{k+1} - I_F^k}{\phi_2(h)} = \dfrac{\beta_F S_F^{k+1} V_F^k}{P_0 + V_F^k} - (\delta_F + \mu_F) I_F^{k+1}, \\ \dfrac{V_F^{k+1} - V_F^k}{\phi_3(h)} = N_f \alpha_f I_F^{k+1} - \mu_V V_F^{k+1}, \end{cases} \tag{2.6.0.1}$$

where the denominator functions are as follows:

$$\begin{cases} \phi_1(h) = \dfrac{e^{h\mu_F} - 1}{\mu_F}, \\ \phi_2(h) = \dfrac{e^{h(\mu_F + \delta_F)} - 1}{\mu_F + \delta_F}, \\ \phi_3(h) = \dfrac{e^{h\mu_V} - 1}{\mu_V}. \end{cases}$$

Rearranging model system (2.6.0.1) yields

$$\begin{cases} S_F^{k+1} = \dfrac{\phi_1(h)\Lambda_F + S_F^k}{1 + \phi_1(h)\left[\mu_F + \frac{\beta_F V_F^k}{P_0 + V_F^k}\right]}, \\ I_F^{k+1} = \dfrac{I_F^k + \frac{\phi_2(h)\beta_F V_F^k S_F^{k+1}}{P_0 + V_F^k}}{1 + \phi_2(h)(\delta_F + \mu_F)}, \\ V_F^{k+1} = \dfrac{V_F^k + \phi_3(h) N_f \alpha_f I_F^{k+1}}{1 + \phi_3(h)\mu_V}. \end{cases} \tag{2.6.0.2}$$

The value of S_F^{k+1} is used to determine the value of I_F^{k+1}, which is then used to determine the value of V_F^{k+1}, hence, model system (2.6.0.2) should be computed in succession. It follows that the solution is positive from the above model system (2.6.0.2), since we consider non-negative initial values, it is important to note that the right-hand side of the model system (2.6.0.2) does not contain any negative terms for all values of $k = 0, 1, 2, 3, \ldots$. This characteristic ensures that the state variables remain non-negative throughout the simulation, preserving the physical meaning of the model. We will determine the stability properties of the numerical scheme in the following subsections.

2.6.1 The fixed points and stability analysis

In this section, we investigate the stability and convergence properties of the fixed points resulting from the application of the proposed NSFDS numerical method. Let X^* be the fixed point of the system (2.6.0.1), which will take the form $X^* = (\hat{S_F}, \hat{I_F}, \hat{V_F})$. Considering the fixed point X^* of the system (2.6.0.1), can be found by solving

$$\begin{cases} f_1(\hat{S_F}, \hat{I_F}, \hat{V_F}) = \hat{S_F}, \\ f_2(\hat{S_F}, \hat{I_F}, \hat{V_F}) = \hat{I_F}, \\ f_2(\hat{S_F}, \hat{I_F}, \hat{V_F}) = \hat{V_F}, \end{cases} \tag{2.6.1.1}$$

where $f_i(\hat{S_F}, \hat{I_F}, \hat{V_F})$, $i = 1, 2, 3$ can be obtained by evaluating the expressions on the right-hand sides of the system (2.6.0.2) as follows:

$$\begin{cases} 1.\ f_1(\hat{S_F}, \hat{I_F}, \hat{V_F}) = \dfrac{\phi_1(h)\Lambda_F + \hat{S_F}}{1 + \phi_1(h)\left[\mu_F + \frac{\beta_F \hat{V_F}}{P_0 + \hat{V_F}}\right]}, \\ 2.\ f_2(\hat{S_F}, \hat{I_F}, \hat{V_F}) = \dfrac{\hat{I_F} + \frac{\phi_2(h)\beta_F \hat{V_F} \hat{S_F}}{P_0 + \hat{V_F}}}{1 + \phi_2(h)(\delta_F + \mu_F)}, \\ 3.\ f_3(\hat{S_F}, \hat{I_F}, \hat{V_F}) = \dfrac{\hat{V_F} + \phi_3(h) N_f \alpha_f \hat{I_F}}{1 + \phi_3(h)\mu_V}. \end{cases} \tag{2.6.1.2}$$

Considering Equation (2.6.1.2), if $\hat{I_F} = 0$ and $\hat{V_F} = 0$, and if the fixed point of each equation satisfies $f_i(X^*) = X^*, i = 1, 2, 3$, then

$$\begin{cases} 1.\ \hat{S_F} = \dfrac{\phi_1(h)\Lambda_F + \hat{S_F}}{1+\phi_1(h)\mu_F} \Rightarrow \hat{S_F} = \dfrac{\Lambda_F}{\mu_F}, \\ 2.\ \hat{I_F} = \dfrac{\hat{I_F}}{1+\phi_2(h)(\delta_F+\mu_F)} \Rightarrow \hat{I_F} = 0, \\ 3.\ \hat{V_F} = \dfrac{\hat{V_F} + \phi_3(h)N_f\alpha_f\hat{I_F}}{1+\phi_3(h)\mu_V} \Rightarrow \hat{V_F} = 0. \end{cases} \tag{2.6.1.3}$$

The unique disease-free equilibrium is denoted as $E_0 = \left(\dfrac{\Lambda_F}{\mu_F}, 0, 0\right)$. This solution represents the Disease-Free Equilibrium (DFE) for the continuous model system (2.2.0.1). However, if at least one of the variables is nonzero, this solution corresponds to the endemic equilibrium of the continuous model (2.2.0.1).

2.6.2 Numerical stability analysis of the fixed points

In this subsection, we examine the following initial conditions applied to the viral model (2.2.0.1): $S_F(0), I_F(0), V_F(0) = (8000, 1000, 2000)$. All the system parameters are provided, and certain values are assumed and listed in Table 2.3. For the purpose of determining the stability properties of system (2.6.0.1), the Jacobian matrix is derived as follows:

$$J = \begin{bmatrix} m_{11} & m_{12} & m_{13} \\ m_{21} & m_{22} & m_{23} \\ m_{31} & m_{32} & m_{33} \end{bmatrix} \tag{2.6.2.1}$$

where

$$\begin{cases} m_{11} &= \dfrac{P_0 + V_F^k}{a_1 V_F^k + a_2 P_0}, \\ m_{12} &= 0, \\ m_{13} &= -\dfrac{\beta_F \phi_1(h)(S_F^k + \Lambda_F \phi_1(h))}{(a_1 V_F^k + a_2 P_0)^2}, \\ m_{21} &= \dfrac{\phi_2(h)\beta_F V_F^k}{b_1(a_1 V_F^k + a_2 P_0)}, \\ m_{22} &= \dfrac{1}{[1 + \phi_2(h)(\delta_F + \mu_F)](a_2 P_0 + a_1 V_F^k)}, \\ m_{23} &= \dfrac{a_2 P_0 \phi_2(h) b_1 \beta_F (S_F^k + \phi_1(h)\Lambda_F)}{(b_1(a_1 V_F^k + a_2 P_0))^2}, \\ m_{31} &= \dfrac{\phi_2(h)\beta_F V_F^k \phi_3(h) N_f \alpha_f}{c_1 b_1 (a_1 V_F^k + a_2 P_0)}, \\ m_{32} &= \dfrac{\phi_3(h) N_f \alpha_f}{c_1 b_1}, \\ m_{33} &= \dfrac{c_1 b_1^2 (a_2 P_0 + a_1 V_F^k)^2 + c_1 b_1 \phi_3(h) N_f \alpha_f a_2 P_0 \phi_2(h) \beta_F (S_F^k + \phi_1(h)\Lambda_F)}{(c_1 b_1 (a_2 P_0 + a_1 V_F^k))^2}, \end{cases}$$

where

$$\begin{cases} a_1 &= 1 + \phi_1(h)(\beta_F + \mu_F), \\ a_2 &= 1 + \phi_1(h)\mu_F, \\ b_1 &= 1 + \phi_2(h)(\delta_F + \mu_F), \\ c_1 &= 1 + \phi_3(h)\mu_V. \end{cases}$$

2.6.3 Stability of disease-free equilibrium

In this section, we investigate the stability of the disease-free equilibrium E_0. By evaluating the Jacobian matrix at the disease-free equilibrium $E_0 = \left(\dfrac{\Lambda_H}{\mu_H}, 0, 0\right)$, we derive the following Jacobian matrix:

$$J(E_0) = \begin{bmatrix} d_1 & 0 & -\dfrac{\Lambda_F \beta_F \phi_1(h)}{P_0 \mu_F a_2} \\ 0 & d_3 & \dfrac{\phi_2(h)\beta_F \Lambda_F}{P_0 \mu_F d_3 P_0} \\ 0 & \phi_3(h) N_f \alpha_f d_3 d_4 & \dfrac{b_1 P_0 + \phi_3(h) N_f \alpha_f \phi_2(h) \beta_F \Lambda_F}{d_4 d_3 \mu_F P_0} \end{bmatrix} \tag{2.6.3.1}$$

where

$$\begin{cases} d_1 &= \dfrac{1}{1+\phi_1(h)\mu_F}, \\ d_2 &= \dfrac{1}{1+\phi_1(h)(\beta_F+\mu_F)}, \\ d_3 &= \dfrac{1}{1+\phi_2(h)(\delta_F+\mu_F)}, \\ d_4 &= \dfrac{1}{1+\phi_3(h)\mu_V}. \end{cases}$$

The characteristic equation corresponding to the above matrix is given by:
$|J(E_0) - \lambda I| = 0 \Longrightarrow (d_1 - \lambda)\Big(\lambda^2 - P_1\lambda + P_2 = 0\Big)$,

where

$$\begin{cases} P_1 &= d_2 + \dfrac{b_1 P_0 + \phi_3(h)\hat{N}_f \alpha_f \phi_2(h)\beta_F \Lambda_F}{d_4 d_3 \mu_F P_0}, \\ P_2 &= \dfrac{d_2 b_1}{d_4 d_3 \mu_F} + \dfrac{\phi_3(h)\hat{N}_f \alpha_f \phi_2(h)\beta_F \Lambda_F (d_3 d_2 - 1)}{d_4 d_3^2 P_0}. \end{cases}$$

We determine the stability of the equilibrium point NSFD scheme at DFE numerically.

Time Step	$\lambda_i(i = 1, 2, 3)$	$\rho(\lambda_i)$	NSFD Scheme
0.001	(0.999928, 0.999998, 0.999934)	0.999998	Converges
0.01	(0.999283, 0.999982, 0.999335)	0.999982	Converges
0.5	(0.965329, 0.999101, 0.967302)	0.999101	Converges
10	(0.579878, 0.982177, 0.514767)	0.982177	Converges

Table 2.1: The spectral radii of the Jacobian matrix associated with the disease-free equilibrium point in the NSFD scheme.

Table 2.1 provides the spectral radii of the Jacobian matrix corresponding to the Disease-Free Equilibrium (DFE) of the NSFD scheme [76]. It can be seen from Table 2.1, regardless of the time step size used in the simulations, it is observed that all the spectral radii are less than one in magnitude. Hence, based on the analysis of the spectral radii, we can conclude that the disease-free equilibrium $E_0 = \left(\frac{\Lambda_H}{\mu_H}, 0, 0\right)$ for the NSFD scheme is unconditionally locally asymptotically stable. In the following subsection, we will assess the stability of the endemic equilibrium point.

2.6.4 Stability of endemic equilibrium point

In this subsection, we examine the stability of the endemic equilibrium point E_1. By substituting the Jacobian matrix with the endemic equilibrium point, we proceed to analyze its stability characteristics:

$$E_1 = \begin{cases} S_F^* &= \dfrac{\Lambda_F[\beta_F + \mu_F R_0]}{(\beta_F + \mu_F)\mu_F R_0}, \\ I_F^* &= \dfrac{\beta_F \Lambda_F (R_0 - 1)}{(\beta_F + \mu_F)(\mu_F + \delta_F) R_0}, \\ V_F^* &= \dfrac{\mu_F P_0}{\beta_F + \mu_F}(R_0 - 1). \end{cases} \tag{2.6.4.1}$$

However, due to the complexity of obtaining the Jacobian matrix at the endemic equilibrium point, we conduct a numerical evaluation of the endemic equilibrium as follows:

Time Step	$\lambda_i(i = 1, 2, 3)$	$\rho(\lambda_i)$	NSFD Scheme
0.001	(0, 0.999999, 0.999933)	0.999999	Converges
0.01	(0, 0.99999, 0.999333)	0.999999	Converges
0.5	(0, 0.999940, 0.967199)	0.999940	Converges
10	(0.998718, 0.008731, 0.504649)	0.998718	Converges

Table 2.2: The spectral radii of the Jacobian matrix associated with the endemic equilibrium point in the NSFD scheme are as follows.

Table 2.2 provides the spectral radii of the Jacobian matrix corresponding to the endemic equilibria of the NSFD scheme. The data in Table 2.2 indicates that all the spectral radii are less than one in magnitude, regardless of the time step size used in the simulations. When $R_0 > 1$, the endemic equilibrium of the NSFD scheme is proven to be locally asymptotically stable.

2.7 Numerical Results

In this section, we present numerical simulations conducted using the NSFD scheme (2.6.0.1). The parameters used in the simulations, as shown in Table 2.3, are primarily obtained from published literature. In cases where certain parameters are not reported in the literature, they were estimated. These simulations aim to study the behavior of the model system under the given parameter values and analyze its dynamics and are coded with MATLAB 2023. The initial conditions used for simulation are given by $S_F(0) = 8000, I_F(0) = 1000, V_F(0) = 1000$.

Variable	Variable Description	Initial value	Source
Λ_F	Supply rate of recruited humans	0.05	Assumed
N_f	Number of viruses produced through replication	100	Assumed
β_F	Infection rate of humans	0.075	[79]
μ_F:	Natural death rate of humans	0.0018	[80]
δ_F	Diseases induced death rate of humans	0.07	[80]
P_0	Half saturation constant associated with the infection of humans.	10000	[79]
α_f	Shedding rate of *viruses*	0.05	[79]
μ_V	Natural decay rate of *viruses*	0.0667	[80]

Table 2.3: Model parameter values used for Simulations

Through numerical simulations, we aim to validate the results obtained from the sensitivity analysis of both R_0 and V_F^*, as well as the analytical results of the single-scale model (2.2.0.1). These

simulations will help substantiate the accuracy and reliability of the obtained findings and provide a deeper understanding of the model's behavior under various scenarios. The numerical simulations are performed using the baseline parameter values listed in Table 2.3. These values serve as the initial set of parameters to observe the system's behavior and dynamics under normal conditions. We illustrate the impact of foodborne virus transmission parameters $(\beta_F, \alpha_f, N_f, \mu_V)$ on the model variables (S_F, I_F, V_F). By varying these parameters, we can observe how the model variables respond and gain insights into the sensitivity and dynamics of the system concerning foodborne virus transmission. These parameters were chosen based on that they are significantly sensitive to both R_0 and V_F^* and also considering that we might have the most control over.

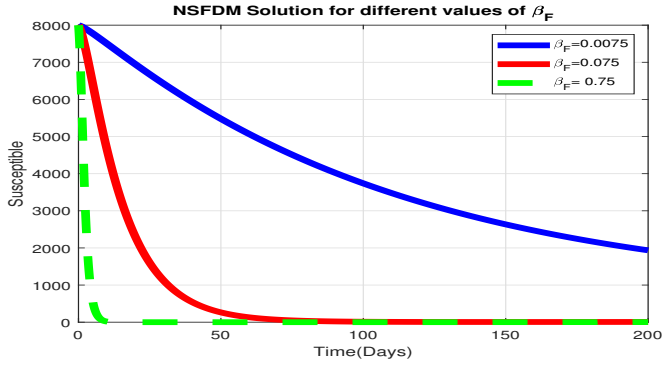

(a)

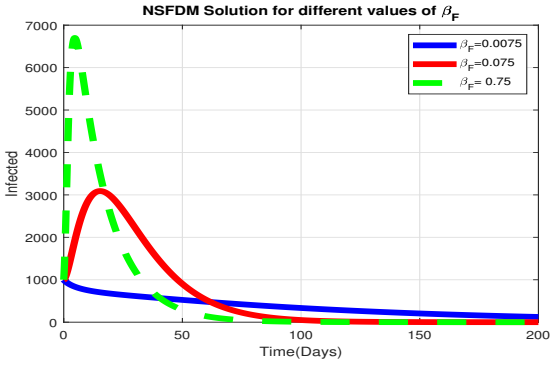

(b)

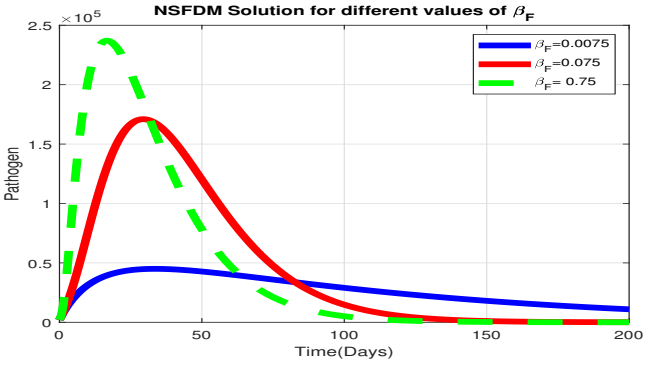

(c)

Figure 2.4: Graphs of numerical solutions of the singlescale model system (2.2.0.1) showing evolution in time of (a) top left: population of susceptible humans (S_F), (b) top right: population of infected humans (I_F), and (c) bottom: population of environmental foodborne viral load (V_F) for different values of humans infection rate β_F : $\beta_F = 0.0075, \beta_F = 0.075, \beta_F = 0.75$

Figure 2.4 illustrates the variations in the populations of (a) susceptible humans (S_F), (b) infected humans (I_F), and (c) environmental viral load (V_F) for different values of the rate β_F.

These plots demonstrate how these model variables change in response to different transmission rates at which humans became infected with foodborne virus infection $\beta_F : \beta_F = 0.0075, \beta_F = 0.075, \beta_F = 0.75$. The findings depicted in Figure 2.4 indicate that higher rates of infection at the human population level (represented by the parameter β_F) lead to an increase in the population of environmental foodborne virus (V_F) and infected humans (I_F). Simultaneously, a significant and noticeable decrease is observed in the population of susceptible humans (S_F). This suggests that an increase in the infection rate among humans has a profound impact on the dynamics of the system, leading to changes in the susceptible, infected, and environmental viral load populations. Hence, implementing environmental-hygiene management measures that prevent humans from coming into contact with the virus in the environment can effectively reduce the transmission risk of the disease at the human population/herd level. By minimizing the exposure to the foodborne virus in the environment, the likelihood of infection among humans can be mitigated, leading to better disease control and prevention.

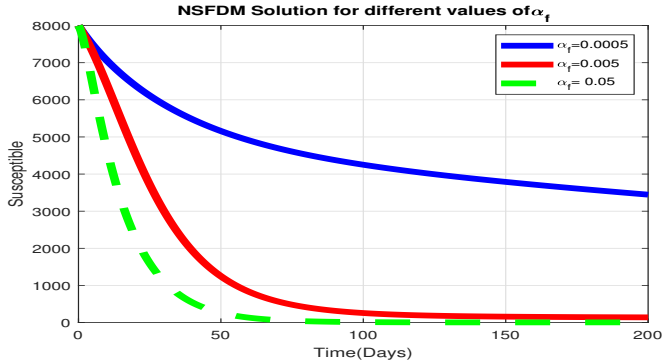

(a)

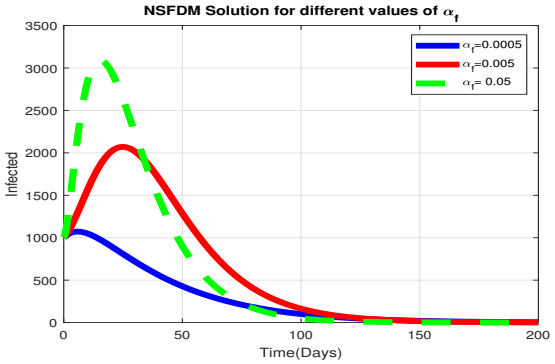

(b)

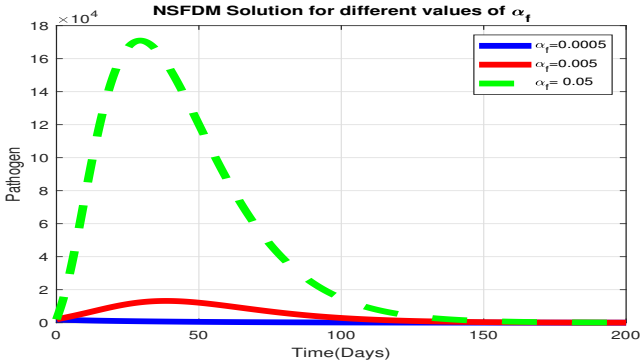

(c)

Figure 2.5: Graphs of numerical solutions of the singlescale model system (2.2.0.1) showing evolution in time of (a) top left: population of susceptible humans (S_F), (b) top right: population of infected humans (I_F), and (c) bottom: population of environmental foodborne viral load (V_F) for different values of humans infection rate α_f : $\alpha_f = 0.0005, \alpha_f = 0.005, \alpha_f = 0.05$.

Figure 2.5 exhibits numerical solutions obtained from the model system (2.2.0.1), showcasing the dynamics of (a) the population of susceptible humans (S_F), (b) the population of infected humans (I_F), and (c) the population of environmental foodborne viral load (V_F) at different values of the excretion rate of the within-host scale foodborne virus into the environment α_f : $\alpha_f = 0.0005, \alpha_f = 0.005, \alpha_f = 0.05$. These plots provide a visual representation of how the model variables evolve over time for varying excretion rates. The findings indicate that an increase in the excretion rate leads to a significant rise in the population of environmental foodborne virus (V_F) and the population of infected humans (I_F), along with a decrease in the population of susceptible humans (S_F). Implementing measures to reduce the shedding rate by infected individuals can have crucial public health implications for the between-host scale dynamics of foodborne viral infections. By reducing the excretion rate, the transmission risk of

the disease can be mitigated, contributing to better disease control and prevention efforts at the human population level.

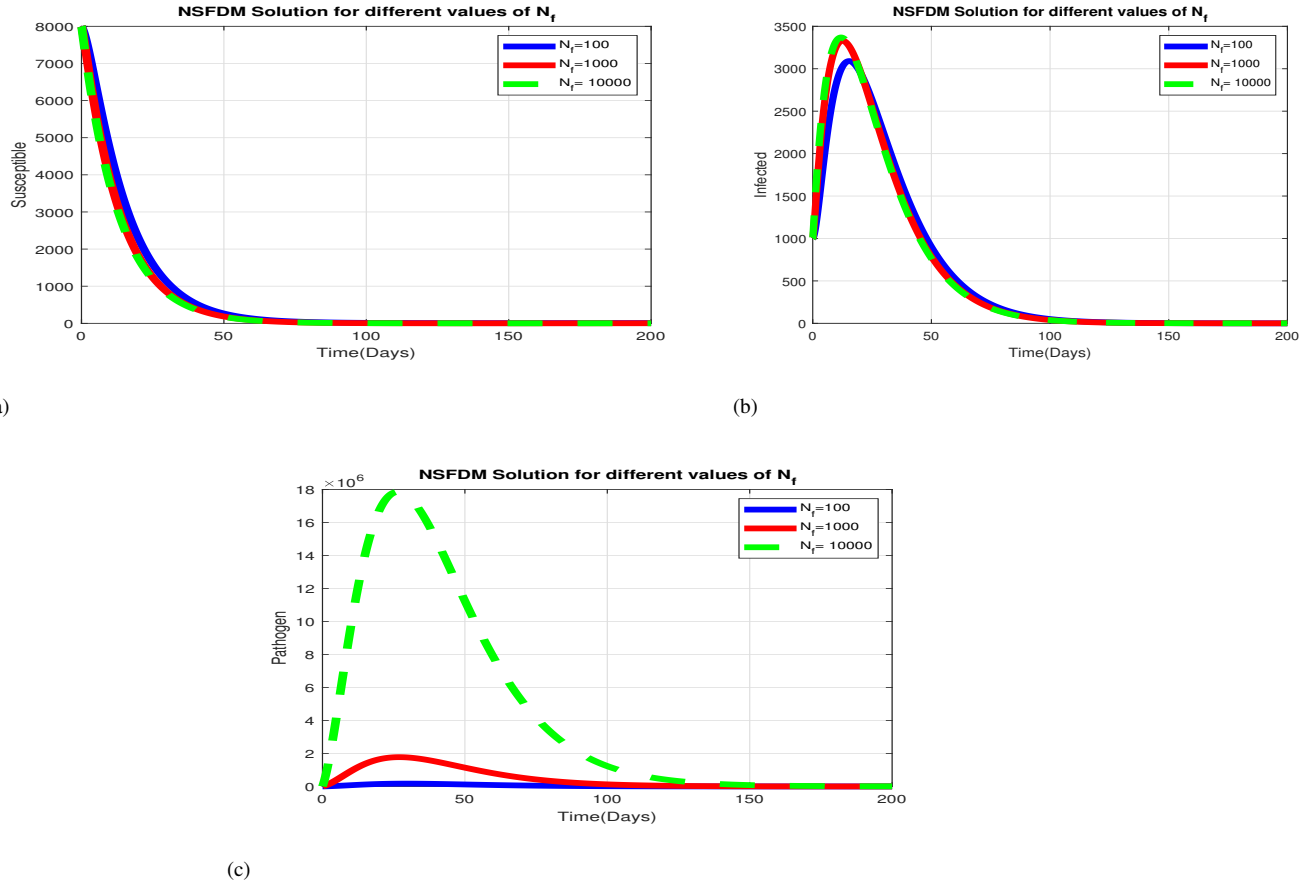

Figure 2.6: Graphs of numerical solutions of the singlescale model system(2.2.0.1) showing evolution in time of (a) top left: population of susceptible humans (S_F), (b) top right: population of infected humans (I_F), and (c) bottom: population of environmental foodborne viral load (V_F) for different values of number of viruses ready for excretion $N_f : N_f = 10, N_f = 1000, N_f = 10000$.

Figure 2.6 displays graphs of the numerical solutions obtained from the between-host scale model system (2.2.0.1), illustrating the dynamics of (a) the population of susceptible humans (S_F), (b) the population of infected humans (I_F), and (c) the environmental viral load (V_F) for different values of the average number of within-host foodborne virus ready for excretion at within-human scale $N_f : N_f = 10, N_f = 1000, N_f = 10000$. The numerical results in Figure 2.6 indicate that as the number of viruses ready for excretion within the human scale increases, there is a corresponding rise in the population of infected humans (I_F) and (c) environmental viral load (V_F), we also observe a decrease in susceptible population (S_F). Results show that any measures

that intend to inhibit the replication of virus within-human scale would have an influence on the transmission risk of foodborne viral infection among humans at population level.

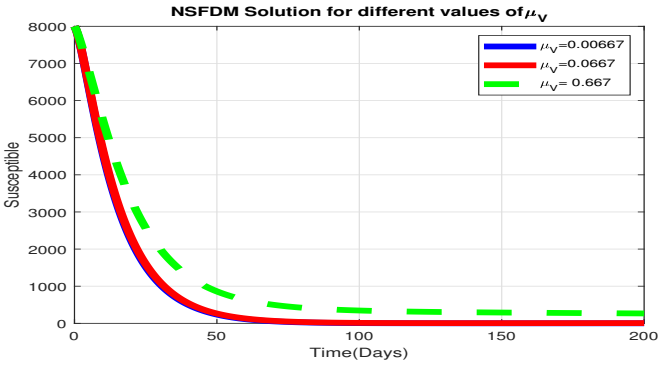

(a)

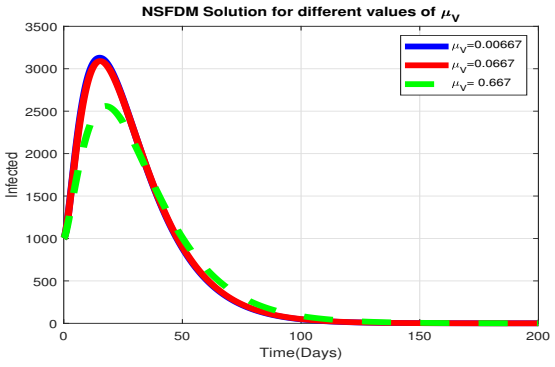

(b)

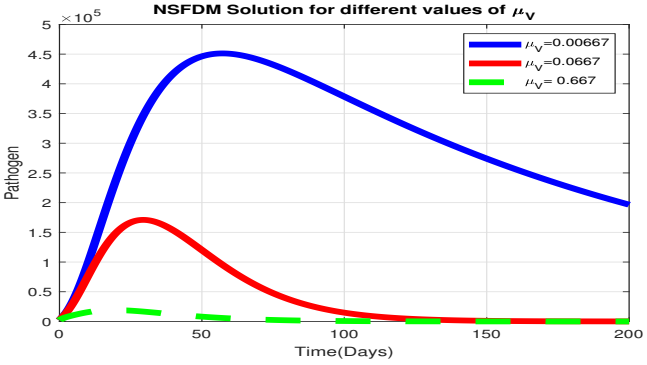

(c)

Figure 2.7: Graphs of numerical solutions of the singlescale model system (2.2.0.1) showing evolution in time of (a) top left: population of susceptible humans (S_F), (b) top right: population of infected humans (I_F), and (c) bottom: population of environmental foodborne viral load (V_F) for different values of environmental pathogen natural death rate μ_V : $\mu_V = 0.00667, \mu_V = 0.0667, \mu_V = 0.667$.

Figure 2.7 depicts graphs of numerical solutions obtained from the between-host scale model system (2.2.0.1) illustrating dynamics of (a) population of susceptible humans (S_F), (b) population of infected humans (I_F), and (c) environmental foodborne viral load (V_F) for different values of the natural death rate of the foodborne virus in the environmental domain μ_V : $\mu_V = 0.00667, \mu_V = 0.0667, \mu_V = 0.667$. The findings demonstrate the influence of environmental conditions on the death rate of foodborne viruses in the environment affect transmission of foodborne viruses on the humans population. This suggests that increasing the death rate of these viruses in the environment will reduce the transmission risk of the disease at the human population level. Hence, implementing environmental-hygiene management practices that enhance the

killing of foodborne viruses in the physical environment can effectively reduce the transmission risk of the disease among humans in the herd. By promoting measures that increase the death rate of viruses in the environment, disease control and prevention efforts can be significantly improved, leading to better public health outcomes.

2.8 Summary

In this chapter, we have introduced a single-scale model that characterizes the intrinsic dynamics of an environmentally-transmitted disease, with a particular focus on foodborne viruses as a paradigm for illustration. The model captures the interactions and transmission dynamics between hosts and the environment, providing valuable insights into the spread and control of the disease at the host level. The model was formulated based on the susceptible-infected endemic framework coupled with the compartment of live virus in the geographical area (SIP) which describes the population dynamics of susceptible humans (S_F), infected humans (I_F), and virus particles (V_F) at any time t. We thoroughly examined the mathematical properties of the model and demonstrated that it is both mathematically and epidemiologically well-posed. This ensures that the model's solutions are meaningful, and its dynamics accurately represent the real-world disease transmission processes. To achieve this, we have proven the positiveness and boundedness of the model solutions and calculated the basic reproductive number for the model. Additionally, we have identified and analyzed the two equilibrium states of the model: the disease-free equilibrium state (E_0) and the endemic equilibrium state (E^*). These analyses provide crucial insights into the stability and behavior of the model over time, enabling a comprehensive understanding of the disease dynamics and potential control strategies. We observed that when the basic reproductive number of the model is less than one, the disease-free equilibrium state is asymptotically stable and globally attracting. On the other hand, when the basic reproductive number of the model exceeds one, there exists a unique endemic equilibrium state that is both locally and globally asymptotically stable. These results provide critical insights into the model's behavior under different conditions and highlight the significance of the basic reproductive number in characterizing the disease dynamics and potential outcomes. We performed a sensitivity analysis of the basic reproductive number R_0 and the endemic value of the infective virus V_F^*. These two disease transmission metrics are crucial in characterizing the dynamics of the disease at the early stage of infection and when it reaches an endemic level, respectively. By examining the sensitivity of these metrics to changes in various model parameters, we gained valuable insights into the factors that significantly influence disease transmission and propagation. This analysis helps in identifying potential targets for disease control and management strategies. A

non-standard finite difference (NSFD) scheme was devised for a mathematical model of foodborne viral infection in humans. Through numerical analysis, it was demonstrated that the discrete systems generated by the NSFD scheme retain essential properties of the original model, including positivity and stability. However, it was observed that the convergence of the solutions to the equilibrium points is influenced by the step-size h used in the numerical simulations. The choice of an appropriate step-size is critical to ensure accurate and reliable results when using the NSFD scheme to approximate the continuous model's dynamics. The fact that this model captures the foodborne virus's replication dynamics in an infected human host in a phenomenological way makes it hard to anticipate the dynamics of the sickness. This is a key weakness in the model. We anticipate that by converting a single-scale model to a multiscale model, this type of single-scale model constraint might be overcomed in terms of predicting the dynamics of environmental disease transmission. In the next chapter we develop a multiscale model for environmentally transmitted pathogens with replication at microscale only using *norovirus* as an example.

Chapter 3

A Nested Multiscale Model Of Norovirus Dynamics In Humans

3.1 Introduction

Extensive research on infectious disease transmission has demonstrated the crucial role of within-host scale processes in the spread of these diseases. The dynamics and interactions that occur at the level of individual hosts can significantly impact the transmission and progression of infectious agents within a population. Depending on the infectious disease system under consideration, the actual functional connection between infectivity and pathogen burden could, however, be very different. Experiments, in particular, proved that a host's ability to transmit an infection grows as the host's pathogen burden rises. Numerous investigations have provided evidence supporting the notion that the infectiousness of a host is influenced by the pathogen load at the within-host scale. These studies have shown that the amount of pathogens present within an infected host can play a significant role in determining the host's ability to transmit the disease to others. [81]. In this chapter, we introduce a nested multiscale model for pathogens with a replication-cycle that occurs only at the microscale, specifically at the host level, wherein the macroscale influences the microscale through initial inoculum and microscale influences macroscale through pathogen shedding using *norovirus* in humans as a paradigm. The multiscale model is used to describe and understand the complex life-cycle of foodborne disease caused by norovirus. The primary goal of this chapter is to examine the influence of pathogen

replication at the microscale on pathogen transmission at the macroscale. Norovirus is among the primary cause responsible for gastroenteritis cases on a global scale due to its multiple modes of transmission, it accounts for more than 67% of foodborne infections [82]. *Noroviruses* are primary causes of both sporadic and epidemic gastroenteritis, as well as being very contagious [83]. Noroviruses are the most common cause of foodborne illnesses, community-acquired diarrhea, and gastroenteritis in people of all ages [82]. The majority of experts agree that a vaccination is the most practical way to lessen the impact of *noroviruses* disease given the natural history of the illness. However, the creation of a *noroviruses* vaccine has advanced steadily while being hampered by significant barriers such as genetic variety, a lack of knowledge of immunity, lack of animal models and inability to multiply in culture system which has prevented the development of assays to determine which antibodies provide protection [84]. Currently, there are no vaccines or specific treatments available for this pathogen. The only available measures are palliative treatments, which involve maintaining good sanitation, practicing personal hygiene, and implementing isolation or quarantine procedures to control its spread and this is the only measure that can be taken against *norovirus* [85]. Insufficient understanding of the connection between the microscale and macroscale dynamics in the progression of such infections is a major barrier to the development of effective treatments for *noroviruses* infections [25]. Many variables can make the *noroviruses* more contagious and worsen the illness that results [82] including immune response against the infection. The complexity of *norovirus* host interactions must be thoroughly understood in order to overcome these infections. The most crucial thing is to learn more about the immune system's defenses against this virus and its effects on the disease progression [86].

Models that depict the dynamics of transmission can show the relative efficacy of various *norovirus* control strategies [86], and hence we need multiscale models that incorporate elements like the immune reaction that fuel the transmission. Most of the existing *norovirus* transmission models use a compartmentalized strategy in which the population is divided according to illness severity. The population is typically divided into three classes, namely susceptible, infected, and recovered (SIR). Some models for *noroviruses* frequently incorporate a latent, or exposed, compartment (E) because to assess the potential efficacy of controls aimed at infected people the latent compartment is required [87]. The basic SEIR structure may be sufficient to describe *norovirus* transmission at the population level, nonetheless, the transmission mechanism theory disregards the complexity of transmission, as it fails to consider that transmission is influenced by processes occurring at multiple scales and frequently across diverse environments. Therefore multiscale modelling is necessary to model the full dynamics of *norovirus* infection through incoporating factors such as the immune response to the infection. As far as we are aware, there is currently no multiscale model for *norovirus* in the existing literature that integrates the dynamics at the microscale level and establishes a linkage with the macroscale submodel. The nested

multiscale model involves a type I reciprocal influence that describes the relationship between the microscale and macroscale at the host level of an infectious disease system. In this model, pathogens move from the microscale to the macroscale through processes such as pathogen shedding or excretion. Given that the effect of super-infection on pathogen burden at the microscale is significantly smaller compared to that of the pathogen replication cycle, a nested multiscale model is better suited for studying these infectious disease systems. This model allows for a more accurate representation of the complex interactions between microscale and macroscale dynamics. Nested multiscale models have the advantage of simplifying the process of minimizing the dimensions of the multiscale model through slow and fast time scale analysis, which makes the multiscale much simpler to evaluate [25]. In this chapter we shall refer to the microcale as within-human scale.

3.2 The Derivation of the Nested Multiscale Model for *Norovirus*

In this subsection, we develop a nested multiscale model of *norovirus* transmission dynamics. Macroscale and within-human scale submodels serve as the foundation for multiscale modelling of infectious disease systems at the host level. It should be highlighted that in order for the nested model to be created, the mathematical representation used to describe both the within-human scale and macroscale submodels must be described by the same formalism. We first develop submodels for *norovirus* transmission dynamics, the macroscale submodel associated with the transmission dynamics of *norovirus* infection and thereafter we develop within-human scale submodel associated with the replication dynamics within-human scale and the final step is to combine all of the submodels into a single multiscale model. We illustrate the derivations of these submodels and how they are linked to form a multiscale model below.

3.3 The macroscale submodel for the *norovirus* multiscale model dynamics

In this part, we develop a macroscale submodel designed to track the behavior of *noroviruses* on a larger scale. This submodel operates by observing the interactions of three populations at a specific time t: susceptible humans denoted as $S_H(t)$, and infected humans denoted as $I_H(t)$ and a population of *noroviruses* $V_H(t)$ in physical environment. The macroscale sumbodel is a modification of between-host single scale model in Chapter 2 through considering norovirus since the one in the previous chapter is for viral transmission in general. The macroscale is linked to the

within-human scale submodel to be developed in the next subsection to form a nested multiscale model for *norovirus* infection. The following assumptions are taken into consideration:

(i) The infection spreads exclusively through direct contact with the *norovirus* present in the physical environment.

(ii) The dynamics of susceptible class S_H, infected class I_H and a pathogen V_H are considered to occur over a relatively slower time scale (t) when compared to the within-human scale variables so that $S_H = S_H(t)$, $I_H = I_H(t), V_H = V_H(t)$.

(iii) The transmission of infection is through ingestion of viral load V_F from the environment. However, if there is any direct transmission, it can be estimated by indirect transmissioon in terms of environmental viral load V_H.

(iv) The average extracellular viruses in each infected individual is modelled phenomenologically by $\widehat{N_h}$, serving as a representation of an individual's level of infectiousness.

The system of ordinary differential equations characterizes the macroscale submodel governing the multiscale dynamics of *norovirus* within the human population.

$$\begin{cases} 1.\ \dfrac{dS_H(t)}{dt} = \Lambda_H - \dfrac{\beta_H S_H V_H}{P_0 + V_H} - \mu_H S_H, \\ 2.\ \dfrac{dI_H(t)}{dt} = \dfrac{\beta_H S_H V_H}{P_0 + V_H} - (\delta_H + \mu_H) I_H, \\ 3.\ \dfrac{dV_H(t)}{dt} = \widehat{N_h}\alpha_h I_H - \mu_V V_H. \end{cases} \tag{3.3.0.1}$$

The macroscale submodel given by model system (3.3.0.1) involves observing the behavior of three distinct populations: susceptible humans denoted as S_H, infected humans represented by I_H, and the viral load in the environment V_H. Equation (1) of the model system (3.3.0.1) presents the dynamics of susceptible humans. New recruits of human population enter this class at a rate Λ_H at any time t through birth, this population is decreased through viral infection at a rate $\dfrac{\beta_H V_H(t) S_H(t)}{P_0 + V_H(t)}$ with β_H the infection rate of humans and P_0 represents the saturation parameter of the norovirus, determining the point at which there is a 50% probability of an individual becoming infected following the ingestion of the virus. The transmission occurs when humans ingest contaminated food from the environment. The number of susceptible individuals declines due to natural mortality, occurring at a rate, μ_H. Equation (2) in the model system (3.3.0.1) outlines the dynamics of the infected human population. This population grows due to the infection

of susceptible humans and diminishes through both natural mortality at a rate of μ_H and disease-induced mortality at a rate of δ_H, resulting in an average lifespan for infected humans within the population of $\frac{1}{(\mu_H + \delta_H)}$. We consider that infected humans transmit the disease by releasing the virus into the environment at a rate of $\widehat{N_h}\alpha_h I_H(t)$, where $\widehat{N_h}$ serves as a phenomenological representation of the mean quantity of viral load at the within-human scale, which is available for discharge into the environment by each infected human, occurring at a rate, α_h. Hence, the population of viral load within the environment, as defined by Equation (3) of the model system (3.3.0.1) increases after viral excretion by the infected human host in feacal material to the environment at a rate $\widehat{N_h}\alpha_h I_H(t)$. The viral load population is presumed to decline due to natural mortality at a rate of μ_V. From the model system (3.3.0.1), it is observed that $\widehat{N_h}$ is treated as a singular value parameter, even though estimating $\widehat{N_h}$ using a single-scale model is challenging. Given this, an alternative approach for estimating $\widehat{N_h}$ involves the utilization of a nested multiscale model focusing on within-human scale dynamics.

Variable	Variable Description
$S_H(t)$	Susceptible humans
$I_H(t)$	Infected humans
$V_H(t)$	Pathogen in the environment

Table 3.1: Description of variables in the system (3.3.0.1).

3.3.1 The within-human scale submodel for the *norovirus* multiscale model dynamics

The dynamics of the norovirus population within humans depict the progression of four distinct populations at the within-human level. These populations encompass the ingested norovirus population denoted as B_h, the susceptible epithelial cell population as S_e, the infected epithelial cell population as I_e, and the immune cell population as I_c. To incorporate this submodel with the single-scale model presented in the model system (3.3.0.1), we introduce the following assumptions:

(i) Infection takes place through interaction with the extracellular viral load B_h at the infection site.

(ii) The disease processes at the within-human scale occur at a fast time scale (τ) as compared to the macroscale *norovirus* submodel so that susceptible epithelial cells $S_e = S_e(\tau)$,

infected epithelial cells $I_e = I_e(\tau)$, immune cells $I_c = I_c(\tau)$ and within-human scale pathogen $B_h = B_h(\tau)$.

(iii) The extracellular viral load $B_h = B_h(\tau)$ serves as proxy of individual human infectivity, and it is eliminated from an individual's body through fecal excretion.

(iv) An immune reaction occurs at the within-human level.

Based on these assumptions, the within-human scale disease dynamics can be described by the following set of ordinary differential equations:

$$\begin{cases} 1. \ \dfrac{dB_h(\tau)}{d\tau} = N_e\alpha_e I_e(\tau) - \phi_t I_c(\tau)B_h(\tau) - \mu_h B_h(\tau) - \alpha_h B_h(\tau), \\ 2. \ \dfrac{dS_e(\tau)}{d\tau} = \Lambda_e - \beta_e S_e(\tau)B_h(\tau) - \mu_e S_e(\tau), \\ 3. \ \dfrac{dI_e(\tau)}{dt} = \beta_e S_e(\tau)B_h(\tau) - \mu_e I_e(\tau) - \alpha_e I_e(\tau), \\ 4. \ \dfrac{dI_c(\tau)}{d\tau} = \Lambda_c + \rho_c I_c(\tau)B_h(\tau) - \mu_c I_c(\tau). \end{cases} \tag{3.3.1.1}$$

Variable	Variable Description
$B_h(t)$	Within-human scale virus
$S_e(t)$	Susceptible epithelial cells
$I_e(t)$	Infected epithelial cells
$I_c(t)$	Immune cells

Table 3.2: Description of variables in the system (3.3.1.1).

Within the context of the norovirus dynamics within humans, infected epithelial cells burst at a rate denoted as α_e, thereby releasing an average number of intracellular viruses, N_e, into the external environment. This results in the total quantity of intracellular viruses being excreted into the extracellular environment, given by, $N_e\alpha_e I_e$, the population of virus at macroscale is reduced through immune cells at a rate, ϕ_t, a natural death, μ_h and shedding rate, α_h. From equation (2) of the model system (3.3.1.1) the susceptible epithelial cells at the infection site receive a constant supply at a rate of Λ_e, but this population decreases due to infections at a rate of β_e and undergoes natural decay at a rate of μ_e. Equation (3) in the model system (3.3.1.1) describes

the behavior of infected epithelial cells. This population experiences growth as a result of the infection of susceptible epithelial cells, while its decline is attributed to the viral replication rate, denoted as α_e, and it is further reduced through natural decay at a rate of μ_e. Equation (4) within the model system (3.3.1.1) characterizes the immune response. The first term reflects a consistent supply rate, Λ_c, while the second term represents the rate of activation of immune cells, denoted as ρ_c, and the final term captures the natural decay rate of immune cells, indicated by μ_c.

3.3.2 Linking the Macroscale and Within-human scale Submodels into a Full Nested Multiscale Model

After introducing the two submodels in systems (3.3.0.1) and (3.3.1.1), which individually describe the key processes of viral load replication and transmission of the *norovirus* at distinct scales (within-human and macroscale), we proceed to link them into a single multiscale model, as illustrated in Figure 3.1. This is achieved by replacing the parameter $\widehat{N_h}$, used to phenomenologically represent human pathogen replication, with a variable $B_h(\tau)$ that mechanistically portrays microorganism reproduction, resulting in

$$
\begin{cases}
1.\ \dfrac{dS_H(t)}{dt} = \Lambda_H - \dfrac{\beta_H S_H V_H}{P_0 + V_H} - \mu_H S_H(t), \\
2.\ \dfrac{dI_H(t)}{dt} = \dfrac{\beta_H S_H V_H}{P_0 + V_H} - (\delta_H + \mu_H) I_H(t), \\
3.\ \dfrac{dV_H(t)}{dt} = \alpha_h B_h(\tau) I_H(t) - \mu_V V_H(t), \\
4.\ \dfrac{dB_h(\tau)}{d\tau} = N_e \alpha_e I_e(\tau) - \phi_t I_c B_h(\tau) - \mu_h B_h(\tau) - \alpha_h B_h(\tau), \\
5.\ \dfrac{dS_e(\tau)}{d\tau} = \Lambda_e - \beta_e S_e B_h(\tau) - \mu_e S_e(\tau), \\
6.\ \dfrac{dI_e(\tau)}{dt} = \beta_e S_e B_h(\tau) - \mu_e I_e(\tau) - \alpha_e I_e(\tau), \\
7.\ \dfrac{dI_c(\tau)}{d\tau} = \Lambda_c + \rho_c I_c B_h(\tau) - \mu_c I_c(\tau).
\end{cases}
\tag{3.3.2.1}
$$

Following the categorization of multiscale models for infectious disease systems outlined in the reference [88], it should be noted that the multiscale model given by (3.3.2.1) can be categorized

under a category known as "nested multiscale models". Now, the complete multiscale model system provided by (3.3.2.1) involves two distinct time scales, which presents a significant challenge in the analysis of the multiscale model. Below is the schematic representation of the nested multiscale model of *norovirus*

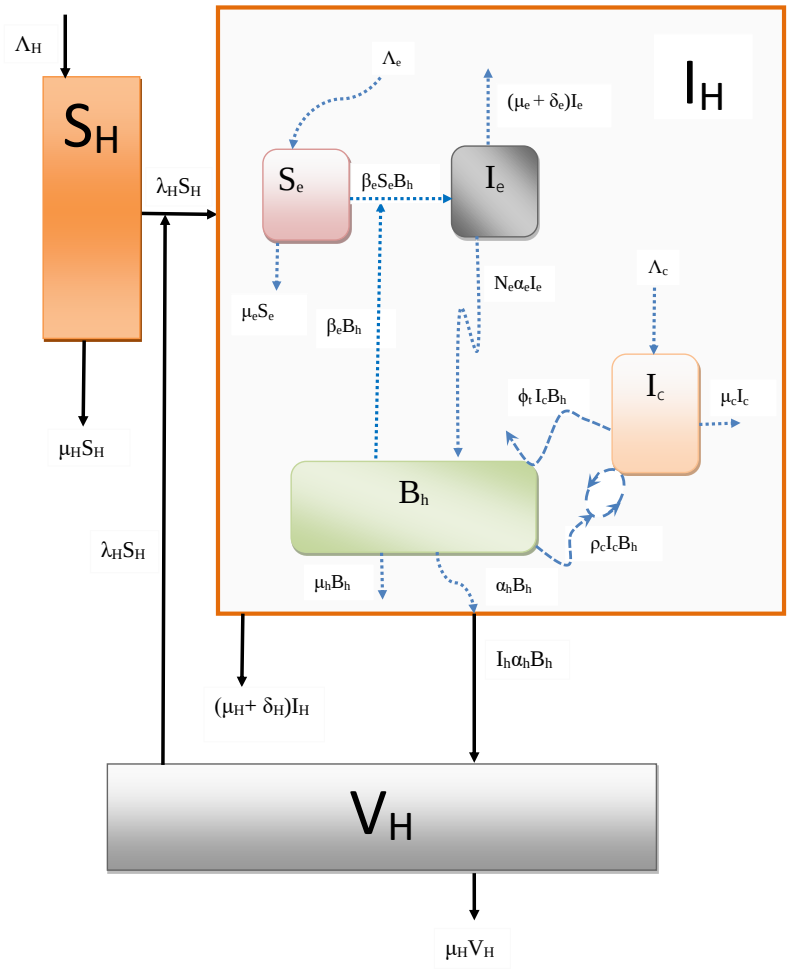

Figure 3.1: A schematic representation of the nested multiscale model of *norovirus*

3.3.3 Simplification of the Full Nested Multiscale Model

Given that the complete nested multiscale model for the transmission dynamics of *norovirus* is introduced in a model system (3.3.2.1) involves two different time scales (the within-human time scale which is a fast time scale, τ and the macroscale time scale which is a slow time scale, t), we analyze it by using fast-slow analysis where we assume a connection between the fast and slow time scales as $\tau = \epsilon t$, with ϵ being a small positive value $0 < \epsilon << 1$. By doing so, we can

now re-write the within-human scale *norovirus* transmission dynamics given in a model system (3.3.1.1) as:

$$\begin{cases} 1.\ \dfrac{dB_h(t)}{d(t)} &= \epsilon[N_e\alpha_e I_e(\tau) - \phi_t I_c B_h(\tau) - \mu_h B_h(\tau) - \alpha_h B_h(\tau)], \\ 2.\ \dfrac{dS_e(t)}{dt} &= \epsilon[\Lambda_e - \beta_e S_e(\tau) B_h(\tau) - \mu_e S_e(\tau)], \\ 3.\ \dfrac{dI_e(t)}{d(t)} &= \epsilon[\beta_e S_e(\tau) B_h(\tau) - \mu_e I_e(\tau) - \alpha_e I_e(\tau)], \\ 4.\ \dfrac{dI_c(t)}{d(t)} &= \epsilon[\Lambda_c + \rho_c I_c(\tau) B_h(\tau) - \mu_c I_c(\tau)]. \end{cases} \tag{3.3.3.1}$$

Here, ϵ is regarded as a fixed parameter indicating the fast time scale of the within-human scale submodel concerning *norovirus* transmission dynamics, relative to the slow time scale of the macroscale submodel for *norovirus* transmission dynamics. Since $0 < \epsilon << 1$, by setting ϵ to zero, the within-human scale submodel of *norovirus* transmission dynamics becomes time-independent, resulting in:

$$\begin{cases} 1.\ N_e\alpha_e I_e^*(\tau) - \phi_t I_c^*(\tau) B_h^*(\tau) - \mu_h B_h^*(\tau) - \alpha_h B_h^*(\tau) = 0, \\ 2.\ \Lambda_e - \beta_e S_e^*(\tau) B_h^*(\tau) - \mu_e S_e^*(\tau) = 0, \\ 3.\ \beta_e S_e^*(\tau) B_h^*(\tau) - \mu_e I_e^*(\tau) - \alpha_e I_e^*(\tau) = 0, \\ 4.\ \Lambda_c + \rho_c I_c^*(\tau) B_h^*(\tau) - \mu_c I_c^*(\tau) = 0. \end{cases} \tag{3.3.3.2}$$

From Equation (3.3.3.2), we get

$$\begin{cases} 1.\ S_e^* &= \dfrac{\Lambda_e}{\beta_e B_h^* + \mu_e}, \\ 2.\ I_e^* &= \dfrac{\beta_e \Lambda_e B_h^*}{(\beta_e B_h^* + \mu_e)(\mu_e + \alpha_e)}, \\ 3.\ I_c^* &= \dfrac{\Lambda_c}{\mu_c - \rho_c B_h^*}, \\ 4.\ B_h^* &= \dfrac{b_1 + \sqrt{b_1^2 + 4b_0 b_2}}{2b_0} \end{cases} \tag{3.3.3.3}$$

where

$$\begin{cases} b_0 &= \beta_e \rho_c (\mu_c + \alpha_e)(\mu_h + \alpha_h), \\ b_1 &= (\mu_e + \alpha_e)(\beta_e a_0 - \mu_e a_1) + N_e \alpha_e \Lambda_e \beta_e \rho_c, \\ b_2 &= Ne \alpha_e \Lambda_e \mu_c - a_2 \mu_c (\mu_e + \alpha_e), \end{cases} \tag{3.3.3.4}$$

and

$$\begin{cases} a_0 &= \phi_t \Lambda_c + \mu_h \mu_e + \alpha_h \mu_c, \\ a_1 &= (\mu_h + \alpha_h)\rho_c, \\ a_2 &= \phi_t \Lambda_c + (\mu_h + \alpha_h)\mu_c. \end{cases} \tag{3.3.3.5}$$

3.4 Computation of the within-human scale basic reproductive number

In this section, we employ the next-generation approach to estimate the basic reproductive number of the model. The equations within the model system (3.3.2.1) can be expressed in the following format:

$$\begin{cases} \dfrac{dX}{dt} &= f(X,Y,Z), \\ \dfrac{dY}{dt} &= g(X,Y,Z), \\ \dfrac{dZ}{dt} &= h(X,Y,Z), \end{cases} \tag{3.4.0.1}$$

where

- $X = (S_e, I_c)$ represents all uninfected components,
- $Y = I_e$ represents infected but not infectious components, and
- $Z = B_h$ represents infected and infectious components.

Following [89], we set

$$\hat{g}(X^*, Z) = \frac{\beta_e \Lambda_e}{\mu_e(\mu_e + \alpha_e)}, \tag{3.4.0.2}$$

By substituting the value of $I_e = \dfrac{\beta_e S_e B_h}{(\mu_e + \alpha_e)}$ and letting $h = \dfrac{dB_h}{dt}$, we obtain

$$h(X^*, \hat{g}(X^*, Z), Z) = N_e \alpha_e I_e - \phi_t I_c B_h - \mu_h B_h - a\alpha_h B_h. \tag{3.4.0.3}$$

Next, we consider $A = D_z(X, \hat{g}(X, 0), 0)$ and also make the assumption that A can be decomposed as $A = M - D$, where $M \geq 0$ and $D > 0$ is a diagonal matrix.

Then A becomes

$$A = \frac{N_e \alpha_e \lambda_e \beta_e}{\mu_e(\mu_e + \alpha_e)} - \left(\frac{\phi_t \Lambda_c}{\mu_c} + \mu_h + \alpha_h \right). \tag{3.4.0.4}$$

Since $A = M - D$, we have

$$M = \frac{N_e \alpha_e \lambda_e \beta_e}{\mu_e(\mu_e + \alpha_e)}. \tag{3.4.0.5}$$

and

$$D = \left(\frac{\phi_t \Lambda_c}{\mu_c} + \mu_h + \alpha_h \right). \tag{3.4.0.6}$$

Hence,

$$D^{-1} = \frac{\mu_c}{\phi_t \Lambda_c + \mu_h \mu_c + \alpha_h \mu_c}. \tag{3.4.0.7}$$

The basic reproductive number is determined by the largest eigenvalue (spectral radius), which is expressed as follows:

$$R_0 = \frac{N_e \alpha_e \Lambda_e \mu_c \beta_e}{\mu_e(\mu_e + \alpha_e)(\phi_t \Lambda_c + \mu_h \mu_c + \mu_c \alpha_h)}. \tag{3.4.0.8}$$

Equation (3.4.0.8) is the expression for R_0 for the within-human scale basic reproductive number for *norovirus*.

Consequently, the application of fast-slow analysis simplifies the system of equations in the within-human scale submodel (3.3.1.1) to the algebraic equations given in system (3.3.3.3) which can be fitted into the parameters of the macroscale submodel and become

$$\begin{cases} 1. \ \dfrac{dS_H(t)}{dt} = \Lambda_H - \dfrac{\beta_H S_H V_H}{P_0 + V_H} - \mu_H S_H, \\ 2. \ \dfrac{dI_H(t)}{dt} = \dfrac{\beta_H S_H V_H}{P_0 + V_H} - (\delta_H + \mu_H) I_H, \\ 3. \ \dfrac{dV_H(t)}{dt} = \alpha_h B_h^* I_H - \mu_V V_H. \end{cases} \tag{3.4.0.9}$$

From Equation (3.4.0.9), it can be observed that the total viral load excreted by each infected individual into the physical environment, denoted as $B_h I_H$, is approximated as $B_h^* I_H$. Therefore we let $N_h = B_h^*$, act as a composite parameter that can be interpreted as the average quantity of within-human scale viral load (B_h) at the endemic equilibrium ready to be shed into the environment by each infected individual. Therefore below we present the full scale multiscale

model (3.3.2.1) which has been simplified or reduced to become:

$$\begin{cases} 1. \ \dfrac{dS_H(t)}{dt} = \Lambda_H - \dfrac{\beta_H S_H V_H}{P_0 + V_H} - \mu_H S_H, \\ 2. \ \dfrac{dI_H(t)}{dt} = \dfrac{\beta_H S_H V_H}{P_0 + V_H} - (\delta_H + \mu_H) I_H, \\ 3. \ \dfrac{dV_H(t)}{dt} = N_h \alpha_h I_H - \mu_V V_H, \end{cases} \tag{3.4.0.10}$$

where the composite parameter N_h, estimating $\widehat{N_h}$, is expressed as follows:

$$N_h = \frac{b_1 + \sqrt{b_1^2 + 4b_0 b_2}}{2b_0}, \tag{3.4.0.11}$$

where

$$\begin{cases} b_0 = \beta_e \rho_c (\mu_c + \alpha_e)(\mu_h + \alpha_h), \\ b_1 = (\mu_e + \alpha_e)(\beta_e a_0 - \mu_e a_1) + N_e \alpha_e \Lambda_e \beta_e \rho_c, \\ b_2 = a_2 \mu_c (\mu_e + \alpha_e)(R_0 - 1), \end{cases} \tag{3.4.0.12}$$

and

$$\begin{cases} a_0 = \phi_t \Lambda_c + \mu_h \mu_e + \alpha_h \mu_c, \\ a_1 = (\mu_h + \alpha_h)\rho_c, \\ a_2 = \phi_t \Lambda_c + (\mu_h + \alpha_h)\mu_c. \end{cases} \tag{3.4.0.13}$$

3.4.1 Invariant Region

In this subsection, we assume the positivity of all variables and parameters in the multiscale model for all $t \geq 0$. The human population, denoted as $N_H = S_H + I_H$, can be determined through:

$$\frac{dN_H(t)}{dt} = \Lambda_H - \mu_H N_H - \delta_H I_H. \tag{3.4.1.1}$$

In the absence of *norovirus*, there is no death from *norovirus* infection, thus $\delta_H = 0$ and therefore:

$$\frac{dN_H(t)}{dt} \leq \Lambda_H - \mu_H N_H. \tag{3.4.1.2}$$

Integrating both sides of (3.4.1.2), the human population approaches

$$N_H(t) \to \frac{\Lambda_H}{\mu_H}. \tag{3.4.1.3}$$

This implies that in the absence of *norovirus* infection, $N_H = \frac{\Lambda_H}{\mu_H}$, indicating the presence of a steady-state population that is globally asymptotically stable. Similarly, by evaluating the third equation in the multiscale model (3.4.0.10), the pathogen population will be given by:

$$V_H = \frac{N_h \alpha_h \Lambda_H}{\mu_H \mu_V}. \tag{3.4.1.4}$$

Consequently, the feasible set for our multiscale model system (3.4.0.10) is provided by

$$\begin{cases} \Omega_1 = (S_H(t), I_H(t), V_H(t)) \in \mathbb{R}_3^+ : \\ \qquad 0 \leq S_H + I_H \leq \dfrac{\Lambda_H}{\mu_H}, \quad 0 \leq V_H \leq \dfrac{N_h \alpha_h \Lambda_H}{\mu_H \mu_V}. \end{cases} \tag{3.4.1.5}$$

Hence, it can be readily demonstrated that all solutions of the simplified multiscale model system (3.4.0.10), starting from positive initial conditions, remain bounded within the invariant region Ω_1 defined by Equation (3.4.1.5). Thus, we deduce that the system holds biological significance and is mathematically well-defined within the domain Ω_1.

3.4.2 The equilibrium states of the multiscale model and the basic reproductive number

In this sub-subsection, we identify the equilibrium points, specifically the disease-free equilibrium (DFE) and the endemic equilibrium, of the model system (3.4.0.10), along with the calculation of the basic reproduction number (R_0) of the nested multiscale model. The disease-free equilibrium point of the nested multiscale model system (3.4.0.10) can be determined by setting the left-hand side equal to zero, and this results in $V_H = I_H = 0$. Thus we get

$$E^0 = (S_H^0, I_H^0, V_H^0) = \left(\frac{\Lambda_H}{\mu_H}, 0, 0\right). \tag{3.4.2.1}$$

The computation of the basic reproductive number aims to ascertain the local asymptotic stability of E^0. In the next subsubsection, we will carry out the calculation of the basic reproductive number.

3.4.2.1 The basic reproductive number

To control *norovirus* infection the major action is to consider reducing R_0 to a value less than a unity. The basic reproductive number is evaluated through the adoption of the next generation operator in [90]. In this method compartments are re-grouped into infected, susceptible and infectious populations. Thus the model system can also be written in the form:

$$\begin{cases} \dfrac{dX}{dt} &= f(X,Y,Z), \\ \dfrac{dY}{dt} &= g(X,Y,Z), \\ \dfrac{dZ}{dt} &= h(X,Y,Z), \end{cases} \tag{3.4.2.2}$$

where

- $X = S_H$ represents all uninfected components, and
- $Y = I_H$ represents infected but not infectious components, and
- $Z = V_H$ represents infected and infectious components.

We let the disease-free equilibrium be $E^0 = \left(\dfrac{\Lambda_H}{\mu_H}, 0, 0\right)$,

we define $(\hat{g}(X^*, Z))$ by

$$(\hat{g}(X^*, Z)) = I_H = \frac{\beta_H S_H V_H}{(P_0 + V_H)(\delta_H + \mu_H)}, \tag{3.4.2.3}$$

therefore, we conclude that

$$h(X,Y,Z) = \frac{N_h \alpha_h I_H}{\mu_V}. \tag{3.4.2.4}$$

Substituting Equation (3.4.2.3) in Equation (3.4.2.4), we get

$$h(X,Y,Z) = \frac{N_h \alpha_h \beta_H S_H V_H}{\mu_V (P_0 + V_H)(\mu_H + \delta_H)}, \tag{3.4.2.5}$$

evaluating $D_Z h(X^*, \hat{g}(X^*, 0), 0)$, we obtain

$$D_Z h(X^*, \hat{g}(X^*, 0), 0) = \frac{N_h \alpha_h \beta_H \Lambda_H}{\mu_H \mu_V P_0 (\mu_H + \delta_H)}, \tag{3.4.2.6}$$

we get a basic reproductive number:

$$R_0 = \frac{N_h \alpha_h \beta_H \Lambda_H}{\mu_H \mu_V P_0 (\mu_H + \delta_H)}. \tag{3.4.2.7}$$

Based on the expression (3.4.2.7) for the reproductive number, it becomes observable that R_0 is influenced by both the parameters associated with the within-human scale and those related to the between-host scale. Consequently, the results reveal a reciprocal interaction between the within-human scale and the between-host scale, illustrating their interconnected influence. This representation of the basic reproductive number can be reformulated as $R_0 = R_{01} R_{02}$ where the quantity R_{01} can be explained as follows:

i. Suppose an individual who has recently become infected entering a previously uncontaminated environment at an equilibrium point. The anticipated count of viral cells generated by this individual, which then proceed to contaminate the environment, is roughly

$$R_{01} = \frac{N_h \alpha_h}{\mu_H (\mu_H + \delta_H)}. \tag{3.4.2.8}$$

By examining equation (3.4.2.8), it becomes obvious that the value of R_{01} depends upon the average viral load of *norovirus* within an infected individual denoted as N_h. This load is excreted into the physical environment at a rate α_h, subsequently rendering it infectious to others upon consumption of contaminated food containing the viral load. We regard N_h as a combined parameter that signifies the endemic level of within-human scale *norovirus* load B_h^*. This value has been previously determined through the within-human scale *norovirus* disease dynamics sub-model, as presented in Equation (3.3.1.1)). Hence, the value of R_{01} indicates the extent to which an infected individual can contribute to the propagation of the disease within the community throughout the entire duration of their infectiousness.

ii. Similarly the expression

$$R_{02} = \frac{\beta_H \Lambda_H}{\mu_V P_0} \tag{3.4.2.9}$$

can be understood as a newly viral infectious dose, introduced into a disease-free community. The anticipated number of individuals likely to be infected by these viral cells is associated with this equation. Consequently, these equations lead us to the conclusion that both the between-host transmission parameters and the within-human scale parameters collectively contribute to the persistence of the infection.

From the equation (3.4.2.9) representing the basic reproductive number for *norovirus* infection, we can deduce that it is influenced by both the within-human scale parameters and the between-host scale parameters. As a result, the findings emphasize that the within-human scale and macroscale aspects of *norovirus* infection mutually influence each other in a reciprocal manner.

3.4.3 Local stability of the disease-free equilibrium

In our scenario, a disease-free state corresponds to a situation where only susceptible humans are present. In this section, we assess the local stability of the disease-free equilibrium. This is accomplished by linearizing the equations of the nested multiscale model (3.4.0.10), which yields a Jacobian matrix. This matrix evaluated at the disease-free equilibrium state becomes.

$$J = \begin{bmatrix} -\mu_H & 0 & \dfrac{-\beta_H \Lambda_H}{P_0 \mu_H} \\ 0 & -(\delta_H + \mu_H) & \dfrac{\beta_H \Lambda_H}{P_0 \mu_H} \\ 0 & N_h \alpha_h & -\mu_V \end{bmatrix}. \tag{3.4.3.1}$$

We analyze the stability by computing the eigenvalues (λ_s) of the Jacobian matrix (3.4.3.1). The characteristic equation is expressed as:

$$(-\mu_H - \lambda)[\lambda^2 + \phi_1 \lambda + \phi_2] = 0. \tag{3.4.3.2}$$

From Equation (3.4.3.2), it is clear that one of the eigenvalues is ($\lambda = -\mu_H$). To draw conclusions about the stability of the disease-free equilibrium (DFE), the Routh-Hurwitz criteria [71] are employed. These criteria are used to determine the signs of the remaining eigenvalues of the polynomial in Equation (3.4.3.3).

$$P(\lambda) = \lambda^2 + \phi_1 \lambda + \phi_2, \tag{3.4.3.3}$$

where:

$$\begin{cases} \phi_1 &= \delta_H + \mu_H + \mu_V, \\ \phi_2 &= (\delta_H + \mu_H)\mu_V - \dfrac{N_h \alpha_h \beta_H \Lambda_H}{P_0 \mu_H}, \\ &= (\delta_H + \mu_H)\mu_V(1 - R_0). \end{cases} \tag{3.4.3.4}$$

By applying the Routh-Hurwitz stability criterion, the equilibrium state linked to the *norovirus* multiscale model system (3.4.0.10) achieves stability only when the determinants of all the Hurwitz matrices associated with the characteristic equation (3.4.3.3) are positive, that is $Det|H_j| > 0; j = 1, 2$. where

$$\det H_1 = \begin{pmatrix} \phi_1 \end{pmatrix} > 0, \quad H_2 = \begin{pmatrix} \phi_1 & 1 \\ 0 & \phi_2 \end{pmatrix} > 0. \tag{3.4.3.5}$$

When the Routh-Hurwitz criterion is applied to the expressions given in Equation (3.4.3.5), it requires that the following conditions must be met to ensure the local stability of the disease-free equilibrium point within the model system (3.4.0.10):

$$\begin{cases} \det(H_1) &= |\phi_1| \\ &= \phi_1 \\ &= \mu_C + \delta_C + \mu_V > 0 \end{cases} \tag{3.4.3.6}$$

To determine the determinant of H_2 we obtain

$$\begin{cases} \det H_2 &= \begin{vmatrix} \phi_1 & 1 \\ 0 & \phi_2 \end{vmatrix} \\ &= \phi_1 \phi_2 \\ &= (\mu_H + \delta_H + \mu_V)(\delta_H + \mu_V)\mu_V(1 - R_0) > 0, \end{cases} \tag{3.4.3.7}$$

Equation (3.4.3.7) provides a clearer view that the coefficients ϕ_1 and ϕ_2 of the polynomial $P(\lambda)$ in Equation (3.4.3.3) are both positive when $R_0 < 1$. Furthermore, it can be observed that the determinants of matrices H_1 and H_2 are positive if and only if $R_0 < 1$. Consequently, all the roots of the polynomial $p(\lambda)$ are either negative or possess negative real parts. Therefore, the theorem provided below offers a summary of the findings.

Theorem 3.1. *[72] The local asymptotic stability of the disease-free equilibrium point within the model system (3.4.0.10) is achieved when* $R_0 < 1$.

3.4.4 Global stability of the disease-free equilibrium

In this subsection, we assess the global stability of the disease-free equilibrium (DFE) within the nested model (3.4.0.10) by employing the next-generation operator, as introduced in [90]. The system (3.4.0.10) can be reformulated as follows

$$\begin{cases} \dfrac{dX}{dt} &= F(X,Y), \\ \\ \dfrac{dY}{dt} &= G(X,Y), \end{cases} \tag{3.4.4.1}$$

where $X = S_H$ signifies the count of uninfected cells, and $Z = (I_H, V_H)$ represents the quantities within the infected compartments and infectious classes. $U_0 = \left(\dfrac{\Lambda_H}{\mu_H}, 0, 0\right)$ corresponds to the disease-free equilibrium of the nested model. To establish the globally asymptotic stability, two conditions need to be met, as outlined in [91]:

H1. for $\dfrac{dX}{dt} = F(X,0)$ is globally asymptotically stable ,

H2. $G(X,Z) = AZ - \hat{G}(X,Z)$, $\hat{G}((X,Z) \geq 0$ for $(X,Z) \in \mathbb{R}^3_+$ where $A = D_Z G(X^*, 0)$ is an M-matrix and $\mathbb{R}^3_+$ is the region where the model have a biological meaning.

Therefore in our case

$$F(X,0) = \begin{bmatrix} \Lambda_H - \mu_H S_H \end{bmatrix}, \tag{3.4.4.2}$$

and matrix A given by

$$A = \begin{bmatrix} -(\delta_H - \mu_H) & \dfrac{\beta_H \Lambda_H}{P_0 \mu_H} \\ \\ N_h \alpha_h & -\mu_V \end{bmatrix} \tag{3.4.4.3}$$

and

$$\hat{G}(X,Z) = \begin{bmatrix} \left(\dfrac{\Lambda_H}{P_0\mu_H} - \dfrac{S_H}{P_0+V_H}\right)\beta_H V_H \\ \\ 0 \end{bmatrix} \tag{3.4.4.4}$$

Since $\dfrac{\Lambda_H}{P_0\mu_H} \geq \dfrac{S_H}{P_0+P_H}$ it is clear that $\hat{G}(X,Z) \geq 0$ for all $(X,Z) \in \mathbb{R}^3_+$. It's clear that

A qualifies as an M-matrix due to the non-negative nature of its off-diagonal elements.

3.4.5 Existence and uniqueness of the endemic equilibrium state

At the endemic state, humans become acutely infected. Let $E^* = (S_H^*, I_H^*, V_H^*)$ refers to the endemic equilibrium point of the model system (3.4.0.10). Equating the left-hand side of the system of equations to zero and determination of the nontrivial solution of the resulting algebraic equations results in the following:

$$E^* = \begin{cases} S_H^* &= \dfrac{\mu_V P_0(\delta_H+\mu_H)(\beta_H+\mu_H) + \mu_H\mu_V P_0(\delta_H+\mu_H)(R_0-1)}{(\beta_H+\mu_H)\beta_H N_h\alpha_h}, \\ \\ I_H^* &= \dfrac{\mu_H\mu_V P_0(R_0-1)}{N_h\alpha_h(\beta_H+\mu_H}, \\ \\ V_H^* &= \dfrac{\mu_H P_0(R_0-1)}{(\beta_H+\mu_H)}, \\ \\ R_0 &= \dfrac{N_h\alpha_h\beta_h\Lambda_H}{(\delta_H+\mu_H)P_0\mu_H\mu_V}. \end{cases} \tag{3.4.5.1}$$

Based on the system (3.4.5.1), our conclusion is that it can be deduced that a unique endemic equilibrium point exists for the *norovirus* nested multiscale model when $R_0 > 1$. Additionally, we deduce that the expressions for the between-host scale endemics, denoted as S_H^*, I_H^*, V_H^*, are determined by a combination of within-human scale disease parameters and between-host scale parameters. Hence, the findings also emphasise that there exists a reciprocal influence between the within-human scale and macroscale aspects.

3.4.6 Local Stability of the Endemic Equilibrium

In this subsection, we assess the local stability of the endemic steady state within the model system (3.4.0.10) using the center manifold theory as outlined in [73].

In case of *norovirus*, the theorem is applied through change of variables as follows: we let $S_H = x_1, I_H = x_2, V_H = x_3$. Furthermore, we let $\phi = \beta^*$, where β^* is regarded as the bifurcation parameter. If we consider $R_0 = 1$ and we solve for β^*

$$1 = \frac{N_h \alpha_h \beta^* \Lambda_H}{P_0 \mu_H (\mu_H + \delta_H) \mu_V}, \tag{3.4.6.1}$$

and hence

$$\beta^* = \frac{P_0 \mu_H \mu_V (\delta_H + \mu_H)}{N_h \alpha_h \Lambda_H}. \tag{3.4.6.2}$$

By employing vector notation $\mathbf{x} = (x_1, x_2, x_3)^T$, we can re-write the model system (3.4.0.10) as follows:

$$\frac{d\mathbf{x}}{dt} = \mathbf{F}(\mathbf{x}, \beta^*), \tag{3.4.6.3}$$

where

$$\mathbf{F} = (f_1, f_2, f_3). \tag{3.4.6.4}$$

So that

$$\begin{cases} \dot{x_1} = f_1 = \Lambda_H - \dfrac{\beta^* x_1 x_3}{P_0 + x_3} - \mu_H x_1, \\ \dot{x_2} = f_2 = \dfrac{\beta^* x_1 x_3}{P_0 + x_3} - (\mu_H + \delta_H) x_2, \\ \dot{x_3} = f_3 = N_h \alpha_h x_2 - \mu_V x_3. \end{cases} \tag{3.4.6.5}$$

Upon linearizing the above model system, we proceed to derive the Jacobian matrix for the system, resulting in:

$$J = \begin{bmatrix} -\mu_H & 0 & -\dfrac{\beta^* \Lambda_H}{\mu_H P_0} \\ 0 & -(\mu_H + \delta_H) & \dfrac{\beta^* \Lambda_H}{\mu_H P_0} \\ 0 & N_h \alpha_h & -\mu_V \end{bmatrix}. \tag{3.4.6.6}$$

The Jacobian matrix of the model system (3.4.0.10) has the right eigenvector $\mathbf{v} = (v_1, v_2, v_3)^T$, where

$$\begin{cases} u_1 = \dfrac{\beta^* \Lambda_H N_h \alpha_h}{\mu_H P_0}, \\ u_2 = 1, \\ u_3 = \dfrac{N_h \alpha_h}{\mu_V}. \end{cases} \tag{3.4.6.7}$$

and the corresponding left eigenvector denoted as $\mathbf{u} = (v_1, v_2, v_3)$, where

$$\begin{cases} v_1 = 0, \\ v_2 = 1, \\ v_3 = \dfrac{N_h \alpha_h}{(\mu_H + \delta_H)}. \end{cases} \tag{3.4.6.8}$$

To determine the sign of a, we use the non-zero second order mixed derivatives of $\mathbf{F}$ with respect to each variable as:

$$\begin{cases} \dfrac{\partial^2 f_1}{\partial x_3^2} = \dfrac{2\beta^* \Lambda_H}{P_0^2 \mu_H}, \\ \dfrac{\partial^2 f_2}{\partial x_3^2} = -\dfrac{2\beta^* \Lambda_H}{P_0^2 \mu_H}. \end{cases} \tag{3.4.6.9}$$

To determine the sign of b, we employ the non-zero partial derivatives concerning each variable and β^*, which is expressed as:

$$\begin{cases} \dfrac{\partial^2 f_1}{\partial x_3 \partial \beta^*} &= -\dfrac{\Lambda_H}{\mu_H P_0}, \\ \dfrac{\partial^2 f_2}{\partial x_3 \partial \beta^*} &= \dfrac{\Lambda_H}{\mu_H P_0}. \end{cases} \tag{3.4.6.10}$$

Substituting Equations (3.4.6.7), (3.4.6.8), (3.4.6.9) and (3.4.6.10) in expressions a and b in (2.4.1.11), respectively, we get

$$\begin{cases} a &= v_1(u_3)^2 \left(\dfrac{\partial^2 f_1}{\partial x_3^2}\right) + v_2(u_3)^2 \left(\dfrac{\partial^2 f_2}{\partial x_3^2}\right), \\ &= \left(\dfrac{2\beta^* \Lambda_H}{P_0^2 \mu_H} u_1 (v_3)^2\right) + \left(\dfrac{-2\beta^* \Lambda_H}{P_0^2 \mu_H} u_2 (v_3)^2\right), \\ &= \left(\dfrac{2\beta^* \Lambda_H}{P_0^2 \mu_H} v_3 (u_1 - u_2)\right) < 0. \end{cases} \tag{3.4.6.11}$$

Since $u_1 - u_2 < 0$ and also

$$\begin{cases} b &= u_1 v_3 \left(\dfrac{\partial^2 f_1}{\partial x_3 \partial \beta^*}\right) + u_2 v_3 \left(\dfrac{\partial^2 f_2}{\partial x_3 \partial \beta^*}\right), \\ &= \left(\dfrac{-\Lambda_H}{P_0 \mu_H} u_1 v_3\right) + \left(\dfrac{\Lambda_H}{P_0 \mu_H} u_1 v_3\right), \\ &= \left(\dfrac{2\beta^* \Lambda_H}{P_0^2 \mu_H} v_3 (u_2 - u_1)\right) < 0. \end{cases} \tag{3.4.6.12}$$

Because $u_2 - u_1 > 0$, it follows that $a < 0$ and $b > 0$. Taking into account the principles of Center Manifold Theory as outlined in item (iv), we conclude that the endemic steady state within the model system (3.4.0.10) is locally asymptotically stable. This stability holds for values of R_0 greater than 1, but in close proximity to 1. For a complete presentation of these findings, refer to [72], where the following theorem summarizes the outcomes.

Theorem 3.2. *The endemic steady state of norovirus multiscale model (3.4.0.10) supported by Center Manifold Theory is locally asymptotically stable for $R_0 > 1$ near 1.*

3.4.7 Global Stability of the Endemic Equilibrium Point

In this section, we establish the global asymptotic stability of the endemic equilibrium E^* within the model system (3.4.0.10), hence we present the following theorem:

Theorem 3.3. *[74] The Endemic Equilibrium E^* of the model system (3.4.0.10) is global asymptotically stable (GAS) whenever $R_0 > 1$.*

Proof. We shall consider a Lyapunov function of the Volterra type denoted as: $L(S_H, I_H, V_H)$, as well as the function $\phi(x) = x - 1 - \ln(x)$. Therefore

$$\begin{aligned} L_1 &= L(S_H, I_H, V_H), \\ &= a_1 S_H^* \phi\left(\frac{S_H}{S_H^*}\right) + a_2 I_H^* \phi\left(\frac{I_H}{I_H^*}\right) + a_3 V_H^* \phi\left(\frac{B_H}{B_H^*}\right), \qquad (3.4.7.1) \\ &= a_1 S_H^* \left[\frac{S_H}{S_H^*} - 1 - ln\frac{S_H}{S_H^*}\right] + a_2 I_H^* \left[\frac{I_H}{I_H^*} - 1 - ln\frac{I_H}{I_H^*}\right] + a_3 V_H^* \left[\frac{V_H}{V_H^*} - 1 - ln\frac{V_H}{V_H^*}\right]. \end{aligned}$$

The derivation of L_1 and substitution yield:

$$\begin{aligned} \dot{L}_1 &= a_1 \frac{dS_H}{dt}\left[1 - \frac{S_H^*}{S_H}\right] + a_2 \frac{dI_H}{dt}\left[1 - \frac{I_H^*}{I_H}\right] + \\ &\quad a_3 \frac{dV_H}{dt}\left[1 - \frac{V_H^*}{V_H}\right], \qquad (3.4.7.2) \\ &= a_1 \left[1 - \frac{S_H^*}{S_H}\right][\Lambda_H - \lambda_H S_H - \mu_H S_H] + a_2 \left[1 - \frac{I_H^*}{I_H}\right][\lambda_H S_H - (\mu_H + \delta_H) I_H] \\ &\quad + a_3 \left[1 - \frac{V_H^*}{V_H}\right][N_h \alpha_h I_H - \alpha_h V_H]. \end{aligned}$$

The following relations holds at the endemic equilibrium point of the model system (3.4.0.10)

$$\begin{cases} \Lambda_H = \lambda_H^* S_H^* + \mu_H S_H^*, \\ (\mu_H + \delta_H) = \dfrac{\lambda_H^* S_H^*}{I_H^*}, \\ \mu_V = \dfrac{N_h \alpha_h I_H^*}{V_H^*}. \end{cases} \qquad (3.4.7.3)$$

Substituting the relations in Equation (3.4.7.3), and rearranging, $\dot{L}_1$ becomes

$$\begin{aligned}
\dot{L}_1 &= a_1\left[1-\frac{S_H^*}{S_H}\right]\left[\lambda_H^* S_H^* + \mu_H S_H^* - \lambda_H S_H - \mu_H S_H\right] \\
&\quad + a_2\left[1-\frac{I_H^*}{I_H}\right]\left[\lambda_H S_H - \frac{\lambda_H^* S_H^* I_H}{I_H^*}\right] \\
&\quad + a_3\left[1-\frac{V_H^*}{V_H}\right]\left[N_h\alpha_h I_H - \frac{N_h\alpha_h I_H^* V_H}{B_H^*}\right], \\
&= -\mu_H S_H a_1\left[1-\frac{S_H^*}{S_H}\right]^2 + a_2\left[\lambda_H^* S_H^* - \lambda_H S_H S_H - \frac{\lambda_H^* S_H^* S_H^*}{S_H} + \frac{\lambda_H S_H S_H^*}{S_H}\right] \\
&\quad + a_2\left[\lambda_H S_H - \frac{\lambda_H^* S_H^* I_H^*}{I_H} - \frac{\lambda_H S_H I_H^*}{I_H} + \lambda_H^* S_H^*\right] - a_3\left[N_h\alpha_h I_H - \frac{N_h\alpha_h I_H^* V_H}{V_H^*} + \hat{N}_h\alpha_h I_H^*\right]. \\
&= -\mu_H S_H a_1\left[1-\frac{S_H^*}{S_H}\right]^2 + \lambda_H^* S_H^*(a_1+a_2) + \lambda_H S_H(a_2-a_1) \\
&\quad + I_H\left[a_3 N_h\alpha_h - \frac{a_2\lambda_H^* S_H^*}{I_H^*}\right] - \frac{a_2\lambda_H S_H I_H^*}{I_H} \\
&\quad - \frac{a_3 N_h\alpha_h I_H^* V_H}{V_H^*} + a_3 N_h\alpha_h I_H.
\end{aligned} \tag{3.4.7.4}$$

We let $a_1 = a_2 = 1$ and we also choose a_3 such that

$$\begin{cases} a_1 = a_2 = 1, \\ a_3\hat{N}_h\alpha_h - \dfrac{a_2\lambda_H^* S_H^*}{I_H^*} = 0, \\ a_3 = \dfrac{\lambda_H^* S_H^*}{N_h\alpha_h I_H^*}, \end{cases} \tag{3.4.7.5}$$

which gives:

Substituting Equation (3.4.7.5) in Equation (3.4.7.4)

$$\begin{aligned}\dot{L}_1 &= \left[1-\frac{S_H^*}{S_H}\right][\lambda_H^* S_H^* + \mu_H S_H^* - \lambda_H S_H - \mu_H S_H] + \left[1-\frac{I_H^*}{I_H}\right][\lambda_H S_H - \lambda_H^* S_H^* \frac{I_H}{I_H^*}] \\ &\quad + \left(\frac{\lambda_H^* S_H^*}{N_h \alpha_h I_H^*}\right)\left[1-\frac{V_H^*}{V_H}\right]\left[N_h \alpha_h I_H - N_h \alpha_h I_H^* \frac{B_H}{B_H^*}\right]. \\ &= -\mu_H S_H \left(1-\frac{S_H^*}{S_H}\right)^2 + \lambda_H^* S_H^* \left(1-\frac{S_H^*}{S_H}\right)\left(1-\frac{\lambda_H S_H}{\lambda_H^* S_H^*}\right) + \\ &\quad \lambda_H^* S_H^* \left(1-\frac{I_H^*}{I_H^*}\right)\left[\frac{\lambda_H S_H}{\lambda_H^* S_H^*} - \frac{I_H}{I_H^*}\right] \\ &\quad + \lambda_H^* S_H^* \left(1-\frac{V_H^*}{V_H}\right)\left(\frac{I_H}{I_H^*} - \frac{V_H}{V_H^*}\right). \end{aligned} \tag{3.4.7.6}$$

Expand Equation (3.4.7.6)

$$\begin{aligned}\dot{L}_1 &\leq \lambda_H^* S_H^* \left(1-\frac{S_H^*}{S_H}\right)\left(1-\frac{\lambda_H S_H}{\lambda_H^* S_H}\right) \\ &\quad + \lambda_H^* S_H^* (1-\frac{I_H^*}{I_H})[\frac{\lambda_H S_H}{\lambda_H * S_H^*} - \frac{I_H}{I_H^*}] \\ &\quad + \lambda_H^* S_H^* \left(1-\frac{V_H^*}{V_H}\right)\left(\frac{I_H}{I_H^*} - \frac{V_H}{V_H^*}\right), \\ &\leq \lambda_H^* S_H^* \left[1 - \frac{\lambda_H S_H}{\lambda_H^* S_H^*}\frac{S_H^*}{S_H} + \frac{\lambda_H}{\lambda_H^*}\right] + \lambda_H^* S_H^* \left[\frac{\lambda_H S_H}{\lambda_H^* S_H^*} - \frac{I_H}{I_H^*} - \frac{\lambda_H S_H I_H^*}{\lambda_H^* S_H^* I_H} + 1\right] \\ &\quad \lambda_H^* S_H^* \left[\frac{I_H}{I_H^*} - \frac{V_H}{V_H^*} - \frac{V_H^* I_H}{V_H I_H^*} + 1\right]. \end{aligned} \tag{3.4.7.7}$$

From Equation (3.4.7.7) we obtain

$$\begin{aligned}\dot{L}_1 &\leq \lambda_H^* S_H^* \left[2 - \frac{S_H^*}{S_H} - \frac{I_H}{I_H^*} + \frac{\lambda_H}{\lambda_H^*} - \frac{\lambda_H S_H I_H^*}{\lambda_H^* S_H^* I_H}\right] \\ &\quad + \lambda_H^* S_H^* \left[1 + \frac{I_H}{I_H^*} - \frac{V_H}{V_H^*} - \frac{V_H^* I_H}{V_H I_H^*}\right]. \end{aligned}$$

Making x the subject of the formula from $\phi(x) = x - 1 - ln(x)$, we have $x = \phi(x) + 1 + ln(x)$ such that:

$$\begin{aligned}\dot{L}_1 \leq\ & \lambda_H^* S_H^* \Bigg[2 - \phi\frac{S_H^*}{S_H} - 1 - lnS_H^* S_H - \frac{I_H}{I_H^*} + \frac{\lambda_H}{\lambda_H^*} \\ & -\phi\left(\frac{\lambda_H S_H I_H^*}{\lambda_H^* S_H^* I_H}\right) - 1 - ln\frac{\lambda_H S_H I_H^*}{\lambda_H^* S_H^* I_H}\Bigg] \\ & +\lambda_H^* S_H^* \left[1 + \frac{I_H}{I_H^*} - \frac{V_H}{V_H^*} - \phi\left(\frac{V_H^* I_H}{V_H I_H^*}\right) - 1 - ln\left(\frac{V_H^* I_H}{V_H I_H^*}\right)\right]\end{aligned} \tag{3.4.7.8}$$

After simplifying Equation (3.4.7.8), we obtain:

$$\begin{aligned}\dot{L}_1 \leq\ & \lambda_H^* S_H^* \Bigg[- \phi\frac{S_H^*}{S_H} - \frac{I_H}{I_H j} - \phi\left(\frac{V_H^* I_H}{V_H I_H^*}\right) - \ln\left(\frac{I_H}{I_H^*}\right) \\ & - \ln\frac{V_H}{V_H^*} + ln\frac{V_0 + V_H}{V_0 + V_H^*} + \frac{\lambda_H}{\lambda_H^*}\Bigg] \\ & +\lambda_H^* S_H^* \left[\frac{I_H}{I_H^*} - \frac{V_H}{V_H^*} - \phi\left(\frac{V_H^* I_H}{V_H I_H^*}\right) - \ln\frac{I_H}{I_H^*} + \ln\frac{V_H}{V_H^*}\right], \\ \leq\ & \lambda_H^* S_H^* \Bigg[- \phi\left(\frac{S_H^*}{S_H}\right) - \frac{I_H}{I_H^*} - \phi\left(\frac{\lambda_H S_H I_H^*}{\lambda_H^* S_H * I_H}\right) \\ & + \ln\left(\frac{I_H}{I_H^*}\right) - \ln\left(\frac{V_H}{V_H^*}\right) + \ln\left(\frac{V_0 + V_H}{V_0 + V_H^*}\right) \\ & + \ln\frac{\lambda_H}{\lambda_H^*}\Bigg] + \lambda_H^* S_H^* \left[\frac{I_H}{I_H^*} - \frac{V_H}{V_H^*} - \phi\left(\frac{V_H^* I_H}{V_H I_H^*}\right) - \ln\left(\frac{I_H}{I_H^*}\right) + \ln\left(\frac{V_H}{V_H^*}\right)\right].\end{aligned} \tag{3.4.7.9}$$

If we put $I_H = I_H^*$ and $V_H = V_H^*$, we get:

$$\begin{aligned}
\dot{L}_1 \leq\ & \lambda_H^* S_H^* \Bigg[-\phi\left(\frac{S_H^*}{S_H}\right) - \phi\left(\frac{\lambda_H S_H I_H^*}{\lambda_H^* S_H^* I_H}\right) + \ln\left(\frac{I_H}{I_H^*}\right) \\
& - \ln\left(\frac{V_H}{V_H^*}\right) - \frac{V_H}{V_H^*} \\
& + \frac{V_H}{V_H^*} - \phi\left(\frac{V_0 + V_H}{V_0 + V_H^*}\right) + \frac{V_0 + V_H}{V_0 + V_H^*} + \frac{V_H(V_0 + V_H^*)}{V_H^*(V_0 + V_H)} - 1 \Bigg] \\
& \lambda_H^* S_H^* [-\phi(\frac{V_H^* I_H}{V_H I_H^*}) + \frac{I_H}{I_H^*} - \frac{V_H}{V_H^*} - \ln(\frac{I_H}{I_H^*}) + \ln\left(\frac{V_H}{V_H^*}\right)\Bigg], \\
\leq\ & \lambda_H^* S_H^* \Bigg[-\phi\left(\frac{\lambda_H S_H I_H^*}{\lambda_H^* S_H^* I_H}\right) - \phi\left(\frac{S_H^*}{S_H}\right) - \frac{I_H}{I_H^*} + \ln\left(\frac{I_H}{I_H^*}\frac{V_H}{V_H^*}\right) - \ln\left(\frac{V_H}{V_H^*}\right) \Bigg] \\
& + \lambda_H^* S_H^* \left[\frac{V_H(V_0 + V_H^*)}{V_H^*(V_0 + V_H)} + \frac{V_0 + V_H}{V_0 + V_H^*} - \phi\left(\frac{V_0 + V_H}{V_0 + V_H^*}\right) - \frac{V_H}{V_H^*} - 1 \right] \\
& \lambda_H^* S_H^* \left[-\phi\left(\frac{V_H^* I_H}{V_H I_H^*}\right) + \frac{I_H}{I_H^*}\frac{V_H}{V_H^*} - \ln\left(\frac{I_H}{I_H^*}\right) + \ln\left(\frac{V_H}{V_H^*}\right)\right], \\
\leq\ & \lambda_H^* S_H^* \left[\frac{V_H}{V_H^*} - \frac{I_H}{I_H^*} + \ln\left(\frac{I_H}{I_H^*}\right) \right. \\
& \left. - \ln\frac{V_H}{V_H^*} \right] + \lambda_H^* S_H^* \left[\frac{I_H}{I_H^*} - \frac{V_H}{V_H^*} + \ln\left(\frac{V_H^*}{V_H}\right) \right] + \lambda_H^* S_H^* \left[\frac{I_H}{I_H^*} - \frac{V_H}{V_H^*} - \ln\left(\frac{I_H}{I_H^*}\right) \right], \\
=\ & 0.
\end{aligned} \tag{3.4.7.10}$$

□

From (3.4.7.10), we have that the largest invariant subset, where $\dot{L} = 0$ is E^* Therefore, we conclude from the LaSelle's Invariance Principle that E^* is globally asymptotically stable (GAS) when $R_0 > 1$.

3.5 Sensitivity Analysis

In this section, we provide an analysis of the model system's sensitivity (3.4.0.10), employing the parameter values outlined in the table labeled as Table 3.3. Very little on *norovirus* mathematical

modelling was done, therefore, it is not easy to find parameter values from the literature, hence some parameter values are estimated:

Variable	Variable Description	Initial value	Source
Λ_H	Supply rate of recruited humans	0.05	Assumed
N_e	Number of viruses produced through replication	100	Assumed
β_H	Infection rate of humans	0.075	[79]
μ_H	Natural death rate of humans	0.0018	[80]
δ_H	Induced death rate of humans	0.076	Assumed
α_h	Shedding rate of *norovirus*	0.05	[79]
μ_V	Natural decay rate of *norovirus*	0.0667	[80]
α_e	Viral replication rate on the site of infection	0.4	[92]
ϕ_t	Decay rate pathogens in the within due to immune cells	0.006	[92]
μ_h	Natural death rate of pathogens in the within	0.01	Assumed
Λ_e	Supply rate of epithelial cells	0.07	Assumed
β_e	Infection rate of susceptible epithelial cells	0.01	[92]
μ_e	Natural death rate of epithelial cells	0.1	[92]
Λ_c	Supply rate of immune cells	0.09	Assumed
ρ_c	Immune activation rate	0.1	[92]
μ_c	Natural death rate of immune cells	0.3	[92]

Table 3.3: Model parameter values

We evaluate the relative change in two transmission metrics (R_0) and (V_H^*) for *norovirus* derived from the nested multiscale model (3.4.0.10) using the sensitivity analysis technique. The analysis is conducted using a combination of Latin Hypercube Sampling and partial rank correlation coefficients (PRCCs) as applied in the previous chapter. For each run, we conduct 1000 simulations to investigate how individual model parameters impact both the basic reproduction numbers (R_0) and the endemic value of the environmental viral load (V_H^*).

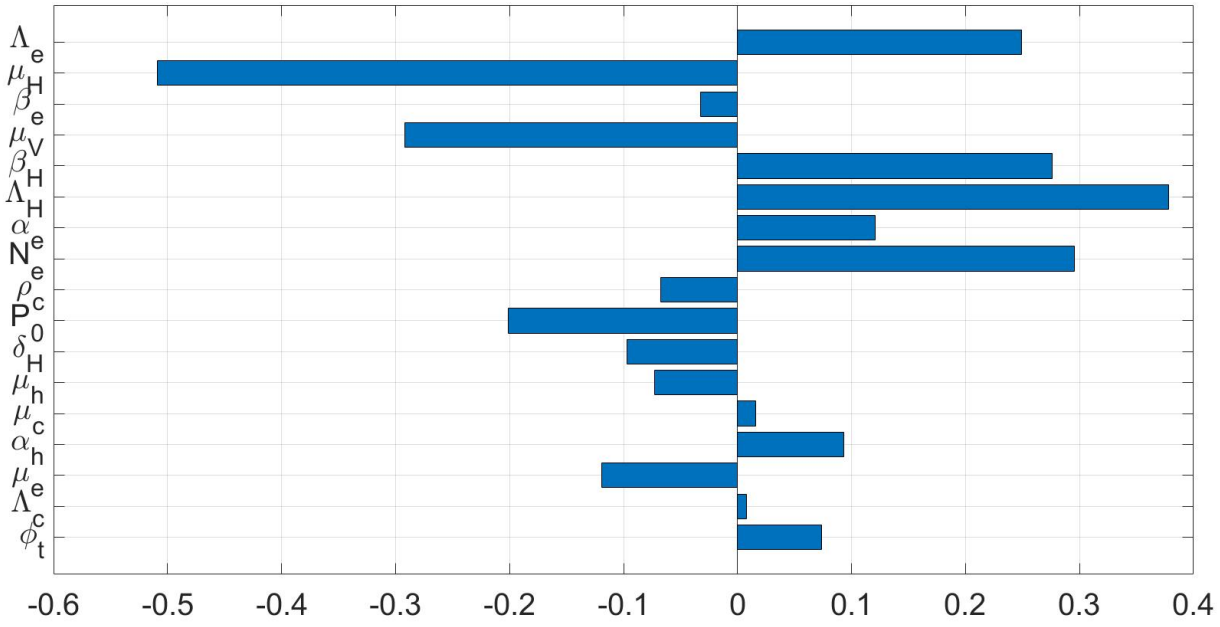

Figure 3.2: Tornado plot of partial rank correlation coefficients (PRCCs) of all the model parameters that influence the viral transmission metric R_0

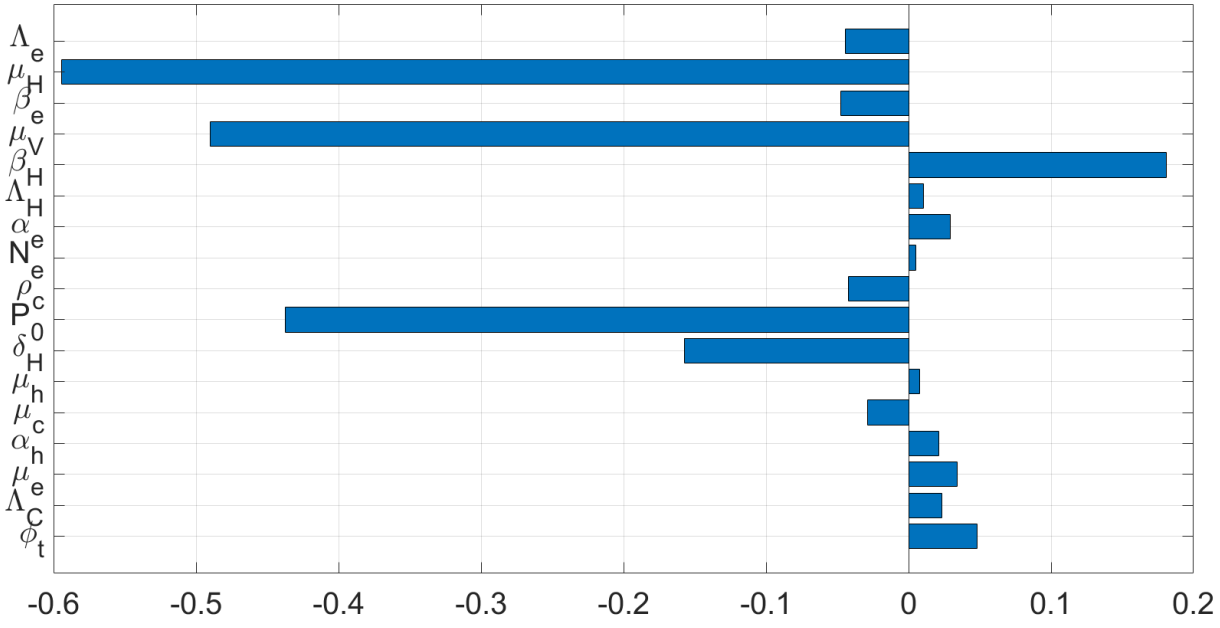

Figure 3.3: Tornado plot of partial rank correlation coefficients (PRCCs) of all the model parameters that influence the viral transmission metric V_H^*

Figures 3.2 and 3.3 present the degree of sensitivity of each parameter on the two *norovirus* transmission metrics to the model parameters to be considered for a sensitivity analysis of the multiscale model (3.4.0.10). Figure 3.2 presents the degree of sensitivity of each parameter on R_0, using parameter values in Table 3.3. The most sensitive parameters at within-human scale are $\Lambda_e, \alpha_e, N_e, \alpha_h, \rho_c$, and μ_h, while the most sensitive parameters at between-host scale are μ_V, β_H and P_0. This suggests that during the initial stages of a *norovirus* infection, special attention should be given to ensuring the precision of the three between-host parameters as well as the six within-human scale parameters when implementing interventions.

Figure 3.3 presents sensitivity analysis to V_H^*, which is found to be much more sensitive to μ_V, β_H, and P_0 parameters that are similar to R_0. Additionally, R_0 and V_H^* both show notable sensitivity to both μ_H (the natural mortality rate of people) and δ_H (the death rate brought on by sickness). This indicates that when *norovirus* infection is endemic, interventions like vaccinations that lessen susceptibility of humans to infection, and also hinder *norovirus* replication at the level of individual humans are likely to have the greatest positive effects on reducing the spread of *norovirus* infection in the community.

In general, these discoveries necessitate that enhancing the reliability and applicability of the multiscale model (3.4.0.10) relies on ensuring the exactness of these parameters during the data collection process. Furthermore, these parameters serve as crucial factors for effective *norovirus* infection management throughout the pathogen's replication-transmission cycle, which should be considered and managed during outbreak at a host-level.

3.6 Construction of NSFD scheme

The method for developing the model (3.4.0.10) is established by employing Micken's approaches, similar to what we did in **Chapter 2**, we use the symbols S_H^k, I_H^k, and V_H^k to represent the estimated values of $S_H(kh)$, $I_H(kh)$, and $V_H(kh)$ respectively, for values of for $k = 0, 1, 2, ...$, and with a constant h representing the time step of the scheme where $h > 0$. For the sequences S_H^k, I_H^k and V_H^k to be consistent with the model's biological nature, the equations should be nonnegative [93]. The objective of formulating the numerical scheme for solving

system (3.4.0.10) is to derive positive approximations through the following procedure:

$$\begin{cases} 1.\ \dfrac{S_H^{k+1}-S_H^k}{\phi_1(h)} = \Lambda_H - \dfrac{\beta_H S_H^{k+1} V_H^k}{P_0+V_H^k} - \mu_H S_H^{k+1}, \\ 2.\ \dfrac{I_H^{k+1}-I_H^k}{\phi_2(h)} = \dfrac{\beta_H S_H^{k+1} V_H^k}{P_0+V_H^k} - (\delta_H+\mu_H) I_H^{k+1}, \\ 3.\ \dfrac{V_H^{k+1}-V_H^k}{\phi_3(h)} = N_h \alpha_h I_H^{k+1} - \mu_V V_H^{k+1}. \end{cases} \tag{3.6.1}$$

Below are the denominator functions considered in this study:

$$\begin{cases} \phi_1(h) = \dfrac{e^{h\mu_H}-1}{\mu_H}, \\ \phi_2(h) = \dfrac{e^{h(\mu_H+\delta_H)}-1}{\mu_H+\delta_H}, \\ \phi_3(h) = \dfrac{e^{h\mu_V}-1}{\mu_V}. \end{cases}$$

Rearranging (3.6.1) we obtain the following expicit scheme

$$\begin{cases} 1.\ S_H^{k+1} = \dfrac{\phi_1(h)\Lambda_H + S_H^k}{1+\phi_1(h)\left[\frac{\beta_H V_H^k}{P_0+V_H^k}+\mu_H\right]}, \\ 2.\ I_H^{k+1} = \dfrac{I_H^k + \phi_2(h)\left[\frac{\beta_H V_H^k S_H^{k+1}}{P_0+V_H^k}\right]}{1+\phi_2(h)(\delta_H+\mu_H)}, \\ 3.\ V_H^{k+1} = \dfrac{\phi_3(h) N_h \alpha_h I_H^{k+1} + V_H^k}{1+\phi_3(h)\mu_V}. \end{cases} \tag{3.6.2}$$

Clearly, from Equation (3.6.2), if the initial conditions $S_H(0)$, $I_H(0)$, and $V_H(0)$ are non-negative, it follows that the right-hand side of Equation (3.6.2) does not contain any negative terms for any value of k. This observation consequently establishes the positiveness of the solution for the NSFD method given by Equation (3.6.2).

3.6.1 The Equilibrium Points

The equilibrium points of the numerical scheme are established by equating S_H^{k+1} to S_H^k, I_H^{k+1} to I_H^k, and V_H^{k+1} to V_H^k.

$$\begin{cases} 1.\ S_H^k &= \dfrac{\phi_1(h)\Lambda_H + S_H^k}{1+\phi_1(h)\left[\frac{\beta_H V_H^k}{P_0+V_H^k}+\mu_H\right]}, \\ 2.\ I_H^k &= \dfrac{I_H^k + \phi_2(h)\left[\frac{\beta_H V_H^k S_H^{k+1}}{P_0+V_H^k}\right]}{1+\phi_2(h)(\delta_H+\mu_H)}, \\ 3.\ V_H^k &= \dfrac{\phi_3(h)N_h\alpha_h I_H^{k+1} + V_H^k}{1+\phi_3(h)\mu_V}, \end{cases} \tag{3.6.1}$$

Through algebraic manipulation, we derive two equilibrium points that can be described as follows: $E^0 = \left(\dfrac{\Lambda_H}{\mu_H}, 0, 0\right)$ and $E^* = S_H^*, I_H^*, V_H^*$ with

$$E^* = \begin{cases} S_H^* &= \dfrac{\mu_V P_0(\delta_H+\mu_H)(\beta_H+\mu_H) + \mu_H\mu_V P_0(\delta_H+\mu_H)(R_0-1)}{(\beta_H+\mu_H)\beta_H N_h\alpha_h}, \\ I_H^* &= \dfrac{\mu_h\mu_V P_0(R_0-1)}{N_h\alpha_h(\beta_h+\mu_h)}, \\ V_H^* &= \dfrac{\mu_H P_0(R_0-1)}{(\beta_H+\mu_H)}, \end{cases} \tag{3.6.2}$$

where, E^0 represents the disease-free equilibrium, while E^* corresponds to the endemic equilibrium. It is important to highlight that the equilibrium points of the discrete model correspond with those of the continuous model (3.4.0.10), and independent of the parameter, ϕ_h. In the next subsection, we proceed to perform a stability analysis for these equilibrium points.

3.6.2 Stability of the equilibrium points

The stability characteristics of the fixed points in the system (3.6.1) have been assessed using the Jacobian matrix concept, as detailed in [76]. For simplicity, we introduce the following function:

$$\begin{cases} f_1(S_H, I_H, V_H) &= \dfrac{S_H^k + \phi_1(h)\Lambda_H(P_0 + V_H^k)}{a_3 V_H^k + a_1 P_0}, \\ f_2(S_H, I_H, V_H) &= \dfrac{I_H^k(a_3 V_H^k + a_1 P_0) + \phi_2(h)\beta_H V_H^k[S_H^k + \phi_1(h)\Lambda_H]}{a_2(a_3 V_H^k + a_1 P_0)}, \\ f_3(S_H, I_H, V_H) &= \dfrac{a_2 a_3 V_H^{k^2} + V_H^k b_0 I_H^k + \phi_2(h)\beta_H(S_H^k + \phi_1(h)\Lambda_H) + I_H^k}{a_2 a_4(a_3 V_H^k + a_1 P_0)}, \end{cases}$$

where

$$\begin{cases} a_1 &= 1 + \mu_h \phi_1(h), \\ a_2 &= 1 + \phi_2(h)(\delta_H + \mu_H), \\ a_3 &= a_1 + \beta_H \phi_1(h), \\ a_4 &= a_1 + \beta_H \phi_1(h), \end{cases}$$

we proceed to formulate the Jacobian matrix in the following way:

$$J = \begin{bmatrix} J_{11} & J_{12} & J_{13} \\ J_{21} & J_{22} & J_{23} \\ J_{31} & J_{32} & J_{33} \end{bmatrix} \tag{3.6.1}$$

where

$$\begin{cases} J_{11} &= \dfrac{P_0 + V_H^k}{a_3 V_H^k + a_1 P_0}, \\ J_{12} &= 0, \\ J_{13} &= \dfrac{(S_H^k + \phi_1(h)\Lambda_H)(a_1 - a_3)P_0}{(a_3 V_H^k + a_1 P_0)^2}, \\ J_{21} &= \dfrac{\phi_2(h)\beta_H V_H^k}{a_2(a_3 V_H^k + a_1 P_0)}, \\ J_{22} &= \dfrac{a_3 V_H^k + a_1 P_0}{a_2(a_3 V_H^k + a_1 P_0)}, \\ J_{23} &= \dfrac{a_1 P_0 \phi_2(h)\beta_H(S_H^k + \phi_1(h))\Lambda_H}{a_2(a_3 V_H^k + a_1 P_0)^2}, \\ J_{31} &= \dfrac{\phi_2(h)\beta_H V_H^k}{a_2 a_4(a_3 V_H^k + a_1 P_0)}, \\ J_{32} &= \dfrac{\phi_3(h) N_h \alpha_h}{a_2 a_4}, \\ J_{33} &= \dfrac{b_3(a_3 V_H^k + a_1 P_0)V_H^k + b_4(a_3 V_H^k + a_1 P_0) + b_5(S_H^k + \phi_1(h)\Lambda_H)}{a_2^2 a_4^2(a_3 V_H^k + a_1 P_0)^2}. \end{cases}$$

where

$$\begin{cases} b_3 &= a_2^2 a_3 a_4, \\ b_4 &= a_1 a_2^2 a_4 P_0, \\ b_5 &= a_1 a_2 a_4 P_0 \phi_2(h)\beta_H. \end{cases}$$

If the absolute value of the eigenvalues is less than one, then the NSFDS converges to the equilibrium points [47].

3.6.3 The stability of the disease-free equilibrium

In this subsection, we demonstrate the stability of the disease-free equilibrium, denoted as E^0. By substituting the disease-free equilibrium E^0 into the Jacobian matrix, we have the following:

$$J(E^0) = \begin{bmatrix} \frac{1}{a_1} & 0 & \frac{\Lambda_H(a_1 - a_3)}{\mu_H a_1 P_0} \\ 0 & \frac{1}{a_2} & \frac{\phi_2(h)\beta_H \Lambda_H}{\mu_H a_2 P_0} \\ 0 & \frac{\phi_3(h) N_h \alpha_h}{a_2 a_4} & \frac{\mu_H a_2 P_0 + \phi_2(h)\beta_H \Lambda_H}{\mu_H a_2 a_4 P_0} \end{bmatrix}. \tag{3.6.1}$$

The characteristic equation linked to the aforementioned matrix is given by $|J(P_0) - \lambda I| = 0$. Nevertheless, we assess the stability of the system (3.6.1)'s fixed points through numerical methods [76].

Time Step	$\lambda_i (i = 1, 2, 3)$	$\rho(\lambda_i)$	NSFD Scheme
0.01	(0.999982, 0.998995, 0.999625)	0.999982	Converges
0.5	(0.999100, 0.950856, 0.981180)	0.999100	Converges
10	(0.982161, 0.342603, 0.659133)	0.982161	Converges
100	(0.835270, -0.011455, 0.835270)	0.999820	Converges

Table 3.4: The spectral radii of the Jacobian matrix corresponding to the free disease point of NSFD scheme.

Table 3.4 displays the spectral radii of the Jacobian matrix associated with the disease-free state of the NSFD scheme, under the condition of $R_0 < 1$. It is noticeable from the table that regardless of the time step size employed in the simulations, all spectral radii remain below one in magnitude. Consequently, we deduce that the disease-free equilibrium point $E^0 = \left(\frac{\Lambda_H}{\mu_H}, 0, 0\right)$ for the system (3.6.1) is unconditionally and locally asymptotically stable when $R_0 < 1$.

3.6.4 The stability of the endemic equilibrium

In this subsection, we establish the stability of the endemic equilibrium, denoted as E^1. By substituting the endemic equilibrium E^* into the Jacobian matrix (3.6.1) and subsequently calculating the eigenvalues.

$$E^* = \begin{cases} S_H^* &= \dfrac{\mu_V P_0(\delta_H+\mu_H)(\beta_H+\mu_H)+\mu_H\mu_V P_0(\delta_H+\mu_H)(R_0-1)}{(\beta_H+\mu_H)\beta_H N_h\alpha_h}, \\ I_H^* &= \dfrac{\mu_h\mu_V P_0(R_0-1)}{N_h\alpha_h(\beta_h+\mu_h)}, \\ V_H^* &= \dfrac{\mu_H P_0(R_0-1)}{(\beta_H+\mu_H)}. \end{cases} \tag{3.6.4.1}$$

with
$R_0 = \dfrac{N_h\alpha_h\beta_H\Lambda_H}{(\delta_H+\mu_H)P_0\mu_H\mu_V}$.

Following a similar approach as employed in assessing the stability of the disease-free equilibrium, we will now proceed to analyze the stability of the endemic point within the context of the system (3.6.1) numerically [76].

Time Step	$\lambda_i(i=1,2,3)$	$\rho(\lambda_i)$	NSFD Scheme
0.01	(0.999997, 0.999501, 0.999115)	0.999997	Converges
0.5	(0.999872, 0.975293, 0.956622)	0.999872	Converges
10	(0.996840, 0.400538,0.600133)	0.996840	Converges
100	(0.960532, -0.008359, 0.010378)	0.960532	Converges

Table 3.5: The spectral radii of the Jacobian matrix corresponding to the free disease point of NSFD scheme.

Table 3.5 provides a presentation of the spectral radii of the Jacobian matrix linked to the endemic point of the NSFD scheme where $R_0 > 1$. From Table 3.5, it becomes observable that all spectral radii maintain values lower than one in magnitude, regardless of the chosen time step size for the simulations. As a result, we can deduce that the endemic equilibrium of the system (3.6.1) attains local asymptotic stability under the condition of $R_0 > 1$.

3.6.5 Numerical Simulations

In this subsection, we conduct simulations of the discrete NSFD scheme multiscale model using Matlab 2023 software. The purpose of these simulations is to validate certain analytical findings that were derived in the preceding section. The primary objective is to examine how the within-human scale parameters influence the between-host variables concerning the infection of

norovirus, for this reason, these numerical results solutions are very important from practical point of view. We illustrate the influence of *norovirus* transmission and replication parameters $(\Lambda_e, \alpha_e, \alpha_h, \mu_V, N_e, \rho_c, \mu_h)$ which were chosen based on their significancy on sensitivity analysis on the nested model variables (S_H, I_H, V_H). The figures are plotted using parameters in Table 3.3 and the following initial values are used: $S_H = 500, I_H = 10; V_H = 300$.

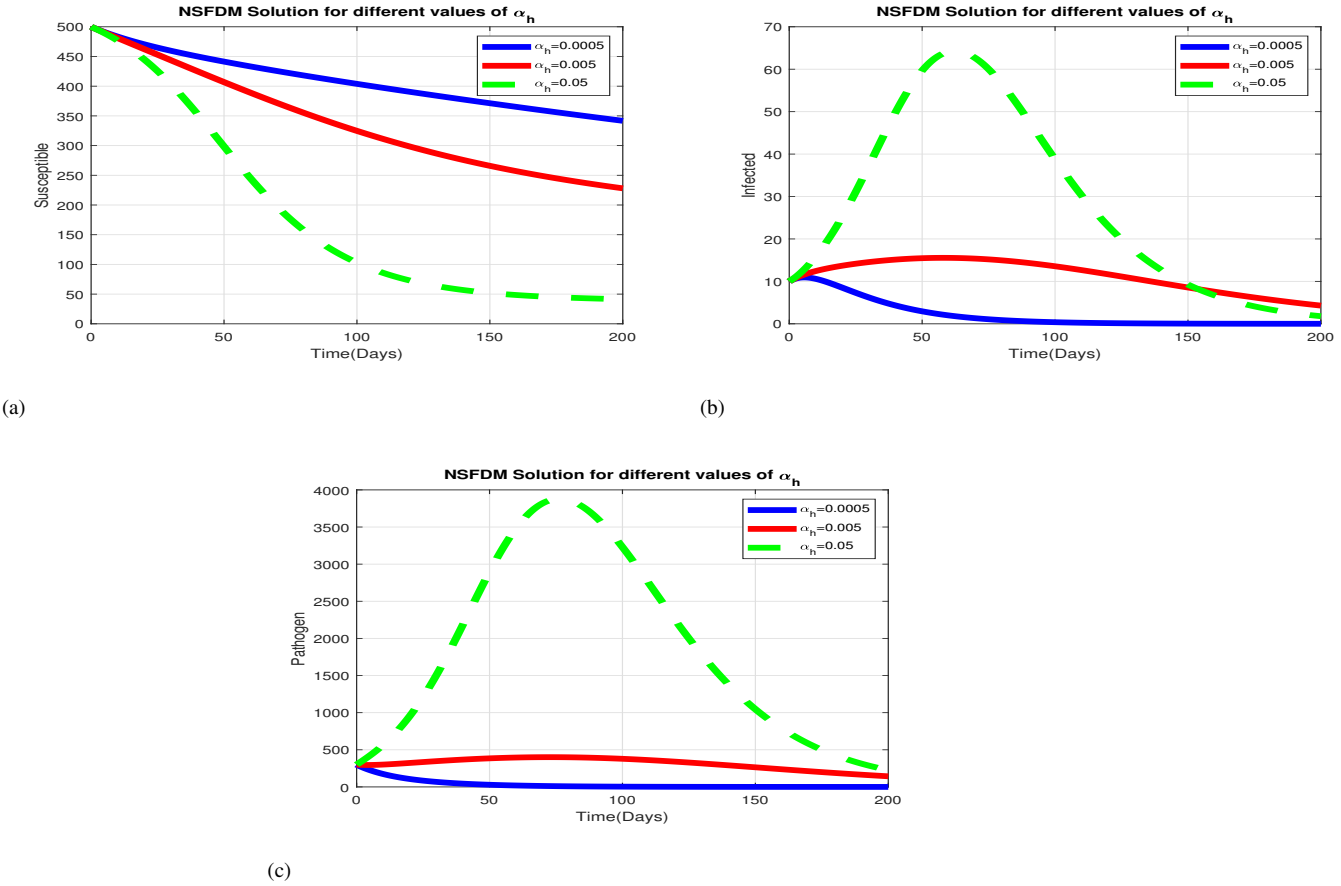

Figure 3.4: Simulations of NSFD scheme showing changes of (a) population of susceptible humans (S_H), (b) population of infected humans (I_H), and (c) population of environmental noroviruses (V_H) for different values of shedding rate by an infected individual α_h : $\alpha_h = 0.0005, \alpha_h = 0.005$, and $\alpha_h = 0.05$.

Figure 3.4 illustrates variations in (a) the population of susceptible humans (S_H), (b) the population of infected humans (I_H), and (c) the environmental load of *norovirus* (V_H) across different values of the shedding rate by an infected individual, α_h: specifically, $\alpha_h = 0.0005$, $\alpha_h = 0.005$, and $\alpha_h = 0.05$. The outcomes indicate that an increase in the excretion rate of within-human scale viral load into the physical environment by each infected human holds significant health

implications at the human population level. This is observable in the notable rise in the between-host *norovirus* levels and the population of infected humans (I_H), coupled with a decrease in the population of susceptible humans (S_H).

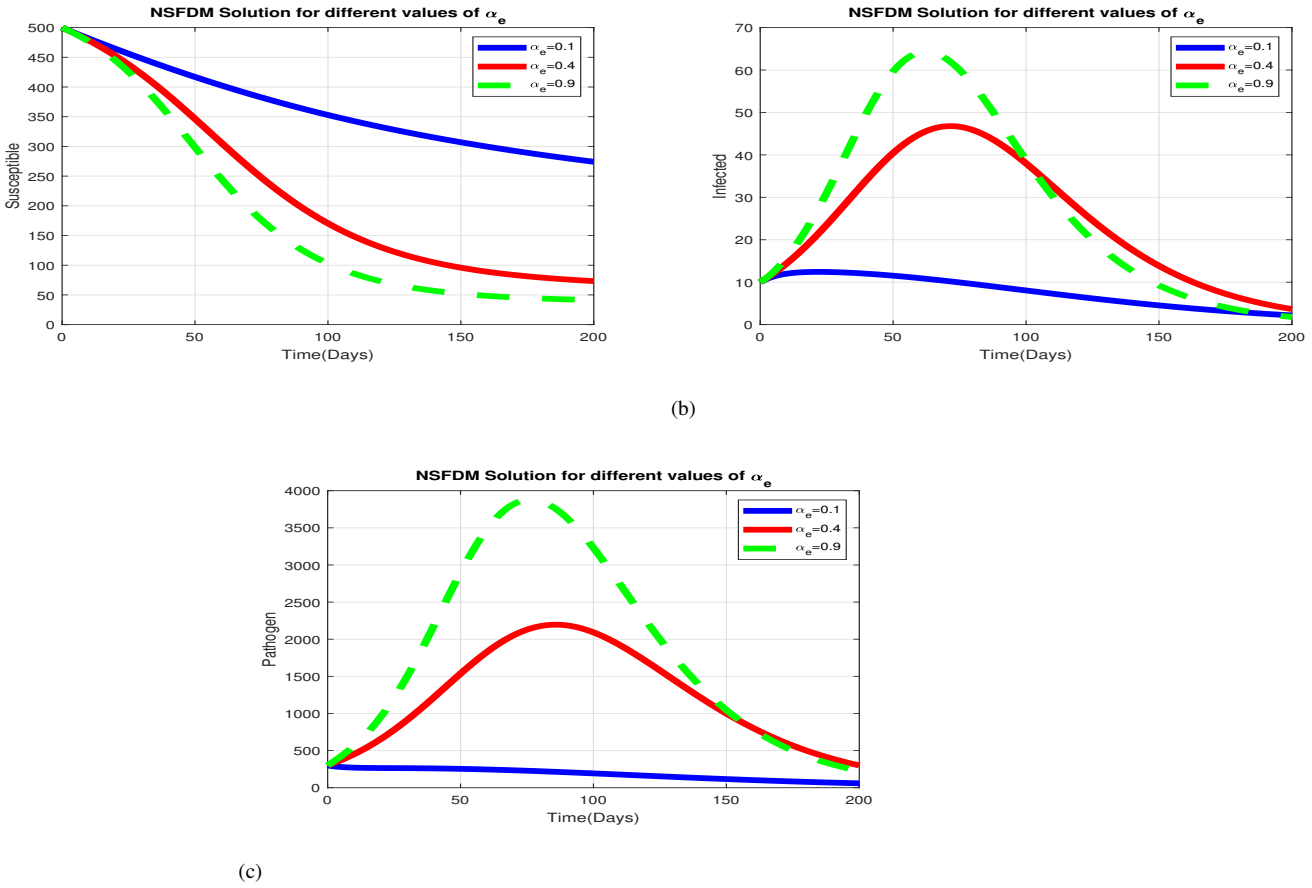

Figure 3.5: Simulations of NSFD scheme showing changes of (a) population of susceptible humans (S_H), (b) population of infected humans (I_H), and (c) population of environmental *noroviruses* (V_H) for different values of replication rate of *norovirus* in the within-human scale $\alpha_e : \alpha_e = 0.1, \alpha_e = 0.4$, and $\alpha_e = 0.9$.

Figure 3.5 illustrates alterations in (a) the population of susceptible humans (S_H), (b) the population of infected humans (I_H), and (c) the environmental load of *norovirus* (V_H) across varying values of the multiplication rate of *norovirus* within the human scale, denoted as α_e: specifically, $\alpha_e = 0.1$, $\alpha_e = 0.4$, and $\alpha_e = 0.9$. The outcomes emphasize the significant health implications of an increased within-human scale replication rate of *norovirus* at the human population level. Notably, there is a substantial rise in both the between-host *norovirus* levels and the population of infected humans (I_H), coupled with a decline in the population of susceptible humans (S_H). Furthermore, it is evident that these two populations experience a reduction over time. These

results emphasize the potential benefits of implementing measures to restrict the replication rate, which could yield positive outcomes in minimizing *norovirus* infections within the human community.

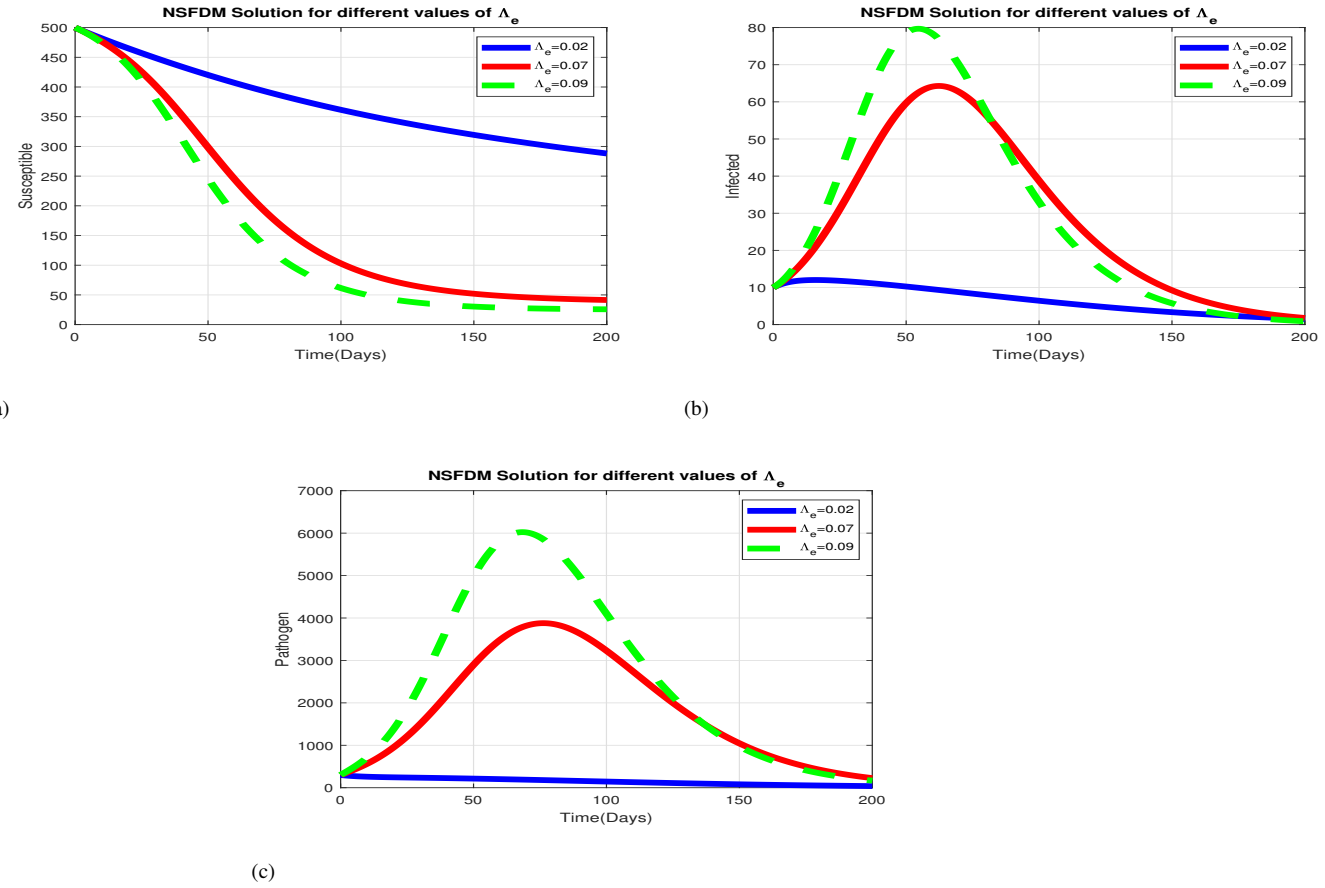

Figure 3.6: Simulations of NSFD scheme showing changes of (a) population of susceptible humans (S_H), (b) population of infected humans (I_H), and (c) population of environmental *noroviruses* (V_H) for different values of epithelial cells supply rate $\Lambda_e = 0.02$, $\Lambda_e = 0.07$, and $\Lambda_e = 0.09$.

Figure 3.6 depicts variations in (a) the susceptible population (S_H), (b) the population of infected humans (I_H), and (c) the community *norovirus* load (V_H) across different values of the supply rate of epithelial cells, denoted as Λ_e: specifically, $\Lambda_e = 0.02$, $\Lambda_e = 0.07$, and $\Lambda_e = 0.09$. The outcomes reveal that with an increase in the supply rate, there is a corresponding rise in the populations of infected individuals and environmental pathogens. These findings suggest that the average supply of susceptible epithelial cells within the human system may indeed influence the dynamics of *norovirus* infection at the broader population and community level.

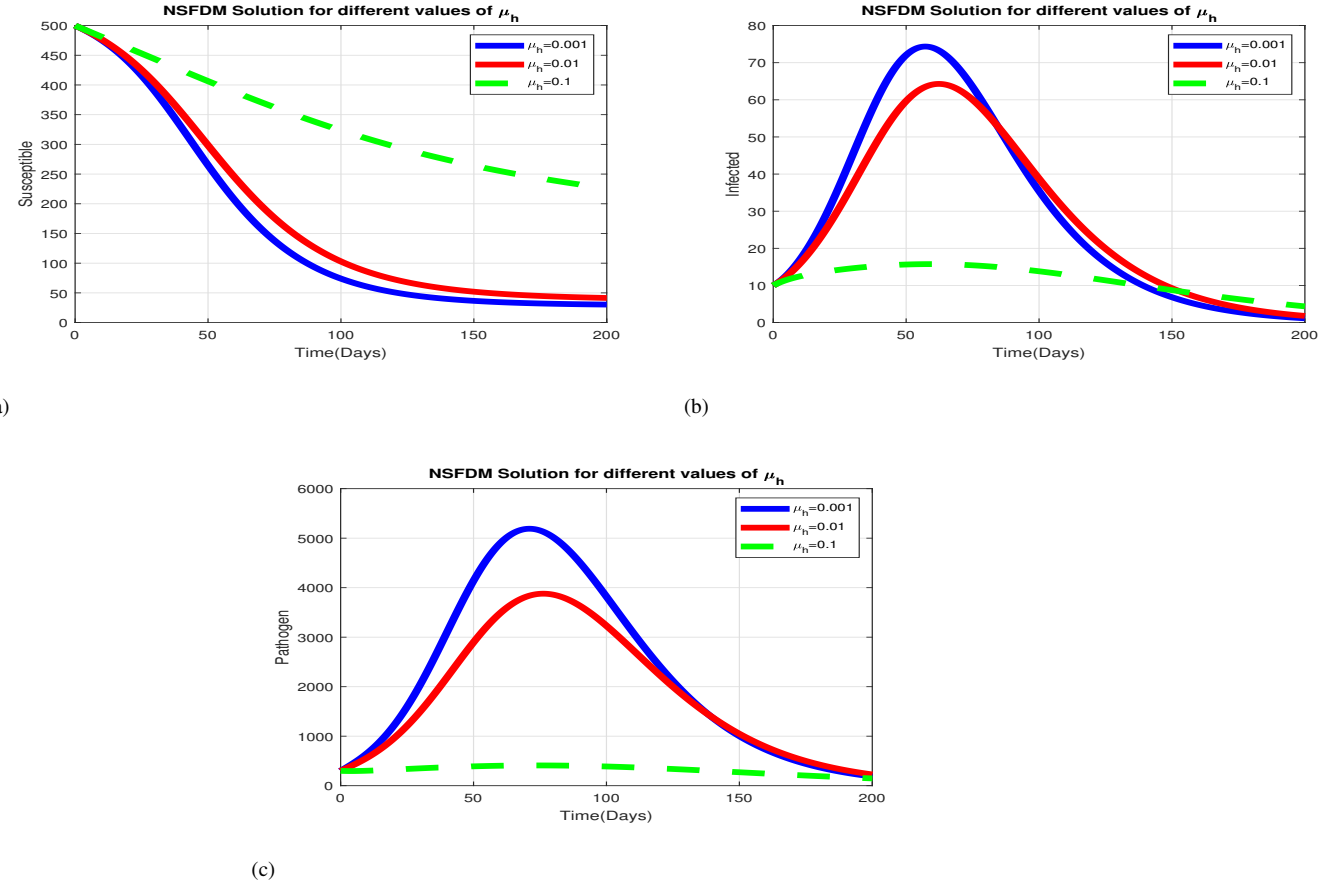

Figure 3.7: Simulations of NSFD scheme showing changes of (a) population of susceptible humans (S_H), (b) population of infected humans (I_H), and (c) population of environmental *noroviruses* (V_H) for different values of within-human scale *norovirus* natural decay rate $\mu_h : \mu_h = 0.1, \mu_h = 0.01, \mu_h = 0.001$.

Figure 3.7 illustrates variations in (a) the population of susceptible humans (S_H), (b) the population of infected humans (I_H), and (c) the environmental load of *norovirus* (V_H) across different values of the natural decay rate of *norovirus* within the human scale, denoted as μ_h: specifically, $\mu_h = 0.1$, $\mu_h = 0.01$, and $\mu_h = 0.001$. The outcomes observed in Figure 3.7 indicate that with an increase in the natural death rate of the within-human scale viral load, there is a noticeable decrease in the populations of environmental *norovirus* (V_H) and infected humans (I_H), along with an increase in the population of susceptible humans (S_H) at the between-host scale. Hence, treatment measures aimed at increasing the decay rate of *norovirus* within the human scale can potentially yield positive effects in reducing *norovirus* infections.

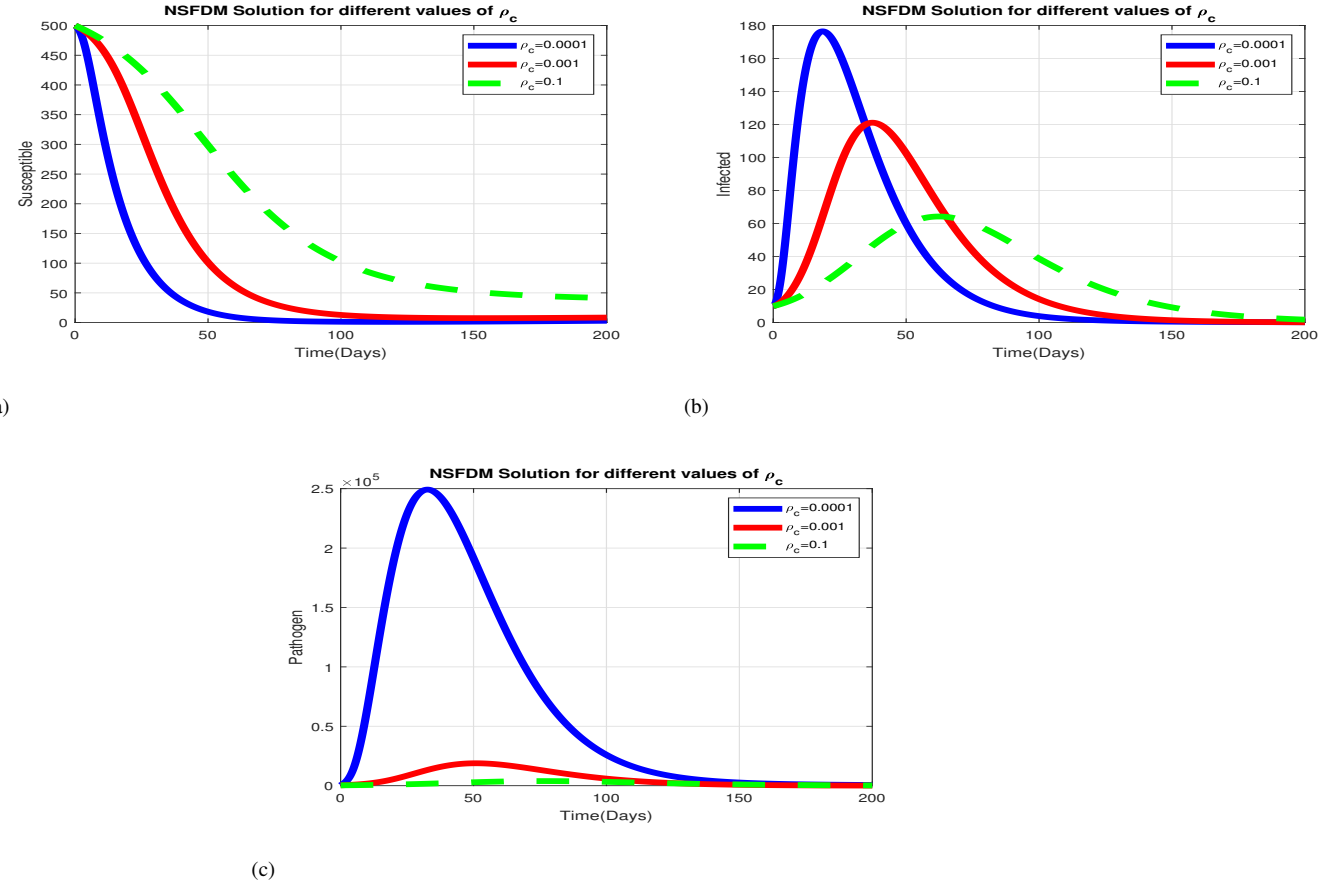

Figure 3.8: Simulations of NSFD scheme showing changes of (a) population of susceptible humans (S_H), (b) population of infected humans (I_H), and (c) population of environmental *noroviruses* (V_H) for for different values of immune cells activation rate ρ_c : $\rho_c = 0.0001, \rho_c = 0.001, \rho_c = 0.1$.

Figure 3.8 presents variations in (a) the population of susceptible humans (S_H), (b) the population of infected humans (I_H), and (c) the environmental load of *norovirus* (V_H) across different values of the immune cells activation rate, denoted as ρ_c: specifically, $\rho_c = 0.0001$, $\rho_c = 0.001$, and $\rho_c = 0.1$. The outcomes depicted in Figure 3.8 demonstrate that with an increase in immune cells activation, there is a corresponding reduction in the populations of infected individuals and environmental pathogens. This observation implies that implementing measures to enhance immune cell activation could have a substantial impact on reducing human infections, as a heightened immune response could effectively neutralize a greater number of viruses.

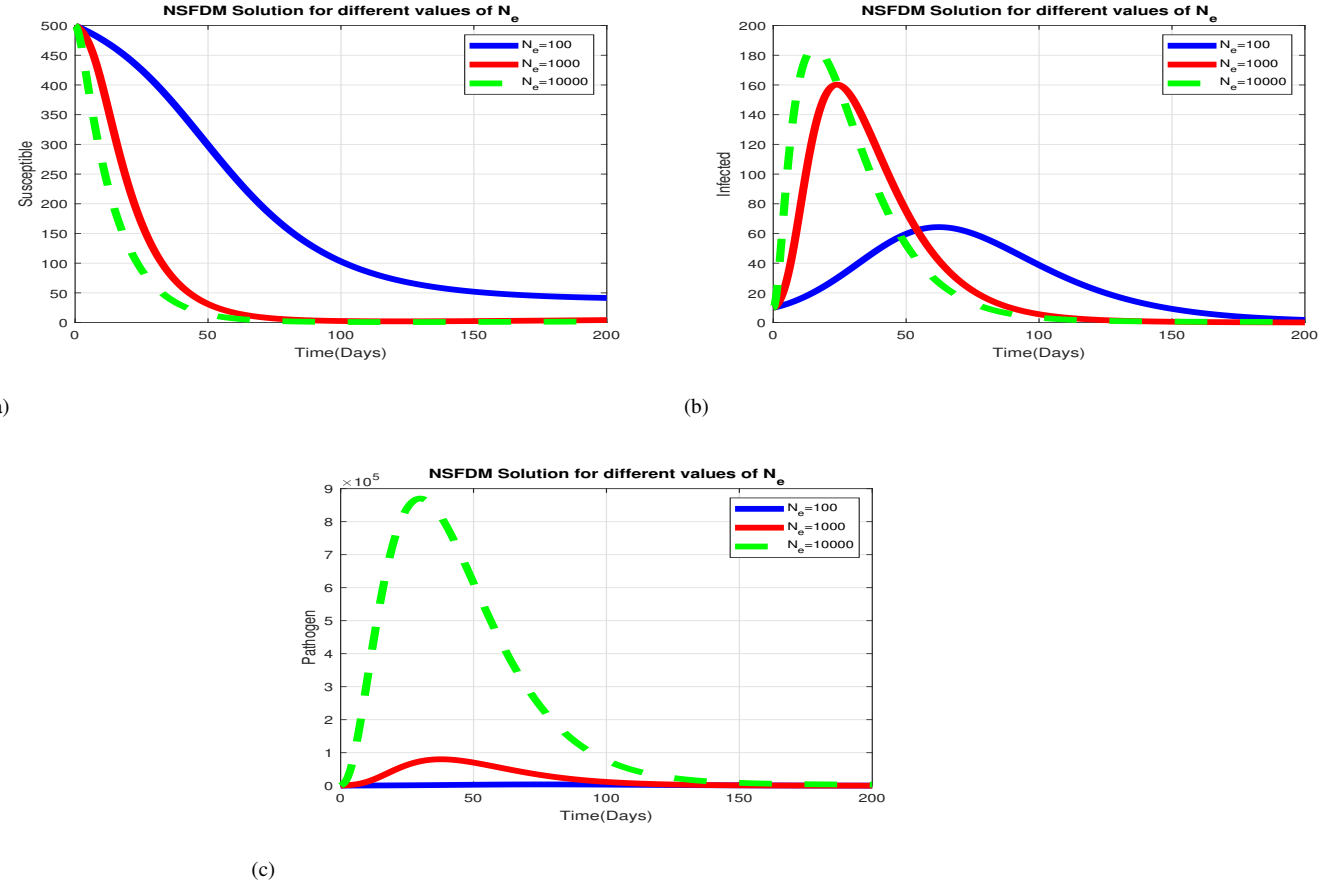

Figure 3.9: Simulations of NSFD scheme showing changes of (a) population of susceptible humans (S_H), (b) population of infected humans (I_H), and (c) population of environmental *noroviruses* (V_H) of the within-human scale produced viral load N_e : $N_e = 100, N_e = 1000, N_e = 10000$.

Figure 3.9 displays graphical representations of the numerical solutions of the model system (3.6.1), indicating the variations in (a) the population of susceptible humans (S_H), (b) the population of infected humans (I_H), and (c) the environmental load of *norovirus* (V_H) across different values of the within-human scale viral load produced per bursting of epithelial cells, denoted as N_e: specifically, $N_e = 100$, $N_e = 1000$, and $N_e = 10000$. The numerical outcomes depicted in Figure 3.9 reveal that with an increase in the number of viruses ready for excretion, there is a corresponding rise in the between-host variables. This finding emphasizes that implementing measures to hinder the replication rate of *norovirus* could have a significant impact on reducing *norovirus* infections at the population level.

3.7 Conclusion

The major innovation in this chapter is the development and the use of nested multiscale model to show that within-human scale disease dynamics has influence on macroscale transmission for foodborne pathogens with replication cycle at within-human scale only. We used a nested multiscale model for infectious disease systems that are transmitted environmentally, wherein the pathogen exclusively replicates within the human scale. We demonstrated the impact of the within-human scale on the macroscale, primarily through shedding or excretion processes. Our approach involved constructing individual submodels for both the within-human scale and the macroscale, which were then interconnected to create a nested multiscale model. We established a connection between the within-human scale model and an epidemiological model by incorporating the within-human scale submodel's dynamics into the epidemiological framework. This integration was achieved by expressing the parameters of the epidemiological model as functions derived from the within-human scale submodel. The nested multiscale was mathematically and numerically analysed. The nested multiscale model incorporates two key metrics: the basic reproductive number (R_0), typically depicting disease dynamics during the initial stages of an infection, and the endemic equilibrium points (E^*), characterizing disease dynamics at the epidemic level. These metrics are defined in relation to both macroscale and within-human scale parameters. This observation leads us to the conclusion that a reciprocal influence exists between the within-human scale and macroscale aspects of the model since both are comprised of within-human scale and macroscale parameters. The sensitivity analysis used to discover the parameters that are sensitive to the decrease or increase of the basic reproductive number R_0 and environmentally pathogen load E^* which help to suggest appropriate health intervention measures. Furthermore, we formulated the NSFD scheme and demonstrated numerically that the discrete systems maintain the essential characteristics of the model, including positivity and stability. Additionally, it is evident that the NSFD scheme converges towards the correct equilibria as the time step h increases. Numerical results show that all the within-human scale parameters varied have great influence on the macroscale variables. It can be observed that all within-human scale parameters, play an important role in minimizing norovirus infection, which can also lead to an extinction of norovirus.

This study highlight the potential influence of within-human dynamics on macroscale dynamics. Additionally, we offer insights into the sensitivity of our model parameters, including the mechanism of vaccine action. Vaccinating individuals who are already infected by targeting the within-human scale parameters is expected to significantly reduce the overall number of infections within the population. This confirms the importance of considering within-human scale dynamics in the modelling of infectious diseases. In the next chapter, we establish a multiscale

model to account for environmentally transmitted pathogens that undergo replication at both the microscale and macroscale levels.

Chapter 4

A Nested Multiscale Model of *E. coli* O157:H7 Dynamics In Cattle

4.1 Introduction

In order to understand pathogen ecology and quantify the impacts of intervention, mathematical models of infection transmission have been introduced into the collection of epidemiologists [94]. Despite the existence of numerous mathematical models, a relatively less explored aspect of infectious disease systems is the fact that their transmission arises from intricate and dynamic interactions between spatial and temporal scales [95]. The dynamics of infectious disease systems can be impacted by the interplay of multiple temporal and spatial scales associated with the cellular, tissue, organ, organism, community, and ecosystem levels of biological organization [20] which will require our focus to shift from transmission theory to transmission-replication theory, a cornerstone of multiscale modelling. The advantages of multiscale modelling include the ability to examine diseases at the scale where infections take place and explore factors that affect disease dynamics. Infections caused by bacteria continue to be a leading cause of death and illness in the world [96]. The development of antibiotics and their use in medicine during the 20th century greatly decreased bacterial illness morbidity and mortality [97]. However, efforts to lessen the burden of bacterial infections are consistently thwarted by the rise in antibiotic resistance to the majority of first-line medicines, antibiotic tolerance, and unequal access to

medications [98–100]. Within this chapter, we create a nested multiscale model for environmentally transmitted infectious diseases wherein, the pathogen undergoes a replication cycle at both the microscale and macroscale levels at host level. To illustrate, we use the example of *E. coli* O157:H7 within a farm setting as there is mounting evidence suggesting that the farm environment plays a significant role in causing a substantial number of isolated cases of *E. coli* O157:H7 infections [101]. Inaccurate representation of the most significant transmission pathway could occur from disregarding a pathogen's growth rates at the macro- and microscales [102]. Understanding the effect of macroscale growth rate on within-cattle pathogen replication and vice-versa could be of value in control of *E. coli* O157:H7 infections. The main objective of this study is to develop a multiscale model that links the macroscale dynamics and within-cattle dynamics in order to assess the relationship between the macroscale bacteria growth rate and within-cattle pathogen replication rate at the site of infection. It is our understanding that there is no existing nested multiscale model in the literature that takes *E. coli* O157:H7 replication cycle into account at the microscale of organization of infectious disease systems. Nested multiscale models are also well-suited for infectious disease systems in which the pathogen undergoes replication at both the microscale and macroscale levels. Symptoms can span from mild diarrhea that resolves on its own to more severe cases characterized by bloody diarrhea and abdominal cramps. In rare instances, these symptoms can escalate to severe conditions such as hemolytic uremic syndrome and renal failure [103, 104]. Infection of humans is primarily transmitted by cattle, either directly or indirectly via their products, hence cattle are considerd as a natural reservoir for this pathogen [105]. However, cattle do not display any disease symptoms, and they consistently test positive while excreting *E. coli* O157:H7 shortly after contracting the infection [106]. The gastrointestinal tract, where *E. coli* O157:H7 replicates, and the external environment, which is linked to *E. coli* O157:H7 transmission on a population level, constitute the two separate environments in which the life cycle of *E. coli* O157:H7 occur. Its ecological and evolutionary dynamics are influenced by the necessity to thrive in both of these environments, resulting in a wide range of life histories and variations in fitness within *E. coli* O157:H7. These variations have significant implications for disease transmission and control strategies. Various interventions have been attempted to combat *E. coli* O157:H7 infection, including strategies aimed at reducing cattle's exposure to the bacteria and enhancing their resistance against it [107]. We follow the same process used in the previous chapter of developing two submodels separately and link them to have a multiscale model. We illustrate the derivations of these submodel and how they are linked to form a multiscale model in the next subsections.

4.1.1 Macroscale Submodel

In this subsection, we formulate a macroscale submodel that tracks the behavior of *E. coli* O157:H7 at the macroscale level. This submodel is constructed by observing the interactions among three populations at a given time t: susceptible cattle ($S_C(t)$), infected cattle ($I_C(t)$), and the population of *E. coli* O157:H7 ($P_W(t)$) present in the physical environment. The formulation of the submodel is established upon the following assumptions:

(i) Infection transmission occurs only through contact with pathogens existing freely in the physical environment. Nevertheless, in cases of direct transmission, it can be approximated in relation to the environmental pathogen load through indirect means.

(ii) All infected cattle cannot recover unless they get treated.

(iii) There is no immune response in the infected cattle host.

(iv) The dynamics of susceptible cattle S_C, infected cattle I_C and environmental pathogen P_W are considered to occur at slow time scale (t) compared to the microscale variables so that $S_C = S_C(t)$, $I_C = I_C(t)$, $P_W = P_W(t)$.

Therefore the system of equations is presented as follows:

$$\begin{cases} 1.\ \dfrac{dS_C(t)}{dt} &= \Lambda_C - \dfrac{\beta_W P_W(t) S_C(t)}{P_0 + P_W(t)} - \mu_C S_C(t), \\ 2.\ \dfrac{dI_C(t)}{dt} &= \dfrac{\beta_W P_W(t) S_C(t)}{P_0 + P_W(t)} - [\mu_C + \delta_C] I_C(t), \\ 3.\ \dfrac{dP_W(t)}{dt} &= r_W P_W(t)\left(1 - \dfrac{P_W(t)}{K_W(t)}\right) + \widehat{N_h}\alpha_h I_C(t) - \mu_W P_W(t). \end{cases} \tag{4.1.1.1}$$

The between-host submodel is characterized by the state variable S_C, which captures the evolution of susceptible cattle dynamics. In Equation (1) of the sub-model system (4.1.1.1), we posit that the influx of new susceptible cattle into the population arises from both births and the introduction of cattle from other farms, occurring consistently at a rate denoted as Λ_C for any given time, t. This susceptible cattle population undergoes a reduction due to infection at a rate,

$$\frac{\beta_W P_W(t) S_C(t)}{P_0 + P_W(t)}$$

and natural death at a constant rate, μ_C. Equation (2) within the sub-model system (4.1.1.1) represents the population of infected cattle, generated from the transition of susceptible cattle to an

infected state. The infected group experiences a decrease due to natural mortality, characterized by a constant rate μ_C, or due to death brought about by the disease at a rate of δ_C. It is assumed that infected cattle contribute to the spread of the disease within the population by contaminating the environment through the excretion of fecal material containing *E. coli* O157:H7 bacterial cells at a variable rate denoted as $\alpha_h \widehat{N_h} I_C$. Consequently, the changes in the population of *E. coli* O157:H7 bacteria within the physical environment, as described by Equation (3) within the sub-model system (4.1.1.1), stem from the excretion or shedding of fecal material containing *E. coli* O157:H7 bacterial cells by infected cattle hosts at a rate of $\alpha_h \widehat{N_h} I_C$. The parameter $\widehat{N_h}$ is regarded as a singular value parameter, yet it actually encapsulates a composite of disease dynamics within an infected individual host. This characteristic renders the model system (4.1.1.1) unrealistic. Furthermore, estimating $\widehat{N_h}$ through a single-scale model proves challenging, thus necessitating the adoption of a nested multiscale approach to accurately estimate $\widehat{N_h}$. This population is assumed to increase in the environment through logistic equation

$$r_W P_W(t) \left(1 - \frac{P_W(t)}{K_W(t)}\right)$$

with r_W environmental pathogen growth rate and the carrying capacity K_W. Furthermore, we also assume that the population of *E. coli* O157:H7 bacteria in the physical environment is reduced due to natural death at a rate, μ_W. All variables within the above system (4.1.1.1) and their corresponding definitions can be found in Table 4.1. Similarly, all parameters and their respective meanings are provided in Table 4.3..

Variable	Variable Description
$S_C(t)$	Susceptible cattle
$I_C(t)$	Infected cattle
$P_W(t)$	Environmental pathogen

Table 4.1: Description of variables in the system (4.1.1.1).

4.1.2 Microscale Submodel

The microscale submodel observes four variables at within-cattle scale that are ingested bacterium B_h, susceptible epithelial cells S_h, infected epithelial cells I_c, and immune cells I_s. We make the following assumptions in order to integrate it with the single-scale submodel given by system (4.1.1.1):

(i) The disease processes occurring at the microscale occur at a fast time scale (τ) compared to the macroscale *E. coli* O157:H7 submodel variable so that $S_h = S_h(\tau)$, $I_h = I_h(\tau)$, $I_s = I_s(\tau)$, $B_h = B_h(\tau)$.

(ii) The extracellular *E. coli* O157:H7 bacterial load $B_h = B_h(\tau)$ serves as an indicator of the infectivity of individual cattle and is excreted through feces.

(iii) *E. coli* O157:H7 bacteria replicate at the at the site of infetion.

These assumptions result in the following formulation of ordinary differential equations:

$$\begin{cases} 1.\ \dfrac{dB_h(\tau)}{d\tau} &= N_e\alpha_e I_h(\tau) - \phi I_s(\tau)B_h(\tau) - [\mu_h + \alpha_h]B_h(\tau), \\ 2.\ \dfrac{dS_h(\tau)}{d\tau} &= \Lambda_h - \beta_h B_h(\tau)S_h(\tau) - \mu_e S_h(\tau), \\ 3.\ \dfrac{dI_h(\tau)}{d\tau} &= \beta_h B_h(\tau)S_h(\tau) - [\alpha_e + \mu_e]I_h(\tau), \\ 4.\ \dfrac{dI_s(\tau)}{d\tau} &= \Lambda_s + \rho_s I_s(\tau)B_h(\tau) - \mu_s I_s(\tau). \end{cases} \tag{4.1.2.1}$$

Equation (1) within the sub-model system (4.1.2.1) captures the evolution of *E. coli* O157:H7 bacterial cells at the within-cattle scale, localized at the site of infection within an individual infected cattle host. The first term corresponds to the bacterial proliferation within epithelial cells, transpiring at a rate denoted as α_e. The second term represents the count of pathogens that are eliminated by immune cells, transpiring at a rate ϕ. It is assumed that the population of *E. coli* O157:H7 bacteria at the within-cattle scale experiences natural decay at a consistent rate, μ_h. We assume that infected cattle facilitate the spread of the disease among the population by contaminating the environment through the excretion of fecal material harboring *E. coli* O157:H7 bacterial cells, occurring at a variable rate of $\alpha_h B_h$. Equation (2) within the sub-model system (4.1.2.1) governs the dynamics of epithelial cells within the within-cattle host. In this equation, the first term represents the supply rate of epithelial cells, characterized as Λ_c. The second term corresponds to the count of epithelial cells destroyed by pathogens, transpiring at a rate β_h. The final term reflects the natural decay rate of epithelial cells, denoted as μ_e. Equation (3) within the submodel system (4.1.2.1) governs the behavior of infected epithelial cells (I_c). These cells experience depletion through the multiplication of *E. coli* O157:H7 at the site of infection, occurring at a steady rate of α_e. This multiplication leads to the release of an average quantity of N_h bacterial units per cell, thereby resulting in a total bacterial count released given

by $N_e\alpha_e I_h$. Equation (4) describes the dynamics of immune cells (I_s). It is assumed that these cells are supplied at a rate Λ_s, and their proliferation is triggered when *E. coli* O157:H7 bacteria are introduced at the within-cattle scale, occurring at a rate of ρ_s. Additionally, the population of immune response cells undergoes natural decay at a constant rate, μ_s. All variables outlined in the aforementioned system (4.1.2.1) and their respective definitions are provided in Table 4.2, while all parameters and their corresponding interpretations can be found in Table 4.3.

Variable	Variable Description
$B_h(\tau)$	*E.coli* inside the after ingested by the cattle
$S_h(\tau)$	Susceptible epithelial cells
$I_h(\tau)$	Infected epithelial cells
$I_s(\tau)$	Immune cells

Table 4.2: Description of variables in the system (4.1.2.1).

4.1.3 Linking the Macroscale and Microscale Submodels into a Full Nested Multiscale Model

In the previous sections we presented the two submodels for the dynamics of *E. coli* O157:H7 transmission dynamics (between-host submodel (4.1.1.1) and within-host submodel (4.1.2.1) that separately describe the two key processes of *E. coli* O157:H7 disease dynamics (transmission and replication of *E. coli* O157:H7 bacteria processes) which occur at two distinct scales (within-host scale and between-host scale). We now integrate them into a single multiscale model as shown in flow diagram in Figure 4.1. We achieve this by replacing the parameter $\widehat{N_h}$ which phenomenologically models within-host scale pathogen replication by a variable $B_h(\tau)$ which mechanistically models the within-host scale pathogen replication to get:

$$
\begin{cases}
\dfrac{dS_C(t)}{dt} &= \Lambda_C - \dfrac{\beta_W P_W(t)}{P_0 + P_W(t)} S_C(t) - \mu_C S_C(t), \\
\dfrac{dI_C(t)}{dt} &= \dfrac{\beta_W P_W(t)}{P_0 + P_W(t)} S_C(t) - [\mu_C + \delta_C] I_C(t), \\
\dfrac{dP_W(t)}{dt} &= r_W P_W(t) \left(1 - \dfrac{P_W(t)}{K_W(t)}\right) + B_h \alpha_h I_C(t) - \mu_W P_W(t), \\
\dfrac{dB_h(\tau)}{d\tau} &= N_e \alpha_e I_h(\tau) - \phi I_s(\tau) B_h(\tau) - [\mu_h + \alpha_h] B_h(\tau), \\
\dfrac{dS_h(\tau)}{d\tau} &= \Lambda_c - \beta_h B_h(\tau) S_h(\tau) - \mu_e S_h(\tau), \\
\dfrac{dI_h(\tau)}{d\tau} &= \beta_h B_h(\tau) S_h(\tau) - [\alpha_e + \mu_e] I_h(\tau), \\
\dfrac{dI_s(\tau)}{d\tau} &= \Lambda_s + \rho_s I_s(\tau) B_h(\tau) - \mu_c I_s(\tau).
\end{cases}
\tag{4.1.3.1}
$$

Considering that the two different time scales involved in the complete multiscale model system given by system (4.1.3.1), this present a crucial challenge in analyzing the multiscale model. The model's conceptual diagram is illustrated in Figure 4.1 below.

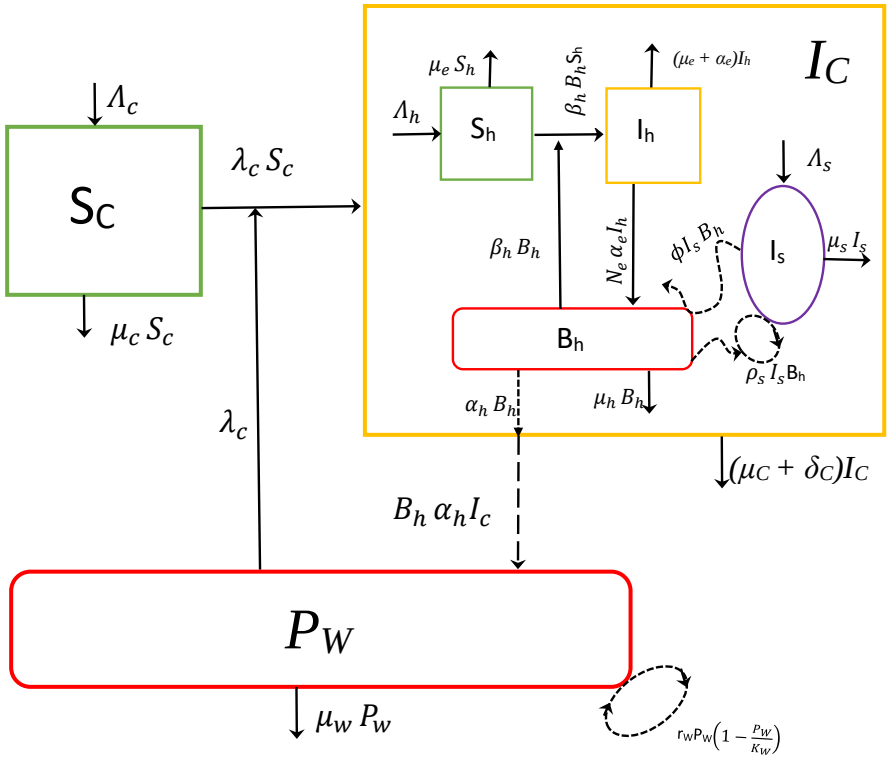

Figure 4.1: A schematic representation of the nested multiscale model of *E.coli* O157:H7 in a farm.

4.1.4 Simplification of the Full Nested Multiscale Model

We reduce the complete multiscale by using fast-slow analysis where we introduce an assumption that establishes a relationship between the fast and slow time scales $\tau = \epsilon t$ where $0 < \epsilon << 1$. By doing so, we can now rewrite the microscale *E. coli* O157:H7 transmission dynamics given

in system (4.1.2.1) as follows:

$$\begin{cases} 1.\ \dfrac{dB_h(\tau)}{d\tau} &= \epsilon[N_e\alpha_e I_h(\tau) - \phi I_s(\tau)B_h(\tau) - [\mu_h + \alpha_h]B_h(\tau)], \\ 2.\ \dfrac{dS_h(\tau)}{d\tau} &= \epsilon[\Lambda_h - \beta_h B_h(\tau)S_h(\tau) - \mu_e S_h(\tau)], \\ 3.\ \dfrac{dI_h(\tau)}{d\tau} &= \epsilon[\beta_h B_h(\tau)S_h(\tau) - [\alpha_e + \mu_I]I_h(\tau)], \\ 4.\ \dfrac{dI_s(\tau)}{d\tau} &= \epsilon[\Lambda_s + \rho_s I_s(\tau)B_h(\tau) - \mu_s I_s(\tau)]. \end{cases} \tag{4.1.4.1}$$

Here, ϵ represents a constant that emphasizes the fast time scale characterizing the microscale *E. coli* O157:H7 transmission dynamics submodel in contrast to the slow time scale of the macroscale *E. coli* O157:H7 transmission dynamics submodel. Given that $0 < \epsilon << 1$, we can effectively consider ϵ to be negligible (close to zero), resulting in the microscale *E. coli* O157:H7 transmission dynamics submodel becoming temporally invariant. As a result, we have the following expression:

$$\begin{cases} 1. & N_e\alpha_e I_h^* - \phi I_s^* B_h^* - (\mu_h + \alpha_h)B_c^* = 0, \\ 2. & \Lambda_h - \beta_h S_h^* B_h^* - \mu_e S_h^* = 0, \\ 3. & \beta_h S_h^* B_h^* - (\alpha_e + \mu_e)I_h^* = 0, \\ 4. & \Lambda_s + \rho_s B_h^* I_s^* - \mu_s I_s^* = 0. \end{cases} \tag{4.1.4.2}$$

From system (4.1.4.2) we get

$$\begin{cases} 1.\ B_h^* &= \dfrac{(\Lambda_h N_e\alpha_e\beta_h) - (\phi I_s^* + \mu_h + \alpha_h)(\mu_e + \alpha_e)\mu_e}{(\phi I_s^* + \mu_h + \alpha_h)(\mu_e + \alpha_e)\beta_h}, \\ 2.\ S_h^* &= \dfrac{\Lambda_h}{(\beta_h B_h^* + \mu_e)}, \\ 3.\ I_h^* &= \dfrac{\Lambda_h\beta_h B_h^*}{\beta_h B_h^* + \mu_e(\mu_e + \alpha_e)}, \\ 4.\ I_s^* &= \dfrac{\Lambda_s}{\mu_s + \rho_s B_h^*}, \end{cases} \tag{4.1.4.3}$$

and the expression

$$R_0 = \frac{N_e \alpha_e \beta_h \Lambda_h}{\mu_e(\mu_h + \alpha_e)(\phi_s + \mu_h + \alpha_h)} \tag{4.1.4.4}$$

represents the basic reproductive number at the microscale. Thus, the application of the fast-slow analysis simplifies the microscale submodel system (4.1.2.1) to the algebraic equations given in system (4.1.4.3) which can be incorporated into the macroscale submodel's parameter to become

$$\begin{cases} \dfrac{dS_C(t)}{dt} &= \Lambda_C - \lambda_W S_C(t) - \mu_C S_C(t), \\ \dfrac{dI_C(t)}{dt} &= \lambda_W S_C(t) - (\mu_C + \delta_C) I_C(t), \\ \dfrac{dP_W(t)}{dt} &= r_W P_W(t)\left(1 - \dfrac{P_W(t)}{K_W(t)}\right) + B_h^* \alpha_h I_C(t) - \mu_W P_W(t). \end{cases} \tag{4.1.4.5}$$

We observe that from the model system outlined in (4.1.4.5), the overall count of *E. coli* O157:H7 bacilli discharged by each infected cattle into the environment ($B_h I_C$) is now approximated as $B_h I_C$. Introducing the notation $N_h = B_h$, where N_h serves as a composite parameter that can be interpreted as the endemic value of the microscale *E. coli* O157:H7 bacterial load (B_h), the complete multiscale model (4.1.3.1) for *E. coli* O157:H7 transmission dynamics is then simplified to:

$$\begin{cases} 1.\ \dfrac{dS_C(t)}{dt} &= \Lambda_C - \lambda_W S_C(t) - \mu_C S_C(t), \\ 2.\ \dfrac{dI_C(t)}{dt} &= \lambda_W S_C(t) - (\mu_C + \delta_C) I_C(t), \\ 3.\ \dfrac{dP_W(t)}{dt} &= r_W P_W(t)\left(1 - \dfrac{P_W(t)}{K_W(t)}\right) + N_h \alpha_h I_C(t) - \mu_W P_W(t), \end{cases} \tag{4.1.4.6}$$

where $\lambda_W = \dfrac{\beta_W P_W}{P_0 + P_W}$ and the composite parameter $\widehat{N}_h$ is given by

$$N_h = \frac{1}{2}\left[Q_2 + \sqrt{Q_2^2 - 4Q_1Q_3}\right] \tag{4.1.4.7}$$

where

$$\begin{cases} Q_1 &= (\alpha_e + \mu_e)(\mu_h + \alpha_h)\beta_h\rho_s, \\ Q_2 &= N_e\alpha_e\Lambda_h\beta_h\rho_s + \phi\Lambda_s\beta_h + (\alpha_e + \mu_e)(\mu_h + \alpha_h)(\mu_s\beta_h - \rho_s\mu_e), \\ Q_3 &= N_e\alpha_e\Lambda_h\beta_h\mu_s - \phi\Lambda_s\mu_e - (\alpha_e + \mu_e)(\mu_h + \alpha_h)\mu_e\mu_s. \end{cases} \tag{4.1.4.8}$$

The analysis of the nested multiscale model (4.1.4.6) is carried out in the upcoming section, wherein we showcase outcomes derived from mathematical analysis and numerical simulations regarding the behavior of the simplified nested multiscale model. Presented below is Table 4.3, containing the parameters of the multiscale model.

Parameter	Description	Initial value	Source
Λ_C	Supply rate of susceptible cattle	10	Assumed
μ_C	Natural death rate of cattle	0.03	Assumed
β_W	Infection rate of cattle	0.038	[108]
δ_C	Disease induced death rate of cattle	0.03	Assumed
r_W	Growth rate of pathogens in the environment	3.5	[108]
μ_W	Death rate of pathogens in the environment	0.06	[108]
K_W	Concentration of pathogens in the environment	10^6	[108]
P_0	Saturation constant of *E. coli* O157:H7	10^9	Assumed
α_h	Shedding rate from cattle infected	0.05	[108]
N_e	Number of pathogens produced	1000	Assumed
ϕ	Death rate of pathogens via immune.	8.6×10^{-6}	[109]
μ_h	Decay rate of E.coli in the microscale	0.03	[108]
α_e	Bacteria replication rate	0.76	Assumed
Λ_h	Supply rate of epithelial cells	5	[109]
β_h	Infection rate of epithelial cells	0.43	Assumed
μ_e	Decay rate of epithelial cells	0.07	[109]
Λ_s	Supply rate of immune cells	3.0×10^5	[109]
ρ_s	Activation rate of immune system	1.4×10^{-9}	[109]
μ_s	Natural death rate of immune cells	0.03	[109]

Table 4.3: Decription of parameters and their values.

4.2 Mathematical analysis

Proposition 1: For non-negative initial conditions, the solutions to the set of equations (4.1.4.6) remain bounded for all $t \geq 0$. Additionally, the domain D_1 serves as a positively invariant and attracting region, ensuring that solutions originating in D_1 will remain within it for all $t \geq 0$.

Consequently, the system of equations (4.1.4.6) exhibits mathematical and epidemiological well-posedness.

$$\begin{cases} D_1 = (S_C(t), I_C(t), P_W(t)) \in \mathbb{R}_3^+ : 0 \leq S_C + I_C \leq \dfrac{\Lambda_C}{\mu_C}, \\ \qquad 0 \leq P_W \leq \dfrac{\Lambda_C N_h \alpha_h}{\mu_W \mu_C}. \end{cases} \tag{4.2.0.1}$$

4.2.1 Feasible region

We denote N_C as the total cattle population count. By summing the first and second equations from the set (4.1.4.6), that is, $N_C = S_C + I_C$, we derive the following expression:

$$\frac{dN_C}{dt} = \Lambda_C - \mu_C N_C - \delta_C I_C,$$

then

$$\frac{dN_C}{dt} \leq \Lambda_C - \mu_C N_C,$$

and hence

$$lim_{x \to \infty}(sup(N_C(t)) \leq \frac{\Lambda_C}{\mu_C}. \tag{4.2.1.1}$$

Using a similar approach, similar expression can be derived for the remaining variable P_W within the system of equations (4.1.4.6). then, we introduce:

$$\begin{cases} D_2 = (S_C(t), I_C(t), P_W(t)) \in \mathbb{R}_3^+ : 0 \leq S_C + I_C \leq \dfrac{\Lambda_C}{\mu_C}, \\ \qquad 0 \leq P_W \leq \dfrac{\Lambda_C N_h \alpha_h}{\mu_W \mu_C}. \end{cases} \tag{4.2.1.2}$$

This indicates that D_2 functions as a positively invariant and attracting region, ensuring that any solution originating in D_2 will remain within it for all $t \geq 0$. Consequently, the system of equations (4.1.4.6) possesses both mathematical and epidemiological well-posedness.

4.2.2 The Disease-free Equilibrium and Reproductive Number of the Simplified Model

The disease-free equilibrium (DFE) of *E. coli* O157:H7 signifies its stable solution when the infection or disease is absent. This equilibrium is represented as E_0, where all the infected compartments are at zero, and the entire population consists only of susceptible individuals. Hence, the disease-free state for the multiscale *E. coli* O157:H7 model, denoted as E_0, can be expressed as:

$$E_0 = (S_C, I_C, P_W) = \left(\frac{\Lambda_C}{\mu_C}, 0, 0\right). \tag{4.2.2.1}$$

4.2.3 The basic reproductive number

Based on our multiscale model which consists of 3 compartments, namely susceptible, infected, and pathogen, the transition occurs from susceptible to infected. To calculate the basic reproduction number (R_0), we only use the infected state and the pathogen compartment, so that our Jacobian matrix can be

$$J_{E_0} = \begin{bmatrix} -(\mu_C + \delta_C) & \dfrac{\beta_W \Lambda_C}{P_0 \mu_C} \\ \\ N_h \alpha_h & r_W - \mu_W \end{bmatrix}, \tag{4.2.3.1}$$

In calculating R_0 we use the Next Generation Matrix method which involves partitioning the matrix J into the submatrix F and V where F is a new non-negative infection matrix and V consists of death, increased state, and other transitions.

$J = FV$
$K = FV^{-1}$

So that matrix

$$F = \begin{bmatrix} 0 & \dfrac{\beta_W \Lambda_C}{P_0 \mu_C} \\ \\ 0 & 0 \end{bmatrix}, \tag{4.2.3.2}$$

and

$$V = \begin{bmatrix} (\mu_C + \delta_C) & 0 \\ \\ -N_h\alpha_h & \mu_W - r_W \end{bmatrix}, \tag{4.2.3.3}$$

are obtained. Whereas the inverse of the matrix V is obtained by

$$V^{-} = \begin{bmatrix} \dfrac{1}{(\mu_C + \delta_C)} & 0 \\ \\ \dfrac{N_h\alpha_h}{(\mu_C + \delta_C)(\mu_W - r_W)} & \dfrac{1}{\mu_W - r_W} \end{bmatrix}, \tag{4.2.3.4}$$

$$K = FV^{-1} = \begin{bmatrix} \dfrac{\beta_W\Lambda_C N_h\alpha_h}{P_0\mu_C(\mu_C + \delta_C)(\mu_W - r_W)} & \dfrac{\beta_W\Lambda_C}{P_0\mu_C} \\ \\ 0 & 0 \end{bmatrix},$$

By using the dominant eigenvalue the basic reproduction number is given by:

$R_0 = \dfrac{\beta_W\Lambda_C N_h\alpha_h}{P_0\mu_C(\mu_C + \delta_C)(\mu_W - r_W)}$, which is biological meaningful provided $\mu_W > r_W$.

4.2.4 Local stability of the Disease-Free Equilibrium

In this subsection, we analyze the local stability of the disease-free equilibrium (DFE) of the model system (4.1.4.6) by linearizing all the equations within the model (4.1.4.6). This linearization process helps us obtain the Jacobian matrix at a state where no infection is present.

$$E_0 = \left(\frac{\Lambda_C}{\mu_C}, 0, 0\right) \tag{4.2.4.1}$$

and evaluate the matrix $det|J(E_0) - \lambda I|$. The Jacobian matrix after linearization is expressed as follows:

$$J_{E_0} = \begin{bmatrix} -\mu_C & 0 & \dfrac{-\beta_W \Lambda_C}{P_0 \mu_C} \\ 0 & -(\mu_C + \delta_C) & \dfrac{\beta_W \Lambda_C}{P_0 \mu_C} \\ 0 & N_h \alpha_h & -(\mu_W - r_W) \end{bmatrix}, \tag{4.2.4.2}$$

In order to assess the stability of the disease-free equilibrium (DFE), we determine the eigenvalues of the Jacobian matrix (4.2.4.2) using the method outlined in [71]. The characteristic equation that yields the eigenvalues is provided as follows:

$$-(\lambda + \mu_C)[\lambda^2 + ((\mu_C + \delta_C)(\mu_W - r_W))\lambda + (\mu_C + \delta_C)(\mu_W - r_W)(1 - R_0)], \tag{4.2.4.3}$$

Equation (4.2.4.3) reveals that one of the eigenvalues corresponds to $(-\mu_C)$. When the eigenvalues are challenging to compute directly, the assessment of the stability of the DFE involves employing the Routh-Hurwitz criterion. This criterion is applied to the coefficients of the characteristic polynomial derived from the linearized Jacobian matrix. Therefore, for stability, the application of the Routh-Hurwitz criteria to the polynomial

$$p(\lambda) = \lambda^2 + a_1\lambda + a_0 = 0,$$

where

$$\begin{cases} a_1 = (\mu_C + \delta_C)(\mu_W - r_W), \\ a_0 = (\mu_C + \delta_C)(\mu_W - r_W)(1 - R_0). \end{cases} \tag{4.2.4.4}$$

and

$$R_0 = \frac{\beta_W \Lambda_C N_h \alpha_h}{P_0 \mu_C (\mu_C + \delta_C)(\mu_W - r_W)}$$

necessitates the satisfaction of the following condition:

$$\begin{cases} a_1 > 0, \\ a_0 > 0. \end{cases} \tag{4.2.4.5}$$

If both conditions are satisfied, the roots of the characteristic equation have negative real parts indicating that the equilibrium is stable.

Therefore, for $a_1 > 0$:

we have $(\mu_C + \delta_C)(\mu_W - r_W)$, and since $(\mu_C + \delta_C) > 0$ and $(\mu_W - r_W) > 0$, provided that $\mu_W > r_W$, we have that $a_1 > 0$.

For $a_0 > 0, (\mu_C + \delta_C)(\mu_W - r_W)(1 - R_0)$. This condition requires that $1 - R_0 > 0$, which implies that $R_0 < 1$.

Hence, it becomes noticeable that the coefficients a_1 and a_0 of the polynomial $p(\lambda)$ are consistently positive under the condition $\mu_W > r_W$ and $R_0 < 1$. Consequently, all the roots of the polynomial $p(\lambda)$ are either negative or possess negative real parts. We summarize the results in the following theorem.

Theorem 4.1. *[72] The local asymptotic stability of the disease-free equilibrium point of the model system (4.1.4.6) is established when the condition $R_0 < 1$ holds.*

4.2.5 Global stability of the disease-free equilibrium

In this subsection, we apply the approach outlined in [70] to analyze the stability of the disease-free equilibrium. To achieve this, we reformulate the system of equations (4.1.4.6) as follows:

$$\begin{cases} \dfrac{dX}{dt} &= F(X,Y), \\ \\ \dfrac{dY}{dt} &= G(X,Y). \end{cases} \tag{4.2.5.1}$$

Here, X represents the count of uninfected cells (S_C), while Z encompasses the infected compartments and infectious classes (I_C and P_W). The disease-free equilibrium is denoted as

$$E_0 = \left(\frac{\Lambda_C}{\mu_C}, 0, 0\right).$$

For the global asymptotic stability of the system, the fulfillment of the following conditions is necessary:

H1. for $\dfrac{dX}{dt} = F(X,0)$ is globally asymptotically stable ,

H2. $G(X,Z) = AZ - \hat{G}(X,Z)$, $\hat{G}((X,Z) \geq 0$ for $(X,Z) \in \mathbb{R}^3_+$ where $A = D_Z G(X^*, 0)$ is an M-matrix and $\mathbb{R}^3_+$ is the region where the model have a biological meaning.

In our case,

$$F(X,0) = \left[\ \Lambda_C - \mu_C S_C\ \right], \tag{4.2.5.2}$$

and

$$A = \begin{bmatrix} -(\delta_C - \mu_C) & \dfrac{\beta_W \Lambda_C}{P_0 \mu_C} \\ N_h \alpha_h & (r_W - \mu_W) \end{bmatrix}, \tag{4.2.5.3}$$

$$\hat{G}(X, Z) = \begin{bmatrix} \left(\dfrac{\Lambda_C}{P_0 \mu_C} - \dfrac{S_C}{P_0 + P_W} \right) \beta_W P_W \\ \dfrac{r_W P_W^2}{K_W} \end{bmatrix}. \tag{4.2.5.4}$$

Since $S_C^0 \left(= \dfrac{\Lambda_C}{\mu_C} \right) \dfrac{1}{P_0} \geq \dfrac{S_C}{P_0 + P_W}$ it is clear that $\hat{G}(X, Z) \geq 0$ for all $(X, Z) \in \mathbb{R}^3_+$.

It can be easily observed that matrix A is an M-matrix due to the non-negative values of its off-diagonal elements. Below we present the theorem to summarize the results:

Theorem 4.2. *[72] The fixed point*

$$E_0 = (X^*, 0) = E_0 \quad = \quad \left(\frac{\Lambda_C}{\mu_C}, 0, 0 \right), \tag{4.2.5.5}$$

The global asymptotic stability of the equilibrium point in the model system (4.1.4.6) is achieved when $R_0 \leq 1$ and the conditions $(H1)$ and $(H2)$ are fulfilled.

4.2.6 The Endemic Equilibrium Points

At the endemic state, cattle experience high levels of *E. coli* O157:H7 infection and excrete bacteria in significant quantities. At this point, the bacteria would have established themselves and persisted within the farm environment. The expressions for the endemic equilibrium point are represented by: $E^* = (S_C^*, I_C^*, P_W^*)$. Therefore evaluating the system of equations (4.1.4.6) at endemic state , the endemic level of bacteria in the environment is given by

$$P_W^*(a_2(P_W^*)^2 + a_1 P_W^* + a_0) = 0. \tag{4.2.6.1}$$

where

$$\begin{cases} a_2 = r_W(\beta_W + \mu_C)(\delta_C + \mu_C) > 0, \\ a_1 = ((\delta_C + \mu_C)(P_0 r_W \mu_C + K_W(\beta_W + \mu_C)(\mu_W - r_W))) > 0. \\ a_0 = P_0 \mu_C K_W(\delta_C + \mu_C)(\mu_W - r_W)(1 - R_0). \end{cases} \tag{4.2.6.2}$$

$P_W^* = 0$ or

$$P_W^* = \frac{-a_1 \pm \sqrt{a_1^2 - 4a_2 a_0}}{2a_2}. \tag{4.2.6.3}$$

The expression above indicates that the size of the susceptible cattle population is directly influenced by both the average duration individuals spend in the susceptible class and the influx of new susceptible cattle through birth. The endemic level of infected cattle is described by the following expression:

$$I_C^* = \frac{P_W^*(P_W^* r_W + K_W(\mu_W - r_W))}{K_W N_h \alpha_h} \tag{4.2.6.4}$$

The above expression reveals that the infected population is directly proportional to the duration individuals spend in the infected compartment, the rate at which susceptible cattle transition into the infected state, and the density of susceptible cattle. The endemic level of susceptible cattle is given by:

$$S_C^* = \frac{-(P_W^*)^2 r_W(\delta_C + \mu_C) + K_W(N_h \alpha_h \Lambda_C + P_W^*(\delta_C + \mu_C)(r_W - \mu_W)}{K_W N_h \alpha_h \mu_C} \tag{4.2.6.5}$$

The biologically meaningful solution would be the non-zero P_W^*. Therefore from the above expressions, we conclude that there exist a positive endemic equilibrium points when $\mu_W > r_W$ and $R_0 > 1$.

4.2.7 Local Stability of the Endemic Equilibrium

$$1 = \frac{\beta_W \Lambda_C N_h \alpha_h}{P_0 \mu_C(\mu_C + \delta_C)(\mu_W - r_W)}. \tag{4.2.7.1}$$

Simplifying we obtain

$$\beta^* = \frac{(\delta_C + \mu_C)(\mu_W - r_W)P_0\mu_C}{N_h\alpha_h\alpha_C}, \tag{4.2.7.2}$$

Additionally, we employ vector notation $\mathbf{x} = (x_1, x_2, x_3)^T$ to represent the variables, enabling us to express the model system (4.1.4.6) in the following way:

$$\frac{d\mathbf{x}}{dt} = \mathbf{F}(\mathbf{x})$$

with

$$\mathbf{F} = (f_1, f_2, f_3),$$

such that:

$$\begin{cases} \dot{x_1} = f_1 = \Lambda_C - \dfrac{\beta^* x_1 x_3}{P_0 + x_3} - \mu_C x_1, \\ \dot{x_2} = f_2 = \dfrac{\beta^* x_1 x_3}{P_0 + x_3} - (\mu_C + \delta_C)x_2, \\ \dot{x_3} = f_3 = r_W x_3\left(1 - \dfrac{x_3}{K_W}\right) + N_h\alpha_h x_2 - \mu_W x_3. \end{cases} \tag{4.2.7.3}$$

The Jacobian matrix corresponding to the system of equations (4.1.4.6), computed at the disease-free equilibrium (E_0), is presented as follows:

$$J = \begin{bmatrix} -\mu_C & 0 & \dfrac{-\beta_W\Lambda_C}{P_0\mu_C} \\ 0 & -b_0 & \dfrac{\beta_F\Lambda_C}{P_0\mu_C} \\ 0 & N_h\alpha_h & -b_1 \end{bmatrix}, \tag{4.2.7.4}$$

where

$$\begin{cases} b_0 = (\mu_C + \delta_C), \\ b_1 = (\mu_W - r_W). \end{cases} \tag{4.2.7.5}$$

The basic reproductive number of model system (4.2.7.3) is

$$R_0 = \frac{\beta_W \Lambda_C N_h \alpha_h}{P_0 \mu_C (\mu_C + \delta_C)(\mu_W - r_W)}. \tag{4.2.7.6}$$

It is clear that the linearized system resulting from the transformed equations (4.2.7.3) with the critical value β^* presents a simple zero eigenvalue. As a result, we can apply the center manifold theory described in [73], which is provided below for clarity. This theory can be utilized to analyze the dynamics of (4.2.7.3) near $\beta_W = \beta$ and establish the local asymptotic stability of the endemic equilibrium point for (4.2.7.3) at $\beta_W = \beta$. This is equivalent to confirming the local stability of the endemic equilibrium point of the original system (4.1.4.6) at the same bifurcation point $\beta_W = \beta^*$.

Theorem 4.3. *[73] Consider the general system of ordinary differential equations characterized by the parameter ϕ.:*

$$\frac{dx}{dt} f(x, \phi), \quad f : \mathbb{R}^n \longrightarrow \mathbb{R}, \quad f : \mathbb{C}^2(\mathbb{R}^2 \times \mathbb{R}), \tag{4.2.7.7}$$

in the system (4.1.4.6), it is notable that the equilibrium point 0, (i.e., $f(0, \phi) = 0, \quad \forall \quad \phi$, and assume that

(1) $A = D_x f(0,0) = \left(\frac{\partial f_i(0,0)}{\partial x_i} \right)$ this represents a linear approximation of the system around the equilibrium point 0, where the parameter ϕ is evaluated at 0;

(2) Zero is an eigenvalue of matrix A, and all other eigenvalues of matrix A have negative real parts;

(3) Matrix A possesses a left eigenvector represented as $\mathbf{u}$ and a right eigenvector represented as $\mathbf{v}$, both corresponding to the eigenvalue zero.

Let f_k represent the kth component of the vector f, and

$$a = \sum_{k,i,j=1}^{n} v_k u_i u_j \frac{\partial^2 f_k}{\partial x_i \partial x_j}(0,0), \tag{4.2.7.8}$$

$$b = \sum_{k,i,j=1}^{n} v_k u_i \frac{\partial^2 f_k}{\partial x_i \partial \phi}(0,0). \tag{4.2.7.9}$$

The behavior of the system near the equilibrium point 0 is entirely determined by the signs of the parameters a and b.

(i) $a > 0$, $b > 0$, *when* $\phi < 0$ *with* $\mid \phi \mid \ll 1$, *0 is locally asymptotically stable, and there exists a positive unstable equilibrium; when* $0 < \phi \ll 1$, *0 is unstable and there exists a negative and locally asymptotically stable equilibrium.*

(ii) $a < 0$, $b < 0$, *when* $\phi < 0$ *with* $\mid \phi \mid \ll 1$, *0 is unstable; when* $0 < \phi \ll 1$, *0 is locally asymptotically stable, and there exists a positive unstable equilibrium point.*

(iii) $a > 0$, $b < 0$, *when* $\phi < 0$ *with* $\mid \phi \mid \ll 1$, *0 is unstable and there exists a locally asymptotically stable negative equilibrium; when* $0 < \phi \ll 1$, *0 is stable and a positive unstable equilibrium appear.*

(iv) $a < 0$, $b > 0$, *when* ϕ *changes from negative to positive, 0 changes its stability from stable to unstable. Correspondingly a negative unstable equilibrium becomes positive and locally asymptotically stable.*

Jacobian matrix (4.2.7.4) has left eigenvector **u** = (u_1, u_2, u_3), where

$$\begin{cases} u_1 = \dfrac{\beta_W \Lambda_C N_h \alpha_h}{P_0 \mu_C (\mu_W - r_W)}, \\ u_2 = 1, \\ u_3 = \dfrac{N_h \alpha_h}{(\mu_W - r_W)}. \end{cases} \tag{4.2.7.10}$$

The right eigenvector of the Jacobian matrix (4.2.7.4) is given by **v** = $(v_1, v_2, v_3)^T$, where

$$\begin{cases} v_1 = 0, \\ v_2 = 1, \\ v_3 = -\dfrac{\beta_W \Lambda_C}{P_0 \mu_C (\mu_W - r_W)}. \end{cases} \tag{4.2.7.11}$$

Calculating the non-zero second-order mixed derivative of **F** with respect to the variables and β^*, which helps us determine the sign of a, yields the following result:

$$\begin{cases} \dfrac{\partial^2 f_1}{\partial x_3^2} = \dfrac{2\beta^*\Lambda_C}{P_0^2\mu_C}, \\ \dfrac{\partial^2 f_2}{\partial x_3^2} = -\dfrac{2\beta^*\Lambda_C}{P_0\mu_C}, \\ \dfrac{\partial^2 f_3}{\partial x_3^2} = -\dfrac{2r_W}{K_W}. \end{cases} \tag{4.2.7.12}$$

The non-zero partial mixed derivative used to determine the sign of b is given by

$$\begin{cases} \dfrac{\partial^2 f_1}{\partial x_3 \partial \beta^*} = -\dfrac{\Lambda_H}{\mu_H P_0}, \\ \dfrac{\partial^2 f_1}{\partial x_3 \partial \beta^*} = \dfrac{\Lambda_H}{\mu_H P_0}. \end{cases} \tag{4.2.7.13}$$

Substituting expression (4.2.7.10), (4.2.7.11), (4.2.7.12) and (4.2.7.13) into a and b in (4.2.7.8) and (4.2.7.9) respectively, we get

$$a = \left[\frac{2\beta^*\Lambda_C}{P_0^2\mu_C}.v_3(u_1-u_2) - \frac{2r_W}{K_W}\right], \tag{4.2.7.14}$$

and

$$b = \frac{k\Lambda_C}{\mu_C P_0}.v_3(u_2-u_1). \tag{4.2.7.15}$$

Since at the DFE $r_W < \mu_W$ and $(u_1 - u_2) < 0$ this implies that $a < 0$ and therefore $u_1 - u_2 < 0$ and if $u_1 > u_2$ then $b > 0$. Using item (iv), based on Theorem 4.3, we can deduce that the endemic steady state of the model system (4.1.4.6) is locally asymptotically stable, and this holds when R_0 is slightly greater than 1. These findings are concisely summarized in the following theorem:

Theorem 4.4. *[72] The E. coli O157:H7 endemic steady state is locally asymptotically stable when $R_0 > 1$ but only if R_0 is close to 1.*

4.3 Sensitivity Analyis

In this section, we employ the multiscale model (4.1.4.6) to derive insights that can provide guidance for formulating strategies to prevent and manage *E. coli* O157:H7 infections. We utilize the parameter values outlined in Table 4.3 for our analysis. The most effective approach to reduce human mortality and morbidity caused by *E. coli* O157:H7 infection involves gaining a full understanding of the varying contributions of different factors influencing the two transmission metrics of the multiscale model system (4.1.4.6), R_0 and P_W^*. Below are the sensitivity results of R_0 and P_W^* on the model parameters when they change, given in the Tornado plots, Figure 4.2 and Figure 4.3, respectively.

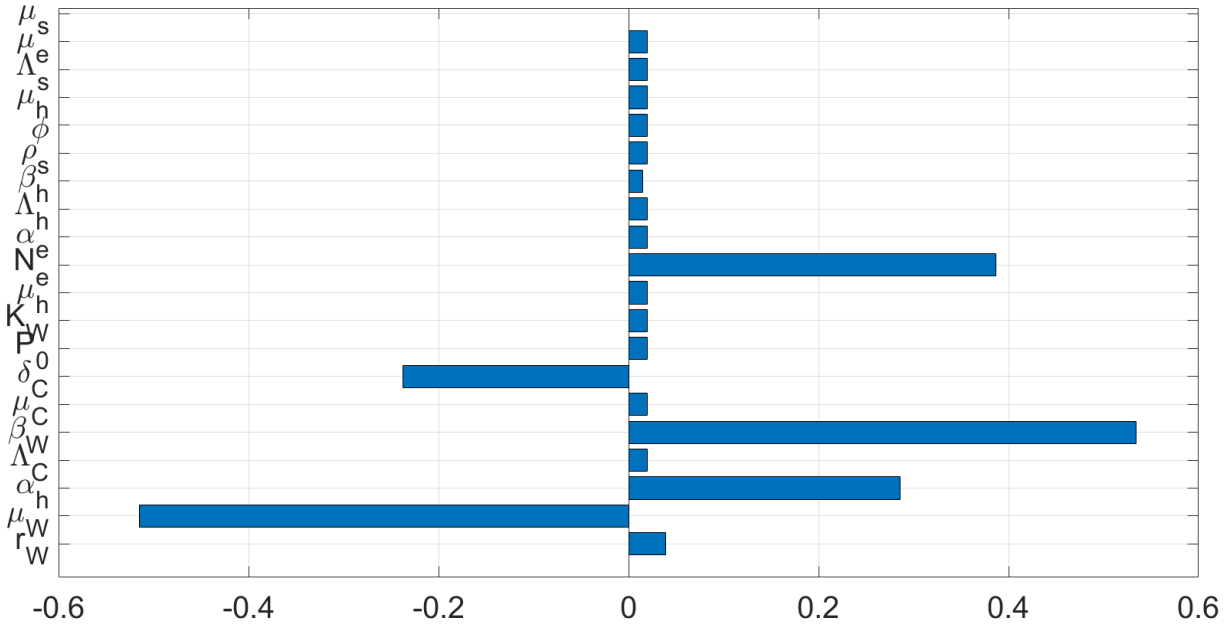

Figure 4.2: Tornado plots illustrate the partial rank correlation coefficients (PRCCs) for all parameters that impact R_0.

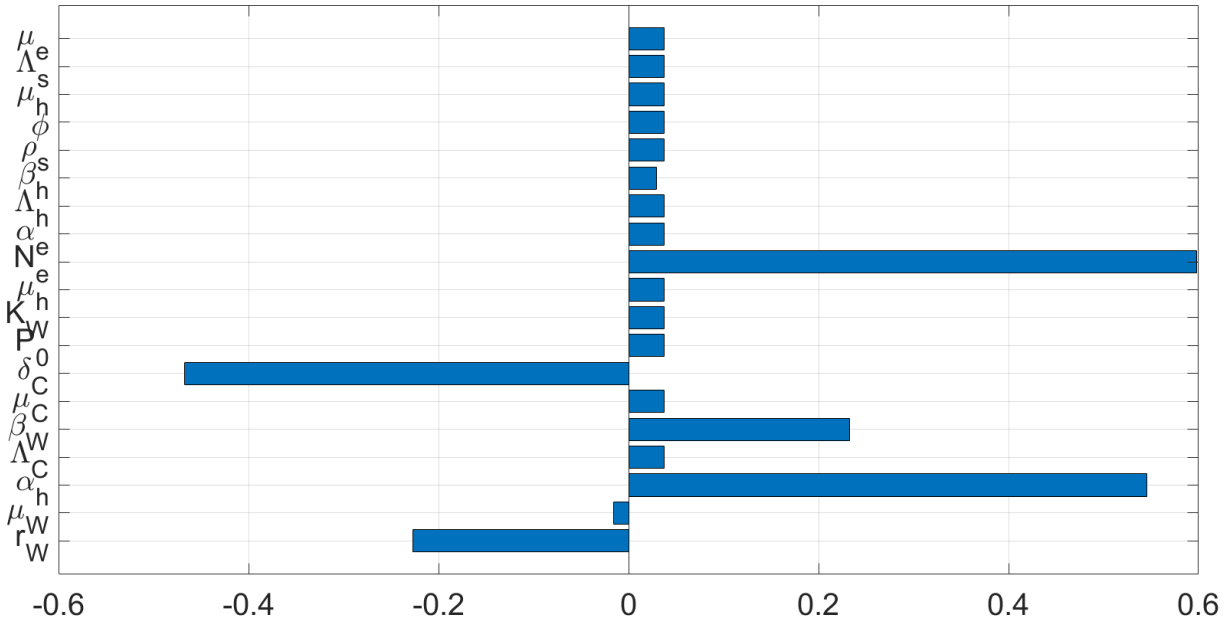

Figure 4.3: Tornado plots of partial rank correlation coefficients (PRCCs) of all seventeen parameters that influence P_W^*.

We observe the following from Figure 4.2 and Figure 4.3:

(i) In Figure 4.2 we observe that the three parameters that we have most control over are the within-host parameters. The parameters N_e and α_h and the between-host parameters β_W and μ_W.

(ii) In Figure 4.3 we observe that there are also four parameters that we have control over. The within-host parameters are N_e and α_h and the between-host parameters are β_h and r_W.

We learn from these results that both R_0 and P_W^* are highly sensitive to similar parameters (β_W, N_e, α_h) and they are both sensitive to δ_C also. Therefore we deduce that, generally, R_0 and P_W^* are comparable. Therefore, it can be inferred that in order to strengthen the validity and usefulness of the nested multiscale model (4.1.4.6), care should be taken in a way to modify the accuracy of these parameters during data collection since these parameters were identified as crucial in the control of foodborne diseases.

4.4 Nonstandard Finite Difference Scheme

Let S_C^k, I_C^k, and P_W^k represent the approximated values of $S_C(kh)$, $I_C(kh)$, and $P_W(kh)$, respectively, where $k = 0, 1, 2, ...$ and h is the time step used in the scheme. These sequences S_C^k, I_C^k, and P_W^k are expected to remain nonnegative to align with the biological context of the model [110]. We implement Micken's scheme by substituting the step-size h with functions $\phi_i(h)$, where $i = 1, 2, 3$, and introduce nonlocal representations for the function terms. The discretization of the simplified multiscale model (4.1.4.6) is carried out as follows:

$$\begin{aligned}
\frac{S_C^{k+1} - S_C^k}{\phi_1(h)} &= \Lambda_C - \frac{\beta_W P_W^k S_C^{k+1}}{P_0 + P_W^k} - \mu_C S_C^{k+1}, \\
\frac{I_C^{k+1} - I_C^k}{\phi_2(h)} &= \frac{\beta_W P_W^k S_C^{k+1}}{P_0 + P_W^k} - (\mu_C + \delta_C) I_C^{k+1}, \\
\frac{P_W^{k+1} - P_W^k}{\phi_3(h)} &= r_W P_W^{k+1} - \frac{r_W P_W^k P_W^{k+1}}{K_W} + N_h \alpha_h I_C^{k+1} - \mu_W P_W^{k+1}.
\end{aligned} \tag{4.4.0.1}$$

Below are the denominator functions considered in this study:

$$\begin{cases}
\phi_1(h) &= \dfrac{e^{h\mu_C} - 1}{\mu_C}, \\[2ex]
\phi_2(h) &= \dfrac{e^{h(\mu_C + \delta_C)} - 1}{\mu_C + \delta_C}, \\[2ex]
\phi_3(h) &= \dfrac{1 - e^{h(r_W - \mu_W)}}{r_W - \mu_W}.
\end{cases}$$

Rearranging Equation (4.4.0.1) we obtain:

$$\begin{cases}
S_C^{k+1} &= \dfrac{S_C^k + \phi_1(h)\Lambda_C}{1 + \phi_1(h)\left(\frac{\beta_W P_W^k}{P_0 + P_W^k} + \mu_C\right)}, \\[2ex]
I_C^{k+1} &= \dfrac{I_c^k + \phi_2(h)\left(\frac{\beta_W P_W^k S_C^{k+1}}{(P_0 + P_W^k)}\right)}{1 + \phi_2(h)(\mu_C + \delta_C)}, \\[2ex]
P_W^{k+1} &= \dfrac{\phi_3(h) N_h \alpha_h I_C^k + P_W^k}{1 + \phi_3(h)\left(\mu_W - r_W(1 - \frac{r_W P_W^k}{K_W})\right)}.
\end{cases} \tag{4.4.0.2}$$

The method described above ensures the positivity of the solution, as it guarantees that if the initial conditions $S_C(0)$, $I_C(0)$, and $P_W(0)$ are non-negative, then the expressions on the right-hand side of Equations (4.4.0.2) do not contain negative terms for any $k = 0, 1, 2, ...$, provided that $\mu_W > \left(1 - \frac{r_W P_W^k}{K_W}\right)$.

4.4.1 The equilibrium points and stability analysis

In this subsection, we investigate the stability and convergence characteristics of equilibrium points within the introduced numerical scheme. We designate X^* as the equilibrium point of the system (4.4.0.1), then it becomes:

$$X^* = (\hat{S_C}, \hat{I_C}, \hat{P_W}),$$

Thus, we observe that the equilibrium point X^* of the system (4.4.0.1) can be found by solving

$$\begin{cases} f_1(\hat{S_C}, \hat{I_C}, \hat{P_W}) = \hat{S_C}, \\ f_2(\hat{S_C}, \hat{I_C}, \hat{P_W}) = \hat{I_C}, \\ f_3(\hat{S_C}, \hat{I_C}, \hat{P_W}) = \hat{P_W}. \end{cases}$$

where $f_i(\hat{S_C}, \hat{I_C}, \hat{P_W}), i = 1, 2, 3$, can be obtained by considering the right hand sides of Equations (4.4.0.2), that is

$$\begin{cases} f_1(\hat{S_C}, \hat{I_C}, \hat{P_W}) = \dfrac{\hat{S_C} + \phi_1(h)\Lambda_C}{1 + \phi_1(h)\left(\frac{\beta_W \hat{P_W}}{P_0 + \hat{P_W}} + \mu_C\right)}, \\ f_2(\hat{S_C}, \hat{I_C}, \hat{P_W}) = \dfrac{\hat{I_C} + \frac{\phi_2(h)\beta_W \hat{P_W} \hat{S_C}}{(P_0 + \hat{P_W})}}{1 + \phi_2(h)(\mu_C + \delta_C)}, \\ f_3(\hat{S_C}, \hat{I_C}, \hat{P_W}) = \dfrac{\phi_3(h) N_h \alpha_h \hat{I_C} + \hat{P_W}}{1 + \phi_3(h)\left(\mu_W - r_W(1 - \frac{r_W \hat{P_W}}{K_W})\right)}. \end{cases} \tag{4.4.1.1}$$

In the system mentioned above, when $\hat{I_C} = \hat{P_W} = 0$ and considering that the equilibrium point of various equations is satisfied by $f_i(X^*) = X^*, i = 1, 2, 3$, then

$$\begin{cases} \hat{S_C} &= \dfrac{\hat{S_C} + \phi_1(h)\Lambda_C}{1 + \phi_1(h)\mu_C} = \dfrac{\Lambda_C}{\mu_C}, \\ \hat{I_C} &= \dfrac{\hat{I_C}}{1 + \phi_2(h)(\mu_C + \delta_C)} = 0, \\ \hat{P_W} &= \dfrac{\phi_3(h)N_h\alpha_h\hat{I_C} + \hat{P_W}}{1 + \phi_3(h)\left(\mu_W - r_W(1 - \frac{r_W\hat{P_W}}{K_W})\right)} = 0. \end{cases} \tag{4.4.1.2}$$

In this case, if both $\hat{I_C}$ and $\hat{P_W}$ are set to zero, the disease-free equilibrium becomes unique and is represented as $\left(\dfrac{\Lambda_C}{\mu_C}, 0, 0\right)$. However, if any of the infected variables is non-zero, it signifies the presence of the endemic equilibrium within the NSFD scheme for the complete model (4.1.4.6).

4.4.2 Numerical stability analysis of the equilibrium points

In this subsection, we examine the following condition for a multiscale model (4.1.4.6) $(S_C(0), I_C(0), P_W(0)) = (1000, 10, 200000)$. The parameter values of the multiscale are given in Table 4.3. To analyze the stability properties of the equilibria in the system (4.1.4.6), we begin by calculating the Jacobian matrix of the system at the disease-free equilibrium point

$$E_0 = \left(\frac{\Lambda_C}{\mu_C}, 0, 0\right)$$

and this matrix is represented as follows:

$$J = \begin{bmatrix} J_{11} & J_{12} & J_{13} \\ J_{21} & J_{22} & J_{23} \\ J_{31} & J_{32} & J_{33} \end{bmatrix}, \tag{4.4.2.1}$$

where

$$
\begin{aligned}
J_{11} &= \frac{1}{1+\phi_1(h\left(\frac{\beta_W P_W^k}{P_0+P_W^k}+\mu_W\right)}, \\
J_{12} &= =0, \qquad (4.4.2.2)\\
J_{13} &= \frac{-(S_C+\phi_1(h)\Lambda_C)[\frac{(P_0+P_W^k)\beta_W-\beta_W P_W^k}{P_0+P_W^k}]}{\left[1+\phi_1(h)\left(\frac{\beta_W P_W^k}{P_0+P_W^k}+\mu_W\right)\right]^2}, \\
J_{21} &= \frac{\phi_2(h)\beta_W P_W^k}{[(P_0+P_W^k)+\phi_1(h)(\beta_W P_W^k+\mu_W(P_0+P_W^k))][1+\phi_2(h)(\mu_C+\delta_C)]}, \\
J_{22} &= \frac{(P_0+P_W^k)+\phi_1(h)(\beta_W P_W^k+\mu_W(P_0+P_W^k))}{[(P_0+P_W^k+\phi_1(h)(\beta_W P_W^k+\mu_W(P_0+P_W^k))][1+\phi_2(h)(\mu_C+\delta_C)]}, \\
J_{23} &= \frac{1}{1+\phi_2(h)(\mu_C+d\delta_C)}\Big[b_0(b_1+b_2)-(b_3+b_4)(1+\phi_1(h)(\beta_W+\mu_W))\Big], \\
J_{31} &= \frac{\phi_3(h)N_h\alpha_h}{1-\phi_3(h)\left(r_w P_W^k+\mu_W-\frac{r_W P_W^k}{K_W}\right)}m_1, \\
J_{32} &= \frac{\phi_3(h)N_h\alpha_h}{1-\phi_3(h)\left(r_w P_W^k+\mu_W-\frac{r_W P_W^k}{K_W}\right)}m_2, \\
J_{33} &= \frac{q_1P_W^{k^2}+a_1q_2P_W^{k^2}+r_12p_1P_W^k+[p_2+t_1]-[p_1P_W^{k^2}[p_2+t_1]P_W^k+a_4I_C^kc_1]2q_1P_W^k+a_1q_2}{(q_1P_W^{k^2}+a_1q_2)P_W^k+r_1}.
\end{aligned}
$$

with

$$
\begin{aligned}
b_0 &= ((P_0+P_W)+\phi_1(h)(\beta_W P_W+\mu_W(P_0+P_W))),\\
b_1 &= I_C(1+\phi_1(h)(\beta_W+\mu_W)),\\
b_2 &= \phi_2(h)\beta_W[S_C+\phi_1(h)\Lambda_C],\\
b_3 &= I_C\Big[(P_0+P_W)+\phi(h)(\beta_W+\mu_W(P_0+P_W))\Big]\Lambda_C,\\
b_4 &= \phi_2(h)\beta_W P_W[S_C+\phi_1(h)\Lambda_C],\\
m_1 &= \frac{\phi_2(h)\beta_W P_W}{\Big[(P_0+P_W)+\phi_1(h)(\beta_W P_W+\mu_W(P_0+P_W))\Big][1+\phi_2(h)(\mu_C+\delta_C)]},\\
m_2 &= \frac{[(P_0+P_W)+\phi_1(h)(\beta_W P_W+\mu_W(P_0+P_W))]}{\Big[(P_0+P_W)+\phi_1(h)(\beta_W P_W+\mu_W(P_0+P_W))\Big][1+\phi_2(h)(\mu_C+\delta_C)]},\\
q_1 &= a_1d_1d_3,\\
q_2 &= k_1d_3+d_1d_2,\\
r_1 &= a_1b_1d_2,\\
p_1 &= a_1c_2,\\
p_2 &= a_1c_1,\\
t_1 &= a_4(c_2I_C^k+a_5[\phi_1(h)\Lambda_C+S_C^k])
\end{aligned}
\tag{4.4.2.3}
$$

and

$$
\begin{aligned}
a_1 &= [1+\phi_2(h(\mu_C+\delta_C))],\\
a_2 &= \phi_1(h)\beta_W,\\
a_3 &= \phi_1(h)\mu_C,\\
a_4 &= \phi_3(h)N_h\alpha_h,\\
a_5 &= \phi_2(h)\beta_W,\\
k_1 &= 1-\phi_3(h)r_W+\phi_3(h)\mu_W,\\
d_1 &= \frac{\phi_3(h)r_W}{K_W},\\
d_2 &= P_0(1+\phi_1(h)\mu_C),\\
d_3 &= (1+\phi(h)\mu_C+\phi_1(h)\beta_W).
\end{aligned}
$$

Substituting the disease-free equilibrium E_0 , into the Jacobian matrix will yield:

$$J(E_0) = \begin{bmatrix} J_{11} & 0 & J_{13} \\ 0 & J_{22} & J_{23} \\ 0 & J_{32} & J_{33} \end{bmatrix}, \tag{4.4.2.4}$$

where

$$\begin{aligned} J_{11} &= \frac{1}{1+\phi_1(h)\mu_W}, \\ J_{13} &= \frac{\Lambda_C(1+\phi_1(h)\mu_C)\beta_W}{\mu_C(1+\phi_1(h)\mu_W)}, \\ J_{22} &= \frac{1}{1+\phi_2(h)(\mu_C+\delta_C)}, \\ J_{23} &= \frac{\phi_2(h)\beta_W\Lambda_C[1+\phi_1(h)\mu_C]}{[1+\phi_2(h)(\mu_C+\delta_C)][1+\phi_1(h)\mu_W]P_0\mu_C}, \\ J_{32} &= \frac{\phi_3(h)N_h\alpha_h}{(1-\phi_3(h)\mu_W)[1+\phi_2(h)(\mu_c+\delta_C)]}, \\ J_{33} &= \frac{[a_1c_1+a_4a_5[\phi_1(h)\Lambda_C+\frac{\Lambda_C}{\mu_C}]]}{a_1b_1d_2}. \end{aligned}$$

The characteristic equation corresponding to the matrix above is obtained by calculating the determinant of the expression $(J(E_0)-\lambda I)$. Nonetheless, the stability of the equilibrium points in the system (4.4.0.2) will be assessed numerically because the model system is highly nonlinear and complex, making it difficult to find exact solutions analytically [76].

Time step	$\lambda_i(i=1,2,3)$	$\rho(\lambda_i)$	NSFD scheme
0.001	$(0.47535, 0.99994, 0)$	0.99944	converges
0.01	$(0.47529, 0.99940, 0)$	0.99940	converges
0.1	$(0.47462, 0.99401, 0)$	0.99401	converges
1	$(0.46789, 0.94176, 0)$	0.94176	converges
10	$(0.40164, 0.5488, 0)$	0.54881	converges
100	$(0.04316, 0.00299, 0)$	0.04316	converges

Table 4.4: Numerical convergence related to the disease-free equilibrium point of the NSFD scheme.

Table 4.4 illustrates the convergence pattern of numerical values towards the disease-free state within the NSFD scheme. The data in Table 4.4 demonstrates that all eigenvalues possess magnitudes less than one, regardless of the chosen time step size. This observation leads us to the conclusion that the disease-free equilibrium $E_0 = \left(\frac{\Lambda_C}{\mu_C}, 0, 0\right)$ within the system is unconditionally locally asymptotically stable [76]. Next, we proceed to assess the stability analysis of the endemic point:

$$E_1^* = \left(S_C^{k^*}, I_C^{k^*}, P_W^{k^*}\right)$$

with

$$\begin{cases} S_C^{k^*} &= \dfrac{\Lambda_C(P_0 + P_W^{k^*})}{(\beta_W + \mu_C)P_W^{k^*} + \mu_C P_0}, \\ I_C^{k^*} &= \dfrac{\beta_W \Lambda_C P_W^{k^*}}{(\delta_C + \mu_C)(\beta_W + \mu_C)P_W^{k^*} + (\delta_C + \mu_C)\mu_C P_0}, \\ P_W^{k^*} &= \dfrac{1}{2}\left[\phi_0 + \sqrt{\phi_0^2 - 4\phi_1}\right]. \end{cases} \tag{4.4.2.5}$$

where

$$\begin{cases} \phi_0 &= \dfrac{r_W K_W k_0 - r_W k_1 - \mu_W K_W k_0}{r_W k_0}, \\ \phi_1 &= \dfrac{\mu_W K_W k_1 (R_0 - 1)}{r_W k_0}, \end{cases} \tag{4.4.2.6}$$

and

$$\begin{cases} k_0 &= (\delta_C + \mu_C)(\beta_W + \mu_C), \\ \\ k_1 &= (\delta_C + \mu_C)\mu_C P_0. \end{cases} \tag{4.4.2.7}$$

Substituting endemic equilibrium pont into the Jacobian matrix gives

$$J(E_1^*) = \begin{bmatrix} a_{11} & a_{12} & a_{13} \\ \\ a_{21} & a_{22} & a_{23} \\ \\ a_{31} & a_{32} & a_{33} \end{bmatrix}, \tag{4.4.2.8}$$

where

$$\begin{aligned}
a_{11} &= \frac{1}{1+\phi_1(h)\left(\frac{\beta_W P_W^{k*}}{P_0+P_W^{k*}}+\mu_W\right)}, \\
a_{12} &= 0, \\
a_{13} &= -\frac{S_C^{k*}+\phi_1(h)\Lambda_C[\frac{(P_0+P_W^{k*})\beta_W-\beta_W k*}{P_0+P^k*}]}{\left[1+\phi_1(h)\left(\frac{\beta_W P_W^{k*}}{P_0+P_W^{k*}}+\mu_W\right)\right]^2}, \\
a_{21} &= \frac{\phi_2(h)\beta_W P_W^{k*}}{[1+\phi_2(h)(\mu_C+\delta_C)][(P_0+P_W^{k*})+\phi_1(h)(\beta_W P_W^{k*}+\mu_W(P_0+P_W^{k*}))]}, \\
a_{22} &= \frac{(P_0+P_W^{k*})+\phi_1(h)(\beta_W P_W^{k*}+\mu_W(P_0+P_W k*))}{[(P_0+P_W^{k*})+\phi_1(h)(\beta_W P_W^{k*}+\mu_W(P_0+P_W^{k*}))][1+\phi_2(h)(\mu_C+\delta_C)]}, \\
a_{23} &= q_1\left[(P_0+P_W^{k*})\phi_1(h)(\beta_W P_W^{k*}+\mu_W(P_0+P_W^{k*}))(a_0+a_1)-(b_0+b_1)(1+\phi_1(h)(\beta_W+\mu_W))\right], \\
a_{31} &= \frac{\phi_3(h)N_h\alpha_h}{1-\phi_3(h)(r_W P_W^{k*}-\mu_W-\frac{r_W P_W^{k*}}{K_W})}m_1, \\
a_{32} &= \frac{\phi_3(h)N_h\alpha_h}{1-\phi_3(h)(r_W P_W^{k*}-\mu_W-\frac{r_W P_W^{k*}}{K_W})}m_2, \\
a_{33} &= \frac{q_1 {P_W^{k*}}^2+a_1q_2{P_W^{k*}}^2+2r_1p_1P_W^{k*}+(p_2+t_1)-[p_1P_W^{k*}(p_2+t_1)P_W^{k*}+a_4I_C^k*c_1]2q_1P_W^*+a_1q_2}{(q_1P_W^k*2+a_1q_2)P_W^k*+r_1},
\end{aligned}$$

with

$$
\begin{aligned}
b_0 &= ((P_0 + P_W^{k*}) + \phi_1(h)(\beta_W P_W^{k*} + \mu_W(P_0 + P_W^{k*}))),\\
b_1 &= I_C^{k*}(1 + \phi_1(h)(\beta_W + \mu_W)),\\
b_2 &= \phi_2(h)\beta_W[S_C^{k*} + \phi_1(h)\Lambda_C],\\
b_3 &= I_C\left[(P_0 + P_W^{k*}) + \phi(h)(\beta_W + \mu_W(P_0 + P_W^{k*}))\right]\Lambda_C,\\
b_4 &= \phi_2(h)\beta_W P_W^{k*}[S_C + \phi_1(h)\Lambda_C],\\
m_1 &= \frac{\phi_2(h)\beta_W P_W^{k*}}{\left[(P_0 + P_W^{k*}) + \phi_1(h)(\beta_W P_W^{k*} + \mu_W(P_0 + P_W^{k*}))\right][1 + \phi_2(h)(\mu_C + \delta_C)]},\\
m_2 &= \frac{[(P_0 + P_W^{k*}) + \phi_1(h)(\beta_W P_W^{k*} + \mu_W(P_0 + P_W^{k*}))]}{\left[(P_0 + P_W^{k*}) + \phi_1(h)(\beta_W P_W^{k*} + \mu_W(P_0 + P_W^{k*}))\right][1 + \phi_2(h)(\mu_C + \delta_C)]},\\
t_1 &= a_4(c_2 I_C^{k*} + a_5[\phi_1(h)\Lambda_C + S_C^{k*}]),\\
q_1 &= a_1 d_1 d_3,\\
q_2 &= k_1 d_3 + d_1 d_2.
\end{aligned}
$$

Applying a similar approach as used for analyzing the stability of the disease-free equilibrium, we also determine the stability of the endemic equilibrium point through numerical calculations. The following table illustrates the convergence of spectral radii associated with the endemic point:

Time step	$\lambda_i (i = 1, 2, 3)$	$\rho(\lambda_i)$	NSFD scheme
0.001	$(0.99987, 0.99940, 0)$	0.99994	converges
0.01	$(0.99872, 0.99940, 0)$	0.99940	converges
0.1	$(0.88537, 0.94177, 0)$	0.99402	converges
1	$(0.88537, 0.94177, 0)$	0.94177	converges
10	$(0.54881, 0.40204, 0)$	0.54881	converges
100	$(0.00248, 0.0068, 0)$	0.00248	converges

Table 4.5: Numerical convergence corresponding to the endemic point of NSFD scheme.

The spectral radii of the Jacobian matrix corresponding to the endemic equilibria of the NSFD scheme are displayed in Table 4.5. It is clear from the data in Table 4.5 that the NSFD scheme

consistently converges across different time steps. Consequently, we deduce that the endemic equilibrium of the system (4.4.0.2) is locally asymptotically stable.

4.4.3 Numerical Results

In this section, we validate through simulations that there exists a reciprocal influence between the microscale and macroscale dynamics. We demonstrate the effectiveness of the bacterial growth rate in the macroscale and microscale on disease transmission and prevalence, this understanding is vital in controlling the diseases caused by *E. coli* O157:H7. This is achieved by varying microscale multiplication N_e holding macroscale bacteria growth rate r_W constant and varying macroscale pathogen growth rate holding microscale multiplication rate constant. The numerical simulations were done using a set of parameters in Table 4.3. The parameter values utilized in the model are sourced from existing literature or estimated, as certain parameters might not be explicitly provided in literature. For parameters that lack direct reporting, their values are estimated based on deductions drawn from published sources. The simulation of the model system (4.4.0.1) is conducted using MATLAB 2023. Below, we present the graphical outcomes of the simulations carried out for the model system (4.4.0.1).

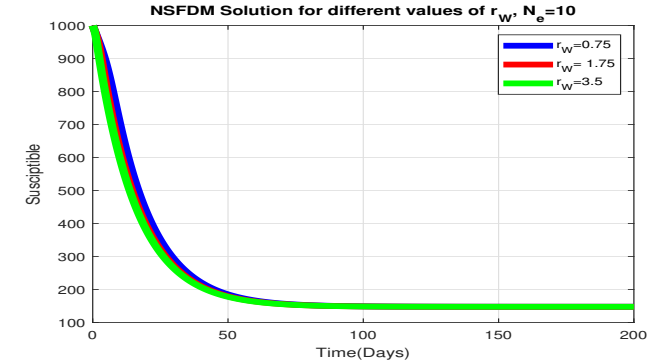

(a)

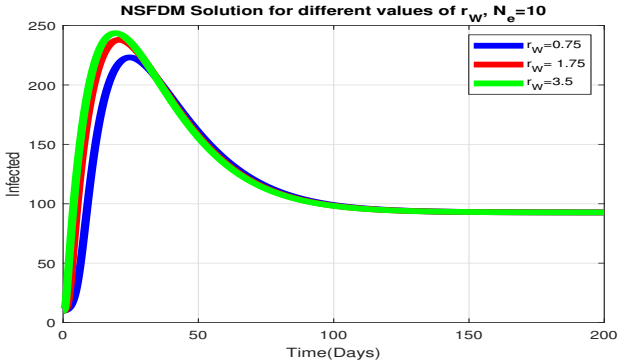

(b)

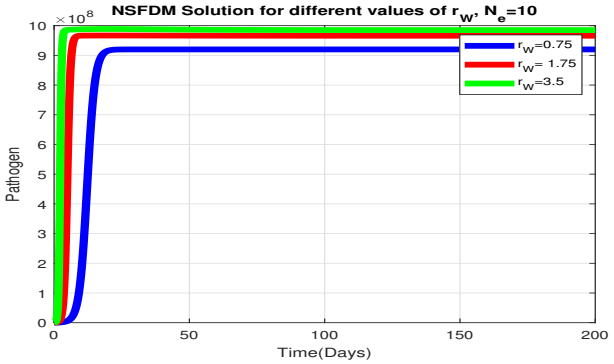

(c)

Figure 4.4: Simulations of discrete model (4.4.0.1) showing changes of (a) population of susceptible cattle (S_C), (b) population of infected cattle (I_C), and (c) environmental bacterial load (P_W) for different values of between-host bacterial growth rate $r_W = 0.75, r_W = 1.75$ and $r_W = 3.5$ when average number of bacteria produced through replication and ready for excretion by an infected cattle $N_e = 10$

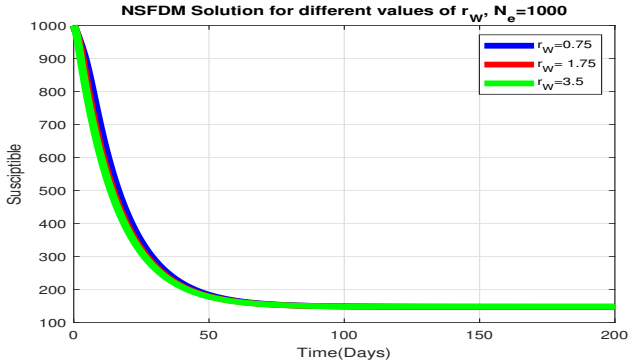

(a)

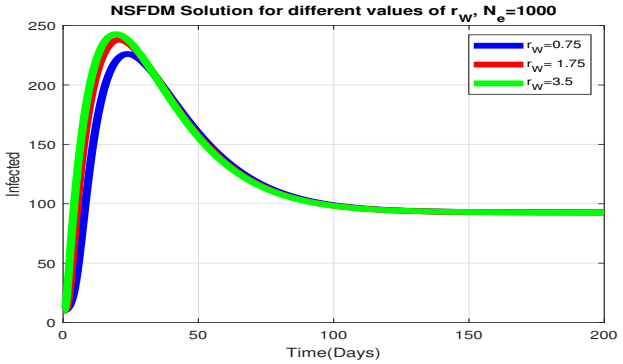

(b)

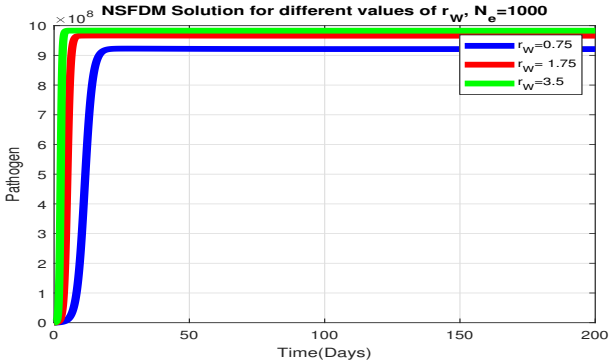

(c)

Figure 4.5: Simulations of discrete model (4.4.0.1) showing changes of (a) population of susceptible cattle (S_C), (b) population of infected cattle (I_C), and (c) environmental bacterial load (P_W) for different values of environmental bacterial growth rate $r_W = 0.75, r_W = 1.75$ and $r_W = 3.5$ when average number of bacteria produced through replication and ready for excretion by an infected cattle $N_e = 1000$

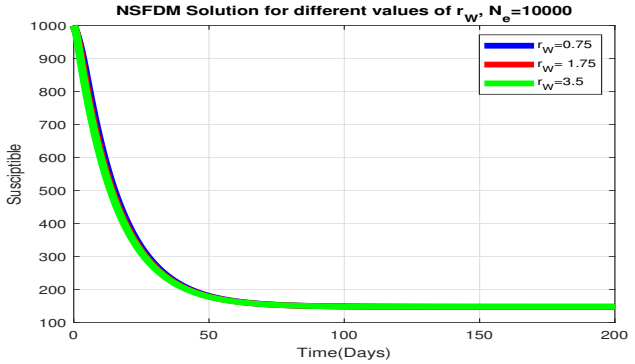

(a)

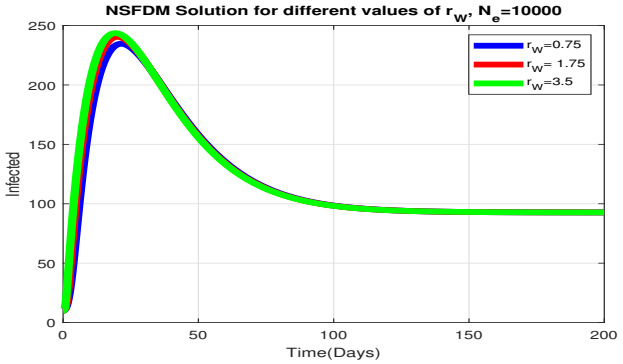

(b)

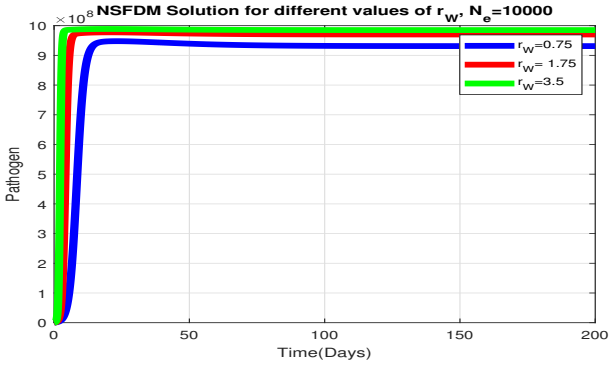

(c)

Figure 4.6: Simulations of discrete model (4.4.0.1) showing changes of (a) population of susceptible cattle (S_C), (b) population of infected cattle (I_C), and (c) environmental bacterial load (P_W) for different values of environmental bacterial growth rate $r_W = 0.75, r_W = 1.75$ and $r_W = 3.5$ when average number of bacteria produced through replication and ready for excretion by an infected cattle $N_e = 10000$

Jointly, 4.4- 4.6, show the effects of increasing the environmental pathogen growth rate $r_W = 0.75, r_W = 1.75, r_W = 3.5$ on between-host populations variables (a) Susceptible population, (b) Infected population and (c) Pathogen population when the number of bacteria ready for excretion $N_e = 10, N_e = 1000, N_e = 10000$. We observe that when $N_e = 10$, there is a noticeable variation as we increase to $N_e = 10000$, the variations in figures 4.4- 4.6 are comparable, meaning that the between-host variables Infected and Pathogen increase and Susceptible decreases as the value of N_e increases. These findings suggest that vaccines capable of inducing protective immunity against incoming *E. coli* O157:H7 could be effective in reducing the growth rate of environmental pathogens. Consequently, such vaccines could play a significant role in controlling *E. coli* O157:H7 infections in cattle.

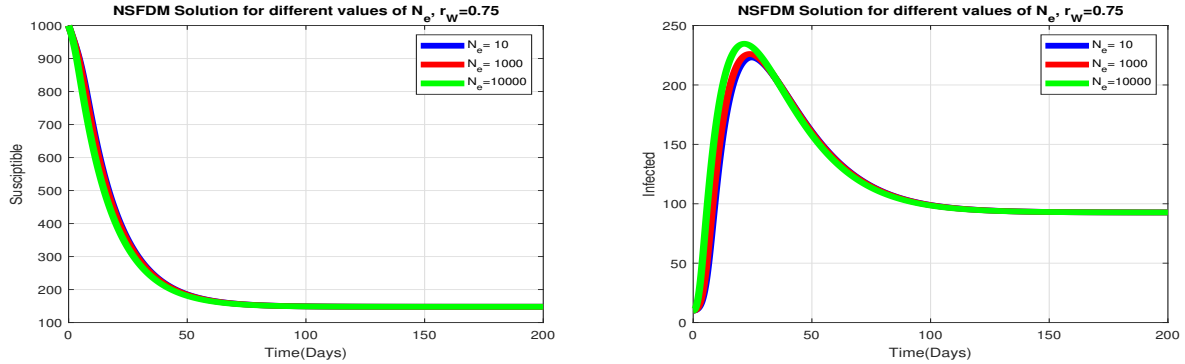

(a)

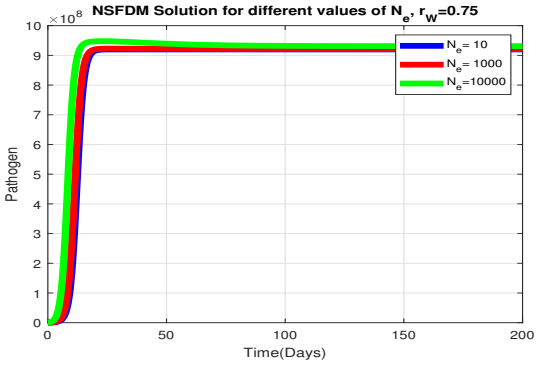

(c)

Figure 4.7: Simulation results of the discrete model (4.4.0.1) depict variations in (a) the susceptible cattle population (S_C), (b) the infected cattle population (I_C), and (c) the environmental bacterial load (P_W) across different scenarios with varying within-cattle scale bacterial replication rates ($N_e = 10$, $N_e = 1000$), and $N_e = 10000$ when average number of between-host bacterial load growth cattle $r_W = 0.75$

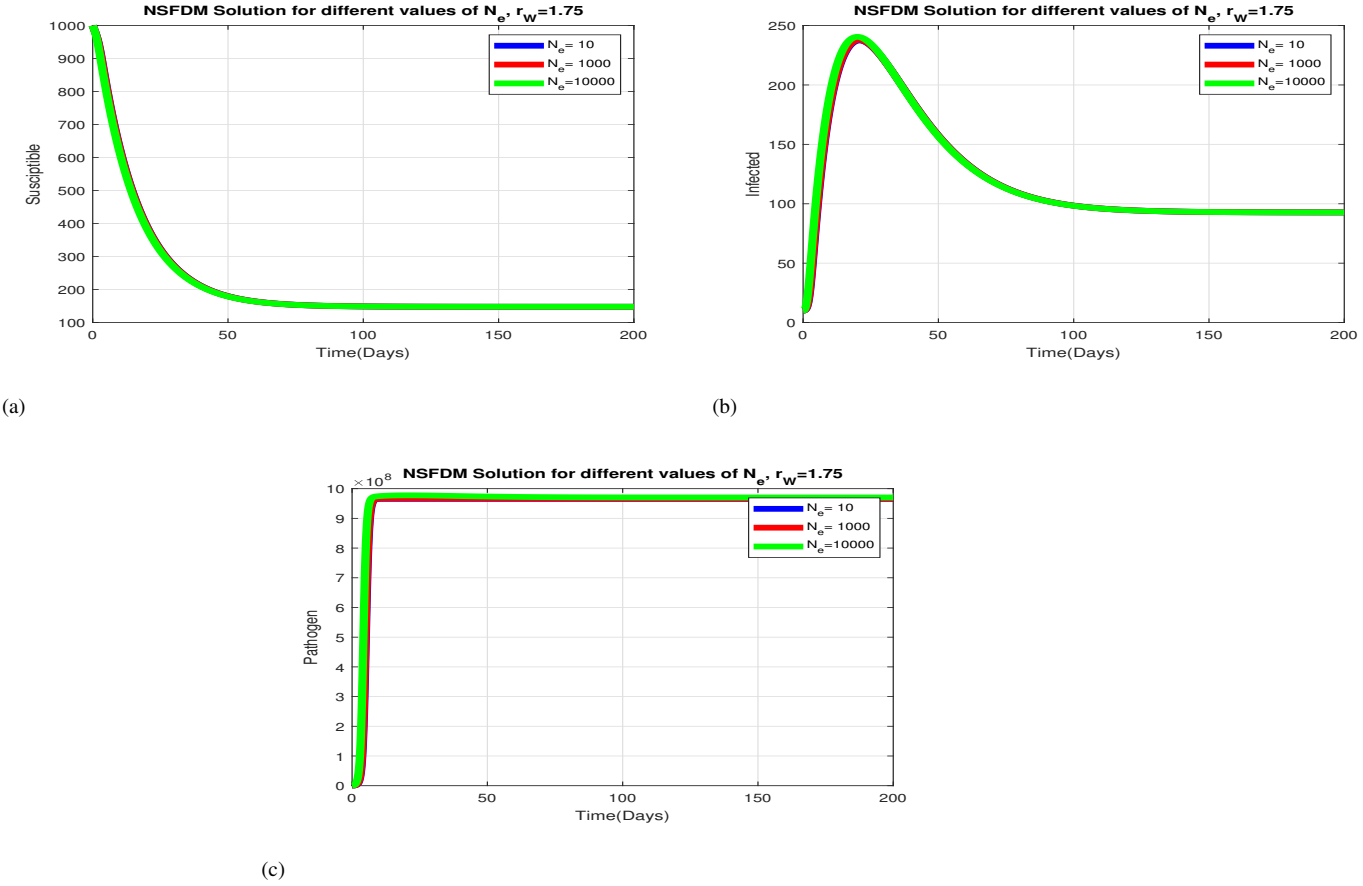

Figure 4.8: Simulation results of the discrete model (4.4.0.1) demonstrate fluctuations in (a) the susceptible cattle population (S_C), (b) population of infected cattle (I_C), and (c) environmental bacterial load (P_W) across various scenarios with different values of the within-cattle scale bacterial replication rate $N_e = 10, N_e = 1000$ and $N_e = 10000$ when average number of between-host bacterial load growth cattle $r_W = 1.75$

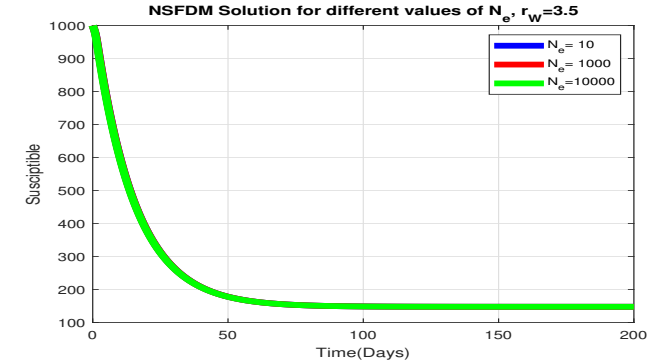

(a)

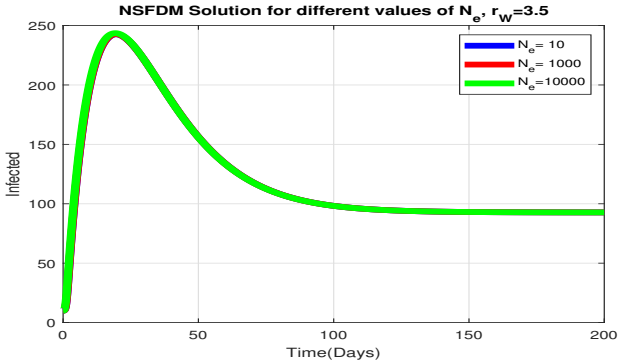

(b)

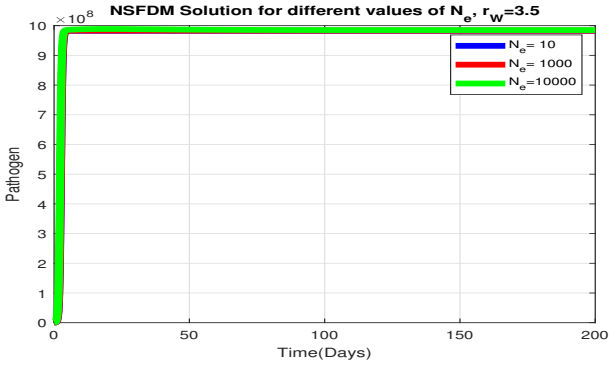

(c)

Figure 4.9: Simulations of the discrete model (4.4.0.1) show the variations in (a) the population of susceptible cattle (S_C), (b) the population of infected cattle (I_C), and (c) the environmental bacterial load (P_W) across different scenarios involving various values of the within-cattle scale bacterial replication rate ($N_e = 10$, $N_e = 1000$, and $N_e = 10000$), while maintaining an average number of environmental bacterial load growth in cattle of $r_W = 3.75$.

Collectively, the combined insights from Figure 4.7, Figure 4.8, and Figure 4.9 illustrate the impacts of increasing the within-host bacterial replication rate ($N_e = 10$, $N_e = 1000$, $N_e = 10000$) on the between-host population variables, including (a) the susceptible population, (b) the infected population, and (c) the pathogen population, while considering different scenarios of the environmental bacterial growth rates ($r_W = 0.75$, $r_W = 1.75$, $r_W = 3.5$). It can be observed that the variations in Figures 4.7 to 4.9 are comparable when $r_W = 0.75$, $r_W = 1.75$, and $r_W = 3.5$. We learn from these three graphs that when $r_W = 0.75$ the pathogen population increase in approximately 10 days and when $r_W = 1.75$ the pathogen population increases in approximately 5 days, we also observe that environmental pathogen increases in approximately 1 day when $r_W = 3.5$. From these results we deduce that any measures that could aim to target pathogen in the environment could have great effect in reducing *E. coli* O157:H7 replication at within-host scale.

4.5 Discussion and Conclusion

The primary aim of this chapter was to construct a nested multiscale model that considers pathogen replication cycles at both the within-host and between-host scales. The goal was to investigate the interaction between the growth rate of environmental pathogens and the microscale pathogen replication rate at the infection site. This was accomplished by considering *E. coli* O157:H7 as a paradigm for analysis. The mathematical analysis of the model has revealed the existence of a domain within which the model is both epidemiologically and mathematically well-defined. During the determination of equilibrium points, we derived the threshold value for the basic reproductive number. Through this process, we identified two significant equilibria: the disease-free equilibrium denoted as E_0 and the endemic equilibrium denoted as E^*. We also conducted a sensitivity analysis of the parameters in the nested multiscale model, focusing on the basic reproductive number (R_0) and the endemic point (P_W^*). This analysis was performed using the Latin Hypercube Sampling (LHS) scheme. The outcomes of the sensitivity analysis regarding the basic reproductive number revealed that parameters such as N_e, β_W, α_h, μ_W, and δ_C exhibited similar sensitivities to those observed for the parameters of the endemic point P_W^*. These results highlight potential influential factors in both the between-host scale and within-host scale dynamics, indicating potential targets for preventive and control measures against *E. coli* O:157H7 infection in cattle. Therefore, we deduce that there is a reciprocal influence between microscale and macroscale in *E. coli* O:157H7 transmission. We constructed the NSFD scheme and hence it is shown numerically that the discrete systems preserve the main properties of the model such as positivity and stability. From the simulation of NSFD scheme, we observe macroscale pathogen growth rate and microscale pathogen replication rate influence each other. A significant contribution of this study is the introduction of a nested multiscale model featuring type I reciprocal influence. The key innovation in this chapter lies in the application of a nested multiscale model to elucidate the connection between the microscale replication rate of *E. coli* O157:H7 and the between-host growth rate of *E. coli* O157:H7. Multiscale modelling offers a framework for incorporating within-host and between-host submodels, as both contribute to the transmission and control of foodborne pathogens. In this study, we have showcased the application of a nested multiscale model to illustrate a one-way connection from the within-host scale to the between-host scale. Specifically, the between-host scale is impacted by the within-host scale, whereas the within-host scale remains unaffected by influences from the between-host scale because the within-host dynamics is the one that sustains the disease. We accomplish this by demonstrating that the within-host replication rate of *E. coli* O157:H7 influences the between-host growth rate of *E. coli* O157:H7, however the between-host pathogen growth rate does not have influence on between-host of *E. coli* O157:H7 growth rate. This suggests that any strategies

that boost protective immunity targeting pathogen killing at the within-cattle scale is critical for achieving successful disease control reducing *E. coli* O157:H7. In the next chapter we present a coupled multiscale model for pathogens with no replication at both macroscale and microscale that we use to study the dynamics of *taenia solium* at host level.

Chapter 5

A Coupled Multiscale Model to Study *Taenia Solium* Dynamics at host level

5.1 Introduction

Several mathematical models have been formulated to describe the dynamics of disease transmission associated with various helminth infections [111]. *Taenia solium (T. solium)*, *Echinococcus granulosus*, *Echinococcus multilocularis*, and *Taenia saginata* are few examples of the zoonotic parasites that belong to this family [38]. Transmission mechanism theory has been used as the foundation to study the transmission of such infections, and also to compare and assess intervention tactics that could be employed for the purpose of managing or eradicating these infections. [13]. SIR models have been used to describe the transmission dynamics of the macroparasites, however, these models neglect the complex life cycle of helminth parasites. In these models, it is assumed that the count of infected individuals is equivalent to the product of susceptible hosts and the probability of avoiding infection through contact with an infected person [112]. The pioneering research conducted by Kostitsyne [44] forms the basis for many current theories regarding helminth infections. Kostitsyne developed a deterministic model featuring an extensive set of differential equations to clarify variations in host populations that can sustain a specific quantity of parasites [113]. The significant contribution of this initial investigation was the realization that traditional epidemic models were insufficient in capturing the intricacies of helminth

parasite dynamics [44]. Based on that, to understand helminth transmission, it must be taken into consideration that these parasites have complex lifecycles that involve several intermediate hosts before transmitting to a definitive host and will require multiscale modelling. In this chapter, we construct a coupled multiscale model for foodborne diseases by using the case of *T. solium*, commonly referred to as the ”pork tapeworm,” at the host level. It is important to note that host behavior plays a crucial role in influencing the disease impact within communities affected with environmentally transmitted infectious diseases. This is due to the fact that specific behaviors, particularly related to sanitation and hygiene practices, can significantly impact the likelihood of disease transmission *T. solium*, is a type of cestode parasite that has the ability to infect both humans and animals. It is prevalent in many parts of the developing world, particularly in regions where wild pigs have contact with human waste [114]. *T. solium* can cause two different diseases in humans, depending on the type of infection: (i) intestinal taeniasis from eating undercooked pork that has been contaminated with cysticercus larvae, and (ii) cysticercosis by ingesting eggs present in food or water that has been polluted with the feces of individuals infected with the human tapeworm [115]. The adult tapeworm that produces eggs is exclusively found in humans (definitive host). As the host excretes, eggs are transmitted along, and when the intermediate host (pigs) consumes them, they hatch and cause the emergence of cysticercosis, a state where larvae form cysts within muscles and organs [116]. Ingesting infectious cysticerci present in inadequately cooked or raw pork products leads to taeniosis in humans, completing the parasite's life cycle. Rather than only monitoring the total number of infected individuals, the multiscale model of the *T. solium* parasite described in this study incorporates the specific parasite load within both human and pig hosts. Moreover, the model also considers the various developmental stages of the parasite's life cycle and explains the interaction between contact, establishment, and parasite fecundity across different life stages within the definitive human host, the environment, and the intermediate host, all within the context of the parasite's life cycle. As of our present knowledge, this study represents the first attempt to thoroughly investigate the complete life cycle of *T. solium* infections. Our aim is to create a coupled multiscale model (CMSM) that covers the entirety of the parasite's life cycle, including both the within-humans interactions and the dynamics within-pigs. CMSMs are built upon the foundation of various multiscale categories, with one of their distinctive concepts being the integration of embedded multiscale models (EMSMs) as submodels. The fundamental characteristic of host-level EMSMs is the ongoing, bidirectional interaction between micro and macroscales throughout the duration when infected hosts are capable of spreading the infection [88]. The primary goal is to evaluate how the within-human and within-pig scales influence the between-host scale, as well as to examine how the between-host scale affect the within-human and within-pig levels in the context of taeniasis disease dynamics. Below we present the *Taenia solium* life cycle:

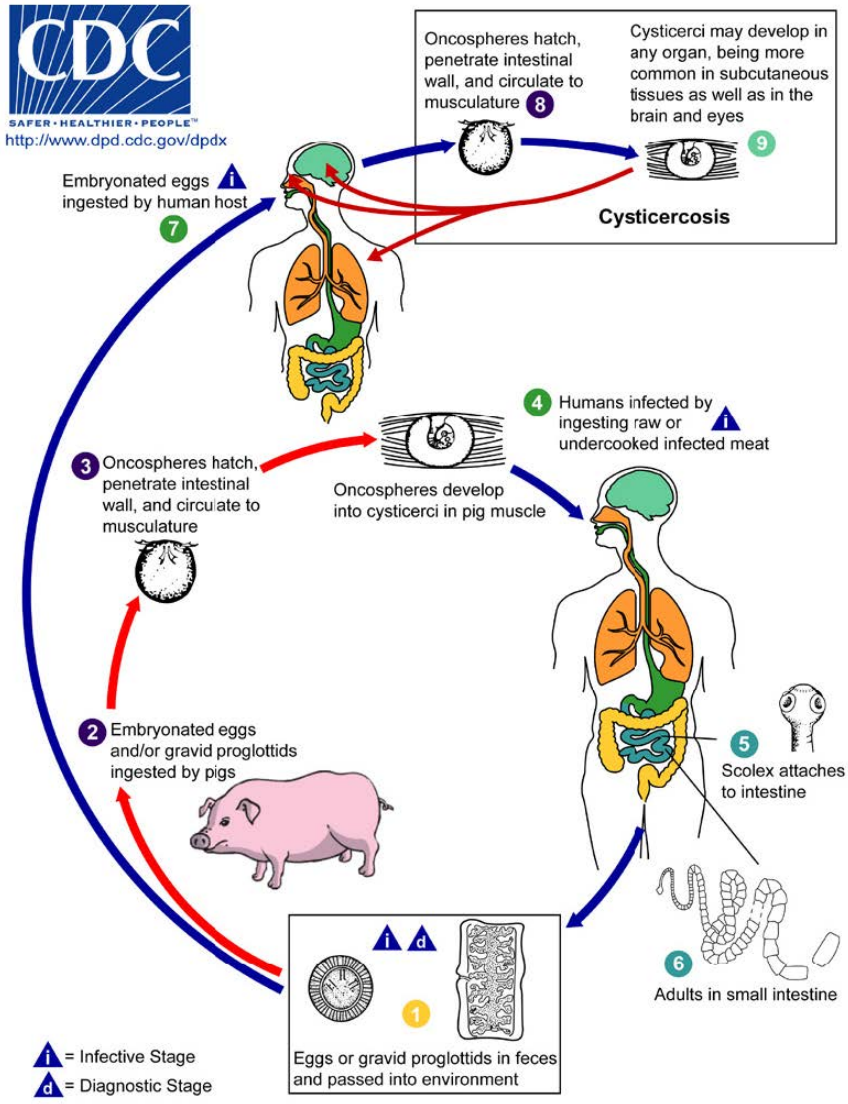

Figure 5.1: *Taenia solium* life cycle obtained from [2]

5.2 Multiscale Model

In this section, we consider and modify the general multiscale model introduced in [117]. In this adapted model, the sub-models at the between-host scale (for both human and animal hosts) are constructed by categorizing the host population into susceptible, infected individuals, and incorporating an additional variable that characterizes the community pathogen load (CPL) (SIP). Given the absence of a pathogen replication cycle at the within-host scale for both human and animal hosts, the within-host sub-models for human taeniasis can be formulated by illustrating the progression of pathogen populations from one life stage to another, using the linear transition functions as outlined in the general multiscale model [117]. We create a linked multiscale model

that follows the life cycle of the intestinal taeniasis parasite, encompassing two separate biological environments: the host environment within humans and the host environment within pigs. This coupled multiscale model is constructed by examining the behaviors of eleven populations at a given time point t. The human-host population is compartmentalized into susceptible humans ($S_H(t)$) and infected humans ($I_H(t)$), plus an additional variable for environmental pathogen *T. solium* load ($E_H(t)$). At the level within humans, the *T. solium* parasite undergoes three primary stages in its life cycle and the within-pig scale the parasite has two main life stages $C_h(t)$, $W_h(t)$ and $E_h(t)$ classes describe the three life stage of parasite within-human scale, ingested cysterci, matured worm and the number of eggs produced by an adult worm at human microscale respectively. The pig population is categorized into two classes denoted as $S_A(t)$ and $I_A(t)$, signifying susceptible pigs and infected pigs, respectively. At the within-pig level, there are representations for ingested parasite eggs ($E_a(t)$) and oncospheres ($O_a(t)$). Additionally, the number of *T. solium* eggs excreted into the environment is represented as $E_H(t)$, while the community pathogen load is denoted as $P_A(t)$. For this model, we assume the following:

(a) Diseases cannot be transmitted vertically.

(b) The spread of the disease within the human population exclusively occurs when individuals consume inadequately cooked pork that contains cysticerci.

(c) Pigs become infected when they consume infected human faeces.

(d) The total population of humans and pigs is constant.

(e) There is an absence of immune responses within both the human and animal populations.

(f) All recently recruited individuals are regarded as being in a state of good health and have not encountered the disease before.

(g) The infected human population do not recover naturally from the infection.

Using the assumptions we have made, we are able to formulate the following multiscale model describing the transmission dynamics of *T. solium* taeniasis:

$$
\begin{cases}
1.\dfrac{dS_H(t)}{dt} = \Lambda_H - \dfrac{\beta_H P_A S_H}{P_0 + P_A} - \mu_H S_H, \\
2.\dfrac{dI_H(t)}{dt} = \dfrac{\beta_H P_A(t) S_H(t)}{P_0 + P_A(t)} - (\delta_H + \mu_H) I_H(t), \\
3.\dfrac{dC_h(t)}{d(t)} = \dfrac{\beta_H P_A(t)[S_H(t) - 1]}{[P_0 + P_A(t)]\Phi_H[I_H(t) + 1]} - (\mu_c + \alpha_c) C_h(t), \\
4.\dfrac{dW_h(t)}{d(t)} = \alpha_c C_h(t) - (\mu_w + \alpha_w) W_h(t), \\
5.\dfrac{dE_h(t)}{d(t)} = \alpha_w W_h(t) - (\mu_e + \alpha_e) E_h(t), \\
6.\dfrac{dE_H(t)}{d(t)} = (I_H(t) + 1)\alpha_e E_h(t) - \alpha_H E_H(t) \\
7.\dfrac{dS_A(t)}{dt} = \Lambda_A - \dfrac{\beta_A S_A E_H(t)}{E_0 + E_H(t)} - \mu_A S_A(t), \\
8.\dfrac{dI_A(t)}{dt} = \dfrac{\beta_A S_A(t) E_H(t)}{E_0 + E_H(t)} - (\mu_A + \delta_A) I_A(t), \\
9.\dfrac{dE_a(t)}{ds} = \dfrac{\beta_A E_H(t)[S_A(t) - 1]}{[E_0 + E_H(t)]\Phi_A[I_A(t) + 1]} - (\alpha_a + \mu_a) E_a(t), \\
10.\dfrac{dO_a(t)}{ds} = \alpha_a E_a(t) - (\mu_o + \alpha_o) O_a(t), \\
11.\dfrac{dP_A(t)}{dt} = O_a(t)\alpha_o(I_A(t) + 1) - \alpha_A P_A(t).
\end{cases}
\tag{5.2.0.1}
$$

This interconnected multiscale model incorporates variables such as susceptible humans $S_H(t)$, infected humans $I_H(t)$, and community parasite load $P_A(t)$, to illustrate the transmission of the taeniasis parasite from pigs to humans. The dynamics of the human population are described by Equation (1) within the coupled multiscale model (Equation 5.2.0.1). The susceptible human population $S_H(t)$ is projected to grow steadily at a consistent rate, Λ_H due to births. Infection in the human population occurs at a rate, β_H, leading to a decrease, while natural mortality transpires at a rate, (μ_H), contributing to a decline. Equation (2) of the submodel (5.2.0.1) presents

the infected humans $I_H(t)$ compartment, this class increases due to infection of the susceptible humans and is reduced due to the rate of mortality caused by the disease, δ_H and through natural death rate, μ_H. Equation (3) presents the population of the initial life stage of the taeniasis parasite within the context of the human scale which begins when humans consume cysticerci $C_h(t)$ via the ingestion of insufficiently cooked pork and has the potential to intensify through super-infection.

$$\lambda_a S_h = \frac{\beta_H P_A(t)[S_H(t) - 1]}{[P_0 + P_A(t)]\phi_H[I_H + 1]}.$$

Superinfection involves downscaling, which involves transferring the between-host scale parameters and variables to the within-human scale, the cysticerci transit to next stage of life cycle through growing to mature worms which attach themselves to the wall of the intestines at a rate, α_c and die naturally at a rate, μ_c. Equation (4) presents second stage of parasite lifecycle which is a worm $W_h(t)$, fully developed worms generate segments containing eggs (referred to as proglottids) denoted as $E_h(t)$ at a rate of α_w, and these segments naturally decrease at a rate of μ_w. Equation (5) gives the dynamics of the final stage of worms which they hatch eggs $E_h(t)$ in the within-human scale stage. Eggs or detached proglottids are passed in stool to the environment at a rate α_e and they naturally decline with a rate of μ_e. The first term of Equation (6) of the multsicale model system (5.2.0.1) given by $(I_H(t+1)\alpha_e E_h(t)$, where every infected human excretes the within-human scale parasite eggs at a rate $\alpha_e E_h(t)$ and when accounting for a total number of $I_h(t) = I_H(t) + 1$ infected humans, this represents the transition from the within-human scale to the between-host scale. Eggs in the environment, $E_H(t)$ deplete naturally at a rate α_H. An additional sub-model is incorporated into the multiscale model (Equation 5.2.0.1), introducing variables such as susceptible pigs denoted as $S_A(t)$, infected pigs $I_A(t)$ and community parasite load $E_H(t)$ to describe the transmission of the taeniasis parasite from environment to pigs. Equation (7) of the multiscale model (5.2.0.1) presents the dynamics of susceptible pigs, the first term of the equation is the increase rate of susceptible pigs through birth, the second term of this equation is the infection rate, β_A with eggs consumed from contaminated human faeces, the compartment of susceptible pigs deplete due to natural death at a rate, μ_A. Equation (8) of the multiscale model (5.2.0.1) is the dynamics of infected pigs $I_A(t)$. Infected class increases due to infection rate of susceptible pigs and reduced due to disease induced death and natural death rate, δ_A and μ_A respectively. Equation (9) presents the population of the initial life stage of the ingested eggs of taeniasis parasite in the within-pig scale which begins when pigs consume eggs from faeces of the infected human $E_H(t)$ and may increase through super-infection at a rate

$$\lambda_h S_a(t) = \frac{\beta_A E_H(t)[S_A(t) - 1]}{[E_0 + E_H(t)]\Phi_A[I_A(t) + 1]},$$

where Φ_A is the proportion of new infection, this class decay naturally at rate μ_a and proceed

to the next stage of life at a rate, α_a. Equation (10) of the multiscale model (5.2.0.1) presents oncospheres, which are released from the ingested eggs through hatching within the intestines, at a rate, α_a, and experience natural mortality at a rate of μ_o also reduced through upscaling to become a community pathogen load at a rate α_o. The last equation presents community cysticersi load ($P_A(t)$), the first term on the right side of Equation (11) in model (5.2.0.1) is represented through the expression $O_a(t)\alpha_o(I_A(t)+1)$, where every infected pig sheds/excretes the within-pig scale pathogens (cysticerci) at a rate $\alpha_o O_a(t)$, additionally, the model requires upscaling (to connect the within-pig scale to the between-human scale) for a total of $I_a(t) = (I_A(t)+1)$ infected pigs, and they naturally expire at a rate of α_A.

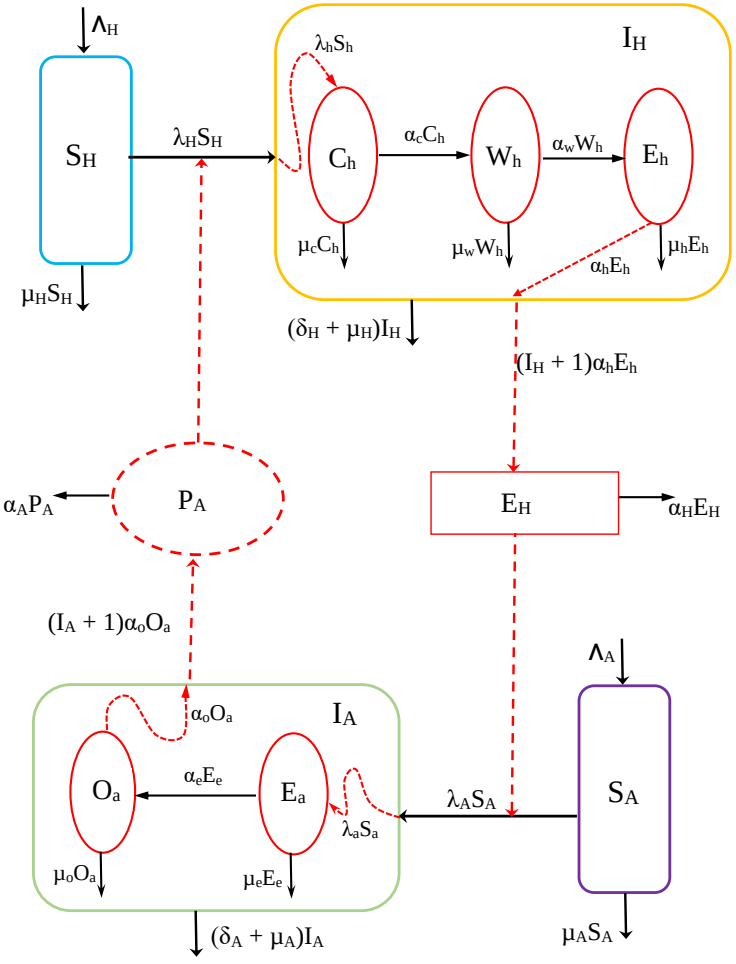

Figure 5.2: A visual representation illustrating the coupled multiscale model (5.2.0.1) portraying the dynamics of taenia-cysticercosis.

Variable	Variable Description	Initial value
$S_H(t)$	Susceptible humans	2000
$I_H(t)$	Infected humans	100
$C_h(t)$	Infective cysticerci	0
$W_h(t)$	Worms inside the human host	0
$E_h(t)$	Eggs hatched by the mature worms	0
$E_H(t)$	Excreted eggs in the environment	0
$S_A(t)$	Susceptible pigs	1000
$I_A(t)$	Infected pigs	0
$E_a(t)$	Parasite eggs within-pig scale	0
$O_a(t)$	Oncosphere (embryonic form of a tapeworm)	0
$P_A(t)$	Community pathogen load	1500

Table 5.1: Description of variables in the system (5.2.0.1).

Parameter	Description	Unit
Λ_H	the rate of supply of susceptible individuals through birth	day^{-1}
β_H	contact rate of susceptible humans with contaminated food	day^{-1}
μ_H	Human mortality rate	day^{-1}
δ_H	human disease-related mortality rate	day^{-1}
Φ_H	proportion of new infecetd humans in the total infected population	day^{-1}
P_0	half saturation constant associated with infection of humans	day^{-1}
μ_c	Natural death rate of cysticerci	day^{-1}
α_c	cysticerci transition rate	day^{-1}
μ_w	worm natural death rate	day^{-1}
α_w	worm transition rate	day^{-1}
μ_e	mortality rate of the eggs	day^{-1}
α_e	excretion rate of eggs	day^{-1}
α_H	eggs in the environment natural death rate	day^{-1}
Λ_A	susceptible pig birth rate	day^{-1}
μ_A	infected pig death rate	day^{-1}
β_A	pig infection rate	day^{-1}
δ_A	pig disease induced death rate	day^{-1}
α_a	eggs in the pig transition rate	day^{-1}
μ_a	within-pig eggs death rate$_1$	day^{-1}
H_0	half saturation constant associated with infection of pig	day^{-1}
μ_0	onchospheres natural death rate	day^{-1}
α_0	rate at which onchospheres are shed/excreted into community$_0$	day^{-1}
α_A	community pathogen load death rate	day^{-1}
E_0	half saturation constant associated with infection of pigs	day^{-1}
Φ_A	proportion of new infected pigs in the total infected pig population	day^{-1}

Table 5.2: Description of parameters.

5.2.1 Feasible Region

Since the coupled multiscale model (5.2.0.1) traces the transmission cycle of human taeniasis parasite which occur within three distinct contexts: (i) the environment at the within-human-host scale, (ii) the environment at the between-host scale, and (iii) the environment within the pig scale. The parameters and state variables within the model system (5.2.0.1) are assumed to possess non-negative values, aligning with the characteristics of human and pig populations. In order to ensure biological and epidemiological relevance, it is crucial to establish that the solutions of the model remain positive and bounded. For all $t > 0$, it is assumed that all parameters and state variables within the multiscale model (5.2.0.1) maintain positive values. By defining $N_H = S_H + I_H$ and summing Equations (1) and (2) within the model system (5.2.0.1), we derive the following:

$$\frac{dN_H}{dt} = \Lambda_H - \mu_H N_H - \delta_H I_H, \tag{5.2.1.1}$$

so that

$$\frac{dN_H(t)}{dt} \leq \Lambda_H - \mu_H N_H. \tag{5.2.1.2}$$

This implies that

$$\lim_{t\to\infty} sup(N_H(t)) \leq \frac{\Lambda_H}{\mu_H}. \tag{5.2.1.3}$$

Similarly, letting $N_A = S_A + I_A$ and adding Equations (7) and (8) in the system (5.2.0.1), we get

$$\frac{dN_A}{dt} = \Lambda_A - \mu_A N_A - \delta_A I_A. \tag{5.2.1.4}$$

so that

$$\frac{dN_A(t)}{dt} \leq \Lambda_A - \mu_A N_A. \tag{5.2.1.5}$$

This implies that

$$\lim_{t\to\infty} sup(N_A(t)) \leq \frac{\Lambda_A}{\mu_A}. \tag{5.2.1.6}$$

Using solutions for N_H and N_A above, solutions for the remaining variables can be obtained. Therefore, all viable solutions of the model system (5.2.0.1) exhibit positivity and fall within a

defined region outlined by

$$\left\{\begin{array}{rcl}\Omega &=& \{(S_H, I_H, C_h, W_h, E_h, E_H, E_a, O_a, S_A, I_A, P_A) \in R_+^{11}: \\ && 0 \leq S_H + I_H \leq S_1,\ 0 \leq C_h \leq S_2,\ 0 \leq W_h \leq S_3, \\ && 0 \leq E_h \leq S_4,\ 0 \leq E_H \leq S_5,\ 0 \leq E_a \leq S_6,\ 0 \leq O_a \leq S_7, \\ && 0 \leq S_A + I_A \leq S_8,\ 0 \leq P_A \leq S_9,\end{array}\right. \tag{5.2.1.7}$$

which remains positively invariant and possesses an attracting nature for all $t > 0$, where:

$$\left\{\begin{array}{l} S_1 = \dfrac{\Lambda_H}{\mu_H}, \\ S_2 = \dfrac{Q_H^* P_A}{P_A + P_0}, \\ S_3 = \dfrac{Q_H^{**} P_A}{P_0 + P_A}, \\ S_4 = \dfrac{Q_H^{***} P_A}{P_0 + P_A}, \\ S_5 = \dfrac{P_0 E_0 (R_0^2 - 1)}{P_0 + Q_A^*}, \\ S_6 = \dfrac{\Lambda_A}{\mu_A}, \\ S_7 = \dfrac{Q_A^* E_H}{E_0 + E_H}, \\ S_8 = \dfrac{Q_A^{**} E_H}{E_0 + E_H}, \\ S_9 = \dfrac{Q_A^* P_0 E_0 (R_0^2 - 1)}{E_0 (P_0 + Q_A^*) + P_0 E_0 (R_0^2 - 1)}. \end{array}\right. \tag{5.2.1.8}$$

Where

$$\begin{cases} Q_H^* = \dfrac{\beta_H(\Lambda_H - \mu_H)}{\Phi_H(\Lambda_H + \mu_H)}, \\ Q_H^{**} = \dfrac{\alpha_c}{\mu_w + \alpha_w}.\dfrac{1}{\mu_c + \alpha_c}.\dfrac{\beta_H(\Lambda_H - \mu_H)}{\Phi_H(\Lambda_H + \mu_H)(\mu_c + \alpha_c)}, \\ Q_H^{***} = \dfrac{\alpha_w}{\mu_e + \alpha_e}.\dfrac{1}{\mu_c + \alpha_c}.\dfrac{\beta_H(\Lambda_H - \mu_H)}{\Phi_H(\Lambda_H + \mu_H)(\mu_c + \alpha_c)}, \\ Q_A^* = \dfrac{\beta_A(\Lambda_A - \mu_A)}{\Phi_A(\Lambda_A + \mu_A)(\alpha_a + \mu_a)}, \\ Q_A^{**} = \dfrac{\alpha_a}{\mu_o + \alpha_o}.\dfrac{\alpha_o}{\alpha_A \mu_A}.\dfrac{\beta_A(\Lambda_A - \mu_A)}{\Phi_A(\Lambda_A + \mu_A)(\alpha_a + \mu_a)}. \\ R_0 = \sqrt{\dfrac{\alpha_0}{\mu_o + \alpha_o}.\dfrac{\alpha_a}{\mu_a + \alpha_a}.b_0.\dfrac{\alpha_e}{\mu_e + \alpha_e}.\dfrac{\alpha_w}{\mu_w + \alpha_w}.\dfrac{\alpha_c}{\mu_c + \alpha_c}.b_1} \end{cases} \tag{5.2.1.9}$$

5.2.2 Disease-Free Equilibrium and Reproductive Number

In order to derive the disease-free equilibrium point of the multiscale model system (5.2.0.1), we equate the left-hand side of the equations to zero and establish that I_H, C_h, W_h, E_h, E_H, I_A, E_a, O_a, and P_A are all set to zero. Therefore we let

$$E_0 = \left(\frac{\Lambda_H}{\mu_H},\ 0,\ 0,\ 0, 0,\ 0,\ \frac{\Lambda_A}{\mu_A}, 0\ 0\ 0,\ 0\right), \tag{5.2.2.1}$$

represent the disease-free equilibrium state within the model system (5.2.0.1). Thus, we continue to compute the basic reproductive number R_0 in order to assess the stability of this disease-free equilibrium. The methodology of the next-generation approach, as outlined in [69], will be employed for the computation of the basic reproduction number within this multiscale model

(5.2.0.1). The representation of the multiscale model (5.2.0.1) can be reformulated in the following way:

$$\begin{cases} \dfrac{dX}{dt} &= f(X,Y,Z), \\ \dfrac{dY}{dt} &= g(X,Y,Z), \\ \dfrac{dZ}{dt} &= h(X,Y,Z), \end{cases} \tag{5.2.2.2}$$

where

(i) $X = (S_H, S_A)$ represents a compartment of susceptible individuals,

(ii) $Y = (I_H, C_h, W_h, E_h, I_A, E_a, O_a)$ denote all states of infected individuals that do not transmit the disease.,

(iii) $Z = (E_H, P_A)$ depicts a compartment containing infected individuals who have the potential to spread the disease.

Following [90] we define $\tilde{g}(X^*, Z)$ by

$$\tilde{g}(X^*, Z) = (\tilde{g}_1(X^*, Z), \tilde{g}_2(X^*, Z), \tilde{g}_3(X^*, Z), \tilde{g}_4(X^*, Z), \tilde{g}_5(X^*, Z), \tilde{g}_6(X^*, Z), \tilde{g}_7(X^*, Z)), \tag{5.2.2.3}$$

with

$$\begin{cases} 1.\ \widetilde{g}_1(X^*,Z) &= \dfrac{\beta_H\Lambda_H P_A}{\mu_H(\mu_H+\delta_H)(P_0+P_A)}, \\ 2.\ \widetilde{g}_2(X^*,Z) &= \dfrac{\beta_H P_A[\Lambda_H-\mu_H]}{\mu_H(\mu_c+\alpha_c)(P_0+P_A)\phi_h[\widetilde{g}_1(X^*,Z)+1]}, \\ 3.\ \widetilde{g}_3(X^*,Z) &= \dfrac{\alpha_c\beta_H[\Lambda_H-\mu_H]P_A}{\mu_H(\mu_w+\delta_w)(\mu_e+\alpha_e)\phi_h(P_0+P_A)[\widetilde{g}_1(X^*,Z)+1]}, \\ 4.\ \tilde{g}_4(X^*,Z) &= \dfrac{\alpha_w\alpha_c\beta_H[\Lambda_H-\mu_H]P_A}{\mu_H(\mu_w+\delta_w)(\mu_e+\alpha_e)\Phi_H(P_0+P_A)[\widetilde{g}_1(X^*,Z)+1]}, \\ 5.\ \tilde{g}_5(X^*,Z) &= \dfrac{\beta_A\Lambda_A E_H}{\mu_A(\mu_A+\delta_A)(E_0+E_H)}, \\ 6.\ \widetilde{g}_6(X^*,Z) &= \dfrac{\beta_A[\Lambda_A-\mu_A]E_H}{\mu_A(\alpha_a+\mu_a)(E_0+E_H)\Phi_A[\tilde{g}_5+1]}, \\ 7.\ \widetilde{g}_7(X^*,Z) &= \dfrac{\alpha_a\beta_A[\Lambda_A-\mu_A]E_H}{\mu_A(\alpha_0+\mu_0)(\alpha_a+\mu_a)(E_0+E_H)\Phi_A[\tilde{g}_6+1]}. \end{cases} \quad (5.2.2.4)$$

We let

$$h(X,Y,Z)=(h_1(X,Y,Z),h_2(X,Y,Z)), \quad (5.2.2.5)$$

where

$$\begin{cases} h_1(X,Y,Z) &= \dfrac{\alpha_e\alpha_w\alpha_c\beta_H[\Lambda_H-\mu_H]P_A}{\mu_H(\mu_e+\alpha_e)(\mu_w+\delta_w)(\mu_c+\alpha_c)\phi_P hi_H(P_0+P_A)}-\alpha_H E_H, \\ h_2(X,Y,Z) &= \dfrac{\alpha_0\alpha_a\beta_A[\Lambda_A-\mu_A]E_H}{\mu_A(\mu_0+\alpha_0)(\alpha_a+\mu_a)\Phi_H(E_0+E_H)}-\alpha_A P_A. \end{cases} \quad (5.2.2.6)$$

Let us define A as $D_Z h(X,\tilde{g}(X,0),0)$, and additionally suppose that A can be expressed in the manner of $A=M-D$, where M is non-negative ($M\geq 0$) and D is positive ($D>0$). This yields a diagonal matrix for A, which can be presented as a matrix.

$$A=D_Z h(X^*,\tilde{g}(X^*,0),0)=\begin{bmatrix} -\alpha_h & \dfrac{a_0}{P_0} \\ \dfrac{a_1}{E_0} & 0 \end{bmatrix}, \quad (5.2.2.7)$$

where

$$\begin{cases} a_0 &= \dfrac{\alpha_e\alpha_w\alpha_c\beta_H[\Lambda_H-\mu_H]}{\mu_H(\mu_e+\alpha_e)(\mu_w+\delta_w)(\mu_c+\alpha_c)Phi_H}, \\ \\ a_1 &= \dfrac{\alpha_0\alpha_a\beta_A[\Lambda_A-\mu_A]}{\mu_A(\mu_0+\alpha_0)(\alpha_a+\mu_a)\Phi_H}. \end{cases} \tag{5.2.2.8}$$

Given that A can be written as $A = M - D$, we deduce that matrices M and D take on the values of:

$$M = \begin{bmatrix} 0 & \dfrac{a_0}{P_0} \\ \\ \dfrac{a_1}{E_0} & 0 \end{bmatrix}, \tag{5.2.2.9}$$

and

$$D = \begin{bmatrix} \alpha_H & 0 \\ \\ 0 & \alpha_A \end{bmatrix}. \tag{5.2.2.10}$$

The basic reproductive number corresponds to the largest eigenvalue of the matrix obtained by multiplying M and the inverse of D, thus MD^{-1}:

$$R_0 = \sqrt{\frac{\alpha_0}{\mu_o+\alpha_o}.\frac{\alpha_a}{\mu_a+\alpha_a}.b_0.\frac{\alpha_e}{\mu_e+\alpha_e}.\frac{\alpha_w}{\mu_w+\alpha_w}.\frac{\alpha_c}{\mu_c+\alpha_c}.b_1}. \tag{5.2.2.11}$$

where,

$$\begin{cases} b_0 &= \dfrac{\beta_H[\Lambda_H-\mu_H]}{\mu_H\Phi_H\alpha_A P_0}, \\ \\ b_1 &= \dfrac{\beta_A[\Lambda_A-\mu_A]}{\mu_A\Phi_A\alpha_H E_0}. \end{cases}$$

In this case

$$R_0 = \sqrt{R_{0AH}, R_{0HA}} \tag{5.2.2.12}$$

In Equation (5.2.2.12), the quantity R_{0AH} can be understood in the following way: imagine a single newly infected pig entering a population of humans that is initially free of the disease and

is in a steady state. The predicted number of people infected by this pig, which is still present and contagious, is roughly

$$R_{0AH} = \frac{\alpha_0}{\mu_o + \alpha_o}.\frac{\alpha_a}{\mu_a + \alpha_a}.b_0. \tag{5.2.2.13}$$

As such, the pig-to-human transmission coefficient R_{0AH} is a combination of parameters related to transmission between human hosts and parameters within individual pigs. Similarly, in Equation (5.2.2.12) the quantity R_{0HA} is interpreted as follows: Consider a single newly infected human entering a disease-free population of pigs at equilibrium. The predicted number of pigs infected by this human, which is still present and contagious, is roughly

$$R_{0HA} = \frac{\alpha_e}{\mu_e + \alpha_e}.\frac{\alpha_w}{\mu_w + \alpha_w}.\frac{\alpha_c}{\mu_c + \alpha_c}.b_1. \tag{5.2.2.14}$$

From the expression (5.2.2.14), we also deduce that the human-to-pig transmission coefficient R_{0HA} is composed of between-host disease parameters and within-pig parameters. We also conclude from the expression of the basic reproductive number of *T. solium* infection that it is a function of both the within-host scale parameters and the between-host scale parameters. Thus, the outcomes derived from this study demonstrate a reciprocal interaction between the microscale and the macroscale in influencing each other within the context of *T. solium* infection.

5.2.3 Local stability of the disease-free equilibrium

In this section, we analyze the stability of the Disease-Free Equilibrium of the model described by equations (5.2.0.1). This is achieved by linearizing all equations within the model (5.2.0.1), resulting in the calculation of the Jacobian matrix. The evaluation of the Jacobian matrix is performed at the DFE point

$$E_0 = \left(\frac{\Lambda_H}{\mu_H},\ 0,\ 0,\ 0, 0,\ 0,\ \frac{\Lambda_A}{\mu_A}, 0\ 0\ 0,\ 0\right). \tag{5.2.3.0.1}$$

Hence, the Jacobian matrix corresponding to the model equations (5.2.0.1) when evaluated at the state of disease-free equilibrium (DFE) can be expressed as follows:

$$J(E_0) = \begin{pmatrix} -\mu_H & 0 & 0 & 0 & 0 & 0 & 0 & 0 & 0 & 0 & q_1 \\ 0 & -a_0 & 0 & 0 & 0 & 0 & 0 & 0 & 0 & 0 & q_2 \\ 0 & 0 & -a_1 & 0 & 0 & 0 & 0 & 0 & 0 & 0 & m_1 \\ 0 & 0 & \alpha_c & -a_2 & 0 & 0 & 0 & 0 & 0 & 0 & 0 \\ 0 & 0 & 0 & \alpha_w & -a_3 & 0 & 0 & 0 & 0 & 0 & 0 \\ 0 & 0 & 0 & 0 & \alpha_e & -\alpha_H & 0 & 0 & 0 & 0 & 0 \\ 0 & 0 & 0 & 0 & 0 & q_3 & -\mu_A & 0 & 0 & 0 & 0 \\ 0 & 0 & 0 & 0 & 0 & q_4 & 0 & -a_4 & 0 & 0 & 0 \\ 0 & 0 & 0 & 0 & 0 & m_2 & 0 & 0 & -a_5 & 0 & 0 \\ 0 & 0 & 0 & 0 & 0 & 0 & 0 & 0 & \alpha_a & -a_6 & 0 \\ 0 & 0 & 0 & 0 & 0 & 0 & 0 & 0 & 0 & \alpha_0 & -\alpha_a \end{pmatrix} \quad (5.2.3.0.2)$$

where

$$
\begin{cases}
a_0 = (\mu_H + \delta_H), \\
a_1 = (\mu_c + \alpha_c), \\
a_2 = (\mu_w + \alpha_w), \\
a_3 = (\mu_e + \alpha_e), \\
a_4 = (\mu_A + \delta_A), \\
a_5 = (\mu_a + \alpha_a), \\
a_6 = (\alpha_0 + \alpha_0), \\
m_1 = \dfrac{\beta_H(\Lambda_H - \mu_H)}{P_0\mu_H\Phi_H}, \\
m_2 = \dfrac{(\Lambda_A - \mu_A)\beta_A}{\mu_A\Phi_A E_0}, \\
q_1 = -\dfrac{\beta_H\Lambda_H}{P_0\mu_H}, \\
q_2 = \dfrac{\beta_H\Lambda_H}{P_0\mu_H}, \\
q_3 = -\dfrac{\beta_A\Lambda_A}{\mu_A P_0}, \\
q_4 = \dfrac{\beta_A\Lambda_A}{\mu_A P_0}.
\end{cases}
\tag{5.2.3.0.3}
$$

Now, considering stability of DFE E_0 by calculating the eigenvalues (λ_s), of the Jacobian matrix given by (5.2.3.0.2), the characteristic equation at the equilibrium E_0 is given by:

$$\begin{aligned} |\ J(E_0) - \lambda_I\ | = 0, \\ (-\mu_H - \lambda)(-a_0 - \lambda)(-a_1 - \lambda)(-a_2 - \lambda)(-a_3 - \lambda), (-\alpha_H - \lambda)(-\mu_A - \lambda)(-a_4 - \lambda) \\ (-a_5 - \lambda)\Big[(-a_6 - \lambda)(-\alpha_A - \lambda)\Big] = 0. \end{aligned}$$

From the above characteristic equation, we notice that there are nine negative eigenvalues $\lambda_1 = -\mu_H$, $\lambda_2 = -a_0$, $\lambda_3 = -a_1$, $\lambda_4 = -a_2$, $\lambda_5 = -a_3$, $\lambda_6 = -\alpha_H$, $\lambda_7 = -\mu_A$, $\lambda_8 = -a_4$ and $\lambda_9 = -a_5$.

The stability of the DFE can be conluded by using Routh-Hurwitz Criteria to determine the sign of the remaining eigenvalues of the polynomial

$$\lambda^2 + \phi_1\lambda + \alpha_a a_6 = 0, \tag{5.2.3.0.4}$$

where

$$\begin{cases} \phi_1 &= (a_6 + \alpha_a), \\ \phi_2 &= \alpha_a a_6. \end{cases} \tag{5.2.3.0.5}$$

Applying the Routh-Hurwitz stability criterion, we can deduce that the equilibrium state with the model system (5.2.0.1) would be stable if and only if the determinants of all the Hurwitz matrices associated with the characteristic equation (5.2.3.0.4) are positive. In this case, we define the following matrices whose elements are the coefficients (ϕ_S) of the characteristic polynomial (5.2.3.0.4):

$$H_1 = \begin{pmatrix} \phi_1 \end{pmatrix}, \quad H_2 = \begin{pmatrix} \phi_1 & 1 \\ 0 & \phi_2 \end{pmatrix}. \tag{5.2.3.0.6}$$

Evaluating the determinant of H_1, we obtain

$$\begin{cases} det(H_1) &= \Big|\ \phi_1\ \Big|, \\ &= \phi_1, \\ &= (a_6 + \alpha_a) > 0. \end{cases} \tag{5.2.3.0.7}$$

The determinant of H_2 is given by:

$$\begin{cases} det(H_2) &= \begin{vmatrix} \phi_1 & 1 \\ 0 & \phi_2 \end{vmatrix}, \\ &= \phi_1\phi_2, \\ &= (a_6 + \alpha_a) > 0, \quad . \end{cases} \tag{5.2.3.0.8}$$

The disease-free equilibrium is stable when all the eigenvalues obtained from $J(E_0)$ are negative or have negative real parts. Clearly, the nine eigenvalues listed above are strictly negative, ensuring the stability of the equilibrium. Now, when examining the stability of the disease-free equilibrium (DFE), we proceeded by using Routh-Hurwitz Criteria to determine the sign of the remaining eigenvalues of the polynomial (5.2.3.0.4). By using the Routh-Hurwitz criterion on our quadratic characteristic equation, we determine that the system is locally stable because both ϕ_1 and ϕ_2 are positive. Consequently, the equilibrium state of the system is stable.

5.2.4 Global stability of the disease-free equilibrium

We establish the global stability of the disease-free equilibrium in the multiscale model represented by equations (5.2.0.1) employing a next-generation operator [90]. Consequently, the system (5.2.0.1) can be re-written in the following manner:

$$\begin{cases} \dfrac{dX}{dt} &= F(X, Z), \\ \dfrac{dY}{dt} &= G(X, Z), \end{cases} \tag{5.2.4.0.1}$$

where

- $X = (S_H, S_A)$ denotes a compartment corresponding to the uninfected category.
- $Z = (I_H, C_h, W_h, E_h, , E_H, I_A, E_a, O_a, P_A)$ represent compartments of infected and infective classes.

We let

$$E_0 = \left(\frac{\Lambda_H}{\mu_H}, \ 0, \ 0, \ 0, 0, \ 0, \ \frac{\Lambda_A}{\mu_A}, 0 \ 0 \ 0, \ 0\right), \tag{5.2.4.0.2}$$

represent the disease-free equilibrium (DFE) state of the interconnected multiscale model described by equations (5.2.0.1). In order for X^* to attain global asymptotic stability, the following conditions, denoted as (H1) and (H2), need to be met:.

H1. $\frac{dX}{dt} = F(X, 0)$ demonstrates globally asymptotically stable (g.a.s),

H2. $G(X, Z) = AZ - \hat{G}(X, Z)$, $\hat{G}((X, Z) \geq 0$ for $(X, Z) \in R^9_+$ where $A = D_Z G(X^*, 0)$ represents an M-matrix, and R^9_+ describes the domain within which the model holds biological significance.

In this case

$$F(X, 0) = \begin{bmatrix} \Lambda_H - \mu_H S_H \\ \Lambda_A - \mu_A S_A \end{bmatrix}, \tag{5.2.4.0.3}$$

and the matrix A is given by

$$A = \begin{pmatrix} -a_0 & 0 & 0 & 0 & 0 & 0 & 0 & 0 & b_0 \\ 0 & -a_1 & 0 & 0 & 0 & 0 & 0 & 0 & b_1 \\ 0 & \alpha_c & -a_2 & 0 & 0 & 0 & 0 & 0 & 0 \\ 0 & 0 & \alpha_w & a_3 & 0 & 0 & 0 & 0 & 0 \\ 0 & 0 & 0 & 0 & -\alpha_H & 0 & 0 & 0 & 0 \\ 0 & 0 & 0 & 0 & b_2 & -a_4 & 0 & 0 & 0 \\ 0 & 0 & 0 & 0 & b_3 & 0 & -a_5 & 0 & 0 \\ 0 & 0 & 0 & 0 & 0 & 0 & \alpha_a & -a_6 & 0 \\ 0 & 0 & 0 & 0 & 0 & 0 & 0 & \alpha_0 & -\alpha_A \end{pmatrix}, \tag{5.2.4.0.4}$$

where

$$\begin{cases} b_0 = \dfrac{\beta_H \Lambda_H}{P_0 \mu_H}, \\ b_1 = \dfrac{\beta_H (\Lambda_H - \mu_H)}{P_0 \mu_H}, \\ b_2 = \dfrac{\beta_A \Lambda_A}{\mu_A P_0}, \\ b_3 = \dfrac{(\Lambda_A - \mu_A \beta_A)}{\mu_A \Phi_A E_0}, \end{cases} \tag{5.2.4.0.5}$$

with $\hat{G}(X, Z)$ given by

$$\hat{G}(X,Z) = \begin{bmatrix} \left(\dfrac{\Lambda_H}{P_0 \mu_H} - \dfrac{S_H}{P_0 + P_A}\right) \beta_H P_A \\ \left(\dfrac{\Lambda_H - \mu_H}{P_0 \mu_H} - \dfrac{S_H - 1}{(P_0 + P_A)\Phi_H (I_H + 1)}\right) \dfrac{\beta_A P_A}{\Phi_H} \\ 0 \\ 0 \\ (I_H + 1)\alpha_e E_H \\ \left(\dfrac{\Lambda_A}{E_0 \mu_A} - \dfrac{S_A}{E_0 + E_H}\right) \beta_A E_H \\ \left(\dfrac{\Lambda_A - \mu_A}{E_0 \mu_A} - \dfrac{S_A - 1}{(E_0 + E_H)\Phi_H (I_A + 1)}\right) \dfrac{\beta_A E_H}{\Phi_A} \\ 0 \\ \alpha_0 O_a - I_A \end{bmatrix}. \tag{5.2.4.0.6}$$

Since $\Lambda_H/(\mu_H P_0) \geq S_H/(P_0+P_A)$, $(\Lambda_H-\mu_H)/(P_0\mu_H\Phi_H) \geq [S_H-1]/[(P_0+P_A)\Phi_H(I_H+1)]$, $\Lambda_A/(\mu_A P_0) \geq S_A/(P_0+P_A)$ and $(\Lambda_A-\mu_A)/(E_0\mu_A\Phi_A) \geq [S_A-1]/[(E_0+P_A)(I_A+1)]$, It is clear that $\hat{G}(X,Z) \geq 0$ for all $(X,Z) \in R_+^{11}$. It is also clear that A is an M-matrix because its

off diagonal elements are non-negative. Consequently, we proceed to formulate a theorem that encapsulates the findings presented above.

Theorem 5.1. *[72] The global asymptotic stability of the disease-free equilibrium in the model described by equations (5.2.0.1) is established when R_0 is less than or equal to 1, and the conditions (H1) and (H2) are fulfilled.*

5.3 The Endemic Equilibrium and Its Stability

This section provides the results related to the presence of a solution in an endemic equilibrium for the model described by equations (5.2.0.1). The endemic equilibrium state of the multiscale model system (5.2.0.1) is determined by equating the left-hand side of the model equations to zero. Letting:

$$E_1^* = (S_H^*, I_H^*, C_h^*, W_h^*, E_H^*, E_H^*, S_A^*, I_A^*, E_a^*, O_a^*, P_A^*), \tag{5.3.0.0.1}$$

be an endemic solution for the multiscale model system (5.2.0.1), the human taeniasis baseline burden can be approximated using the endemic solutions of E_1^*. We now give expression for the

endemic variables and their interpretation as follows:

$$
\begin{cases}
S_H^* &= \dfrac{\Lambda_H(P_0+P_A^*)}{\beta_H P_A^* + \mu_H(P_0+P_A^*)}, \\
I_H^* &= \dfrac{\Lambda_H \beta_H P_A^*}{[\beta_H P_A^* + \mu_H(P_0+P_A^*)](\delta_H+\mu_H)}, \\
C_h^* &= \dfrac{\beta_H P_A^*[S_H^*-1]}{[P_o+P_A]\Phi_H[I_H^*+1]]}a_4, \\
W_h^* &= \dfrac{\beta_H P_A^*[S_H^*-1]}{[P_o+P_A^*]\Phi_H[I_H^*+1]]}a_1a_4, \\
E_h^* &= a_1a_2\dfrac{\beta_H P_A^*[S_H^*-1]}{[P_o+P_A^*]\Phi_H[I_H^*+1]]}a_4, \\
E_H^* &= \dfrac{(I_H^*+1)\alpha_e}{\alpha_H}a_1a_2\dfrac{\beta_H P_A^*[S_H^*-1]}{[P_o+P_A^*]\Phi_H[I_H^*+1]]}a_4, \\
S_A^* &= \dfrac{\Lambda_A(E_0+E_H^*)}{\beta_A E_H^* + \mu_A(E_0+E_H^*)}, \\
I_A^* &= \dfrac{\beta_A S_A^*}{(E_0+E_H^*)(\mu_A+\delta_A)}\dfrac{(I_H^*+1)\alpha_e}{\alpha_H}\dfrac{\beta_H P_A^*[S_H^*-1]}{[P_o+P_A^*]\Phi_H[I_H^*+1]]}a_1a_2a_4, \\
E_a &= \dfrac{\beta_A[S_A^*-1]}{(\mu_a+\alpha_a)[E_0+E_H^*]\Phi_A[I_A^*+1]}\dfrac{(I_H^*+1)\alpha_e}{\alpha_H}\dfrac{\beta_H P_A^*[S_H^*-1]}{[P_o+P_A^*]\Phi_H[I_H^*+1]]}a_1a_2a_4, \\
O_a &= E_a^*\dfrac{\beta_A[S_A^*-1]}{[E_0+E_H^*]\Phi_A[I_A^*+1]}\dfrac{(I_H^*+1)\alpha_e}{\alpha_H}\dfrac{\beta_H P_A^*[S_H^*-1]}{[P_o+P_A^*]\Phi_H[I_H^*+1]]}a_1a_2a_3a_4, \\
P_A^* &= \dfrac{\alpha_o(I_A^*+1)}{\alpha_A}E_a^*\dfrac{\beta_A[S_A^*-1]}{[E_0+E_H^*]\Phi_A[I_A^*+1]}\dfrac{(I_H^*+1)\alpha_e}{\alpha_H}\dfrac{\beta_H P_A^*[S_H^*-1]}{[P_o+P_A^*]\Phi_H[I_H^*+1]]}a_1a_2a_3a_4.
\end{cases}
\tag{5.3.0.0.2}
$$

where

$$\begin{cases} a_1 &= \dfrac{\alpha_c}{\mu_w + \alpha_w}, \\ a_2 &= \dfrac{\alpha_w}{\mu_e + \alpha_e}, \\ a_3 &= \dfrac{\alpha_a}{(\mu_o + \alpha_o)(\mu_a + \alpha_a)}, \\ a_4 &= \dfrac{1}{\mu_c + \alpha_c}, \\ a_5 &= \dfrac{\alpha_e}{\mu_c + \alpha_c}. \end{cases} \tag{5.3.0.0.3}$$

$$S_H^* = \frac{\Lambda_H(P_0 + P_A^*)}{\beta_H P_A^* + \mu_H(P_0 + P_A^*)}. \tag{5.3.0.0.4}$$

In Equation (5.3.0.0.4), we can observe that the susceptible human population in a state of endemic equilibrium is influenced by both the average duration individuals remain in the susceptible category and the rate at which new susceptible individuals join this category due to births. Individuals within the susceptible category transition out of it due to either infection or mortality. The quantity of infected humans during the endemic state is expressed as follows:

$$I_H^* = \frac{\Lambda_H \beta_H P_A^*}{[\beta_H P_A^* + \mu_H(P_0 + P_A^*)](\delta_H + \mu_H)}. \tag{5.3.0.0.5}$$

It can be observed from Equation (5.3.0.0.5) that the number of infected human individuals at the state of endemic equilibrium is determined by both the average duration individuals spend in the infected category and the rate at which susceptible individuals get infected. The within-host infective cysticerci in the human intestine during the endemic phase is described as follows:

$$C_h^* = \frac{\beta_H P_A^*[S_H^* - 1]}{[P_o + P_A]\Phi_H[I_H^* + 1](\mu_c + \alpha_c)]}. \tag{5.3.0.0.6}$$

By examining Equation (5.3.0.0.6), we can observe that the average population of infective cysticerci within an individual infected human is determined by both the typical lifespan of infective

cysticerci within a single infected human host and the rate at which a susceptible individual becomes infected. The quantity of first-stage worm larvae population within an infected human host during the endemic state is expressed as follows:

$$W_h^* = \frac{\beta_H P_A^*[S_H^* - 1]}{[P_o + P_A^*]\Phi_H[I_H^* + 1](\mu_c + \alpha_c)]} a_1. \tag{5.3.0.0.7}$$

It can be observed from Equation (5.3.0.0.7) that the population of tapeworm at the state of endemic equilibrium is determined by the rate at which humans become infected, the rate at which cysticerci develop into mature worms, and the average lifespan of infective worm eggs within the internal human environment. The established quantity of within-host infective worm eggs in the human intestine during the endemic phase is described as follows:

$$E_h^* = \frac{\beta_H P_A^*[S_H^* - 1]}{[P_o + P_A^*]\Phi_H[I_H^* + 1](\mu_c + \alpha_c)]} a_1 a_2. \tag{5.3.0.0.8}$$

We observe from Equation (5.3.0.0.8) that the population of tapeworm eggs at the endemic equilibrium state is determined by the rate at which humans become infected, the rate at which cysticerci develop into mature worms, the rate at which tapeworm hatch eggs, and the average lifespan of infective eggs within the within-human environment. The established quantity of infective tapeworm eggs in the environment during the endemic phase is expressed as follows:

$$E_H^* = \frac{(I_H^* + 1)\alpha_e}{\alpha_H} \frac{\alpha_w}{\mu_e + \alpha_e} \frac{\alpha_c}{\mu_w + \alpha_w} \frac{\beta_H P_A^*[S_H^* - 1]}{[P_o + P_A^*]\Phi_H[I_H^* + 1](\mu_c + \alpha_c)]}. \tag{5.3.0.0.9}$$

We note from Equation (5.3.0.0.9) that the tapeworm eggs population in the environment at equilibrium point is equal to the rate at which humans get infected, the rate at which cysticerci develop into mature worms,, the rate at which tapeworm eggs are hatched, the rate at which tapeworm eggs are shed to the environment and the average life span of infective eggs in the outside environment. The endemic value of infective tapeworm eggs in the environment is given by

$$S_A^* = \frac{\Lambda_A(E_0 + E_H^*)}{\beta_A E_H^* + \mu_A(E_0 + E_H^*)}. \tag{5.3.0.0.10}$$

By examining Equation (5.3.0.0.10), we can observe that the susceptible pig population at the

state of endemic equilibrium is influenced by both the average duration that individuals remain in the susceptible category and the rate at which new susceptible pigs join this category through births. Pigs within the susceptible category transition out of it due to either infection or mortality. The quantity of infected pigs during the endemic phase is expressed as follows:

$$I_A^* = \frac{\beta_A S_A^*}{(E_0+E_H^*)(\mu_A+\delta_A)}\frac{(I_H^*+1)\alpha_e}{\alpha_H}\frac{\beta_H P_A^*[S_H^*-1]}{[P_o+P_A^*]\Phi_H[I_H^*+1]]}a_1a_2a_4. \quad (5.3.0.0.11)$$

It can be observed from Equation (5.3.0.0.11) that the number of infected pigs at the state of endemic equilibrium is determined by the rate at which susceptible individuals become infected, and the average duration that individuals remain in the infected category. The quantity of within-pig host tapeworm eggs during the endemic phase is described as follows:

$$E_a = \frac{[S_A^*-1]}{(\mu_a+\alpha_a)[E_0+E_H^*]\Phi_A[I_A^*+1]}\frac{(I_H^*+1)}{\alpha_H}\frac{P_A^*[S_H^*-1]}{[P_o+P_A^*]\Phi_H[I_H^*+1]]}Z_1. (5.3.0.0.12)$$

where $Z_1 = \alpha_e\beta_A\beta_H a_1a_2a_4$. Notice from Equation (5.3.0.0.12) that the tapeworm eggs at within-pig scale at the endemic equilibrium point is given by the rate at which susceptible pigs become infected, the rate at which eggs are ingested and the rate at which they grow to release onchospheres. The endemic value of within-pig host onchospheres is given by

$$O_a = \frac{E_a^*\beta_A[S_A^*-1]}{[E_0+E_H^*]\Phi_A[I_A^*+1]}\frac{(I_H^*+1)\alpha_e}{\alpha_H}\frac{\beta_H P_A^*[S_H^*-1]}{[P_o+P_A^*]\Phi_H[I_H^*+1]]}a_1a_2a_3a_4. (5.3.0.0.13)$$

Note from Equation (5.3.0.0.13) that onchospheres at the endemic equilibrium point is given by the rate at which susceptible individuals and pigs become infected and the rate at which onchospheres are released from ingested eggs within-pig host. The endemic value of community pathogen load is given by

$$P_A^* = \frac{(I_A^*+1)}{\alpha_A}\frac{E_a^*[S_A^*-1]}{[E_0+E_H^*]\Phi_A[I_A^*+1]}\frac{(I_H^*+1)\alpha_e}{\alpha_H}\frac{P_A^*[S_H^*-1]}{[P_o+P_A^*]\Phi_H[I_H^*+1]]}Z_2 (5.3.0.0.14)$$

where $Z_2 = a_1a_2a_3a_4a_o\beta_A\beta_H$.

Note from Equation (5.3.0.0.14) that community pathogen load at the endemic equilibrium point is given by the rate at which susceptible individuals and pigs become infected, the rate at which onchospheres are released from ingested eggs within-pig host and the rate at which onchospheres

develop into cycticerci in muscles within an infected pig host.

Therefore, we conclude that the between-host scale endemic expressions for $S_H^*, I_H^*, E_H^*, S_A^*, I_A^*, P_A^*$ are determined by both within-host scale disease parameters and between-host scale parameters and in turn, the within-host scale endemic expressions for $C_h^*, W_h^*, E_h^*, E_a^*, O_a^*$ are dependent on both within-host scale and between-host scale parameters. Therefore, the obtained results here also show that the microscale (within-host scale) and the macroscale (between-host scale) influence each other in a reciprocal way.

5.3.1 Local stability of the endemic equilibrium state

In this subsection, we investigate the local asymptotic stability of the endemic steady state within the model system (5.2.0.1) using the Center Manifold Theory introduced in [73]. To apply the Center Manifold Theory, we proceed to alter the variables within the model system as follows: defining $S_H = x_1$, $I_H = x_2$, $C_h = x_3$, $W_h = x_4$, $E_h = x_5$, $E_H = x_6$, $S_A = x_7$, $I_A = x_8$, $E_a = x_9$, $O_a = x_{10}$, and $P_A = x_{11}$. Additionally, we employ the vector notation $\mathbf{x} = (x_1, x_2, x_3, x_4, x_5, x_6, x_7, x_8, x_9, x_{10}, x_{11})^T$, which enables us to express the model system (5.2.0.1) in the following form:

$$\frac{d\mathbf{x}}{dt} = \mathbf{f}(\mathbf{x}, \beta^*), \tag{5.3.1.0.1}$$

where

$$\mathbf{f} = (f_1, f_2, f_3, f_4, f_5, f_6, f_7, f_8, f_9, f_{10}, f_{11}). \tag{5.3.1.0.2}$$

Therefore, model system (5.2.0.1) can be re-written as:

$$
\begin{cases}
\dot{x_1} = \Lambda_H - \dfrac{\beta^* x_1 x_{11}}{P_0 + x_{11}} - \mu_H x_1 = f_1, \\
\dot{x_2} = \dfrac{\beta^* x_1 x_{11}}{P_0 + x_{11}} - (\mu_H + \delta_H) x_2 = f_2, \\
\dot{x_3} = \dfrac{\beta_H x_{11}[x_1 - 1]}{[P_0 + x_{11}]\Phi_H[x_2 + 1]} - (\mu_c + \alpha_c) x_3 = f_3, \\
\dot{x_4} = \alpha_c x_3 - (\mu_w + \alpha_w) x_4 = f_4, \\
\dot{x_5} = \alpha_w x_4 - (\mu_e + \alpha_e) x_5 = f_5, \\
\dot{x_6} = (x_2 + 1)\alpha_e x_5 - \alpha_H x_6 = f_6, \\
\dot{x_7} = \Lambda_A - \dfrac{\beta_A x_7 x_6}{E_0 + x_6} - \mu_A x_7 = f_7, \\
\dot{x_8} = \dfrac{\beta_A x_7 x_6}{E_0 + x_6} - (\mu_A + \delta_A) x_8 = f_8, \\
\dot{x_9} = \dfrac{\beta_A x_6[x_7 - 1]}{(E_0 + x_6)\Phi_A(x_8 + 1)} - (\alpha_a + \mu_a) x_9 = f_9, \\
\dot{x_{10}} = \alpha_a x_9 - \mu_o + \alpha_o x_{10} = f_{10}, \\
\dot{x_{11}} = x_{10}\alpha_a(x_8 + 1) - \alpha_A x_{11} = f_{11}.
\end{cases}
\tag{5.3.1.0.3}
$$

Since we are using the Center Manifold Theory method, thus, the Jacobian matrix of the system (5.3.1.0.3) will be computed at the disease-free equilibrium point E^0, represented as $J(E^0)$. The Jacobian matrix corresponding to the set of Equations (5.3.1.0.3) when evaluated at the disease-free equilibrium E_0 is formulated as follows:

$$J_{\beta^*} = \begin{pmatrix} -\mu_H & 0 & 0 & 0 & 0 & 0 & 0 & 0 & 0 & 0 & b_0 \\ 0 & -a_0 & 0 & 0 & 0 & 0 & 0 & 0 & 0 & 0 & b_1 \\ 0 & 0 & -a_1 & 0 & 0 & 0 & 0 & 0 & 0 & 0 & b_2 \\ 0 & 0 & \alpha_c & -a_2 & 0 & 0 & 0 & 0 & 0 & 0 & 0 \\ 0 & 0 & 0 & \alpha_w & -a_3 & 0 & 0 & 0 & 0 & 0 & 0 \\ 0 & 0 & 0 & 0 & \alpha_e & -\alpha_H & 0 & 0 & 0 & 0 & 0 \\ 0 & 0 & 0 & 0 & 0 & b_3 & -\mu_A & 0 & 0 & 0 & 0 \\ 0 & 0 & 0 & 0 & 0 & b_4 & 0 & -a_4 & 0 & 0 & 0 \\ 0 & 0 & 0 & 0 & 0 & b_5 & 0 & 0 & -a_5 & 0 & 0 \\ 0 & 0 & 0 & 0 & 0 & 0 & 0 & 0 & \alpha_a & -a_6 & 0 \\ 0 & 0 & 0 & 0 & 0 & 0 & 0 & 0 & 0 & \alpha_0 & -\alpha_A \end{pmatrix} \quad (5,3.1.0.4)$$

where

$$\begin{cases} a_0 = (\mu_H + \delta_H), \\ a_1 = (\mu_c + \alpha_c), \\ a_2 = (\mu_w + \alpha_w), \\ a_3 = (\mu_e + \alpha_e), \\ a_4 = (\mu_A + \delta_A), \\ a_5 = (\mu_a + \alpha_a), \\ a_6 = (\alpha_0 + \alpha_0), \\ b_0 = -\dfrac{\beta_H \Lambda_H}{P_0 \mu_H}, \\ b_1 = \dfrac{\beta_H \Lambda_H}{P_0 \mu_H}, \\ b_2 = \dfrac{\beta_H (\Lambda_H - \mu_H)}{P_0 \mu_H}, \\ b_3 = \dfrac{\beta_A \Lambda_A}{\mu_A P_0}, \\ b_4 = -\dfrac{\beta_A \Lambda_A}{\mu_A P_0}, \\ b_5 = \dfrac{(\Lambda_A - \mu_A)\beta_A}{\mu_A \Phi_A E_0}. \end{cases} \tag{5.3.1.0.5}$$

The basic reproductive number of our model system is

$$R_0 = \sqrt{M_1 \frac{\beta_A[\Lambda_A - \mu_A]}{\mu_A \Phi_A \alpha_H E_0} . \frac{\alpha_e}{\mu_e + \alpha_e} . \frac{\alpha_w}{\mu_w + \alpha_w} . \frac{\alpha_c}{\mu_c + \alpha_c} . \frac{\beta_H[\Lambda_H - \mu_H]}{\mu_H \Phi_H \alpha_A P_0}}. \tag{5.3.1.0.6}$$

where

$$M_1 = \frac{\alpha_0}{\mu_o + \alpha_o} . \frac{\alpha_a}{\mu_a + \alpha_a}.$$

Consider $\beta_A = k\beta_H$, where k lies within the interval $(0, 1)$ or $k \geq 1$. Additionally, let $\beta_H = \beta^*$. Assuming β^* as the bifurcation parameter and adopting $R_0 = 1$, we can solve for β^*, yielding:

$$\beta^* = \sqrt{\frac{M_2\mu_A\Phi_A\alpha_H E_0.\mu_H\Phi_H\alpha_A P_0}{k\alpha_0\alpha_a\alpha_e\alpha_w\alpha_c(\Lambda_A - \mu_A)(\Lambda_H - \mu_H)}}. \tag{5.3.1.0.7}$$

where $M_2 = (\mu_o + \alpha_o)(\mu_a + \alpha_a)(\mu_e + \alpha_e)(\mu_w + \alpha_w)(\mu_c + \alpha_c)$.

It is clear that the linearized version of the transformed Equations (5.3.1.0.3), when examined near $\beta_H = \beta^*$ with the bifurcation point β^*, demonstrates a simple occurrence of a zero eigenvalue.

It is necessary for us to have the following computations in order to apply Theorem (2.4.1.11), (It is important to highlight that we are utilizing β^* as the parameter for bifurcation, replacing ϕ as presented in Theorem (2.4.1.11).

Eigenvectors of J_{β^*}: In situations where $R_0 = 1$, it is possible to demonstrate that the Jacobian matrix (5.3.1.0.4) at $\beta_H = \beta^*$ (referred to as J_{β^*}) possesses a corresponding right eigenvector linked to the zero eigenvalue, which is expressed as:

$$\mathbf{u} = [u_1, u_2, u_3, u_4, u_5, u_6, u_7, u_8, u_9, u_{10}, u_{11}]^T, \tag{5.3.1.0.8}$$

where

$$\begin{cases} u_1 &= -\dfrac{\beta^*\Lambda_H}{\mu_H^2 P_0}, \\ u_2 &= \dfrac{\beta^*\Lambda_H}{P_0\mu_H(\mu_H+\delta_H)}, \\ u_3 &= \dfrac{\beta^*(\Lambda_H-\mu_H)}{P_0\mu_H\Phi_H(\mu_c+\alpha_c)}, \\ u_4 &= \dfrac{\alpha_c}{\mu_c+\alpha_c}\dfrac{\beta^*(\Lambda_H-\mu_H)}{(\mu_w+\alpha_w)P_0\mu_H\Phi_H}, \\ u_5 &= \dfrac{\alpha_w}{\mu_w+\alpha_w}\dfrac{\alpha_c}{\mu_c+\alpha_c}\dfrac{\beta^*(\Lambda_H-\mu_H)}{(\mu_e+\alpha_e)P_0\mu_H\Phi_H} \\ u_6 &= \dfrac{\alpha_e}{\mu_e+\alpha_e}\dfrac{\alpha_w}{\mu_w+\alpha_w}\dfrac{\alpha_c}{\mu_c+\alpha_c}\dfrac{\beta^*(\Lambda_H-\mu_H)}{\alpha_A\mu_H\Phi_H P_0}, \\ u_7 &= \dfrac{-k\beta^*\Lambda_A\alpha_e}{\mu_A^2 E_0}\dfrac{\alpha_e}{\mu_e+\alpha_e}\dfrac{\alpha_w}{\mu_w+\alpha_w}\dfrac{\alpha_c}{\mu_c+\alpha_c}\dfrac{\beta^*(\Lambda_H-\mu_H)}{\alpha_A\mu_H\Phi_H P_0}, \\ u_8 &= \dfrac{k\beta^*\Lambda_A}{\mu_A E_0(\mu_A+\delta_A)}\dfrac{\alpha_e}{\mu_e+\alpha_e}\dfrac{\alpha_w}{\mu_w+\alpha_w}\dfrac{\alpha_c}{\mu_c+\alpha_c}\dfrac{\beta^*(\Lambda_H-\mu_H)}{\alpha_A\mu_H\Phi_H P_0}, \\ u_9 &= \dfrac{\alpha_A}{\alpha_a}\dfrac{(\mu_o+\alpha_o)}{\alpha_o}, \\ u_{10} &= \dfrac{\alpha_A}{\alpha_o}, \\ u_{11} &= 1. \end{cases} \tag{5.3.1.0.9}$$

In addition, the left eigenvector of the Jacobian matrix (5.3.1.0.4) associated with the zero eigenvalue at $\beta_H = \beta^*$ is given by

$$\mathbf{v} = [v_1, v_2, v_3, v_4, v_5, v_6, v_7, v_8, v_9, v_{10}, v_{11}]^T, \tag{5.3.1.0.10}$$

where

$$
\begin{cases}
v_1 &= 0, \\
v_2 &= 0, \\
v_3 &= \dfrac{\alpha_e}{\mu_e+\alpha_e}\dfrac{\alpha_w}{\mu_w+\alpha_w}.\dfrac{\alpha_c}{\mu_c+\alpha_c}.\dfrac{k\beta^*(\Lambda_A-\mu_A)}{\alpha_H\mu_A\Phi_A E_0}, \\
v_4 &= \dfrac{\alpha_e}{\mu_e+\alpha_e}.\dfrac{\alpha_w}{\mu_w+\alpha_w}.\dfrac{k\beta^*(\Lambda_A-\mu_A)}{\alpha_H\mu_A\Phi_A E_0}, \\
v_5 &= \dfrac{\alpha_e}{\mu_e+\alpha_e}.\dfrac{k\beta^*(\Lambda_A-\mu_A)}{\alpha_H\mu_A\Phi_A E_0}, \\
v_6 &= \dfrac{k\beta^*(\Lambda_A-\mu_A)}{\alpha_H\mu_A\Phi_A E_0}, \\
v_7 &= 0, \\
v_8 &= 0, \\
v_9 &= 1, \\
v_{10} &= \dfrac{\mu_a+\alpha_a}{\alpha_a}, \\
v_{11} &= \dfrac{\mu_a+\alpha_a}{\alpha_a}.\dfrac{\mu_o+\alpha_o}{\alpha_o}.
\end{cases}
\tag{5.3.1.0.11}
$$

Computation of bifurcation parameters a and b:

To determine the signs of a and b, we analyze the non-zero second-order mixed derivatives of vector **f** with respect to the variables and β^*. The determination of the sign of a is connected to the existence of the following non-vanishing partial derivatives of vector **f**:

$$
\begin{cases}
\dfrac{\partial^2 f_1}{\partial x_1 \partial x_{11}} = \dfrac{-\beta^*}{P_0}, \\
\dfrac{\partial^2 f_1}{\partial x_{11}^2} = -\dfrac{2\beta^* \Lambda_H}{P_0^2 \mu_H}, \\
\dfrac{\partial^2 f_2}{\partial x_1 \partial x_{11}} = -\dfrac{\beta^*}{P_0}, \\
\dfrac{\partial^2 f_2}{\partial x_{11}^2} = \dfrac{-2\beta^* \Lambda_H}{P_0^2 \mu_H} \\
\dfrac{\partial^2 f_3}{\partial x_1 \partial x_{11}} = -\dfrac{\beta^*}{P_0 \Phi_H} \\
\dfrac{\partial^2 f_3}{\partial x_{11}^2} = -\dfrac{-2\beta^*(\Lambda_H - \mu_H)}{P_0 \mu_H \Phi_H}, \\
\dfrac{\partial^2 f_6}{\partial x_2 \partial x_5} = \alpha_e, \\
\dfrac{\partial^2 f_7}{\partial x_7 \partial x_6} = \dfrac{-k\beta^*}{E_0}, \\
\dfrac{\partial^2 f_7}{\partial x_6^2} = \dfrac{2k\beta^* \Lambda_A}{E_0^2 \mu_A}, \\
\dfrac{\partial^2 f_8}{\partial x_2 \partial x_6} = \dfrac{k\beta^*}{E_0}, \\
\dfrac{\partial^2 f_8}{\partial x_6^2} = \dfrac{-2k\beta^* \Lambda_A}{E_0^2 \mu_A}, \\
\dfrac{\partial^2 f_9}{\partial x_7 \partial x_6} = \dfrac{k\beta^*}{E_0 \Phi_A}, \\
\dfrac{\partial^2 f_9}{\partial x_8 \partial x_6} = \dfrac{-k\beta^*[\Lambda_A - \mu_A]}{E_0 \Phi_A \mu_A}, \\
\dfrac{\partial^2 f_9}{\partial x_6^2} = \dfrac{-k\beta^*[\Lambda_A - \mu_A]}{E_0^2 \Phi_A \mu_A}, \\
\dfrac{\partial^2 f_3}{\partial x_{11} \partial x_2} = \dfrac{\beta^*[\Lambda_H - \mu_H]}{P_0 \Phi_H \mu_H}, \\
\dfrac{\partial^2 f_{11}}{\partial x_{10} \partial x_8} = \alpha_e
\end{cases}
\tag{5.3.1.0.12}
$$

The sign of b is connected to the following non-vanishing derivatives within vector $\mathbf{f}$:

$$\begin{cases} \dfrac{\partial^2 f_1}{\partial x_{11}\partial\beta^*} = -\dfrac{\Lambda_H}{\mu_H P_0}, \\ \dfrac{\partial^2 f_2}{\partial x_{11}\partial\beta^*} = \dfrac{\Lambda_H}{\mu_H P_0}, \\ \dfrac{\partial^2 f_3}{\partial x_{11}\partial\beta^*} = \dfrac{(\Lambda_H-\mu_H)}{\mu_H P_0\Phi_H}, \\ \dfrac{\partial^2 f_7}{\partial x_6\partial\beta^*} = -\dfrac{k\Lambda_A}{\mu_A E_0}, \\ \dfrac{\partial^2 f_8}{\partial x_6\partial\beta^*} = \dfrac{k\Lambda_A}{\mu_A E_0}, \\ \dfrac{\partial^2 f_9}{\partial x_6\partial\beta^*} = \dfrac{k(\Lambda_A-\mu_A)}{\mu_A E_0\phi_A}. \end{cases} \tag{5.3.1.0.13}$$

Substituting expressions (5.3.1.0.9), (5.3.1.0.11), (5.3.1.0.12) and (5.3.1.0.13) into a and b in (2.4.1.11)

$$\begin{cases} a = \sum_{k,i,j=1}^{n} u_k v_i v_j \dfrac{\partial^2 f_k}{\partial x_i \partial x_j}(0,0), \\ = -2\beta^*\left[\dfrac{\Lambda_H^2}{P_0^3\mu_H^3}\dfrac{(\mu_a+\alpha_a)^*}{\alpha_a^2}\dfrac{(\mu_o+\alpha_o)^*}{\alpha_o^2}+\right. \\ \dfrac{\Lambda_H^2}{P_0^3\mu_H^2(\mu_H+\delta_H)}\dfrac{(\mu_a+\alpha_a)^2}{\alpha_a^2}\dfrac{(\mu_o+\alpha_o)^2}{\alpha_o^2}+\dfrac{(\Lambda_H-\mu_H)^2}{P_0^3\mu_H^2\Phi_H(\mu_c+\alpha_c)}\dfrac{(\mu_a+\alpha_a)^2}{\alpha_a^2}\dfrac{(\mu_o+\alpha_o)^2}{\alpha_o^2}+ \\ \dfrac{k^2\Lambda_A^2}{\mu_A^3E_0^3}\dfrac{\alpha_e}{\mu_e+\alpha_e}\dfrac{\alpha_w}{\mu_w+\alpha_w}\dfrac{\alpha_c}{\mu_c+\alpha_c}\dfrac{\beta^*(\Lambda_H-\mu_H)}{\alpha_A\mu_H\Phi_H P_0}\dfrac{(\Lambda_A-\mu_A)^2k^2\beta^*2}{\alpha_H^2\mu_A^2\Phi_A^2E_0^2}+ \\ \dfrac{k^2\Lambda_A^2}{\mu_A^2E_0^3(\mu_A+\delta_A)}\dfrac{\alpha_e}{\mu_e+\alpha_e}\dfrac{\alpha_w}{\mu_w+\alpha_w}\dfrac{\alpha_c}{\mu_c+\alpha_c} \\ \left.\dfrac{\beta^*(\Lambda_H-\mu_H)}{\alpha_A P_0\mu_H\Phi_H}\dfrac{(\Lambda_A-\mu_A)^2k^2\beta*2}{\alpha_H^2\mu_A^2\Phi_A^2E_0^2}\dfrac{k\beta^*(\Lambda_A-mu_A)}{E_0^2\mu_A\Phi_A}\dfrac{\alpha_A}{\alpha_a}\dfrac{(\mu_o+\alpha_o)}{\alpha_o}\dfrac{(\Lambda_A-\mu_A)^2k^2}{\alpha_H^2\mu_A^2\Phi_A^2E_0^2}\right] < 0. \end{cases} \tag{5.3.1.0.14}$$

and

$$
\begin{cases}
b = \sum_{k,i=1}^{n} u_k v_i \frac{\partial^2 f_k}{\partial x_i \partial \phi}(0,0), \\
= \left[\frac{\beta^* \Lambda_H^*}{\mu_H^3 P_0^2} \frac{(\mu_a+\alpha_a)}{\alpha_a} \frac{(\mu_o+\alpha_o)}{\alpha_o} + \frac{\beta^* \Lambda_H^2}{\mu_H^2 P_0^2 (\mu_H+\delta_H)} \frac{(\mu_a+\alpha_a)}{\alpha_a} \frac{(\mu_o+\alpha_o)}{\alpha_o} + \right. \\
\frac{\beta^*(\Lambda_H-\mu_H)^2}{\mu_H^2 P_0^2 \Phi_H^2} (\mu_c+\alpha_c) \frac{\mu_a+\alpha_a}{\alpha_a} \frac{(\mu_o+\alpha_o)}{\alpha_o} + \frac{k^2\beta * \Lambda_A^2}{\mu_A^3 E_0^2} \frac{\alpha_e}{(\mu_e+\alpha_e)} \frac{\alpha_w}{(\mu_w+\alpha_w)} \\
\frac{\alpha_c}{(\mu_c+\alpha_c)} \frac{\beta^*(\lambda_H-\mu_H)}{\alpha_A \mu_H \Phi_H P0} \frac{(\Lambda_A-\mu_A)k\beta^*}{\alpha_H \mu_A \Phi_A E_0} + \frac{k^2\beta * \Lambda_A^2}{\mu_A^2 E_0^2 (\mu_A+\delta_A)} \frac{\alpha_e}{\mu_e+\alpha_e} \\
\frac{\alpha_w}{(\mu_w+\alpha_w)} \frac{\alpha_c}{(\mu_c+\alpha_c)} \frac{\beta^*(\Lambda_H-\mu_H)}{\alpha_A P0 \mu_H \Phi_H} \frac{\beta^*(\Lambda_H-\mu_H)}{\alpha_A P_0 \mu_H \Phi_H} \\
\frac{(\Lambda_A-\mu_A)k\beta^*}{\alpha_H \mu_A \Phi_A E_0} \frac{k^2\beta^* \Lambda_A^*}{\mu_A^2 E_0^2 (\mu_A+\delta_A)} \frac{\alpha_e}{(\mu_e+\alpha_e)} \frac{\alpha_w}{(\mu_w+\alpha_w)} \frac{\alpha_c}{(\mu_c+\alpha_c)} \\
\left. \frac{\beta^*(\Lambda_H-\mu_H)}{\alpha_A P_0 \mu_H \Phi_H} \frac{(\Lambda_A-\mu_A)k\beta^*}{\alpha_H \mu_A \Phi_A E_0} + \frac{k^2(\Lambda_A-\mu_A)^2\beta^*}{\alpha_H \mu_A^2 E_0^2 \Phi_A^2} \frac{\alpha_A}{\alpha_a} \frac{(\mu_0+\alpha_0)}{\alpha_o} \right] > 0.
\end{cases}
\tag{5.3.1.0.15}
$$

Thus $a < 0$ and $b > 0$ whenever $\Lambda_H > \mu_H$ and $\Lambda_A > \mu_A$. Applying point (iv) of the Center Manifold Theory, we have derived the following outcome, which is valid within a range of R_0 values greater than 1 and approaching 1. The Center Manifold Theory ensures that the endemic equilibrium is locally asymptotically stable when R_0 is slightly above 1.

Theorem 5.2. *The local stability of the endemic equilibrium of the coupled multiscale model (5.2.0.1), by the Center Manifold Theorem in [73], is established when the basic reproduction number (R_0) is slightly greater than 1.*

5.4 Sensitivity Analysis

In this section, we perform a sensitivity analysis on the basic reproductive number to assess the relative change in the metric of taeniasis disease dynamics. This assessment focuses on observing changes to the within-host scale and between-host scale parameters within the coupled

multiscale model system (Equation (5.2.0.1)). We accomplish this by using Latin hypercube sampling (LHS) and partial rank correlation coefficients (PRCCs). The outcomes of the investigation into the sensitivity of the basic reproductive number (R_0) for taeniasis disease in response to variations in the parameters of the baseline coupled multiscale model system (5.2.0.1) are presented in the Tornado plot, shown in Figure (5.3) for the parameters in Table 5.3.

Parameter	Initial values	Unit	Source
Λ_H	2247	day^{-1}	[118]
β_H	0.036	day^{-1}	Estimated
μ_H	0.0141	day^{-1}	[119]
δ_H	0.0925	day^{-1}	[119]
Φ_H	0.009	day^{-1}	Estimated
P_0	10000	day^{-1}	Estimated
μ_c	0.007	day^{-1}	Estimated
α_c	0.0001	day^{-1}	Estimated
μ_w	0.8	day^{-1}	Estimated
α_w	0.14-0.33	day^{-1}	[120]
μ_e	10.42	day^{-1}	[119]
α_e	0.150	day^{-1}	[45]
α_H	50	day^{-1}	[121]
Λ_A	1450	day^{-1}	Estimated
μ_A	0.0996	day^{-1}	[112]
β_A	0.25	day^{-1}	[122]
δ_A	0.0001	day^{-1}	Estimated
α_a	0.01	day^{-1}	Estimated
μ_a	0.0001	day^{-1}	Estimated
E_0	100000	day^{-1}	Estimated
μ_o	0.001	day^{-1}	Estimated
α_o	0.0001	day^{-1}	Estimated
α_A	00.007	day^{-1}	Estimated
E_0	10000	day^{-1}	Estimated
Φ_A	0.0001	day^{-1}	Estimated

Table 5.3: Parameter values.

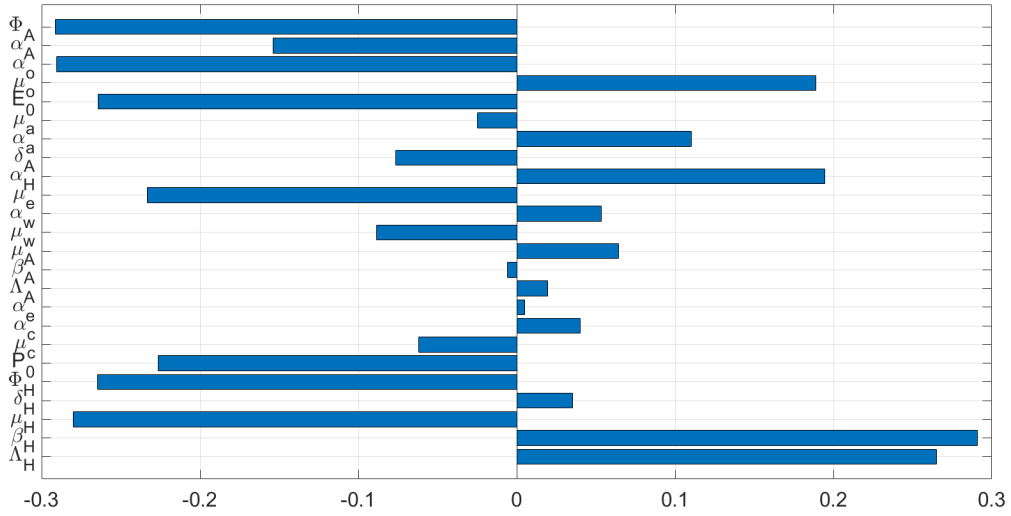

Figure 5.3: Global Sensitivity for Reproductive number (R_0)

Referring to Figure (5.3), we draw the following conclusions: The parameters that show the highest sensitivity to the taeniasis disease dynamics metric (R_0) are α_o, α_c, μ_e, α_e, μ_o, and μ_w, all of which relate to the within-host scale of taeniasis disease dynamics. This suggests that special attention should be given to enhancing the accuracy of these five parameters related to the within-host scale when gathering data, as doing so could lead to enhancements in the reliability and usefulness of the multiscale model for understanding taeniasis disease dynamics as described by Equation (5.2.0.1). The between-host scale parameters that demonstrate the highest sensitivity are β_H, P_0, Φ_H, Φ_A, α_A, E_0, and α_H. Consequently, when initiating interventions for human taeniasis disease, it becomes crucial to ensure the accuracy of these seven between-host parameters to achieve effective outcomes. In conclusion, we observe that evaluating the sensitivity of (R_0) to the parameters of the multiscale model offers valuable insights into guiding the collection of data for model parameterization. Additionally, this assessment helps identify parameters that play a vital role in controlling taeniasis infection in humans and pigs, both at the within-host and between-host scales.

5.5 Numerical Analysis of the Coupled Multiscale Model

In this section of the study, we conduct numerical simulations of a coupled multiscale model for the taeniasis disease system. This is done with the aim of visually demonstrating certain analytical findings that have been derived in this research. We undertake numerical analysis

to describe the impact of various parameters. The dynamics of the coupled multiscale model system (5.2.0.1) were examined using a Python program, specifically version 2.7, running on the Windows 10 operation system which differs from the method used in the first three models because the coupled multiscale is highly nonlinear and not easy to apply NSFD scheme. The values of parameters employed for model simulation are presented in Table 5.3. Several of the parameter values utilized in this research were extracted from established literature. The reason for assuming or estimating certain parameter values lies in the current lack of development and analysis of multiscale modelling for taeniasis infectious disease, particularly within the framework of replication theory. We demonstrate (a) the impact of within-host scale factors on human taeniasis disease at the between-host level, and (b) the influence of between-host scale factors on the within-host scale. The initial conditions used for simulation are given by $S_H(0) = 2000$, $I_H(0) = 100$, $C_h(0) = 0$, $W_h(0) = 0$, $E_h(0) = 0$, $E_H(0) = 0$, $S_A(0) = 1000$, $I_A(0) = 0$, $E_a(0) = 0$, $O_a(0) = 0$ and $P_A(0) = 1500$.

5.5.1 The influence of within-host scale on between-host scale human taeniasis dynamics

In this subsection through numerical analysis we investigate reciprocal influence of the within-human scale parameters (α_c, α_w, α_e, μ_c, μ_w, μ_e) and within-pig scale parameters (α_a, α_o, μ_a, μ_o) on four key between-host variables (I_H, E_H, I_A, P_A). These parameters and variables were selected as illustrative examples to showcase how within-host scale disease processes can affect the human taeniasis transmission dynamics at the between-host scale.

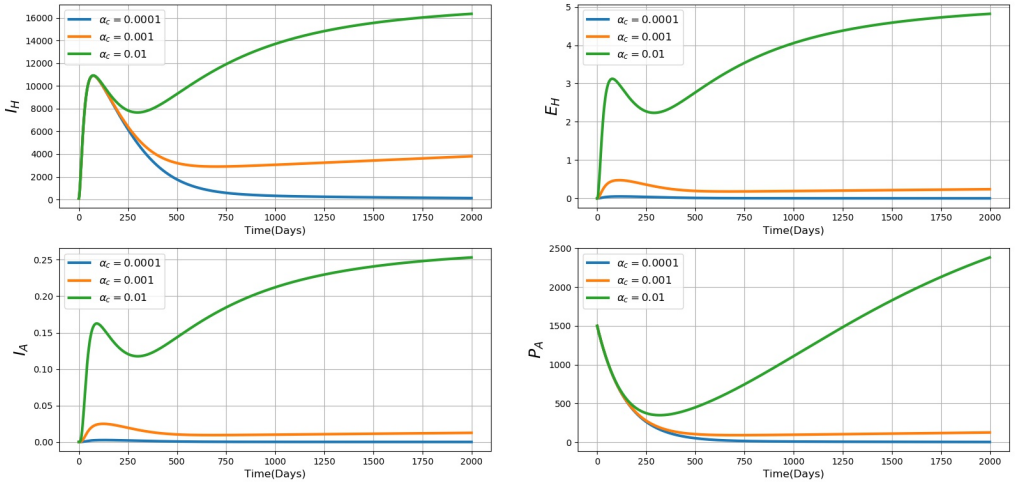

Figure 5.4: *Graph of numerical solutions of model system (5.2.0.1) of average progresssion rate of cysticerci C_h to a worm W_h within-human scale on the between-host scale population dynamics of infected individuals (I_H), environmental pathogen (E_H), infected pig (I_A) and community pathogen load (P_A) for different values of α_c: α_c = 0.0001, α_c = 0.001, and α_c = 0.01.*

Figure 5.4 shows the impact of the average progression of cysticerci (C_h) transforming into a worm (W_h) at the within-human scale on between-host variables, with α_c values of $\alpha_c = 0.0001, \alpha_c = 0.001, \alpha_c = 0.01$. The numerical outcomes depicted in Figure 5.4 reveal a rise in between-host variables: infected individuals (I_H), environmental pathogen (E_H), infected pigs (I_A), and community pathogen load (P_A). This increase is attributed to an increase of α_c values. As of now, we are not aware of any interventions specifically aimed at addressing this particular life stage. These findings imply that implementing control strategies directed at the initial life stages of the pathogen within the definitive host's within-host scale would yield optimal advantages in terms of reducing both parasite load and environmental impact.

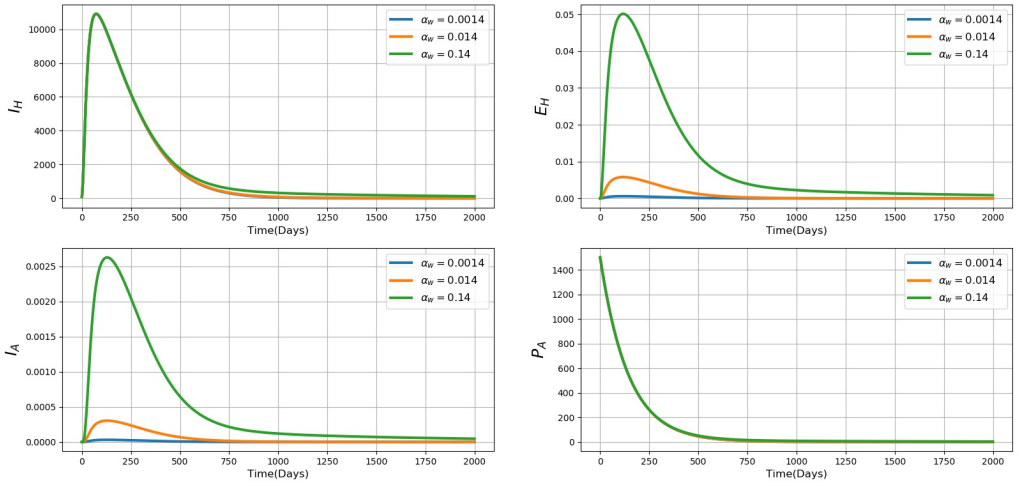

Figure 5.5: *Graph of numerical solutions of model system (5.2.0.1) showing the influence of eggs excretion rate by mature worms within-human scale where* $\alpha_w = 0.0014$, $\alpha_w = 0.014$, $\alpha_w = 0.14$ *on the between-host scale population dynamics of infected individuals* (I_H), *environmental pathogen* (E_H), *infected pigs* (I_A) *and community pathogen load* (P_A).

Figure 5.5 presents graphs of numerical solutions for the model system (5.2.0.1). The results show the effects of increasing matured tapeworm eggs release rate in the within-human scale α_w on between-host variables. The outcomes depicted in Figure 5.5 illustrate a rise in the population of infected people (I_H), environmental pathogens (E_H), and infected pigs (I_A) for various levels of eggs excretion rate by mature worms at the human scale $\alpha_w = 0.0014$, $\alpha_w = 0.014$, and $\alpha_w = 0.14$. The outcomes propose that employing measures to constrain the matured worm to release eggs at the within-human scale may have benefits in reducing the environmental pathogen load and hence infected humans.

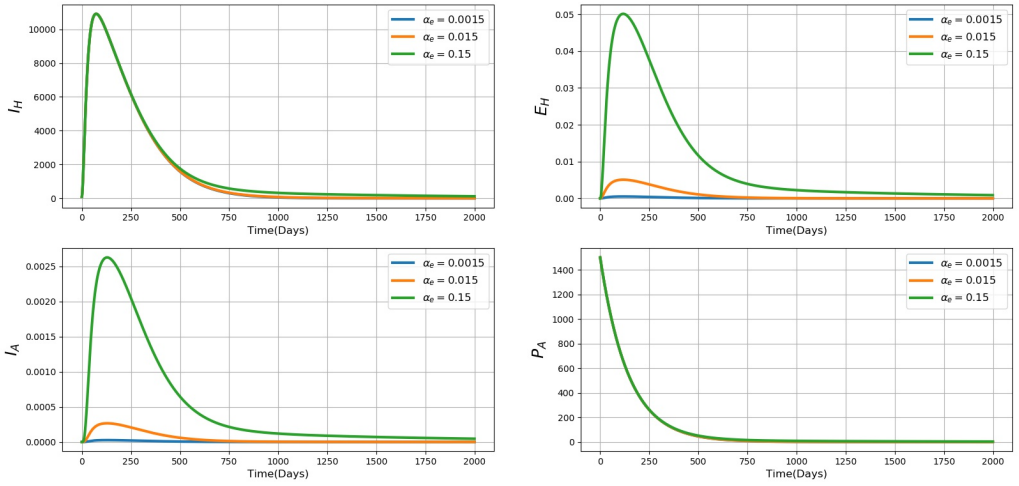

Figure 5.6: *Graphs of numerical solutions of model system (5.2.0.1) illustrating the effect of human excretion rate to the environment* α_e *where* $\alpha_e = 0.0015$, $\alpha_e = 0.015$, $\alpha_e = 0.15$ *on the between-host scale population dynamics of infected individuals* (I_H)*, environmental pathogen* (E_H)*, infected pigs* (I_A) *and community pathogen load* (P_A).

Figure 5.6 displays graphical representations of numerical solutions for the model system (5.2.0.1). The outcomes illustrate the impact of varying egg excretion rates on the environment by the infected human on between-host variables $\alpha_e = 0.0015$, $\alpha_e = 0.015$, $\alpha_e = 0.15$ in population of the infected individuals I_H, environmental pathogen E_H, infected pigs I_A and community pathogen P_A. The results of these graphs show an increase in infected humans I_H, environmental pathogen E_H, infected pigs I_A, when a significant quantity of eggs is released into the environment by the infected human at a high rate. The findings indicate that implementing control measures aimed at reducing the rate of shedding by an infected human may have benefits in reducing the environmental pathogen load and hence infected humans.

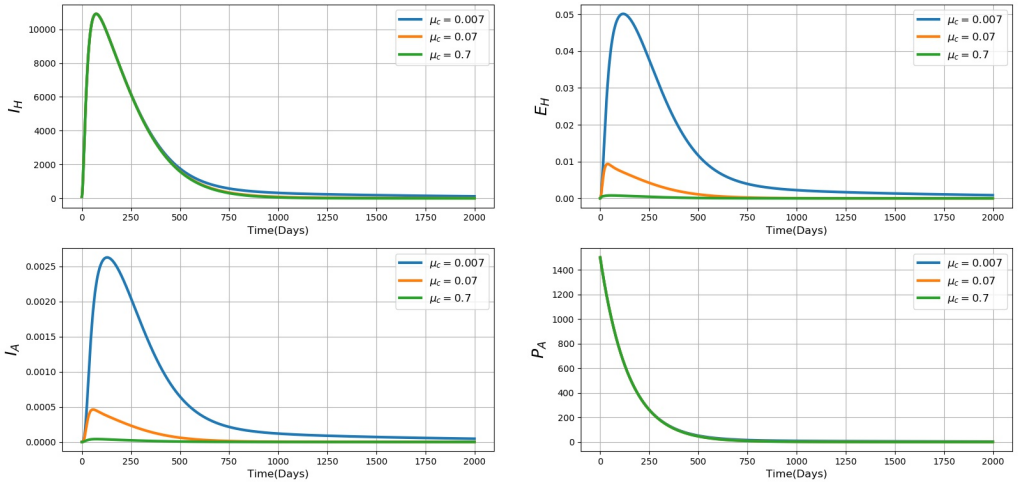

Figure 5.7: *Simulations of model system (5.2.0.1) presenting the effect of death rate of cysticerci in the within-human scale μ_c where $\mu_c = 0.0.007$, $\mu_c = 0.07$, $\mu_c = 0.7$ on the between-host scale population dynamics of infected individuals (I_H), environmental pathogen (E_H), infected pigs (I_A) and community pathogen load (P_A).*

Figure 5.7 displays graphical representations of numerical solutions for the model system (5.2.0.1), illustrating changes in the populations of infected humans (I_H), environmental pathogens (E_H), infected pigs (I_A), and community pathogen load (P_A) across various values of the natural decay rate of cysticerci within the human scale, denoted as μ_c: $\mu_c = 0.007$, $\mu_c = 0.07$, and $\mu_c = 0.7$. The numerical outcomes depicted in Figure 5.7 demonstrate that with an increase in the natural decay rate of cysticerci within the human scale, there is a corresponding reduction in the variables that pertain to interactions between hosts E_H, I_A and P_A. Therefore, control measures intended to kill cysticerci within-human scale may have maximum effect on reducing transmission of human taeniasis at population/community level.

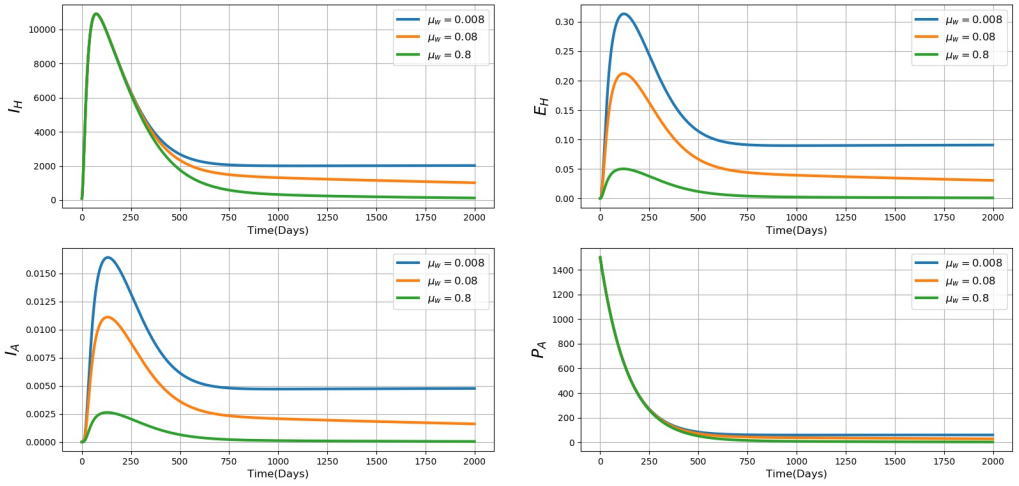

Figure 5.8: *Simulations of model system (5.2.0.1) presenting the effect of death rate of matured worm in the within-human scale μ_w where $\mu_w = 0.008$, $\mu_w = 0.08$, $\mu_w = 0.8$ on the between-host scale population dynamics of infected individuals (I_H), environmental pathogen (E_H), infected pigs (I_A) and community pathogen load (P_A).*

Figure 5.8 presents graphical representations of numerical solutions for the model system (5.2.0.1), illustrating changes in the populations of infected humans (S_H) and environmental pathogens (E_H), population of infected pigs (I_A) and population of community pathogen load (P_A) across various levels of the natural decay rate within the human scale matured worm for $\mu_w = 0.008$, $\mu_w = 0.08$, and $\mu_w = 0.8$. The numerical findings illustrated in Figure 5.8 indicate that with an increase in the decay rate of mature worms within the human scale, there is a corresponding decline in the variables related to interactions between hosts I_H, E_H, I_A and P_A. Therefore, these results suggest that any control measures intended to kill matured tapeworms within an infected individual may have maximum effect on reducing transmission of human taeniasis at population/community level.

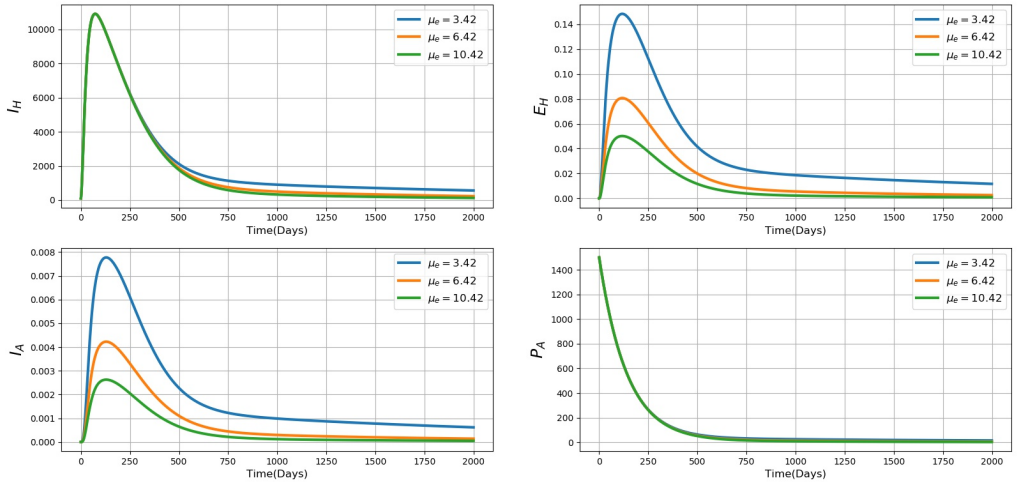

Figure 5.9: *Simulations of model system (5.2.0.1) showing the effect of death rate of eggs within-human scale μ_e where $\mu_e = 3.42$, $\mu_e = 6.42$, $\mu_e = 10.42$ on the between-host scale population dynamics of infected individuals (I_H), environmental pathogen (E_H), infected pigs (I_A) and community pathogen load (P_A).*

Figure 5.9 showcases visual representations of numerical solutions for the model system (5.2.0.1), depicting variations in the populations of infected humans (I_H) and environmental pathogens (E_H), population of infected pigs (I_A) and population of community pathogen load (P_A) across different values of the natural decay rate of tapeworm eggs within the context of a human scale, represented as μ_e: $\mu_e = 3.42$, $\mu_e = 6.42$, and $\mu_e = 10.42$. The numerical findings shown in Figure 5.9 indicate that with an increase in the natural decay rate of tapeworm eggs within the human scale, there is a corresponding reduction in the variables related to interactions between hosts I_H, E_H, I_A and P_A. Therefore, control measures intended to kill tapeworms eggs within an infected individual may yield great achievement on the reduction of human taeniasis transmission at an individual level and population/community level.

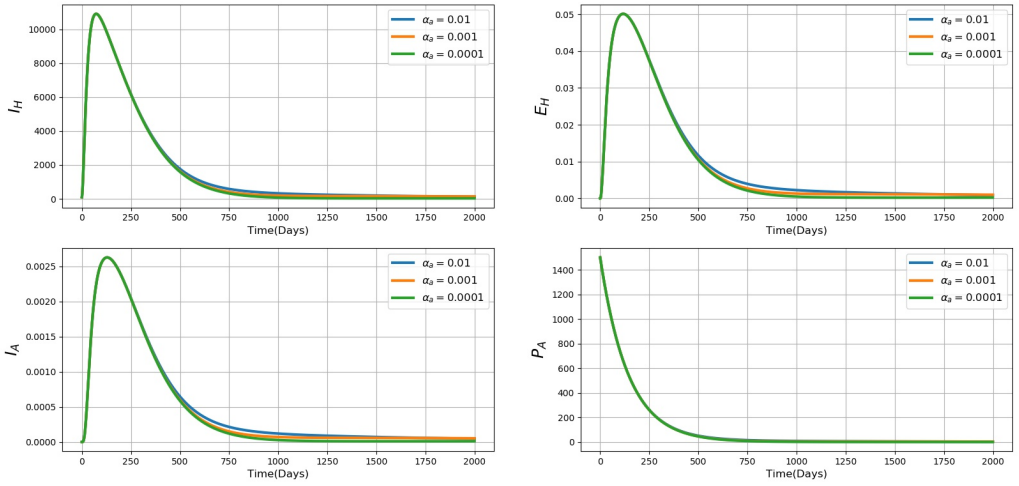

Figure 5.10: Simulations of model system (5.2.0.1) presenting the effect of eggs progression rate to onchospheres in the within-pig scale for $\alpha_a = 0.0001$, $\alpha_a = 0.001$, $\alpha_a = 0.01$ on the between-host scale population dynamics of infected individuals (I_H), environmental pathogen (E_H), infected pig (I_A) and community pathogen load (P_A).

Figure 5.10 presents graphs of numerical solutions for the model system (5.2.0.1). The results show the effects of eggs in the within-pig scale progression rate to become onchospheres α_a where $\alpha_a = 0.0001$, $\alpha_a = 0.001$, $\alpha_a = 0.01$. The results in Figure 5.10 show variations in population of the infected individuals I_H, environmental pathogen E_H, infected pig I_A and community pathogen P_A for different values of eggs transition rate within-pig scale. The outcomes presented in Figure 5.10 indicate that raising α_a leads to only marginal rises in the interplay of population dynamics between hosts, including infected individuals (I_H), environmental pathogens (E_H), infected pigs (I_A), and community pathogen load (P_A). These findings imply that strategies focused on addressing the initial life stages of the pathogen within the pig scale are likely to yield limited benefits in reducing parasite burden at the pig scale and lessening the burden of human taeniasis at the broader population/community level.

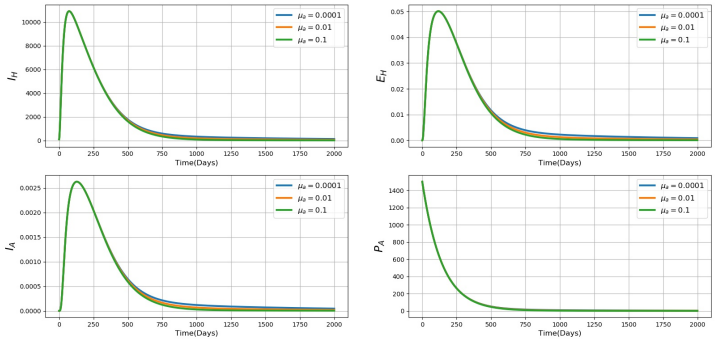

Figure 5.11: *Simulations of model system (5.2.0.1) presenting the effect of eggs death rate within-pig scale μ_a where $\mu_a = 0.0001$, $\mu_a = 0.001$, $\mu_a = 0.01$ on the between-host scale population dynamics of infected individuals (I_H), environmental pathogen (E_H), infected pigs (I_A) and community pathogen load (P_A).*

Figure 5.11 presents graphs of numerical solutions for the model system (5.2.0.1). The results show the effect of eggs death rate in the within pig μ_a where $\mu_a = 0.0001$, $\mu_a = 0.001$, $\mu_a = 0.01$. The results of these graphs illustrate a small variation on environmental pathogen E_H, infected pig I_A and infected humans. Figure 5.11 shows that increasing μ_a resulted in very small changes in between-host scale population dynamics of infected individuals (I_H), environmental pathogen (E_H), infected pigs (I_A), and community pathogen burden (P_A). These findings imply that control methods aimed at eliminating tapeworm eggs at the within-pig scale will have little effect on parasite load and community pathogen load burden.

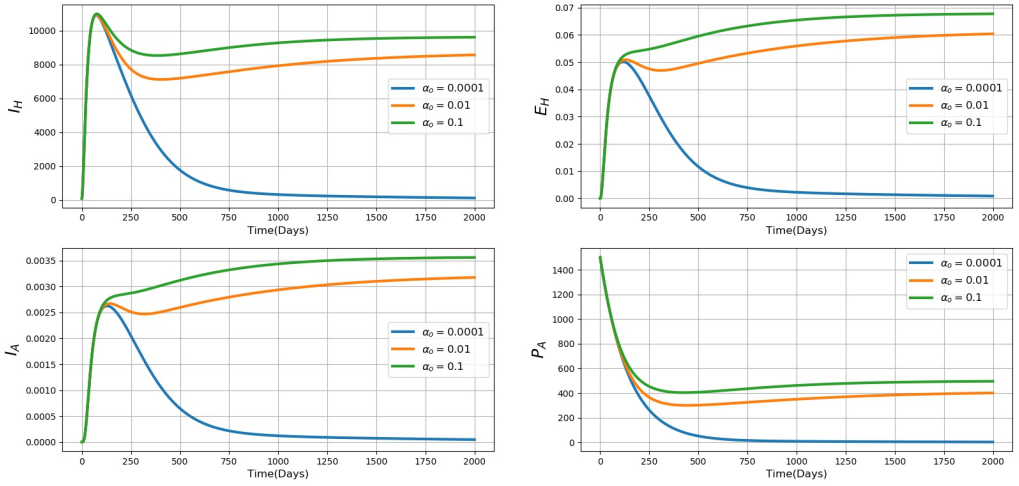

Figure 5.12: Simulations of model system (5.2.0.1) presenting the effect of rate at which onchospheres are shed/excreted into the community by pig α_o with $\alpha_o = 0.0001$, $\alpha_o = 0.01$, $\alpha_o = 0.1$ on the between-host scale population dynamics of infected individuals (I_H), environmental pathogen (E_H), infected pig (I_A) and community pathogen load (P_A).

Figure 5.12 presents graphs of numerical solutions for the model system (5.2.0.1). The results display the consequences of the rate at which pigs release or excrete oncospheres into the community α_o where $\alpha_o = 0.0001$, $\alpha_o = 0.01$, $\alpha_o = 0.1$ on the between-host scale population dynamics of infected individuals (I_H), environmental pathogen (E_H), infected pig (I_A) and community pathogen load (P_A). The results in Figure 5.12 show that an increase in α_o results in increases in between-host scale population dynamics of infected individuals (I_H), environmental pathogen (E_H), infected pigs (I_A) and community pathogen load (P_A). These findings imply that implementing control measures focusing on the second life stage of the pathogen within the pig scale would be advantageous for decreasing parasite burden within the pig population and weakening human taeniasis at the broader human population/community level.

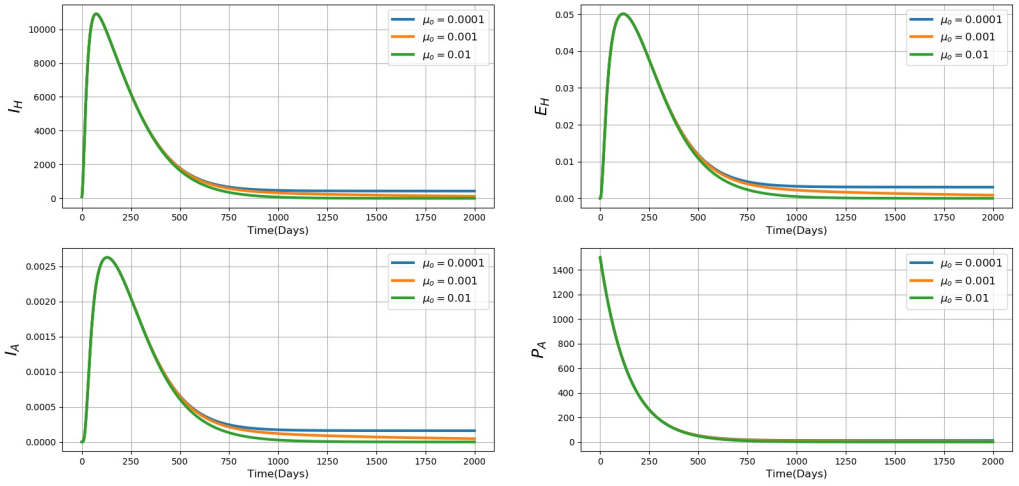

Figure 5.13: Simulations of model system (5.2.0.1) illustrating the effect of scalonchospheres death rate at the within-pig scale μ_o with $\mu_o = 0.0001$, $\mu_o = 0.001$, $\mu_o = 0.01$ on the between-host scale population dynamics of infected individuals (I_H), environmental pathogen (E_H), infected pig (I_A) and community pathogen load (P_A).

Figure 5.13 displays graphical representations of numerical solutions for the model system (5.2.0.1), illustrating changes in the populations of infected humans (I_H) and environmental pathogens (E_H), population of infected pigs (I_A) and population of community pathogen load for different values of natural decay rate of onchospheres in the within-pig scale across various levels of the natural decay rate of oncospheres within the pig-scale μ_o: $\mu_o = 0.0001$, $\mu_o = 0.001$, and $\mu_o = 0.01$. The results in Figure 5.13 show that an increase in α_o results in very minimal increases in between-host scale population dynamics of infected individuals (I_H), environmental pathogen (E_H), infected pig (I_A) and community pathogen load (P_A). These findings indicate that implementing control measures aimed at affecting the death rate of oncospheres within the pig scale would result in limited advantages for reducing parasite load within the pig population and addressing the burden of human taeniasis at the population/community level.

5.5.2 The influence of between-host scale on the within-host taeniasis disease dynamics

In this subsection, we examine how the parameters at the between-host scale, namely β_H, P_0, β_A, and E_0, impact the variables within the human scale (W_h, E_h) and within the pig scale (E_a, O_a)

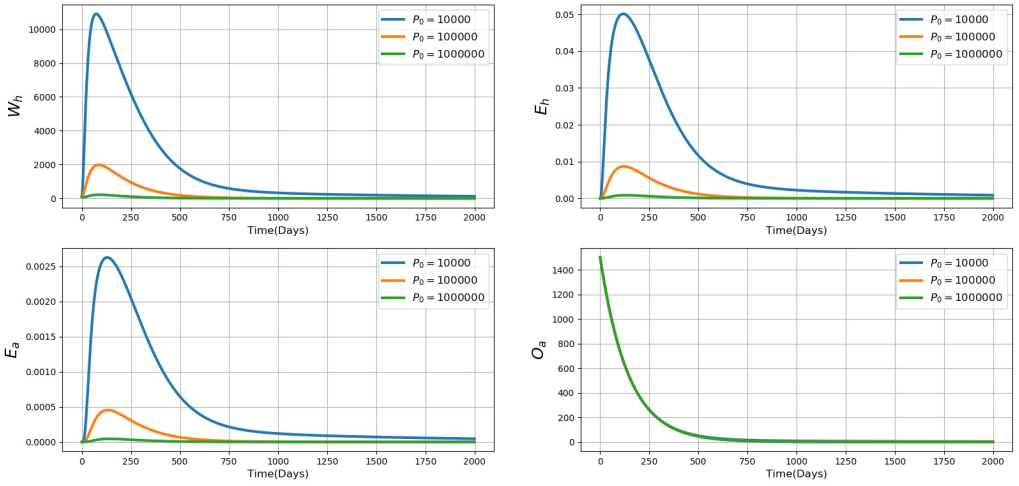

Figure 5.14: *Simulations of model system (5.2.0.1) showing the influence of half saturation constant associated with (P_0) on the within-humans scale variables (W_h, E_h) and within-pig scale variables (E_a, O_a).*

In Figure 5.14, we illustrate the outcomes resulting from changing the half-saturation constant linked to human infection P_0 using the values $P_0 = 10000$, $P_0 = 100000$, and $P_0 = 1000000$. Increasing P_0 is associated with the decrease in within-human scale variables (W_h, E_H) and within-pig scale variables (E_a, O_a). The findings indicate that as P_0 increases, there is a considerable decrease in the variables within the human scale and within-pig scale taeniasis intensity. Therefore, adequate distribution of vaccines in the population to reduce susceptibility of human to the disease will significantly reduce the infection intensity of the disease at an individual level.

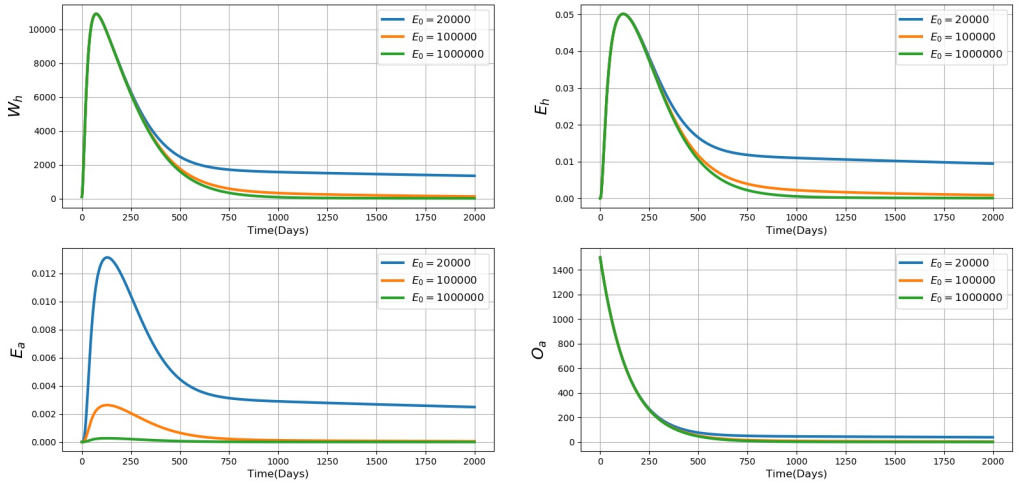

Figure 5.15: *Simulations of model system (5.2.0.1) showing the influence of half saturation constant associated with pig infection (E_0) on the within-host scale variables of within-human scale (W_h, E_h) and within-pig scale variables (E_a, O_a)*

.

In Figure 5.15, we present the consequences of the half-saturation constant linked to pig infection E_0 using the values $E_0 = 20000$, $E_0 = 100000$, and $E_0 = 1000000$. Increasing E_0 is associated with the decrease in within-human scale variables (W_h, E_H) and within-pig scale variables (E_a, O_a). The findings reveal that an increase in E_0 leads to a notable reduction in both the within-human scale and within-pig scale taeniasis intensity. Therefore, adequate distribution of vaccines in the population to reduce susceptibility of pigs to the disease will significantly reduce the infection intensity of the disease at an pig level.

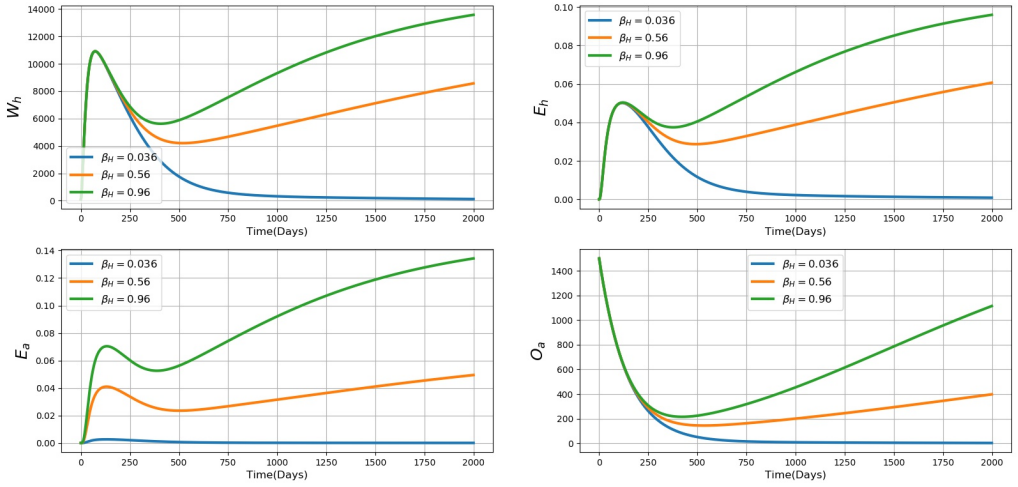

Figure 5.16: *Graph of numerical solutions of model system (5.2.0.1) showing the influence of between-host transmission rate parameter (β_H) on the within-host scale population dynamics of matured worms (W_h), eggs released by tapeworm in the human intestines (E_h), eggs within an pig (E_a), and onchosphers (O_a) for different values of β_H: β_H = 0.036, β_H = 0.56, and β_H = 0.96.*

Figure 5.16 illustrates graphs of numerical solution showing the variations in the within-human scale cycsticerci (C_h), the within-human scale eggs released by matured worm (E_h), ingested eggs in the within-pig scale (E_a), oncospheres (O_a) within-pig scale for different values of β_H: $\beta_H = 0.036$, $\beta_H = 0.56$, and $\beta_H = 0.96$. The outcomes presented in Figure 5.16 indicate that with an increase in β_H, there is a corresponding rise in the variables within the human scale (W_h,E_h) and within-pig scale variables (E_a,O_a). This implies that interventions that include improving pig husbandry thus avoiding free-roaming pig, enhanced meat inspection and improved meat product processing will effectively prevent humans from consuming contaminated food.

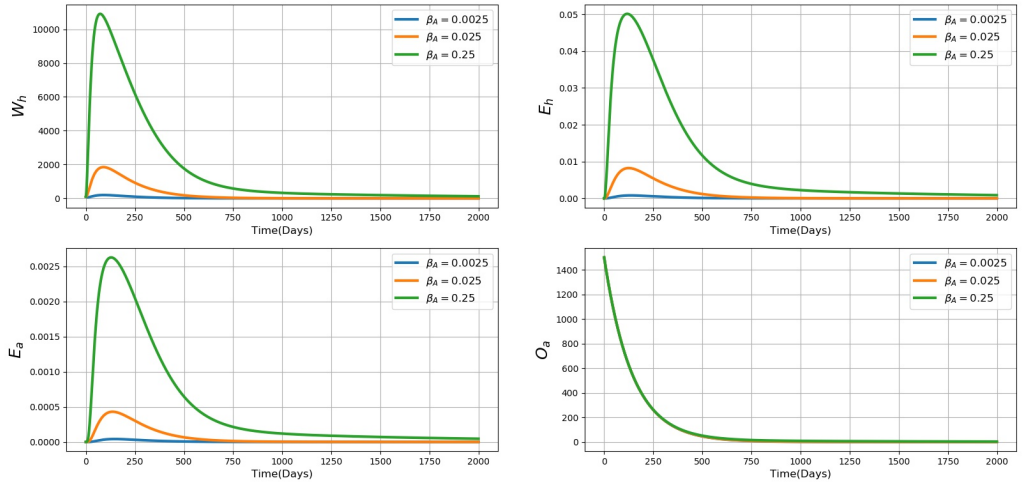

Figure 5.17: *Graph of numerical solutions of model system (5.2.0.1) showing the influence of between-host transmission rate parameter of pigs (β_A) on the within-host scale population dynamics of matured worms (W_h), eggs released by tapeworm in the human intestines (E_h), eggs within an pig (E_a), and onchosphers (O_a) for different values of β_A: β_H = 0.0025, β_H = 0.025, and β_H =0.25.*

Figure 5.17 illustrates graphs of numerical solution showing the variations in the within-human scale matured worms (W_h), the within-human pig eggs released by matured worm (E_h), ingested eggs in the within-pig scale (E_a), oncospheres (O_a) within-pig scale for different values of β_A: $\beta_A = 0.0025$, $\beta_A = 0.025$, and $\beta_A = 0.25$. The findings presented in Figure 5.17 demonstrate that as β_A increases, there is also an increase in the variables within the human scale (W_h,E_h) and within-pig scale variables (E_a,O_a). This suggests that interventions encompassing community health education, which addresses hygiene and food safety, along with enhanced sanitation practices and termination of open defecation, these will prevent pigs to feed on infected human faeces.

5.5.3 Discussion and conclusion

In this chapter, we formulated a multiscale model to represent a type I environmentally transmitted disease system within hosts, where there is no pathogen replication cycle at either the within-human host scale or the within-pig host scale. In the case of such type I foodborne diseases, the pathogen load within infected hosts (both human and pig hosts) can only increase through

super-infection, which refers to the occurrence of infection again before a host has fully recovered from a previous infection. We conducted a comprehensive mathematical analysis of the multiscale model, including considerations of the feasible region, the basic reproductive number, stability analyses for both the disease-free equilibrium and the endemic equilibrium. The basic reproductive number R_0 is defined based on a combination of parameters associated with interactions between hosts and factors within individual hosts. From the formulation of the reproductive number, it becomes clear that a component of it, represented by the pig-to-human transmission coefficient R_{0AH}, is comprised of disease parameters that operate between hosts and within pigs. Additionally, from the expression of the basic reproductive number, R_{0HA}, it is apparent that this value is influenced by a combination of parameters at both the within-host scale and the between-host scale. Furthermore, we can deduce that the expressions for endemic values at the between-host scale, such as S_H^*, I_H^*, E_H^*, S_A^*, I_A^*, and P_A^*, are influenced by both within-host disease parameters and between-host parameters. Conversely, the expressions for endemic values at the within-host scale, namely C_h^*, W_h^*, E_h^*, E_a^*, and O_a^*, are dependant on a combination of within-host scale and between-host scale parameters. As a result, the outcomes derived here emphasize a reciprocal interaction between the microscale and macroscale factors in the context of *T. solium* infection. We also conducted a sensitivity analysis to evaluate the parameters that exert the most significant influence on either increasing or decreasing the dynamics of taeniasis disease. From the numerical outcomes presented in Figures 5.4 to Figures 5.13, we observe that changes in the chosen within-host scale parameters (α_c, α_w, α_e, μ_c, μ_w, μ_e, α_a, α_o, μ_a, μ_o) lead to corresponding changes in the variables at the between-host scale (I_H, E_H, I_A, P_A). This confirms that throughout the progression of disease dynamics, the within-host scale plays a role in influencing the between-host scale for human taeniasis infection. We also noted that the variations observed in Figures 5.14 to Figure 5.17 of the selected between-host scale parameters (β_H, P_0, β_A, and E_0) correspond with changes in the four important selected within-host scale variables (W_h, E_h, E_a, and O_a). This validates that throughout the progression of disease dynamics, the between-host scale impacts the within-host scale for human taeniasis infection. To conclude, the outcomes substantiate that both the between-host scale and the within-host scale reciprocally influence each other during human taeniasis infection. The results of this study are useful for policymakers and members of the community in teanisis-endemic areas to use better strategies in improving disease management.

Chapter 6

Conclusion and Future Research Directions

In this study, we developed multiscale models of foodborne diseases caused by three different pathogens which are environmentally transmitted for describing and understanding the complex life cycle of foodborne pathogens considering the role of humans, plants, animals and the environment and their interconnectedness in sustaining the transmission of foodborne diseases. The multiscale models were developed with a main purpose of illustrating the reciprocal influence between microscale and macroscale for foodborne diseases based on replication-relativity theory. The three environmental transmitted pathogens considered in the study are *norovirus* which represent foodborne pathogens with replication-cycle at microscale only, *E. coli* O157:H7 which represent foodborne pathogens with replication-cycle at both macroscale and microscale and *tapeworm* which represent foodborne pathogens which do not replicate at both macroscale and microscale. Traditionally, foodborne diseases have been modelled based on transmission theory which considers transmission to be the primary cause of infectious disease spread at the macroscale. It is important to consider that disease dynamics is influenced by interaction between two scales where pathogen replication occurs microscale (within the host) and transmission occurs at macroscale (between-hosts). We started by developing a single-scale model that we progressively extend to develop the nested multiscale for *norovirus*. To be more specific:

Chapter 2, we formulated a single-scale model to represent the transmission dynamics of foodborne disease systems, focusing on viral infections in a general context. The model was developed following the transmission mechanism theory, which emphasizes single-scale modelling at each level of organization within an infectious disease system [20]. The specifics of the pathogen replication-transmission interactions are not clearly modeled in this single scale model. Instead, a single parameter serves as the sole phenomenological representation of pathogen proliferation [33]. By means of mathematical examination, the single-scale model has demonstrated robustness both in mathematical terms and from an epidemiological standpoint. Additionally, a sensitivity analysis was conducted to evaluate the model's two key disease transmission metrics, the basic reproduction number (R_0) and the endemic value of the environmental viral load (V_F^*), with respect to all model parameters. This analysis employed the Latin hypercube sampling scheme. In terms of numerical analysis and computational considerations, we introduced the NSFD (Non Standard Finite Difference) approach. Through numerical simulations, we demonstrated that our NSFD scheme maintains dynamic consistency concerning the essential properties of the continuous model, specifically positivity and equilibrium stability. In this chapter, we demonstrated that although the model analyses were simple, a significant limitation of the model was its depiction of the pathogen's replication dynamics within an infected host, which was characterized in a phenomenological manner which makes the model being unrealistic in predicting the dynamics of foodborne disease systems. We anticipated that this kind of limitation of single-scale models can be overcome by extending the single-scale model to a multiscale model.

In **Chapter 3**, we extended and modified the single-scale model for viral foodborne infection from **Chapter 2**. The primary goal of this chapter was to construct microscale and macroscale submodels and interconnect them to establish a nested multiscale model. The aim was to demonstrate that the microscale disease dynamics significantly influence the macroscale disease dynamics of norovirus infection. Given the extensive impact of human norovirus infections worldwide, there is an urgent need to devise strategies for prevention and treatment. In this chapter, we introduce a nested multiscale model for norovirus infection that combines microscale and macroscale submodels, allowing us to evaluate the impact of microscale disease dynamics on macroscale disease dynamics based on replication-relativity theory. The connection between the scales was usually established by relating the transmission rate at the macroscale to the pathogen load at the microscale [55]. Gaining insights into the replication cycle of norovirus and its interactions with cellular processes and innate immune responses is crucial for identifying molecular targets that can be utilized to manage human norovirus infections and mitigate the occurrence of outbreaks [123], because viruses develop strategies to counteract host immune responses in order to infect their hosts and replicate within them. We established a connection between the within-human

scale model and an epidemiological model by incorporating the within-human scale submodel's dynamics into the epidemiological framework. The results in this study reveals that within-human pathogen replication rate, the epithelial supply rate, the amount of pathogens produced through replication, pathogen shedding rate to the environment, immune system activation and within-host pathogen natural death rate have great influence on the transmission dynamics of norovirus infection. In particular, microscale parameters have shown to have great impact on macroscale variables through shedding or excretion processes. These parameters represent key targets for therapeutic and vaccine design since they show the impact on norovirus transmission. A research investigation indicated that regular immunization has the potential to decrease the occurrence of norovirus by as much as 70.5%, even if the vaccines do not offer full protection against the disease. The authors developed a dynamic, age-specific mathematical model of norovirus transmission and vaccination, utilizing available data, especially age-stratified time series case notification data. Their findings demonstrated that focusing on infants and toddlers is a more effective strategy for infection prevention [124]. Their findings demonstrate the effectiveness of the norovirus vaccine, with outcomes varying based on specific age groups. Our study suggests the development of a vaccine that induces the production of protective antibodies, the design of the vaccine should prioritize the engulfment of norovirus cells, thereby enhancing virus clearance and preventing viral replication at the site of infection. We emphasize the potential impact of vaccines at the individual level, with the goal of restricting replication and minimizing the shedding of norovirus into the environment. Our results concur with the sensitivity analysis results in [124], their findings revealed that the most critical vaccine attributes are the ability to clear infection and susceptibility. Additionally, they suggested that while reductions in infectiousness and symptoms also play a role, their impact is comparatively less significant. However, they differ with our results, because we concluded that infectiousness plays a big role in disease progresssion because we found that within-host scale is the scale that sustains the disease. Furthermore, their results emphasized that the primary advantages of vaccination would be individual-focused rather than through herd effects. We also offer insights into the sensitivity of our findings to model parameters, such as the vaccine mode, allowing us to underscore areas where further research is needed. Our results emphasize the importance of addressing within-host disease dynamics on par with between-host disease dynamics. This confirms that the microscale dynamics for any infection cannot be ignored in modelling of infectious disease. Considering that currently there is no vaccines or specific treatments available for *norovirus* infection, except palliative treatment, therefore the findings imply that the creation of drugs targeting the elimination and suppression of *norovirus* replication at the microscale could yield advantageous outcomes in mitigating the disease transmission risk among the human population at a broader level.

A new mathematical model for the transmission of norovirus on cruise ships, considering both direct and environmental transmission was developed. The findings suggest that isolating symptomatic passengers is not guaranteed to effectively control outbreaks. The study highlighted that direct person-to-person contact plays a major role in overall transmission. The conclusion suggests that implementing personal hygiene measures, like thorough handwashing, is a potentially effective strategy to reduce the probability of infection through contact with contaminated surfaces or individuals [125].

In **Chapter 4**, the key innovation in this study lies in the application of a nested multiscale model to clarify the connection between the within-host replication rate of *E. coli* O157:H7 and the between-host growth rate of *E. coli* O157:H7. Multiscale modelling offers a framework for incorporating within-host and between-host submodels, as both contribute to the transmission and control of foodborne pathogens. In this study, we have showcased the application of a nested multiscale model to illustrate a one-way connection from the within-host scale to the between-host scale. Specifically, the between-host scale is impacted by the within-host scale, whereas the within-host scale remains unaffected by influences from the between-host scale. We accomplish this by demonstrating that the within-host replication rate of *E. coli* O157:H7 influences the between-host growth rate of *E. coli* O157:H7, however the between-host pathogen growth rate does not have influence on between-host of *E. coli* O157:H7 growth rate. Based on our numerical analysis, we discover that the within-host replication can be regulated through vaccination. Vaccines exert biological effects at the individual level, aiming to either diminish the susceptibility of cattle to colonization by *E. coli* O157:H7 or reduce the duration of such colonization. For *E. coli* O157:H7 to be expelled, it must initially endure in the gastrointestinal tract of cattle. A vaccine capable of eliciting the production of antibodies against these virulence factors could hinder the organism's adherence, leading to its elimination from the gastrointestinal tract [126]. Our findings align with those of a study conducted by [127], where they employed a simulation model for *E. coli* O157:H7 infection in cattle to evaluate pre-slaughter intervention strategies. They concluded that vaccinating cattle against *E. coli* O157:H7 and employing substances to minimize fecal shedding of the organism held the most significant potential for reducing contamination of beef carcasses. The outcomes of this study are in agreement with the findings reported in [128]. Their findings revealed that in the progression of PTB infection in ruminants, once the infection has effectively established within the host, the impact of superinfection on the overall pathogen load at this scale becomes insignificant in comparison to the contribution of pathogen replication [128]. The multiscale model developed in this study offers novel perspectives on how the within-host pathogen replication rate contributes to the dynamics of environmental disease systems, where pathogens replicate at both the individual host and population levels. While the primary focus of this investigation was on *E. coli* O157:H7 in cattle, the multiscale modeling

framework employed is sufficiently broad and can be applied to provide guidance for the control and elimination of numerous other environmentally transmitted diseases that share a transmission mode similar to *E. coli* O157:H7.

In **Chapter 5** we have presented a coupled multiscale model of taeniasis infection, wherein no pathogen replication cycle occurs at either the individual human scale or the individual pig scale. In cases of such type I environmentally transmitted diseases, the volume of pathogens within the infected hosts (both human and pig hosts) can solely escalate through super-infection, denoting instances of recurring infection transpiring before the host has recuperated from the initial infectious episode. Multiscale models of this type include the actual burden of parasites across the distinct life stages within the parasite's life cycle, observed both at the microscale and macroscale, rather than only monitoring the number of afflicted hosts. This study demonstrates a diverse range of mass intervention strategies that can be employed to eradicate taenia/cysticercosis.

To assess the accuracy of the model, we examined the impact of the parameters at the individual level (cysticerci transition rate α_c, worm transition rate α_w, excretion rate of eggs α_e, natural death rate of cysticerciμ_c, natural death rate of a tapeworm μ_w, natural death rate of eggs μ_e) and within-pig scale parameters (eggs transition stage α_a, onchospheres shedding rate α_o, within-pig eggs natural death rate μ_a, onchospheres natural death rate μ_o) on four key between-host variables (Infected humans I_H, environmental eggs E_H, infected animals I_A, community pathogen load P_A). These specific parameters and variables were chosen as examples to highlight the impact of disease processes at the individual host level on the transmission dynamics of human taeniasis at the broader between-host scale. Our findings indicated that inhibiting the advancement of the three primary life stages of a parasite within the human host (cysticerci, adult worm, and eggs) can lead to the elimination of pig and human cysticercosis, as well as human taeniasis. However, our findings demonstrated that the parameters related to the two primary life stages at the within-pig scale are likely to provide minimal benefits in decreasing the parasite load at the pig scale and reducing the prevalence of human taeniasis at the broader population or community level. These results suggest that strategies targeting the eradication of tapeworm eggs at the within-pig scale will have minimal impact on both the parasite load and the overall pathogen burden within the community. Conversely, we investigated the influence of between-host scale parameters, specifically β_H, P_0, β_A, and E_0, on the variables within-human scale (W_h, E_h) and within-pig scale (E_a, O_a). Additionally, we observed that the changes identified in these specified between-host scale parameters align with fluctuations in the four essential within-host scale variables we selected.

This validates that throughout the progression of disease dynamics, the between-host scale impacts the within-host scale for human taeniasis infection and vice versa. For this reason our

coupled multiscale model suggest the development of vaccine that will effectively kill or restrict the cisterci within-human scale from growing to become an adult worm, or the vaccine that will kill the matured tapeworm within-human scale or hinder the tapeworm to release eggs or the vaccine that will kill the eggs at within-human scale. In terms of vaccine, our model supports the model developed in [46], their model is recommended for pig vacination to reduce infections caused by tapeworm, however, they concluded that if the vaccine efficacy is 100% but the coverage of pig vaccination is 82%, pig cysticercosis will be eliminated as predicted by herd immunity. [46], these results were also supported by other mathematical models with vaccine reported in the literature [129].

Most of the interventions that have been tested for T. solium to date have relied on the treatmentof the definitive hosts (humans) to remove tapeworm infections[130]. These interventions agree with our study because our study has revealed that strategies focused on addressing the initial life stages of the pathogen within the pig scale, the death rate of oncospheres within the pig scale and eliminating tapeworm eggs at the within-pig scale would result in limited effect for reducing parasite load within the pig population and hence little success on addressing the burden of human taeniasis at the population/community level. However, our results further find that implementing control measures focusing on the second life stage of the pathogen within the pig scale would be advantageous for decreasing parasite burden within the pig population and weakening human taeniasis at the broader human population/community level. Results in [46], further shown that implementing campaigns to inform the population in combination with the vaccination of pigs and chemotherapy to humans is the best strategy to combat taeniasis/cysticercosis in any country, even though it generates high costs in a short time, the health problems caused by the infection will be reduced and it will be eliminated. Another study has recommended that a combination of both vaccination/oxfendazole treatment of pigs together with anthelmintic treatment of the human population to eliminate the adult tapeworms, particularly when control procedures were first implemented, would have the greatest and most rapid impact on reducing the incidence of neurocysticercosis [44, 131, 132]. Given that multiscale modelling allows the examination of the disease at the scale of infection occurrence, our research demonstrated that gaining insights into the life stages of the tapeworm at both within-human and within-pig scales can result in substantial cost reduction. This is because interventions can be targeted specifically at a particular life stage in both hosts. Our study carried on to assess the influence of between-host scale disease dynamics on within-human and within-pig scales disease dynamics. The findings indicate that as half saturation constant associated with humans infection P_0 and pigs E_0 increases respectively, there is a considerable decrease in the variables within the human scale and within-pig scale taeniasis intensity. Therefore, adequate distribution of vaccines at the population to reduce susceptibility of human and pigs to the disease will significantly reduce the infection intensity

of the disease at an individual level. Further, our results suggest that with an increase in human infection β_H and pig infection β_A respectively, there is a corresponding rise on the within-human scale and within-pig scale variables. This implies that interventions that include improving pig husbandry thus avoiding free-roaming pig, enhanced meat inspection and improved meat product processing will effectively prevent humans from consuming contaminated food, and suggests also that interventions encompassing community health education, which addresses hygiene and food safety, along with enhanced sanitation practices and termination of open defecation, will prevent pigs to feed on infected human faeces.

Based on the numerical outcomes, the multiscale model addressing human taeniasis highlights several potential intervention points that are appropriate for testing strategies aimed at managing the proliferation of this foodborne illness. The control measures can be categorized into two groups: those focusing on the animal host to manage susceptible pigs, S_A (possibly involving animal population control or decreasing parasite load within the animal host scale), and those concentrating on the human host to modify susceptible humans, S_H (likely involving regulating human-animal contact or reducing parasite load across different life stages within the human host scale). In general, the outcomes of this investigation affirm the bidirectional impact between public health interventions aimed at curtailing human taeniasis within communities and populations (on a macroscale) on one side, and medical interventions intended to address individual well-being and disease treatment (on a microscale) on the other. These findings emphasise the significant medical and public health implications that need to be taken into account during the planning stages for controlling and eradicating human taeniasis. Our model allowed us to assess the impact of combined human-pig intervention upon the infection of T. solium in humans and human cysticercosis. The application of the model is not restricted to a community or a country. It can be applied worldwide but not with a single strategy. Our model has the potential for designing optimal strategies to achieve the control, reduction, or to eliminate the infection. Multiscale modelling can be used to study or characterize an infectious disease system at more than one scale, thus studying disease through consideration of different scales can improve the predictions used to inform public health strategies, by adding patient-specific dynamics to population-level pathogen spread and it can save costs since interupting one or all the main stages at within-human scale can reduce these infections greatly. To sum up the findings from the three multiscale models created within this study, it becomes obvious that the two disease transmission metrics, namely, the basic reproductive number R_0 and the points of endemicity are influenced by a combination of disease parameters at the within-host scale and parameters governing interactions between hosts at the between-host scale. Nevertheless, as is the case with any

model development, our multiscale models have their limitations. The limitations of the multiscale modeling framework outlined in this study involve the omission of recovery, rendering the models unrealistic by implying that an individuals infected remains infectious until death. While we acknowledge individual variations in infection response, our multiscale models assumes homogeneity. Additionally, the models do not account for the impact of infection control measures. Furthermore, the reliability of the model studied here, depends on their validation against empirical data and ability to accurately represent the dynamics of the system designed to model. However, the multiscale models empirical data is scarce to validate the models. The models are more of theoretical approach because they aimed at laying a foundation on the use of multiscale modelling of foodborne diseases.

The primary contributions of this study to scientific understanding are as follows:

(i) Introduction and utilization of a nested multiscale model to demonstrate that the disease dynamics at the microscale level exert an impact on the macroscale level for environmentally transmitted foodborne pathogens that undergo replication only at the microscale, (ii) Creation and application of a nested multiscale model to establish a correlation between the replication rate of pathogens at the microscale and the growth rate of environmental pathogens for environmentally transmitted foodborne pathogens that replicate at both the microscale and macroscale, (iii) the use of a coupled multiscale model to illustrate how the dynamics within a host influence the dynamics between hosts in the context of human taeniasis, and vice versa, for pathogens that do not undergo replication at either scale, and development of the NSFD scheme as a means to demonstrate both positivity and stability for the proposed multiscale models.

6.1 Future Research Directions

As the primary objective of this research was only the creation of nested and interconnected multiscale models for evaluating the mutual impact between microscale and macroscale factors concerning environmentally transmitted foodborne diseases, for future research directions the following aspects can be taken into consideration:

1. The multiscale model for environmentally transmitted foodborne diseases can be extended by explicitly incorporating age because all ages affected including children under the age of 5 years who account for almost one third of the deaths from foodborne diseases.

2. Temperature is commonly regarded as the predominant factor influencing the rate of development in free-living pathogens, and it is therefore anticipated that temperature will have

an impact on the possibility that hosts would be exposed to a pathogen dose large enough to result in infection [133].

3. Regarding the coupled multiscale model, we will create an NSFD scheme, known for its efficiency compared to the well known numerical techniques. This scheme ensures both solution positivity and numerical stability across broader domains.

4. It is imperative to consider cost effectiveness when designing and implementing foodborne diseases interventions. The two nested multiscale models may be extended by incorporating cost effectiveness.

Bibliography

[1] S.M. Pires, B.N. Desta, L. Mughini-Gras, B.T. Mmbaga, O.E. Fayemi, E.M Salvador, T. Gobena, S.E Majowicz, T. Hald, and P.S. Hoejskov. Burden of foodborne diseases: Think global, act local. *Current Opinion In Food Science*, 39:152–159, 2021.

[2] D. Subedi, S. Subedi, A. Gautam, S. Bhandari, and M. Kandel. Cysticercosis in nepal: A review. *Nepalese Veterinary Journal*, 37(1):148–162, 2020.

[3] M. El Fatini, A. Lahrouz, R. Pettersson, A. Settati, and R. Taki. Stochastic stability and instability of an epidemic model with relapse. *Applied Mathematics and Computation*, 316:326–341, 2018.

[4] A.W. Taylor, D.M. Blau, Q. Bassat, D. Onyango, K.L. Kotloff, S. El Arifeen, I. Mandomando, R. Chawana, V.L. Baillie, and V. Akelo. Initial findings from a novel population-based child mortality surveillance approach: a descriptive study. *The Lancet Global Health*, 8(7):e909–e919, 2020.

[5] M.Y Li. *An introduction to mathematical modeling of infectious diseases*, volume 2. Springer, 2018, Cham.

[6] V.O. Ezenwa, A.H. Prieur-Richard, B. Roche, X. Bailly, P. Becquart, G.E. Garcia-Pena, P.R. Hosseini, F. Keesing, A. Rizzoli, and G. Suzan. Interdisciplinarity and infectious diseases: an ebola case study. *PLoS Pathogens*, 11(8):e1004992, 2015.

[7] N.I. Nii-Trebi. Emerging and neglected infectious diseases: insights, advances, and challenges. *BioMed Research International*, 2017, 2017.

[8] D.M. Morens and A.S. Fauci. Emerging infectious diseases: threats to human health and global stability. *PLoS Pathogens*, 9(7):e1003467, 2013.

[9] M.W Borgdorff and D. Van Soolingen. The re-emergence of tuberculosis: what have we learnt from molecular epidemiology? *Clinical Microbiology and Infection*, 19(10): 889–901, 2013.

[10] WHO et al. Antimicrobial resistance global report on surveillance: 2014 summary. Technical report, World Health Organization, 2014.

[11] R.P. Singh, M. Javaid, A. Haleem, R. Vaishya, and S. Bahl. Significance of health information technology (hit) in context to covid-19 pandemic: Potential roles and challenges. *Journal of Industrial Integration and Management*, 5(04):427–440, 2020.

[12] S. Enayati and O.Y Özaltın. Optimal influenza vaccine distribution with equity. *European Journal of Operational Research*, 283(2):714–725, 2020.

[13] R. Netshikweta and W. Garira. A multiscale model for the world's first parasitic disease targeted for eradication: guinea worm disease. *Computational and Mathematical Methods in Medicine*, 2017, 2017.

[14] C.C Adley and M.P Ryan. The nature and extent of foodborne disease. In *Antimicrobial Food Packaging*, pages 1–10. Elsevier, 2016.

[15] J. Perumal, Y. Wang, A.B.E. Attia, U.S Dinish, and M. Olivo. Towards a point-of-care sers sensor for biomedical and agri-food analysis applications: A review of recent advancements. *Nanoscale*, 13(2):553–580, 2021.

[16] A.G. Taiwo. Prevalence and antibiogram of pathogenic foodborne escherichia coli and salmonella spp. in developing african countries. *Foodborne Pathogens and Antibiotic Resistance*, pages 431–439, 2016.

[17] A. Chlebicz and K. Śliżewska. Campylobacteriosis, salmonellosis, yersiniosis, and listeriosis as zoonotic foodborne diseases: a review. *International Journal of Environmental Research and Public health*, 15(5):863, 2018.

[18] P.A. de Jonge, F.L. Nobrega, S.J.J. Brouns, and B. Dutilh. Molecular and evolutionary determinants of bacteriophage host range. *Trends in Microbiology*, 27(1):51–63, 2019.

[19] S. Patterson and B. Jones. *Bioequivalence and statistics in clinical pharmacology*. Chapman and Hall/CRC, 2017, New York.

[20] W. Garira. The replication-transmission relativity theory for multiscale modelling of infectious disease systems. *Scientific Reports*, 9(1):1–17, 2019.

[21] F. Pappalardo, G. Russo, F.M. Tshinanu, and M. Viceconti. In silico clinical trials: concepts and early adoptions. *Briefings in Bioinformatics*, 20(5):1699–1708, 2019.

[22] W. Garira. A complete categorization of multiscale models of infectious disease systems. *Journal of Biological Dynamics*, 11(1):378–435, 2017.

[23] W. Garira, D. Mathebula, and R. Netshikweta. A mathematical modelling framework for linked within-host and between-host dynamics for infections with free-living pathogens in the environment. *Mathematical Biosciences*, 256:58–78, 2014.

[24] W. Garira and D. Mathebula. A coupled multiscale model to guide malaria control and elimination. *Journal of Theoretical Biology*, 475:34–59, 2019.

[25] W. Garira. The research and development process for multiscale models of infectious disease systems. *PLoS Computational Biology*, 16(4):e1007734, 2020.

[26] T. Bintsis. Foodborne pathogens. *AIMS microbiology*, 3(3):529, 2017.

[27] K.K. Shah, B.S. Pritt, and M.P Alexander. Histopathologic review of granulomatous inflammation. *Journal of Clinical Tuberculosis and other Mycobacterial Diseases*, 7:1–12, 2017.

[28] A.B. Pigozzo, G.C. Macedo, R. Weber dos Santos, and M. Lobosco. Computational modeling of microabscess formation. *Computational and Mathematical Methods in Medicine*, 2012, 2012.

[29] K.A. Pawelek, S. Liu, and M.U Lolla. Modeling the spread of hookworm disease and assessing chemotherapy programs: mathematical analysis and comparison with surveillance data. *Journal of Biological Systems*, 24(01):167–191, 2016.

[30] G. Magombedze, C.N. Ngonghala, and C. Lanzas. Evalution of the "iceberg phenomenon" in johne's disease through mathematical modelling. *PloS One*, 8(10):e76636, 2013.

[31] I.H. Spicknall, J.S. Koopman, M. Nicas, J.M. Pujol, S. Li, and J.N.S Eisenberg. Informing optimal environmental influenza interventions: how the host, agent, and environment alter dominant routes of transmission. *PLoS Computational Biology*, 6(10):e1000969, 2010.

[32] C.B. Beggs, C.J. Noakes, P.A. Sleigh, L.A. Fletcher, and K. Siddiqi. The transmission of tuberculosis in confined spaces: an analytical review of alternative epidemiological models. *The International Journal of Tuberculosis and Lung Disease*, 7(11):1015–1026, 2003.

[33] W. Garira and B. Maregere. The transmission mechanism theory of disease dynamics: Its aims, assumptions and limitations. *Infectious Disease Modelling*, 8(1):122–144, 2023.

[34] Constantinos I Siettos and Lucia Russo. Mathematical modeling of infectious disease dynamics. *Virulence*, 4(4):295–306, 2013.

[35] L. Alfaro, A. Chari, A.N. Greenland, and P.K. Schott. Aggregate and firm-level stock returns during pandemics, in real time. Technical report, National Bureau of Economic Research, 2020.

[36] J.A. Souza-Neto, J.R. Powell, and M. Bonizzoni. Aedes aegypti vector competence studies: A review. *Infection, Genetics and Evolution*, 67:191–209, 2019.

[37] S. Narison and S. Maltezos. Scrutinizing the spread of covid-19 in madagascar. *Infection, Genetics and Evolution*, 87:104668, 2021.

[38] E.A. Mordecai, J.M Caldwell, M.K Grossman, C.A. Lippi, L.R Johnson, M. Neira, J.R. Rohr, S.J. Ryan, V. Savage, M.S. Shocket, et al. Thermal biology of mosquito-borne disease. *Ecology Letters*, 22(10):1690–1708, 2019.

[39] P. Ayscue, C. Lanzas, R Ivanek, and Y.T Gröhn. Modeling on-farm escherichia coli o157: H7 population dynamics. *Foodborne Pathogens and Disease*, 6(4):461–470, 2009.

[40] S. Widgren, S. Engblom, U. Emanuelson, and A. Lindberg. Spatio-temporal modelling of verotoxigenic escherichia coli o157 in cattle in sweden: exploring options for control. *Veterinary Research*, 49(1):1–13, 2018.

[41] J. Vanderpas, J. Louis, M. Reynders, G. Mascart, and O. Vandenberg. Mathematical model for the control of nosocomial norovirus. *Journal of Hospital Infection*, 71(3):214–222, 2009.

[42] Sarah M Bartsch, Susan S Huang, Kim F Wong, Taliser R Avery, and Bruce Y Lee. The spread and control of norovirus outbreaks among hospitals in a region: a simulation model. In *Open forum infectious diseases*, volume 1, page ofu030. Oxford University Press, 2014.

[43] Bruce Y Lee, Zachary S Wettstein, Sarah M McGlone, Rachel R Bailey, Craig A Umscheid, Kenneth J Smith, and Robert R Muder. Economic value of norovirus outbreak control measures in healthcare settings. *Clinical microbiology and infection*, 17(4):640–646, 2011.

[44] M.V. José, J.R. Bobadilla, N.Y. Sánchez-Torres, and J.P. Laclette. Mathematical model of the life cycle of taenia-cysticercosis: transmission dynamics and chemotherapy (part 1). *Theoretical Biology and Medical Modelling*, 15(1):1–19, 2018.

[45] J.A. Mwasunda, J.I. Irunde, D. Kajunguri, and D. Kuznetsov. Modeling and analysis of taeniasis and cysticercosis transmission dynamics in humans, pigs and cattle. *Advances in Difference Equations*, 2021(1):1–23, 2021.

[46] N.Y. Sánchez-Torres, J.R. Bobadilla, J.P. Laclette, and M.V. José. How to eliminate taeniasis/cysticercosis: porcine vaccination and human chemotherapy (part 2). *Theoretical Biology and Medical Modelling*, 16(1):1–14, 2019.

[47] M.Z. Ndii, D. Tambaru, and B.S. Djahi. A nonstandard finite difference scheme for water-related disease mathematical model. *Appl Math Inf Sci*, 13(4):545–551, 2019.

[48] T. Berge, J.M.S. Lubuma, G.M. Moremedi, N. Morris, and R. Kondera-Shava. A simple mathematical model for ebola in africa. *Journal of Biological Dynamics*, 11(1):42–74, 2017.

[49] S. Treibert, H. Brunner, and M. Ehrhardt. A nonstandard finite difference scheme for the svicdr model to predict covid-19 dynamics. *Math. Biosci. Eng*, 19(2):1213–1238, 2022.

[50] R.B. Garabed, A. Jolles, W. Garira, C. Lanzas, J. Gutierrez, and G. Rempala. Multi-scale dynamics of infectious diseases, 2020.

[51] Andreas Handel and Pejman Rohani. Crossing the scale from within-host infection dynamics to between-host transmission fitness: a discussion of current assumptions and knowledge. *Philosophical Transactions of the Royal Society B: Biological Sciences*, 370 (1675):20140302, 2015.

[52] Christoforos Hadjichrysanthou, Emilie Cauët, Emma Lawrence, Carolin Vegvari, Frank De Wolf, and Roy M Anderson. Understanding the within-host dynamics of influenza a virus: from theory to clinical implications. *Journal of The Royal Society Interface*, 13 (119):20160289, 2016.

[53] Hayriye Gulbudak and Cameron J Browne. Infection severity across scales in multi-strain immuno-epidemiological dengue model structured by host antibody level. *Journal of mathematical biology*, 80:1803–1843, 2020.

[54] Sebastian J Schreiber, Ruian Ke, Claude Loverdo, Miran Park, Prianna Ahsan, and James O Lloyd-Smith. Cross-scale dynamics and the evolutionary emergence of infectious diseases. *Virus evolution*, 7(1):veaa105, 2021.

[55] James WG Doran, Robin N Thompson, Christian A Yates, and Ruth Bowness. Mathematical methods for scaling from within-host to population-scale in infectious disease systems. *Epidemics*, page 100724, 2023.

[56] Dephney Mathebula. *Multi-Scale Modelling of Vector-Borne Diseases*. PhD thesis, 2018.

[57] Mathieu Legros and Sebastian Bonhoeffer. A combined within-host and between-hosts modelling framework for the evolution of resistance to antimalarial drugs. *Journal of the Royal Society Interface*, 13(117):20160148, 2016.

[58] Jessica L Hite and Clayton E Cressler. Resource-driven changes to host population stability alter the evolution of virulence and transmission. *Philosophical Transactions of the Royal Society B: Biological Sciences*, 373(1745):20170087, 2018.

[59] Folashade B Agusto, MCA Leite, and Maria E Orive. The transmission dynamics of a within-and between-hosts malaria model. *Ecological Complexity*, 38:31–55, 2019.

[60] Francesco Bosia. The influence of viral within-host evolution on transmission chain reconstruction: a simulation study. Master's thesis, ETH Zurich, 2017.

[61] K.F. Gurski. A simple construction of nonstandard finite-difference schemes for small nonlinear systems applied to sir models. *Computers & Mathematics with Applications*, 66 (11):2165–2177, 2013.

[62] A. Suryanto and I. Darti. On the nonstandard numerical discretization of sir epidemic model with a saturated incidence rate and vaccination. *AIMS Math*, 6:141–155, 2021.

[63] A.M. Niewiadomska, B. Jayabalasingham, J.C. Seidman, L. Willem, B. Grenfell, D. Spiro, and C. Viboud. Population-level mathematical modeling of antimicrobial resistance: a systematic review. *BMC Medicine*, 17(1):1–20, 2019.

[64] G. Di Cola, A.C. Fantilli, M.B. Pisano, and V.E. Ré. Foodborne transmission of hepatitis a and hepatitis e viruses: A literature review. *International Journal of Food Microbiology*, 338:108986, 2021.

[65] H. Liu, W. Zhu, Y. Cao, J. Gao, T. Jin, N. Qin, and X. Xia. Punicalagin inhibits biofilm formation and virulence gene expression of vibrio parahaemolyticus. *Food Control*, 139: 109045, 2022.

[66] J. Bhardwaj, S. Hong, J. Jang, C. Han, J. Lee, and J. Jang. Recent advancements in the measurement of pathogenic airborne viruses. *Journal of Hazardous Materials*, 420: 126574, 2021.

[67] R. Netshikweta et al. *Multiscale Modelling of Environmentally Transmitted Infectious Diseases*. PhD thesis, 2021.

[68] H.W. Hethcote. The mathematics of infectious diseases. *SIAM Rev.*, 42(4):599–653, 2000.

[69] C. Castillo, Z. Feng, and W. Huang. On the computation of r0 and its role on global stability. *Mathematical Approaches for Emerging and Reemerging Infectious Disease: An Introduction*, 125:229–250, 2003.

[70] P. Van den Driessche and J. Watmough. Reproduction numbers and sub-threshold endemic equilibria for compartmental models of disease transmission. *Mathematical Biosciences*, 180(1-2):29–48, 2002.

[71] R. Mahardika, Widowati, and Y.D. Sumanto. Routh-hurwitz criterion and bifurcation method for stability analysis of tuberculosis transmission model. In *Journal of Physics: Conference Series*, volume 1217, page 012056. IOP Publishing, 2019.

[72] R. Netshikweta and W. Garira. A nested multiscale model to study paratuberculosis in ruminants. *Frontiers in Applied Mathematics and Statistics*, 8:817060, 2022.

[73] C. Keidies and W. Mathis. Application of center manifolds to oscillator analysis. In *Proc. 12th European Conf. on Circuit Theory and Design (ECCTD'95), Istanbul, Türkei*, volume 1, pages 447–450, 1995.

[74] C. Vargas-De-León. On the global stability of infectious diseases models with relapse. *Abstraction and Application Magazine*, 9, 2014.

[75] A.D. Polyanin and V.F. Zaitsev. *Handbook of ordinary differential equations: exact solutions, methods, and problems*. CRC Press, 2017.

[76] N.H. Sweilam, I.A. Soliman, and S.M. Al-Mekhlafi. Nonstandard finite difference method for solving the multi-strain tb model. *Journal of the Egyptian Mathematical Society*, 25 (2):129–138, 2017.

[77] K.C. Patidar. Nonstandard finite difference methods: recent trends and further developments. *Journal of Difference Equations and Applications*, 22(6):817–849, 2016.

[78] N.H. Sweilam, S.M. Al-Mekhlafi, A.O. Albalawi, and J.A.T. Machado. Optimal control of variable-order fractional model for delay cancer treatments. *Applied Mathematical Modelling*, 89:1557–1574, 2021.

[79] M.O. Milbrath, I.H. Spicknall, J.L. Zelner, C.L. Moe, and J.N.S. Eisenberg. Heterogeneity in norovirus shedding duration affects community risk. *Epidemiology & Infection*, 141(8): 1572–1584, 2013.

[80] H. Namawejje, L.S Luboobi, D. Kuznetsov, and E. Wobudeya. Mathematical model for the effects of treatment and vaccination controls on the dynamics of rotavirus disease with reference to uganda. *J. Math. Comput. Sci.*, 4(5):958–991, 2014.

[81] W. Garira and D. Mathebula. Development and application of multiscale models of acute viral infections in intervention research. *Mathematical Methods in the Applied Sciences*, 43(6):3280–3306, 2020.

[82] K. Bányai, M.K. Estes, V. Martella, and U.D. Parashar. Viral gastroenteritis. *The Lancet*, 392(10142):175–186, 2018.

[83] P. Chhabra, M. de Graaf, G.I. Parra, M.C. Chan, K. Green, V. Martella, Q. Wang, P.A. White, K. Katayama, H. Vennema, et al. Updated classification of norovirus genogroups and genotypes. *The Journal of General Virology*, 100(10):1393, 2019.

[84] L.A. Ford-Siltz, K. Tohma, and G.I. Parra. Understanding the relationship between norovirus diversity and immunity. *Gut Microbes*, 13(1):1900994, 2021.

[85] A. Nilghaz, S.M. Mousavi, M. Li, J. Tian, R. Cao, and X. Wang. based microfluidics for food safety and quality analysis. *Trends in Food Science & Technology*, 118:273–284, 2021.

[86] L.F. Barrett. *How emotions are made: The secret life of the brain*. Pan Macmillan, 2017.

[87] C. McCall, H. Wu, B. Miyani, and I. Xagoraraki. Identification of multiple potential viral diseases in a large urban center using wastewater surveillance. *Water Research*, 184: 116160, 2020.

[88] W. Garira. A primer on multiscale modelling of infectious disease systems. *Infectious Disease Modelling.*, 3:176–191, 2018.

[89] C. Chavez, Z. Feng, and W. Huang. On the computation of r0 and its role on global stability. *Mathematical Approaches for Emerging and Re-emerging Infection Diseases: An Introduction*, 125:31–65, 2002.

[90] C. Castillo-Chavez, Z. Feng, and W. Huang. *"On the computation Ro and its stability,"In: Mathematical Approaches for Emerging and Reemerging Infectious Diseases: An Introduction, IMA*, volume Vol. 125 of *229-250.* Springer - Velgar, 2002.

[91] R. Sameni. Mathematical modeling of epidemic diseases; a case study of the covid-19 coronavirus. *arXiv preprint arXiv:2003.11371*, 2020.

[92] J. Reyes-Silveyra and A.R. Mikler. Modeling immune response and its effect on infectious disease outbreak dynamics. *Theoretical Biology and Medical Modelling*, 13:1–21, 2016.

[93] S. Kumar, B. Panna, and R.K. Jha. Medical image encryption using fractional discrete cosine transform with chaotic function. *Medical & Biological Engineering & Computing*, 57:2517–2533, 2019.

[94] F. Battiston, G. Cencetti, I. Iacopini, V. Latora, M. Lucas, A. Patania, J.G Young, and G Petri. Networks beyond pairwise interactions: structure and dynamics. *Physics Reports*, 874:1–92, 2020.

[95] G. Russo, P. Reche, M. Pennisi, and F. Pappalardo. The combination of artificial intelligence and systems biology for intelligent vaccine design. *Expert Opinion on Drug Discovery*, 15(11):1267–1281, 2020.

[96] WHO et al. World health statistics overview 2019: monitoring health for the sdgs, sustainable development goals. Technical report, World Health Organization, 2019.

[97] D.M. Lin, B. Koskella, and H.C. Lin. Phage therapy: An alternative to antibiotics in the age of multi-drug resistance. *World Journal of Gastrointestinal Pharmacology and Therapeutics*, 8(3):162, 2017.

[98] U. Hofer. The cost of antimicrobial resistance. *Nature Reviews Microbiology*, 17(1):3–3, 2019.

[99] A. Brauner, O. Fridman, O. Gefen, and N.Q. Balaban. Distinguishing between resistance, tolerance and persistence to antibiotic treatment. *Nature Reviews Microbiology*, 14(5): 320–330, 2016.

[100] Economics & Policy Center for Disease Dynamics. Access barriers to antibiotics, 2019.

[101] Samiran Banerjee and Marcel GA van der Heijden. Soil microbiomes and one health. *Nature Reviews Microbiology*, 21(1):6–20, 2023.

[102] A. Maciel-Guerra, M. Baker, Y. Hu, W. Wang, X. Zhang, J. Rong, Y. Zhang, J. Zhang, J. Kaler, D. Renney, et al. Dissecting microbial communities and resistomes for interconnected humans, soil, and livestock. *The ISME Journal*, 17(1):21–35, 2023.

[103] Z. Haiwen, H. Rui, Z. Bingxi, G. Qingfeng, Z. Jifeng, W. Xuemei, and W. Beibei. Oral administration of bovine lactoferrin-derived lactoferricin (lfcin) b could attenuate enterohemorrhagic escherichia coli o157: H7 induced intestinal disease through improving intestinal barrier function and microbiota. *Journal of Agricultural and Food Chemistry*, 67 (14):3932–3945, 2019.

[104] R. Das, P. Palit, M.D.A. Haque, T. Ahmed, and A.S.G Faruque. Association between pathogenic variants of diarrheagenic escherichia coli and growth in children under 5 years of age in the global enteric multicenter study. *The American Journal of Tropical Medicine and Hygiene*, 1(aop), 2022.

[105] O.O. Alegbeleye, I. Singleton, and A.S. Sant'Ana. Sources and contamination routes of microbial pathogens to fresh produce during field cultivation: A review. *Food Microbiology*, 73:177–208, 2018.

[106] C.C. Conrad, K. Stanford, C. Narvaez-Bravo, T. Callaway, and T. McAllister. Farm fairs and petting zoos: a review of animal contact as a source of zoonotic enteric disease. *Foodborne Pathogens and Disease*, 14(2):59–73, 2017.

[107] N.A. Jarvis, C.A. O'Bryan, T.M. Dawoud, S.H. Park, Y.M. Kwon, P.G Crandall, and S.C. Ricke. An overview of salmonella thermal destruction during food processing and preparation. *Food Control*, 68:280–290, 2016.

[108] J.T. LeJeune, T.E. Besser, N.L. Merrill, D.H. Rice, and D.D. Hancock. Livestock drinking water microbiology and the factors influencing the quality of drinking water offered to cattle. *Journal of Dairy Science*, 84(8):1856–1862, 2001.

[109] C. Roth. Modeling immune response to bacterial infection. *The Journal of Undergraduate Research*, 5(1):9, 2007.

[110] S. Stević, B. Iričanin, and Z. Šmarda. On a product-type system of difference equations of second order solvable in closed form. *Journal of Inequalities and Applications*, 2015: 1–15, 2015.

[111] J. Firth, N. Siddiqi, A.I. Koyanagi, D. Siskind, S. Rosenbaum, C. Galletly, S. Allan, C. Caneo, R. Carney, A.F. Carvalho, et al. The lancet psychiatry commission: a blueprint for protecting physical health in people with mental illness. *The Lancet Psychiatry*, 6(8): 675–712, 2019.

[112] P. Winskill, W.E. Harrison, M.D. French, M.A. Dixon, B. Abela-Ridder, and M. Basáñez. Assessing the impact of intervention strategies against taenia solium cysticercosis using the epicyst transmission model. *Parasites & Vectors*, 10:1–14, 2017.

[113] N. Bellomo, R. Bingham, M.A.J. Chaplain, G. Dosi, G. Forni, D.A. Knopoff, J. Lowengrub, R. Twarock, and M.E. Virgillito. A multiscale model of virus pandemic: Heterogeneous interactive entities in a globally connected world. *Mathematical Models and Methods in Applied Sciences*, 30(08):1591–1651, 2020.

[114] O.H. Del Brutto, T.E. Nash, A.C. White Jr, V. Rajshekhar, P.P. Wilkins, G. Singh, C.M. Vasquez, P. Salgado, R.H. Gilman, and H.H. Garcia. Revised diagnostic criteria for neurocysticercosis. *Journal of the Neurological Sciences*, 372:202–210, 2017.

[115] A. Ito and C.M. Budke. Focus: Zoonotic disease: Genetic diversity of taenia solium and its relation to clinical presentation of cysticercosis. *The Yale Journal of Biology and Medicine*, 94(2):343, 2021.

[116] A.C. White Jr, C.M. Coyle, V. Rajshekhar, G. Singh, W.A. Hauser, A. Mohanty, H.H. Garcia, and T.E. Nash. Diagnosis and treatment of neurocysticercosis: 2017 clinical practice guidelines by the infectious diseases society of america (idsa) and the american society of tropical medicine and hygiene (astmh). *Clinical Infectious Diseases*, 66(8):e49–e75, 2018.

[117] W. Garira and F. Chirove. A general method for multiscale modelling of vector-borne disease systems. *Interface Focus*, 10(1):20190047, 2020.

[118] L. Wu, B. Song, W. Du, and Jie Lou. Mathematical modelling and control of echinococcus in qinghai province, china. *Math. Biosci. Eng*, 10(2):425–444, 2013.

[119] M.A. Dixon, U.C. Braae, P. Winskill, M. Walker, B. Devleesschauwer, S. Gabriel, and M.G. Basanez. Strategies for tackling taenia solium taeniosis/cysticercosis: A systematic review and comparison of transmission models, including an assessment of the wider taeniidae family transmission models. *PLoS Neglected Tropical Diseases*, 13(4): e0007301, 2019.

[120] V. Dermauw, P. Dorny, U.C. Braae, B Devleesschauwer, L.J. Robertson, A Saratsis, and L.F Thomas. Epidemiology of taenia saginata taeniosis/cysticercosis: a systematic review of the distribution in southern and eastern africa. *Parasites & Vectors*, 11(1):1–12, 2018.

[121] M. Coral-Almeida, S. Gabriël, E.N Abatih, N. Praet, W. Benitez, and P. Dorny. Taenia solium human cysticercosis: a systematic review of sero-epidemiological data from endemic zones around the world. *PLoS Neglected Tropical Diseases*, 9(7):e0003919, 2015.

[122] A.L Okello and L.F. Thomas. Human taeniasis: current insights into prevention and management strategies in endemic countries. *Risk Management and Healthcare Policy*, pages 107–116, 2017.

[123] Wadzanai P Mboko, Preeti Chhabra, Marta Diez Valcarce, Veronica Costantini, and Jan Vinjé. Advances in understanding of the innate immune response to human norovirus infection using organoid models. *The Journal of general virology*, 103(1), 2022.

[124] KAM Gaythorpe, CL Trotter, and AJK Conlan. Modelling norovirus transmission and vaccination. *Vaccine*, 36(37):5565–5571, 2018.

[125] Mary E Wikswo, Jennifer Cortes, Aron J Hall, George Vaughan, Christopher Howard, Nicole Gregoricus, and Elaine H Cramer. Disease transmission and passenger behaviors during a high morbidity norovirus outbreak on a cruise ship, january 2009. *Clinical infectious diseases*, 52(9):1116–1122, 2011.

[126] Jose M Lorenzo, Paulo E Munekata, Ruben Dominguez, Mirian Pateiro, Jorge A Saraiva, and Daniel Franco. Main groups of microorganisms of relevance for food safety and stability: General aspects and overall description. In *Innovative technologies for food preservation*, pages 53–107. Elsevier, 2018.

[127] Amit Vikram, Joelle Woolston, and Alexander Sulakvelidze. Phage biocontrol applications in food production and processing. *Current issues in molecular biology*, 40(1): 267–302, 2021.

[128] Rendani Netshikweta, Winston Garira, et al. An embedded multiscale modelling to guide control and elimination of paratuberculosis in ruminants. *Computational and Mathematical Methods in Medicine*, 2021, 2021.

[129] Hector H Garcia, Armando E Gonzalez, Victor CW Tsang, Seth E O'Neal, Fernando Llanos-Zavalaga, Guillermo Gonzalvez, Jaime Romero, Silvia Rodriguez, Luz M Moyano, Viterbo Ayvar, et al. Elimination of taenia solium transmission in northern peru. *New England Journal of Medicine*, 374(24):2335–2344, 2016.

[130] WHO First Ever Licensed Vaccine. Anthelmintic against the major cause of epilepsy in the developing world, 2017.

[131] Marshall W Lightowlers and Meritxell Donadeu. Designing a minimal intervention strategy to control taenia solium. *Trends in parasitology*, 33(6):426–434, 2017.

[132] Hector H Garcia, Armando E Gonzalez, and Robert H Gilman. Taenia solium cysticercosis and its impact in neurological disease. *Clinical microbiology reviews*, 33(3):10–1128, 2020.

[133] M. Konboon, M. Bani-Yaghoub, P.O. Pithua, N. Rhee, and S.S. Aly. A nested compartmental model to assess the efficacy of paratuberculosis control measures on us dairy farms. *PloS One*, 13(10):e0203190, 2018.